Interlaminaire vertaaiing van composietlaminaten
door middel van nanovezelmembranen

Interlaminar Toughening of Composite Laminates
by Electrospun Nanofibrous Interleaves

Lode Daelemans

Promotoren: prof. dr. ir. K. De Clerck, prof. dr. ir. W. Van Paepegem
Proefschrift ingediend tot het behalen van de graad van
Doctor in de ingenieurswetenschappen: materiaalkunde

UNIVERSITEIT
GENT

Vakgroep Materialen, Textiel en Chemische Proceskunde
Voorzitter: prof. dr. P. Kiekens
Faculteit Ingenieurswetenschappen en Architectuur
Academiejaar 2017 - 2018

ISBN 978-94-6355-039-0
NUR 971
Wettelijk depot: D/2017/10.500/74

Examination board

Chairman

prof. Gert De Cooman (UGent)

Secretary

prof. Paul Kiekens (UGent)

Reading committee

prof. Véronique Michaud (EPFL)

prof. Ludwig Cardon (UGent)

prof. Hubert Rahier (VUB)

dr. ir. Ives De Baere (UGent)

prof. Dagmar D'Hooge (UGent)

Promotors

prof. Karen De Clerck (UGent)

prof. Wim Van Paepegem (UGent)

Funding

Financial support from the Agency for Innovation by Science and Technology of Flanders (IWT) and the Special Research Fund (BOF) of Ghent University is gratefully acknowledged. Results in this PhD were obtained within the framework of the IWT Strategic Basic Research Grant 141344 and the BOF 13/24J/020 project.

Preface

At the start of my PhD, I was not sure what to expect from the coming four years. On the one hand, I felt excited to go into materials science research, being able to extend my knowledge and hoping to discover something new. On the other hand, four years of focusing on a very specific topic seemed like a daunting task. Yet now that these years are over, I can say that I would have happily added another four years to my research career. Apart from gaining more in-depth knowledge in the field of textiles, nanofibres and composites personally, my colleagues and I were also able to bring some novel insights into the field, which is the most rewarding outcome I could imagine.

Writing this PhD would not have been possible without the help of my promoters. I cannot thank Karen De Clerck and Wim Van Paepegem enough for their support. They always made time for me in their busy schedules whenever I wanted to discuss something. I could not have asked for better promoters and I am glad I was able to perform this PhD under their supervision. I would also like to thank Hubert Rahier, Ives De Baere, Sam van der Heijden and Timo Meireman for their help and advice.

During these past years, I was lucky to be able to work with the kindest colleagues of which many I can call good friends now. Their support during stressful times and frequent discussions over some coffee have not only positively influenced my research, they also helped me grow on a personal level. For that, I would like to express my sincere gratitude and I hope that I will be able to return the favour someday.

Special thanks go to my colleague Sam van der Heijden with whom I have worked intensively together. Without his collaboration, this book would have contained a lot less pages.

My friends and family deserve a word of thanks as well, for their patience whenever I could not make time for them and for their on-going support throughout this period. I would also like to thank Charlotte, for always being there for me and for making sure I wanted for nothing.

Lastly, I would like to dedicate this PhD to my mother, who, above everything else, always put her children first and gave them everything in her reach to make them follow their dreams. I am where I am today because of her.

Contents

Publications in international peer reviewed journals

1* **Novel composite materials with tunable delamination resistance using functionalizable electrospun SBS fibers**
Sam van der Heijden, Lode Daelemans, Kevin De Bruycker, Robin Simal, Ives De Baere, Wim Van Paepegem, Hubert Rahier and Karen De Clerck
(2017) COMPOSITE STRUCTURES. 159. p.12-20
IF 2015: 3.853; Q1

2 **A hybrid micro-meso-scale unit cell model for homogenization of the nonlinear orthotropic material behavior of coated fabrics used in tensioned membrane structures**
Tien Dung Dinh, Ali Rezaei, Lode Daelemans, Marijke Mollaert, Danny Van Hemelrijck and Wim Van Paepegem
(2017) COMPOSITE STRUCTURES. 162. p.271-279
IF 2015: 3.853; Q1

3 **Finite element simulation of the woven geometry and mechanical behaviour of a 3D woven dry fabric under tensile and shear loading using the digital element method**
Lode Daelemans, Jana Faes, Samir Allaoui, Gilles Hivet, Manuel Dierick, Luc Van Hoorebeke and Wim Van Paepegem
(2016) COMPOSITES SCIENCE AND TECHNOLOGY. 137. p.177-187
IF 2015: 3.879; Q1

4* **Improved fatigue delamination behaviour of composite laminates with electrospun thermoplastic nanofibrous interleaves using the Central Cut-Ply method**
Lode Daelemans, Sam van der Heijden, Ives De Baere, Hubert Rahier, Wim Van Paepegem and Karen De Clerck
(2016) COMPOSITES: PART A: APPLIED SCIENCE AND MANUFACTURING. 94. p.1-31
IF 2015: 3.719; Q1

5 **Creation of a nanovascular network by electrospun sacrificial nanofibers for self-healing applications and its effect on the flexural properties of the bulk material**
Ana Torre Muruzabal, Lode Daelemans, Guy Van Assche, Karen De Clerck and Hubert Rahier
(2016) POLYMER TESTING. 54. p.78-83
IF 2015: 2.35; Q1

6 **Finite element simulations to evaluate deformation of polyester tubular braided structures**
Jerry Ochola, Benny Malengier, Lode Daelemans and Lieva Van Langenhove
(2016) TEXTILE RESEARCH JOURNAL. p.1-9
IF 2015: 1.299; Q1

7* **Using aligned nanofibres for identifying the toughening micromechanisms in nanofibre interleaved laminates**
Lode Daelemans, Sam van der Heijden, Ives De Baere, Hubert Rahier, Wim Van Paepegem and Karen De Clerck
(2016) COMPOSITES SCIENCE AND TECHNOLOGY. 124. p.17-26
IF 2015: 3.879; Q1

8* **Damage-resistant composites using electrospun nanofibers: a multiscale analysis of the toughening mechanisms**
Lode Daelemans, Sam van der Heijden, Ives De Baere, Hubert Rahier, Wim Van Paepegem and Karen De Clerck
(2016) ACS APPLIED MATERIALS & INTERFACES. 8(18). p.111806-11818
IF 2015: 7.145; Q1

9 **Interlaminar toughening of resin transfer molded laminates by electrospun polycaprolactone structures: effect of the interleave morphology**
Sam van der Heijden, Lode Daelemans, Timo Meireman, Ives De Baere, Hubert Rahier, Wim Van Paepegem and Karen De Clerck
(2016) COMPOSITES SCIENCE AND TECHNOLOGY. 136. p.10-17
IF 2015: 3.879; Q1

10 Bisphenol A based polyester binder as an effective interlaminar toughener
Lode Daelemans, Sam van der Heijden, Ives De Baere, Irfan Muhammad, Wim Van Paepegem, Hubert Rahier and Karen De Clerck
(2015) COMPOSITES PART B-ENGINEERING. 80. p.145-153
IF 2015: 3.85; Q1

11* Nanofibre bridging as a toughening mechanism in carbon/epoxy composite laminates interleaved with electrospun polyamide nanofibrous veils
Lode Daelemans, Sam van der Heijden, Ives De Baere, Hubert Rahier, Wim Van Paepegem and Karen De Clerck
(2015) COMPOSITES SCIENCE AND TECHNOLOGY. 117. p.244-256
IF 2015: 3.879; Q1

12* Interlaminar toughening of resin transfer moulded glass fibre epoxy laminates by polycaprolactone electrospun nanofibres
Sam van der Heijden, Lode Daelemans, Bert De Schoenmaker, Ives De Baere, Hubert Rahier, Wim Van Paepegem and Karen De Clerck
(2014) COMPOSITES SCIENCE AND TECHNOLOGY. 104. p.66-73
IF 2014: 3.569; Q1

*Papers directly related to the work presented in this PhD.

Conference contributions

1* **Nano-engineering highly toughened fibre reinforced polymer composites by interleaving electrospun nanofibres for advanced applications**
Lode Daelemans, Timo Meireman, Ives De Baere, Hubert Rahier, Wim Van Paepegem and Karen De Clerck
(2017) International Conference on Electrospinning.

2* **Interlaminar toughening of resin transfer molded laminates by electrospun polycaprolactone structures: effect of the interleave morphology**
Timo Meireman, Lode Daelemans, Ives De Baere, Hubert Rahier, Wim Van Paepegem and Karen De Clerck
(2017) International Conference on Electrospinning.

3* **Toughening micromechanisms in composites enhanced with electrospun thermoplastic nanofibrous interleaves**
Lode Daelemans, Sam van der Heijden, Timo Meireman, Ives De Baere, Hubert Rahier, Wim Van Paepegem and Karen De Clerck
(2016) 4th International Conference on Nanomechanics and Nanocomposites.

4* **Increasing the damage resistance of composites by interleaving them with electrospun nanofibrous veils**
Lode Daelemans, Sam van der Heijden, Ives De Baere, Hubert Rahier, Wim Van Paepegem and Karen De Clerck
(2016) 17th European Conference on Composite Materials.

5* **Towards damage resistant composites using electrospun nanofibers: a multiscale analysis of the toughening mechanisms**
Sam van der Heijden, Lode Daelemans, Ives De Baere, Hubert Rahier, Wim Van Paepegem and Karen De Clerck
(2016) 4th International Conference on Electrospinning.

6 **Electrospinning of sacrificial nanofibers for the creation of a self-healing nanovascular network and its effect on the properties of an epoxy matrix**
Ana Torre Muruzabal, Lode Daelemans, Guy Van Assche, Karen De Clerck and Hubert Rahier
(2016) 4th International Conference on Electrospinning.

7 **Virtual mechanical testing of a complex 3D woven fabric: a unified simulation methodology for deformation mechanics of textile structures during tension, shear and draping**
Lode Daelemans, Jana Faes, Samir Allaoui, Gilles Hivet and Wim Van Paepegem
(2016) 17th European Conference on Composite Materials.

8 **Using a polyester binder for the interlaminar toughening of glass/epoxy composite laminates**
Lode Daelemans, Sam van der Heijden, Ives De Baere, Hubert Rahier, Wim Van Paepegem and Karen De Clerck
(2015) 20th International Conference on Composite Materials.

9* **Interlaminar toughening of resin transfer moulded glass fibre epoxy laminates by polycaprolactone electrospun nanofibres**
Sam van der Heijden, Lode Daelemans, Ives De Baere, Hubert Rahier, Wim Van Paepegem and Karen De Clerck
(2015) 20th International Conference on Composite Materials.

10 **From dry yarns to complex 3D woven fabrics: a unified simulation methodology for deformation mechanics of textiles in tension, shear and draping**
Lode Daelemans and Wim Van Paepegem
(2015) SIMULIA Benelux Regional User Meeting 2015.

11 **Added value of micro-tomography measurements in mechanical characterization of materials: some case studies in engineering applications**
Wim Van Paepegem, Lode Daelemans et al.
(2015) 2nd UGCT seminar.

*Contributions directly related to the work presented in this PhD.

Symbols and abbreviations

CAI	Compression After Impact
CBBM	Compliance Based Beam Method
CCP	Central Cut-Ply
CF	Carbon Fibre
***R*-curve**	Resistance curve
DCB	Double Cantilever Beam
DIC	Digital Image Correlation
DLC	Double Layer Coated
ENF	End Notched Flexure
FRP	Fibre Reinforced Polymer
GF	Glass Fibre
LVI	Low Velocity Impact
PA	Polyamide
PA6	Polyamide 6
PA66	Polyamide 6.6
PA69	Polyamide 6.9
PCL	Polycaprolactone
RH	Relative Humidity
SBS	Styrene-Butadiene-Styrene
SEM	Scanning Electron Microscopy
SENB	Single Edge Notched Bending
SENT	Single Edge Notched Tension
SLB	Single Led Bend
SLC	Single Layer Coated
SSI	Self-Supporting Interlayer
TCD	Tip-to-Collector Distance
UD	Unidirectional
VARTM	Vacuum Assisted Resin Transfer Moulding

a	Crack or delamination length
C	Compliance
δ	Displacement
da/dN	Delamination growth rate
G_I	Mode I interlaminar fracture toughness
G_{II}	Mode II interlaminar fracture toughness
P	Load

Summary

Fibre reinforced polymer (FRP) composites have already been used by mankind from as early on as 2000 BC as a structural material under the form of straw reinforced clay bricks. Technology has come a long way since then and nowadays, composite materials are used for many high-end applications such as wind turbines, airplanes, construction materials, bicycles and bridge decks. These relatively new materials typically consist of layers of continuous fibres with high stiffness and high strength embedded in a polymer matrix. The combination of the reinforcing fibres and the polymer matrix results in materials with outstanding mechanical properties at low weight. Therefore, they are mainly used in structural applications in which weight is a critical factor, such as the aerospace sector. Most composite structures are formed by stacking unidirectional or woven plies of reinforcing fibres under different angles in order to tune the properties in the in-plane directions. This is referred to as a composite laminate. Although the laminated structure of many FRP materials allows one to engineer the properties in various directions, it also results in the biggest downside associated with these materials: failure by delamination. The reinforcing plies are prone to debond and separate due to a mismatch in elastic properties between adjacent reinforcing plies, a relatively weak resin rich interlayer between the reinforcing plies and the fact that there is no through-thickness reinforcement. Delamination results in a loss of stiffness and strength of the composite part and is one of the major failure modes encountered in composites during use. Hence, increasing the resistance to delamination would result in better materials, allowing engineers to design new and optimized composite applications.

This PhD investigates the novel interlaminar toughening technique based on interleaving electrospun nanofibrous veils. These veils can be thought of as a new class of materials consisting of very thin polymeric fibres with typical diameters below 500 nm. This is substantially lower than the diameter of the classical reinforcing fibres that have diameters between 5 and 25 µm. It is this small diameter that gives nanofibrous veils interesting characteristics such as a large surface area, a high porosity and improved mechanical properties compared to the bulk polymer. They are formed as self-supporting veils or can be directly electrospun on the reinforcing fibre plies. This makes it exceptionally

easy to integrate them into composite laminates in comparison to many traditional toughening techniques by interleaving them between reinforcing plies. Although the expected benefits are numerous, the research into these nanofibre interleaved composite materials is still very limited.

The primary goal of this PhD is to develop highly toughened nanofibre enhanced composite laminates while at the same time, getting a thorough understanding of the micromechanisms and generic parameters of this novel toughening method. This has been done by a broad mechanical investigation concerned with not only fundamental loading cases, but also a real-life loading case such as impact. The interleaved composites can be thought to have three different levels at which the nanofibres affect the properties. These levels coincide with the hierarchical nature of the laminate itself: (i) the nanotoughened epoxy resin, (ii) the nanotoughened interlayer and (iii) the nanotoughened laminate. The effect of the nanofibres was analysed on each level separately. This multilevel analysis led to a significant advancement of the understanding of these materials in a more structured and general sense, a step that is crucial to be able to design better damage resistant composite structures. Nanofibre interleaved composites with excellent delamination resistance were designed, while obtaining a lot more fundamental knowledge about the prerequisites for effective nanofibre toughening. The improvements were in-line with and often even better than those obtained with traditional toughening methods.

At the nanotoughened epoxy level, the effect of electrospun nanofibres on the fracture toughness of the epoxy resin was analysed. Using SENB experiments on relatively thick nanotoughened epoxy specimens, we found that there are two distinct mechanisms causing an increased fracture toughness compared to neat epoxy resin. The first one is the yielding of nanofibres in the fracture processing zone in front of the crack tip (intrinsic toughening) which caused an increase in the initiation fracture toughness of about 20 – 30 % for PCL nanofibre toughened epoxy. However, the main increase in fracture toughness was due to the extrinsic toughening mechanism of nanofibre bridging. If the crack propagates, nanofibres will bridge the newly formed crack surfaces and take up energy by straining, yielding and eventually (tensile) fracture. At the same time, they provide closing tractions on the crack which relieves the stress at the crack tip. Both effects will cause an increase in the fracture toughness. Using in-situ

microscopy, the development of the nanofibre bridging zones was visualised. These experiments provided many new insights into the way nanofibres result in an improved fracture toughness.

At the level of a nanotoughened interlayer, other factors such as the delamination path will come into play. Microscopic analysis of delaminated specimens showed that the delamination did not progress solely through the nanotoughened interlayer. Thus, nanofibre bridging zones did not just develop over the whole delamination plane. Rather, the delamination was deflected towards the reinforcing ply boundary where it progressed by "classical" interfacial failure of the reinforcing fibres. However, regular crossings of the nanotoughened interlayer by the delamination path occurred, and it was mainly at these interlaminar crossings that nanofibre bridging zones developed. SEM analysis of the fracture surface of delaminated specimens showed the same fracture morphology of the nanofibre bridging zones with protruding, plastically deformed nanofibres visible as in the nanotoughened epoxy. It was found that the delamination mode affects the development of nanofibre bridging zones. Not only did a Mode I loading mode typically result in less interlaminar crossings, it also exerted peeling forces to the nanofibres, making their adhesion with the epoxy very important. Indeed, nanofibres with a low adhesion to the epoxy matrix did not improve the Mode I delamination resistance. Mode II loadings on the other hand typically resulted in a higher amount of interlaminar crossings while exerting straining forces to the nanofibres. This resulted in very effective load transfer to the nanofibres which readily increased the Mode II delamination resistance.

The interaction between the delamination path and the nanotoughened interlayers – which determines the amount of nanofibre bridging zones – was found to be dependent on parameters related to the nanofibres themselves, the veil morphology, the interleaving technique, the reinforcing fabric architecture and even the way in which the delamination experiment is performed. These effects are very important not only to design optimally toughened laminates, but also to comprehend the results reported in literature. Indeed, while one type of nanofibrous veil might result in good improvements for one type of composite laminates, it does not necessarily result in the same improvements for other types of laminates. Generally, in order to increase the fracture

toughness on the interlaminar level, the interaction between the delamination path and the nanotoughened interlayer characteristics are of crucial importance and should both be considered in order to design damage resistant composite materials.

Although the nanotoughened epoxy and nanotoughened interlayer level provided the essential insights into the toughening micromechanisms acting in an interleaved composite, the crack and delamination growth were always carefully initiated and controlled. Furthermore, the delamination specimens typically had a unidirectional layup, which is not often encountered in applications. To provide a link between the fundamental insights and the mechanical response that can be expected in real-life situations, fully interleaved composite laminates were analysed. Using multidirectional laminates interleaved with nanofibres, the general mechanical properties and open hole tensile strength were analysed. While the (in-plane) tensile, shear and flexural stiffness and strength were retained, the open hole strength of PCL nanofibre interleaved laminates even increased about 8% compared to the virgin material.

The low velocity impact resistance of fully interleaved laminates increased considerably compared to the virgin material. The (projected) damage decreased up to 50 – 60 %, especially at higher impact energies where the virgin material showed much delamination. PCL nanofibre interleaved laminates performed better than PA6.9 nanofibre interleaved ones. This was attributed to the strain rate sensitivity of PA6.9 and its low adhesion strength with the epoxy matrix. The interleaved laminates also showed less permanent indentation for the same impact energy than the virgin material. As more energy was absorbed in the interleaved laminates by the nanofibres, less damage to reinforcing fibres and matrix resin was produced. Analysis of the fracture surface of impacted specimens showed the development of nanofibre bridging zones, providing the link between the three levels. The PCL nanofibre bridging zones were more effective as much more plastic deformation and no peeling was observed compared to the PA6.9 bridging zones. The residual compressive strength of the impacted specimens was not influenced much by the presence of the nanotoughened interlayers. This was attributed to the relatively high impact

energies that were used and the shape of the delaminations in the cross-ply specimens.

Samenvatting

Al sinds 2000 voor Christus gebruikt de mens vezelversterkte composietmaterialen. Destijds onder de vorm van stro-versterkte kleistenen om huizen te bouwen. Ondertussen is de technologie enorm geëvolueerd en vindt men composietmaterialen terug in vele hoogperformante toepassingen zoals windturbines, vliegtuigen, schepen, fietsen en brugdekken. Deze relatief nieuwe materialen bestaan meestal uit lagen van continue vezels met een hoge stijfheid en hoge sterkte, ingebed in een kunststofmatrix. De combinatie van versterkende vezels in een kunststofmatrix resulteert in materialen met uitstekende mechanische eigenschappen en een zeer laag gewicht. Dit maakt ze uitermate interessant voor structurele toepassingen waarbij het gewicht een kritische rol speelt, zoals in de luchtvaartsector. De lagen, die bestaan uit unidirectionele vezels of een geweven structuur, worden gestapeld onder verschillende hoeken om zo een dikkere structuur te vormen, waarbij de eigenschappen in het vlak kunnen worden afgestemd naargelang de toepassing. Deze gestapelde structuur wordt ook wel een (composiet)laminaat genoemd. De gelamineerde structuur maakt het mogelijk om de eigenschappen in het vlak nauwkeurig af te stemmen, maar zorgt tegelijk voor één van de grootste gebreken van deze materialen: materiaalfalen door delaminatie. De versterkende lagen zijn geneigd los te komen van elkaar door een mismatch in elastische eigenschappen tussen verschillend georiënteerde lagen, de aanwezigheid van een relatief zwakke harsrijke zone tussen de versterkingslagen en de afwezigheid van een versterking in de dikterichting.

Delaminaties resulteren in een verlies van stijfheid en sterkte van het composietmateriaal en zijn één van de belangrijkste oorzaken van materiaalfalen tijdens gebruik. Dit betekent dat de verhoging van de delaminatieweerstand zou resulteren in betere composietmaterialen, waarmee ingenieurs niet alleen geoptimaliseerde, maar ook nieuwe toepassingen kunnen ontwerpen.

In dit doctoraat wordt een nieuwe interlaminaire vertaaiingstechniek onderzocht om de delaminatieweerstand te verhogen. Deze techniek is gebaseerd op de incorporatie van elektrogesponnen nanovezel membranen in de composietlaminaten. Een nanovezelmembraan kan worden beschouwd als

een nieuw soort materiaalklasse bestaande uit zeer dunne polymeervezels met diameters kleiner dan 500 nm. Dit is aanzienlijk kleiner dan de diameter van de klassieke versterkingsvezels die tussen de 5 en 25 µm ligt. Dankzij deze kleine diameter vertonen de nanovezelmembranen zeer interessante eigenschappen, waaronder een groot specifiek oppervlak, een hoge porositeit en verbeterde mechanische eigenschappen in vergelijking met het bulkpolymeer. Tijdens het elektrospinnen worden nanovezels afgezet als zelfondersteunende membranen of kan men ze onmiddellijk afzetten op de versterkingsvezellagen. Door de membranen tussen de versterkende lagen te leggen, of door gebruik te maken van versterkingslagen met opgesponnen nanovezels, zijn ze bijzonder makkelijk te integreren in composietlaminaten. Dit biedt een enorm voordeel in vergelijking met vele andere vertaaiingstechnieken. Desondanks is het onderzoek naar deze nieuwe nanovezelverbeterde composietmaterialen nog steeds zeer beperkt.

Het doel van dit doctoraat was tweeledig. Niet alleen wilden we nanovezelvertaaide composietlaminaten ontwikkelen, ook wilden we een grondig inzicht krijgen in de micromechanismen en generieke parameters die gerelateerd zijn aan deze nieuwe vertaaiingstechniek. Een breed mechanisch onderzoek op verschillende materiaalniveaus lag daarom aan de basis van dit doctoraat. De nanovezelverbeterde composieten kunnen immers worden onderverdeeld in drie verschillende niveaus, waarin de nanovezels de eigenschappen beïnvloeden. Deze niveaus vallen samen met de hiërarchische aard van het laminaat: (i) het nanovezelvertaaide epoxyhars, (ii) de nanovezelvertaaide tussenlaag en (iii) het nanovezelvertaaide laminaat. Op elk van deze niveaus werd het vertaaiingseffect van de nanovezels afzonderlijk geanalyseerd. Het is deze analyse op drie niveaus die leidde tot een meer generiek inzicht in deze materialen: een cruciale stap om betere schadebestendige toepassingen te kunnen ontwerpen.

Op het laagste niveau, dat van het nanovezelvertaaide epoxy, werd het effect van de nanovezels op de breuktaaiheid van het epoxyhars geanalyseerd. Door gebruik te maken van SENB experimenten op relatief dikke nanovezelvertaaide epoxy proefstukken, werden twee mechanismen ontdekt die voor een verhoogde breuktaaiheid zorgen. Het eerste mechanisme is de plastische vervorming van nanovezels in de spanningszone die optreedt aan de scheurtip

(intrinsieke vertaaiing). Hierdoor stijgt de energie die nodig is voor scheurinitiatie in het epoxy. Het PCL nanovezelvertaaide epoxy had bijvoorbeeld een 20% tot 30% hogere breuktaaiheid. De belangrijkste stijging van de breuktaaiheid was echter het gevolg van de vorming van nanovezelbruggen tussen scheuroppervlakken (extrinsieke vertaaiing). Wanneer een scheur in het nanovezelvertaaide epoxy ontstaat en groeit, zullen nanovezels de nieuw gevormde breukoppervlakken overbruggen. Tijdens dit proces zullen de nanovezels uitgerokken worden en uiteindelijk zelfs breken, waardoor er enorm veel energie wordt geabsorbeerd. Tegelijkertijd zorgen de nanovezelbruggen ook voor een sluitende actie tussen de scheuroppervlakken, waardoor de spanningsintensiteit aan de scheurtip daalt. Beide effecten veroorzaken een verhoging van de waargenomen breuktaaiheid van het nanovezelvertaaide epoxy. In-situ microscopie maakte het mogelijk om de ontwikkeling van nanovezelbruggen te visualiseren tijdens de scheurexperimenten. Deze experimenten leverden vele nieuwe inzichten op in de werking van het vertaaiingsmechanisme in nanovezelvertaaid epoxy.

Op het niveau van de nanovezelvertaaide tussenlaag spelen andere factoren een rol, waaronder het delaminatiepad. Het nanovezelvertaaide epoxyhars bevindt zich nu namelijk tussen vezellagen. Uit microscopische analyse van gedelamineerde proefstukken bleek dat de delaminatie niet doorheen de volledige vertaaide tussenlaag ontstond. Dit betekent dat er zich geen nanovezelbruggen zullen vormen over het ganse oppervlak van de delaminatie. In plaats daarvan wijkt de delaminatie grotendeels uit naar het grensvlak van de versterkingslagen. De tussenlaag wordt echter nog regelmatig doorkruist door de delaminatie. Deze doorkruisingen zorgen voor de ontwikkeling van nanovezelbruggen, en bijgevolg voor een verhoging van de delaminatieweerstand. Uit SEM-analyse van de gedelamineerde proefstukken bleek dat de doorkruisingen dezelfde morfologie hadden als het gebroken nanovezelvertaaide epoxyhars. Er waren restanten van nanovezelbruggen te zien waarin uitstekende en plastisch vervormde nanovezels zichtbaar waren.

Ook de belastingsmode bleek een invloed te hebben op de ontwikkeling van nanovezelbruggen tijdens delaminatie. Een Mode I-belasting (opening) leidde meestal tot minder doorkruisingen van de vertaaide tussenlaag. Daarboven op zorgde de Mode I-belasting voor "afpel"-krachten op de nanovezels. Bijgevolg is

een goede hechting tussen de nanovezels en het epoxy cruciaal om de delaminatieweerstand te verbeteren. Bij een Mode II-belasting (afschuiving) daarentegen, waren meer doorkruisingen van de tussenlaag zichtbaar. Hierbij werden de nanovezels uitgerokken in plaats van afgepeld. Dit resulteerde in een zeer effectieve belastingsoverdracht door de nanovezels, waardoor de Mode II-delaminatieweerstand aanzienlijk verhoogde. Bijkomend bleek dat de interactie tussen het delaminatiepad en de vertaaide tussenlaag afhankelijk was van het nanovezeltype, de morfologie van het nanovezelmembraan, de manier waarop de nanovezels geïntegreerd worden, de architectuur van de vezelversterking en zelfs van de manier waarop een delaminatie-experiment wordt uitgevoerd. Het is zeer belangrijk om inzicht te krijgen in deze parameters, niet alleen om optimaal vertaaide laminaten te bekomen, maar ook om de in de literatuur beschreven resultaten beter te begrijpen. Deze parameters verklaren waarom één type nanovezelmembraan kan leiden tot een goede delaminatieweerstand voor één bepaald type composietlaminaat, maar niet noodzakelijk leidt tot dezelfde verbeteringen voor een ander soort laminaat. Over het algemeen kan men stellen dat, om de delaminatieweerstand te verbeteren op het interlaminaire niveau, de interactie tussen het delaminatiepad en de nanovezelvertaaide tussenlaag van cruciaal belang is en in acht moet worden genomen om schadebestendige composietmaterialen te kunnen ontwerpen.

Hoewel de bovengenoemde twee niveaus essentiële inzichten gaven in de micromechanismen van vertaaiing door middel van nanovezels, werden de scheur- en delaminatiegroei altijd zorgvuldig geïnitieerd en gecontroleerd. Bovendien hadden de delaminatieproefstukken meestal een unidirectionele stapeling; een stapeling die niet vaak in applicaties voorkomt. Om een verband te kunnen leggen tussen de fundamentele inzichten en de mechanische respons die in werkelijke situaties kan worden verwacht, werden multidirectionele composietlaminaten geanalyseerd die nanovezelmembranen hadden in elke tussenlaag. Terwijl de delaminatieweerstand verhoogde, bleven ook de algemene mechanische eigenschappen zoals de trek-, schuif- en buigstijfheid en trek-, schuif-, en buigsterkte behouden. Een positief resultaat, aangezien traditionele vertaaiingstechnieken doorgaans een negatief effect hebben op de algemene mechanische eigenschappen. De sterkte van de proefstukken waarin een gat werd geboord (modelsysteem voor structuren met bv. een klinknagel of een beschadiging) nam zelfs toe in vergelijking met het referentiemateriaal

wanneer er PCL nanovezelmembranen aanwezig waren in de tussenlagen. Ook de impactweerstand verhoogde aanzienlijk. Het geprojecteerde schadeoppervlak nam af met 40% tot 50%. Dit effect was voornamelijk zichtbaar bij hoge impactenergieën waarbij het referentiemateriaal zeer veel delaminatie vertoonde. De permanente indeuking van nanovezelvertaaide laminaten was daarenboven beperkter, wat duidt op een betere impactweerstand. Aangezien de nanovezels energie absorbeerden, bleef de schade aan de versterkingsvezels en het matrixhars beperkt. Analyse van het breukoppervlak toonde opnieuw de ontwikkeling van nanovezelbruggen aan, wat de nauwe relatie tussen de drie niveaus bevestigde.

PART I

Interlaminar Toughening of Composite Laminates Using Electrospun Nanofibrous Interleaves

1

GENERAL INTRODUCTION

Fibre reinforced polymer composites are finding their way into many high-end applications. Airplanes, wind turbines, ships, and formula 1 vehicles are just a few examples in which composites play a major role. However, due to their laminated structure, they are prone to failure by delamination. Improving the delamination resistance is thus one of the major research topics in the field. In this PhD, the use of electrospun nanofibres is investigated to create delamination resistant composite materials. This chapter will give a concise introduction into the topic of fibre reinforced composites, delamination failure and toughening techniques, followed by the objectives of the research and an outline of the work.

1.1 FIBRE REINFORCED COMPOSITE MATERIALS

According to the most general definition, a "composite" material is a material which contains at least two physically distinctive constituents and has properties which cannot be achieved with either component alone[1]. They can be natural materials such as wood, which consists out of cellulosic fibres in a lignin matrix making it flexible but strong allowing trees to withstand windy weather[2], or man-made materials with specific engineered properties such as reinforced concrete. Due to its generality, this definition of course covers a wide variety of materials which are used for all kinds of applications and purposes. Nevertheless, the term composite is often used to refer to one specific subclass of composite materials, i.e. the fibre reinforced polymer (FRP) composite materials. As the name suggests, these materials consist out of fibres embedded in a polymer matrix (Figure 1).

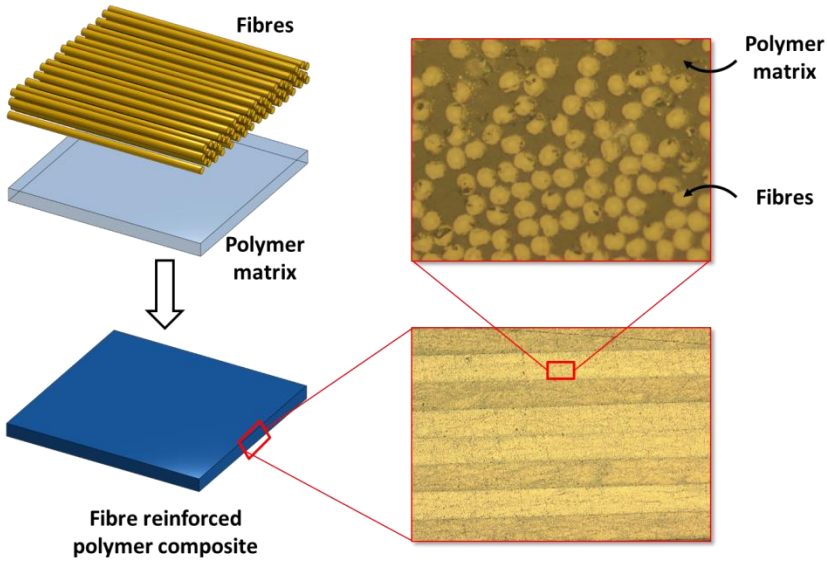

Figure 1 – Illustration of a fibre reinforced polymer composite.

The fibres, which are usually high modulus/high strength fibres such as carbon fibre (CF) or glass fibre (GF), have a reinforcing effect on the polymer matrix,

thus, improving its mechanical properties. On the other hand, the polymer matrix is a necessity to keep the fibres in their position and transferring an external load to them. It defines the shape of the composite and will protect the fibres from the environment. The fibre/matrix combination results in a relatively light material with excellent mechanical properties. This makes them interesting for high-end applications in which the combination of a low weight and high mechanical properties are important such as in the aerospace industry for example[3]. Over the past decades, these materials have gained interest from all kinds of sectors and are perhaps one of the most important subclasses of composite materials. As the research performed in this PhD work is solely on FRP composites, the term composite will be used to refer to a FRP composite material throughout the text.

Fibre reinforced composites have already been used by mankind for many centuries. One of the earliest examples is the use of grass and straw to reinforce natural clay for better building materials by the Mesopotamians. This building composite material can still be found today (Figure 2a). Other historic examples include the use of plaster soaked linen for death masks by the Egyptians or composite bows which contained silk fibres and natural pine resin by the Mongols. The real surge of FRP composites however dates back to the beginning of the 20th century with the invention of synthetic polymer resins (Bakelite, polyester, epoxy, …) and the introduction of the first glass fibres by Owens Corning. These events – which were well timed in retrospect – led to the possibility of obtaining high-end lightweight materials with mechanical properties which were previously unattainable. Their production was accelerated by World War II in which glass fibre reinforced composites were used in radar domes due to their transparency for radio signals and the first boat hulls and cars, such as the 1953 Corvette C1 (Figure 2b), found rapid commercialisation after the war effort. During the next decades, the processing methods improved, new reinforcing fibres such as carbon fibre were produced and better types of matrix polymer became available resulting in more composite applications. Nowadays, composite materials are used for wind turbines, airplanes such as the Airbus A380 (Figure 2c), construction materials, motorbikes, canoes, trucks, fishing rods, snowboards, bicycles, bridge decks and many other applications. They are even finding ground in designer goods where the aesthetically pleasing look of carbon fibre is a sign of excellence and luxury.

It is clear that there is a bright future ahead for these materials as they will become one of our main engineering materials.

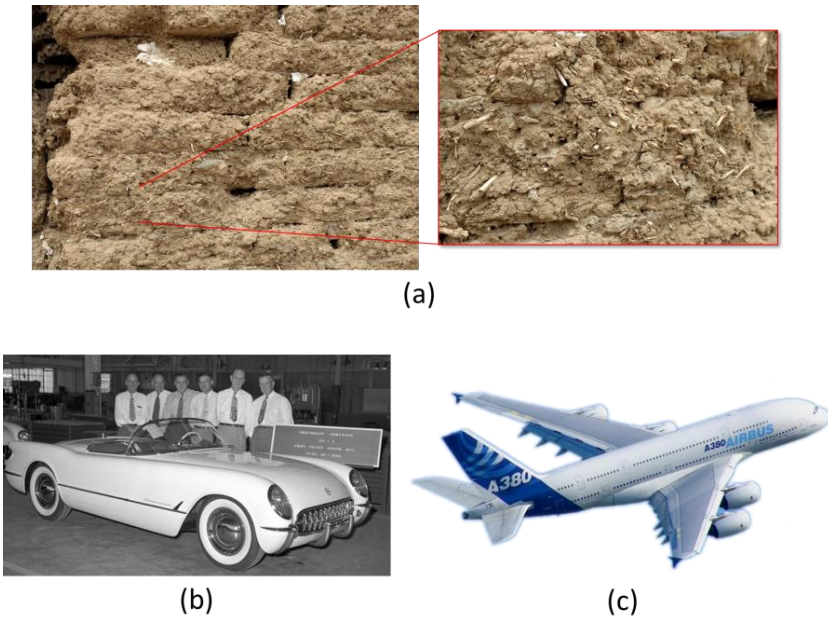

Figure 2 – Straw/clay composite bricks found behind the plaster of a house in Nicosia, Cyprus (a), the first ever produced 1953 Corvette C1 (b) and the Airbus A380 which has about 50% of its structural parts made from composites (c).

The fibres make up the principal load-bearing component in a composite material[2]. The choice of fibre type, volume fraction, length and orientation of the fibres inside the matrix determines the efficiency of the reinforcement. Low-end composites are typically made by mixing in short (staple) fibres with a polymer and processing it through traditional thermoplastics processing[4]. However, to produce high-end composites, long continuous fibres are much better suited as they will result in better mechanical performance. Just like common clothing, the fibres typically come as a textile product in which thousands of them are arranged in mats, e.g. fabrics, non-wovens, braids or unidirectional tapes. This improves there handling considerably as it would be very time consuming if every fibre in a composite needs to placed one at a time.

Traditionally, most composites are built up by layering several plies of the reinforcing fibres on top of each other and filling the free space with a polymer matrix resulting in a laminated structure referred to as a composite laminate[2]. The fibre orientation and fabric architecture of the reinforcing plies as well as the manner in which they are stacked can have a profound effect on the in-plane as well as out-of-plane mechanical properties[5]. Most composite laminates are formed by stacking unidirectional plies under different angles in order to tune the properties in the in-plane directions (Figure 3). Similarly, woven fabrics are also used, especially for less critical parts as they typically perform less than an equivalent unidirectional ply-based composite due to fibre waviness coming from the woven architecture[6,7].

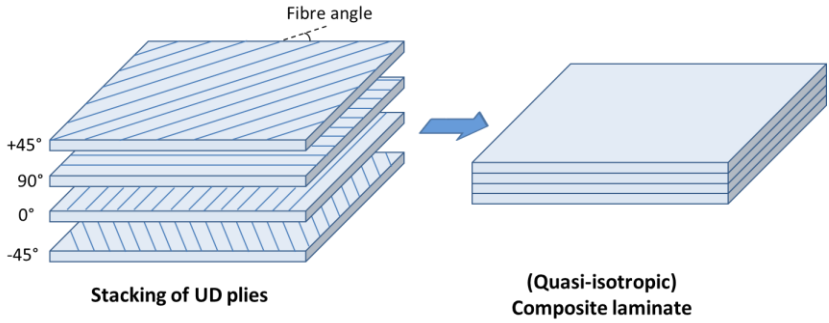

Figure 3 – Stacking of (unidirectional) reinforcing plies showing the laminated structure of composite laminates.

A wide range of thermoplastic and thermosetting polymers can be used as a matrix material. Thermoset matrices however form the main material for structural composites today[8]. Typical matrix materials are polyester, vinylester and epoxy resin. The ester-based matrices were historically important as they were one of the early available synthetic matrix resins, but are now mainly used for low-end and mid-range products. Epoxy resin is the material of choice for high-end applications such as the aerospace or wind energy sector due to its good temperature stability, chemical resistance, mechanical properties and adaptability to manufacturing methods[9]. Nevertheless, one big disadvantage of

many epoxy resins is their brittleness which can cause early failure of the composite part[10,11].

The combination of reinforcing fibres with a matrix naturally results in an interface between the fibres and the matrix (Figure 4). Generally, one can think of the interface as being responsible for load transfer to the reinforcing fibres. Therefore, its performance will have a profound effect on the overall composite properties[12]. If there is no bonding between the reinforcing fibres and the matrix, the resulting composite will have a low stiffness and strength as the reinforcing fibres will not be able to take up any stresses. On the other hand, perfect bonding can lower the damage tolerance as there is no stress relief possible, resulting in a brittle composite[2]. As such there is often an optimal interface performance window which will result in the best overall performance of the composite[13].

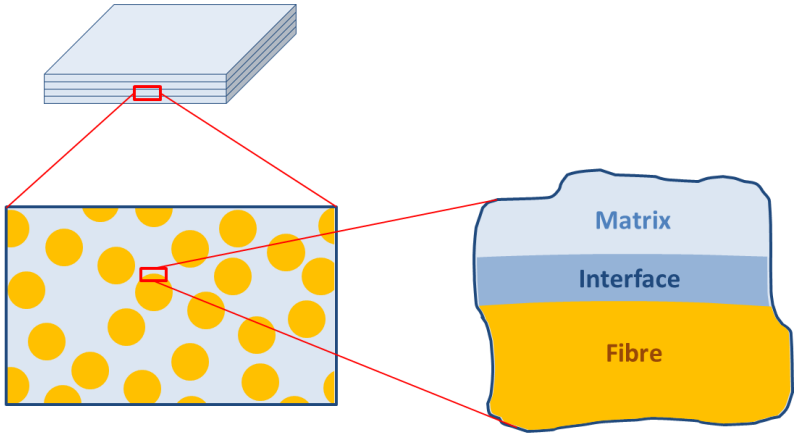

Figure 4 – Illustration of the interface between the reinforcing fibres and the matrix.

1.2 DELAMINATION FAILURE IN COMPOSITE LAMINATES

Although the laminated structure of many FRP materials allows one to engineer the properties in various directions, it also results in the biggest downside associated with these materials: failure by delamination[14]. The reinforcing plies will debond and separate, resulting in a loss of stiffness and strength of the composite part. Delamination is one of the major failure modes encountered in composites during service and substantial research has been devoted to decrease the risk of delamination[14,15].

Delamination is a failure mechanism which is typical for laminated composite structures as opposed to other engineering materials. There are several factors related to FRP materials which cause the relatively poor delamination resistance. Due to their laminated structure, a resin rich interlayer is formed between adjacent reinforcing plies (Figure 5). This interlayer is a weak spot as there are no reinforcement fibres present. Furthermore, the reinforcing fibres are placed in the plane of the laminate, increasing its in-plane properties, but providing no reinforcement in the through-thickness direction of the composite. Hence, the through-thickness properties are dependent on the matrix resin which has a relatively low stiffness and strength compared to the reinforcing fibres and is usually quite brittle. Furthermore, by stacking the reinforcing plies under different (in-plane) orientations, the mismatch in elastic properties of adjacent plies causes strong interlaminar stresses at free edges.

The development of delaminations can be easily understood by considering a block of post-it notes (Figure 6). When you push the block from both sides, the notes buckle out relative to each other to accompany for the deformation. This causes an opening delamination (Mode I) between some of the notes. If you push the block forward at its surface, the sliding force causes the block to deform in a step-like geometry due to shearing delaminations (Mode II). In the case of a composite laminate, the opening and shearing motion is prevented due to the rigid matrix resin which "glues" the layers together. This results in the development of stresses between the layers, i.e. interlaminar stresses. If these stresses overcome the local matrix or interface strength, the layers will debond and separate, and the failure can be classified as a delamination.

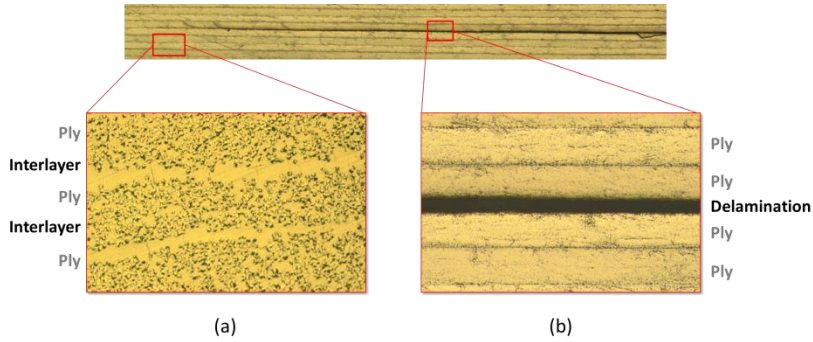

Figure 5 – Optical micrograph of a delaminated composite specimen showing the resin rich layer between reinforcing plies (a) and delamination between reinforcing plies (b).

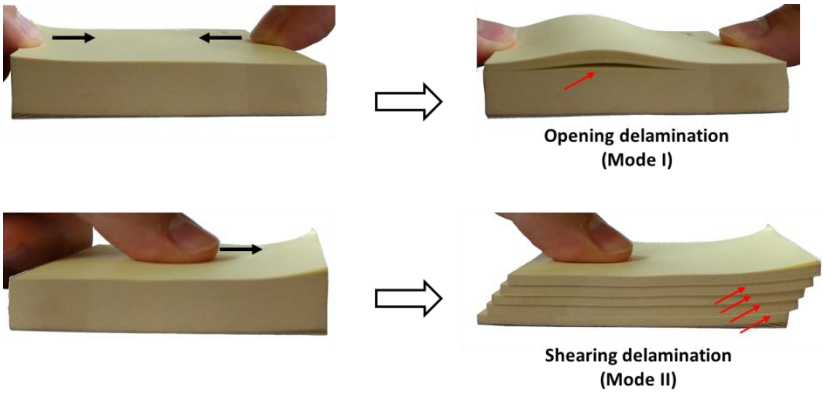

Figure 6 – Development of opening (Mode I) and shearing (Mode II) delaminations in a block of post-it notes.

Delaminations are usually located to damage prone areas where the interlaminar stresses are more severe than in the bulk of the part. These severe interlaminar stresses are caused by out-of-plane external loads, geometry

effects or local stress concentrations[15,16] (Figure 6). Out-of-plane external loads are often found at joints where two composite parts are connected such as those found in aircraft wings. Geometric effects such as tapered structures can cause a stress redistribution in the tapered section resulting in local shear and through-thickness stresses although the external load is in-plane. Local stress concentrations occur when there are discontinuities or abrupt changes in material properties. These occur for example at free edges, ply drops or prior cracks. In practice, all of these mechanisms often arise together and interact with one other. Since the damage prone region is often known during the design phase prior to production, there would be serious benefits if there is a method to locally toughen the interlayer at those regions making the part more delamination resistant.

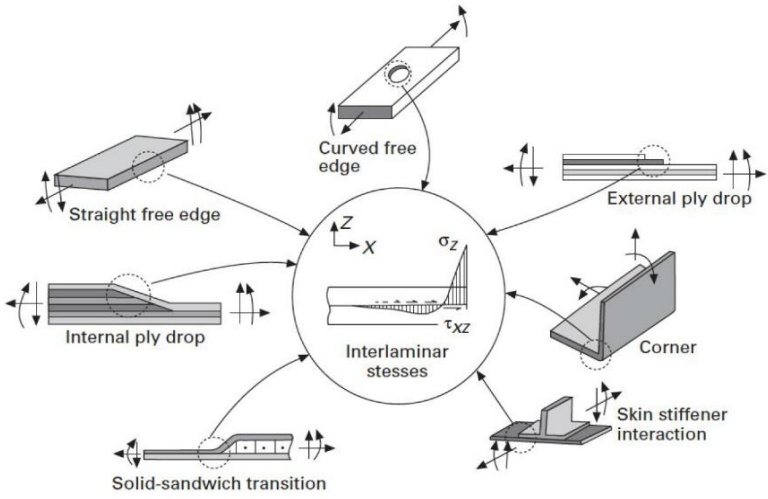

Figure 7 – Structural designs which promote delamination failure.[16]

Besides the above mentioned mechanisms triggering delamination failure, there is one specific case of external loading which – due to its importance in real-life – is treated here separately: impact. In general, the impact resistance of FRP composite laminates is fairly low[17,18]. This is often stated to be one of the major drawbacks of using these materials. During impact loading, which is a through-thickness loading, delamination is a critical and major failure event (Figure 8). It

is generated by two major mechanisms: (i) interlaminar shear owing to the impact contact force and (ii) transverse intralaminar tensile cracks developing in the bottom layers of the composite due to bending[15]. Although the impact damage is typically interlaminar shear dominated, both mechanisms play a major role in thin laminates where bending is more severe. However, it is often not the impact event itself which will cause sudden failure of the composite part, but the reduced load-bearing capability of the impacted composite[19,20]. Indeed, even relatively small impact events such as tool drops (when technicians are working on a wing), hail or tossed up debris such as pebbles can cause an important degradation of the mechanical properties of the structure[21]. Furthermore, this kind of damage is often not visible to the naked eye as it is internal and composites are often black, opaque or painted. Since this might lead to a sudden and unexpected failure of the composite, improving the impact resistance of composites is thus a very important research topic in the community.

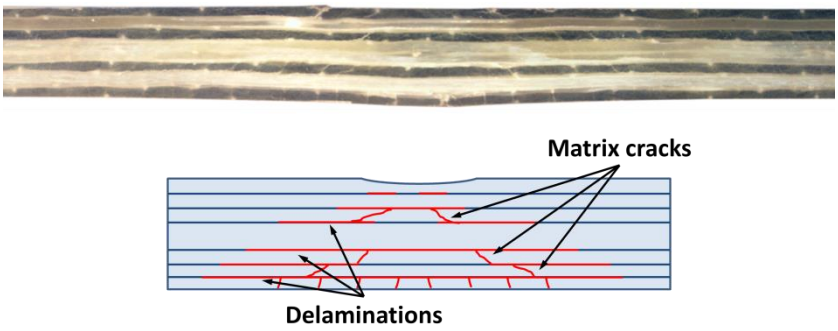

Figure 8 – Illustration of impact damage showing delamination failure and matrix cracks based on optical micrograph of an impact GFRP cross-ply specimen (through-thickness view).

It is clear that delamination resistance is of utmost importance in many composite applications. There is a need to develop methods of delaying and/or preventing this type of damage. It is thus of no surprise that improving this delamination resistance is a large field of study and many methods exist today. Nevertheless, much improvement can still be made as current toughening methods have serious disadvantages which limit their effectiveness and

prevents their use in applications. The next section deals with the current state-of-the-art toughening techniques for composite laminates, followed by a section on the toughening technique researched and developed in this PhD.

1.3 CURRENT TOUGHENING TECHNIQUES

Several methods have been developed to improve the (interlaminar) fracture toughness of composites and prevent delamination failure. These methods can be more or less classified based on the scale at which they provide an increased toughness:

- → Matrix resin toughening;
- → Addition of toughening particles;
- → Through-thickness reinforcement.

1.3.1 Matrix resin toughening

In the case of epoxy resins, matrix toughening is usually achieved by adding another component which is more "flexible" than the epoxy cross-linked network. There are various options for the secondary component, ranging from longer branched or hyper-branched resin additives[22–24], to mixing in reactive rubbers or thermoplastics[25–27]. In all cases, the added component will have a plasticizing effect on the finally obtained matrix.

The longer or hyperbranched additives will be integrated in the primary epoxy network with local plasticized regions resulting in an improved fracture toughness of the bulk resin (Figure 9a). The current state-of-the-art commercial composite resin systems are already well-developed in terms of fracture toughness. For example, Momentive's EPIKOTE RIMR135 resin formulation designed for infusion applications reaches a fracture toughness of 1500 J/m² which is an order of magnitude higher than their basic EPIKOTE 828 DGEBA based epoxy system[28]. Other resin producers provide similar high toughness resins.

Reactive rubbers and thermoplastics are dissolved into the liquid unreacted epoxy formulation. Upon curing of the epoxy resin, the increase in molecular

weight of the cross-linked network causes a phase separation process to take place[29]. This results in a complex multiphase microstructure where, dependent on the exact formulation and curing conditions, epoxy rich regions and toughening polymer rich regions co-exist. The increase in fracture toughness is typically dependent on which polymers are added, the amount in which they are added and on the obtained microstructure after phase separation[26]. Studies have shown that an epoxy rich matrix filled with small rubber particles results in an optimal improvement, while for thermoplastics a co-continuous phase morphology is often desirable[26,30] (Figure 9b).

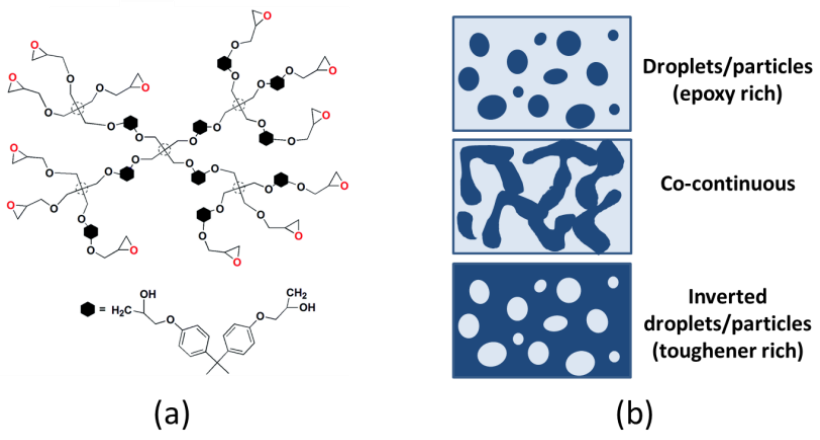

Figure 9 – Hyperbranched epoxy monomer (image adapted from Ref.[31]) (a) and typical phase separation morphologies obtained in rubber/thermoplastic toughening (b).

Several researchers have proven that adding reactive rubbers can increase the fracture toughness of the bulk resin tremendously. Willner and McGarry[32] already reported in 1968 that carboxyl terminated copolymers of butadiene and acrylonitrile (CTBN) enabled a ten-fold increase in fracture toughness. Since then, many other researchers have used similar liquid rubber systems and reported good results. However, this technique also results in disadvantages which cannot be disregarded. Typically, the addition of a rubber phase decreases the mechanical properties such as stiffness and strength and results in

a lower temperature resistance due to a lower glass transition temperature[33–36]. In addition, mixing in the liquid rubbers increases the viscosity of the resin[37]. As such, the technique is unsuitable for many composite production methods where a low viscosity resin is required in order to wet out the reinforcing fibres, such as infusion processing.

The use of a thermoplastic toughening phase allowed an increase in fracture toughness without a drastic reduction in stiffness and strength. A lot of research has been performed on many different thermoplastics, e.g. poly-ethersulphone[38–41], polycaprolactone[42] polyetherimide[43,44], poly-(phenylene oxide)[45], … . Although good improvements of fracture toughness are reported, the problems related to an increased resin viscosity remain[26]. Furthermore, the phase separation process is not easily controllable as it tends to depend on the used curing conditions which can vary depending on the application and differs when the phase separation takes place in a confined region such as in between the reinforcing fibres in a laminate.

Figure 10 illustrates the main toughening micromechanisms which act in rubber and thermoplastic toughened epoxy. Extrinsic mechanisms, i.e. mechanisms that work behind the crack tip, include particle bridging and particle debonding. Bridging particles create a closing traction between both crack surfaces resulting in a decrease of the stress intensity at the crack tip. Furthermore, the particles will keep bridging the crack if the adhesion with the matrix is good, until they are completely torn apart, absorbing a lot of energy through plastic deformation. If the adhesion is insufficient, the particles tend to debond, initiating crack path deflection resulting in a higher crack surface area and thus higher energy. Intrinsic toughening mechanisms, i.e. mechanisms that work in front of the crack tip, include particle yielding, shear banding, crack pinning, crazing and plastic void growth. A more thorough description and analysis of these toughening micromechanisms can be found in Refs. [30,35,45,46].

Matrix resin toughening has proven to be a viable method to increase the resin's fracture toughness. It is done by either developing new epoxy formulations or mixing in rubber/thermoplastic. The research in this field has already resulted in commercialised products, for example high toughness infusion resins or toughened prepreg materials. Yet, despite the fact that the resin's fracture

toughness is increased, the resulting composite laminates are still prone to delamination failure. This proves that there is more to composite toughening than just using a high toughness resin. Furthermore, the disadvantages related to these methods limit further application in industrial processes.

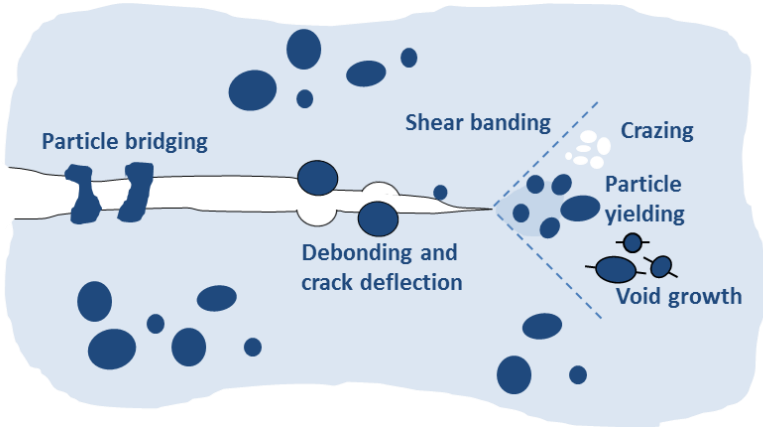

Figure 10 – Illustration of the different toughening mechanisms acting in a rubber/thermoplastic toughened epoxy including particle bridging, debonding, crack deflection, particle yielding, shear banding, crazing and void growth.

1.3.2 Addition of rigid nanoparticles

The development of nanotechnology provided new materials with interesting properties such as carbon nanotubes (CNTs), graphene, nanosilica and nanoclays, and spiked interest in many sectors. Although inherently different from the tough and flexible particles described in Section 1.3.1, these high stiffness high strength particles also had potential to increase the fracture toughness, stiffness and strength of FRP composites. Over the past decades, this field has been extensively studied using a wide array of nanoparticles[47–57]. There are two crucial aspects to achieve improvements in mechanical properties: a homogeneous dispersion of the particles in the matrix and good adhesion between the particles and the matrix [58–60]. The major toughening micromechanisms associated to rigid nanoparticles are crack pinning, crack deflection and particle bridging/pull-out[61,62]. Although the mechanical properties

of some nanoparticles are unprecedented, e.g. CNTs have a (theoretical) E-modulus and tensile strength of 1 TPa and 10 – 100 GPa[63], this is hardly reflected in nanoparticle modified FRP composites. Due to their poor natural adhesion with the matrix resin and the difficulty to obtain homogeneously dispersed particles, the reported improvements in toughness are only moderate in most cases. Even more, agglomeration of the nanoparticles can induce stress concentrations leading to an overall reduction in properties of the modified composites[64]. Therefore, surface modifications and specialised production techniques such as growing nanotubes directly on carbon fibres are often required which immediately hinders the applicability in an industrial setting. Handling of these small nanoparticles – which are easily airborne – requires special safety precautions in order to eliminate health risks. Besides the disadvantages related to their nanoscale, adding nanoparticles can also increase the resin's viscosity similar to the rubber/thermoplastic toughened epoxies[65].

1.3.3 Through-thickness reinforcements

Another method to increase the delamination resistance is to add through-thickness reinforcements to a laminate such as the use of 3D woven fabrics, stitching and Z-pinning (Figure 11a). The added reinforcement will provide a physical link between the plies in the out-of-plane direction. With 3D woven fabrics, laminates can be built up from thick woven preforms which have reinforcing fibres in the in-plane as well as out-of-plane directions[66–69]. Similarly, by stitching the dry reinforcing plies of a laminate with a yarn before resin infusion, a through-thickness reinforcement is created[70–73]. In the Z-pinning method, structural pins made for example out of CFRP or titanium are inserted through the thickness of the composite prior to production[74–77]. Although these methods achieve significant increases in delamination resistance, they cause a decrease of the in-plane properties of the composite up to 30%[78]. The through-thickness reinforcements typically cause fibre misalignment, formation of resin pockets and fibre damage due to hammering in pins or stitching (Figure 11b). The decrease in in-plane properties often outweighs the increase in delamination resistance and the use of these methods has not found much practical application in high-end composites today.

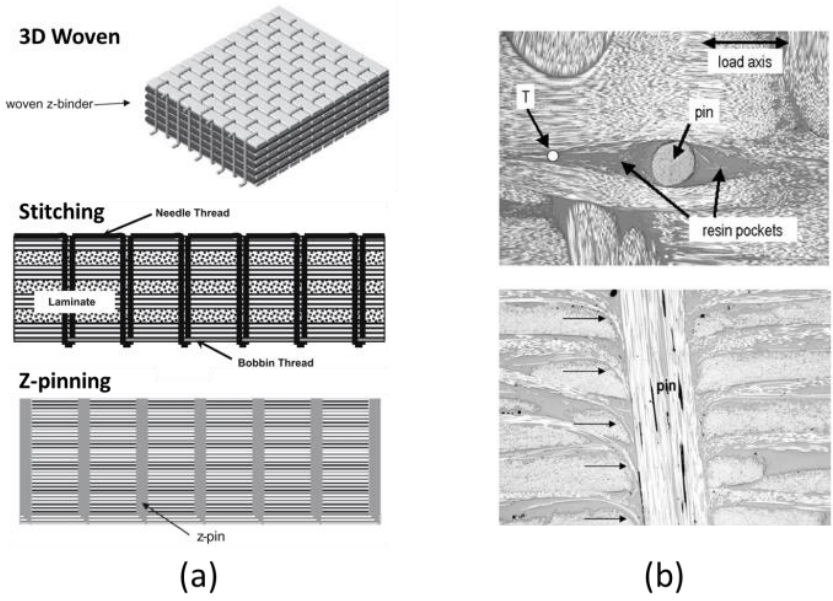

Figure 11 – Concept of 3D woven, stitching and Z-pin toughening (a). Distorted fibre orientation and resin rich zones typical for through-thickness reinforcements (b). Images are adapted from Ref.[78]

1.4 ELECTROSPUN NANOFIBRES AS A NOVEL TOUGHENING TECHNIQUE

From the discussion in the previous section, it is clear that a new toughening method is needed which can circumvent the disadvantages related to existing techniques. Ideally, this method has following aspects:

- → High improvements in delamination resistance;
- → No decrease in in-plane properties such as stiffness and strength;
- → Simple integration in current composite production routes;
- → Easy to handle without health risks;
- → Economically viable on large scale;
- → Easily dispersed in damage prone regions (interlayers).

This is where electrospun nanofibres come into the picture. Electrospun nanofibrous veils can be thought of as a novel class of materials consisting of very thin polymeric fibres with typical diameters below 500 nm. As a comparison, classical reinforcing fibres such as carbon or glass fibres have diameters between 5 and 25 µm. The small diameter gives nanofibrous veils interesting characteristics such as a large surface area, a high porosity and improved mechanical properties compared to the bulk polymer.

Electrospinning is currently the most efficient technique to produce nanofibrous veils from a polymer solution or melt[79]. Nozzle electrospinning (Figure 12) is the most conventional technique in which a polymer solution is pumped through a nozzle at a constant flow rate to form a drop at the nozzle tip. A high voltage applied at the nozzle creates an electric field between the nozzle tip and the collector. When the drop of polymer solution leaves the nozzle and enters the electric field, the particles become similarly charged. A Taylor cone is formed and when the electrostatic repulsion outweighs the surface tension of the droplet, a continuous jet of polymer solution is expelled from the cone towards the collector. Before the jet reaches the collector while the solvent evaporates, instabilities occur which stretch the jet into a fibre, resulting in a non-woven membrane of nanofibres on the collector. The technique offers the possibility of electrospinning many types of polymers ranging from rubbers[80,81], to thermoplastics[82–84] and even silica[85,86]. Furthermore, by changing electrospinning

parameters such as the flow rate or polymer concentration a wide variety of morphologies can be obtained in a controllable manner[87–89].

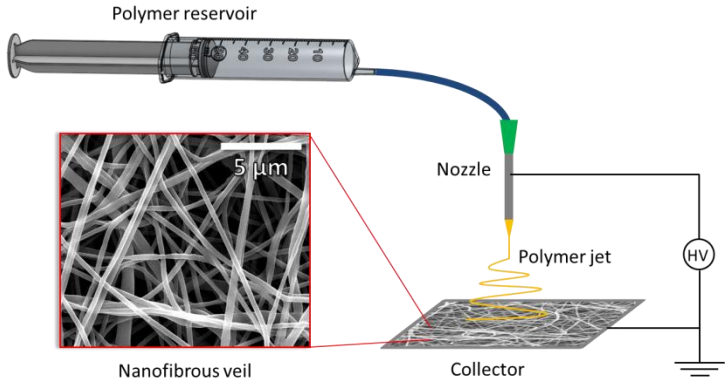

Figure 12 – Schematic illustration of a typical nozzle electrospinning setup. Nanofibres are deposited in a random manner resulting in a self-supporting nanofibrous veil.

Electrospun nanofibrous veils have the potential to serve as a toughening material while fulfilling the conditions mentioned in the beginning of this section. They are formed as a self-supporting non-woven membrane which can be easily handled similar to regular fabrics. They can also be deposited directly on reinforcing fibres by guiding dry fabric through an electrospinning set-up. Hence, the veils can easily be placed in between the primary reinforcing plies either as self-supporting membranes or as nanofibre "coated" fabrics prior to composite production and there is no change in the composite manufacturing process required (Figure 13). As they are not mixed in the resin, the viscosity is unaffected. The nanoscale diameter of the nanofibres offers relatively thin interlayers, while their macroscopic length (continuous fibres) poses no health hazards in comparison with other nanomaterials. The electrospinning process itself is relatively simple in design and proven to be scalable making it a cost-effective nanofibre production method[90,91]. They can be made from many polymers ranging from rubbers to thermoplastics and thus can readily improve the delamination resistance in a similar way as rubber/thermoplastic toughened epoxies.

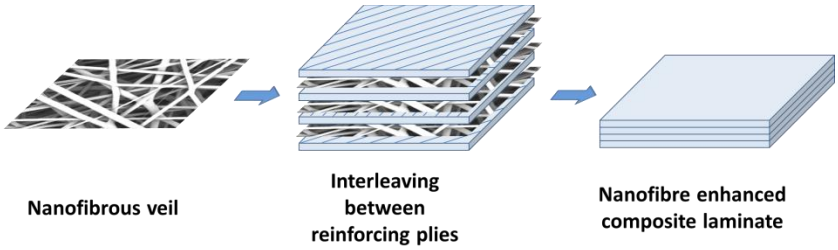

Figure 13 – Concept of interleaving electrospun nanofibrous veils for toughened composite laminates.

Although there are many obvious benefits, the research on composites enhanced with (electrospun) thermoplastic nanofibres is still very limited. Reneker, Kim and Dzenis[92–94] produced the pioneering work of interlaminar toughened composites using electrospun polybenzimidazole fibres in 1999 and showed that they could increase the interlaminar fracture toughness of carbon fibre/epoxy laminates up to 15 – 130%. Since then, published work from other research groups has confirmed the toughening potential of electrospun nanofibres for composite laminates. At the start of this PhD in 2013, only a handful of research groups investigated this type of materials and few literature was available[95–106]. Since then, the number of articles published each year on this topic has only increased. The emergence of this research topic in published literature was thus parallel with our own findings[89,107–113]. The following paragraphs give a concise overview of the published literature regarding electrospun nanofibre toughened composites including articles that were published during this PhD research.

Several researchers focused on using electrospun nanofibres which dissolve in the matrix resin such as polycaprolactone (PCL), polyetherketone-cardo (PEK-C), polysulfone (PSF) or phenoxy-based nanofibres[96,98,102,103,106]. They reported improvements in interlaminar toughness due to a phase separation of the dissolved nanofibres which resulted in a tough particulate phase at the interlayer. Although this is an in interesting technique as no prior resin/thermoplastic mixture is necessary, the phase separation process is still difficult to control. Furthermore, as the nanofibrous morphology is lost,

potential toughening mechanisms related to a fibre morphology instead of a particulate phase will not be present.

Another approach to produce nanofibre enhanced composite laminates is to use thermoplastic nanofibres which retain their nanofibrous structure in the final laminate. This is advantageous as the nanofibres' physical and mechanical properties are unaffected while there is no increase in viscosity of the matrix resin due to dissolution of the nanofibres. Furthermore, the interlayer will automatically consist out of a co-continuous epoxy and thermoplastic phase microstructure. Several polymer types which retain their nanofibrous structure in the final laminate have already been investigated, e.g. polyacrylonitrile (PAN)[106], PCL[107], P(St-coGMA)[103,114], polyimide (PI)[115], polyamide 6 (PA6)[116–118] and polyamide 6.6 (PA6.6)[97,99,104,119–121]. Regular non-woven veils, with a larger diameter of the fibres, have also been investigated to study the interlaminar toughening effect[122–125].

The Mode I and Mode II interlaminar fracture toughness, G_I and G_{II} respectively, are most often studied since they can be used to assess the damage resistance of composite laminates [122,123,126]. A variety of effects on the G_I and G_{II} are reported in literature when laminates are interleaved with electrospun nanofibrous veils. Zhang et al.[106] reported no improvements in G_I upon interleaving of PAN nanofibres as compared to using dissolvable PCL or PEK-C nanofibres. Bilge et al.[103] used P(St-coGMA) nanofibres which improved the delamination toughness. Saghafi et al.[119] and Beckermann et al.[120] reported an increase in G_I and G_{II} of unidirectional laminates interleaved with PA6.6 nanofibres. However, these improvements in G_I only occur during precracking or crack initiation, while G_I was not affected or even decreased at further crack growth. The effect of PA6.6 nanofibres on woven laminates has been studied by Hamer et al.[99] and Palazzetti et al.[104,121]. Although Hamer et al. report an increase in G_I, only minor improvements and even decreases on both G_I and G_{II} are reported by Palazetti et al.[99,104,121]. De Schoenmaker et al.[116] state that G_I increases slightly upon addition of PA6 nanofibres in UD laminates.

Although some excellent work has already been carried out of which the results illustrate the potential of interleaving laminates with nanofibrous veils, improvements only occur under very specific cases such as crack initiation or

some of the findings even seem to contradict each other. This indicates that some fundamental aspects of nanofibre toughening have not been analysed in these previous works. One important reason for this is that most of the reported literature deals with interleaving one specific type of nanofibre in one specific laminate structure. This results in a large scatter in data as the underlying toughening principles are unclear.

An in-depth understanding of the fracture and toughening mechanisms is clearly needed in order to link the presence of nanofibres to the observed increase or decrease in interlaminar fracture toughness. These micromechanical fracture mechanisms and the generic parameters to obtain toughened composites have not been reported before. Nevertheless, such a generic understanding is crucial in order to select the right type of nanofiber and design novel toughened composites.

1.5 MULTISCALE NATURE OF INTERLEAVED COMPOSITE LAMINATES

An interleaved composite can be thought to have three different levels at which the nanofibres will affect its properties, see Figure 14. These levels coincide with the hierarchical nature of the laminate itself: (i) the nanotoughened epoxy resin, (ii) the nanotoughened interlayer and (iii) the nanotoughened laminate. By considering the effect of nanofibres on each level simultaneously, much better insights can be attained into the micromechanisms of toughening and the crucial parameters resulting in highly toughened composite materials.

The major research results obtained in this PhD work are arranged in Chapter 3 according to the level to which they belong. At the nanotoughened epoxy level, the main focus is the effect of electrospun nanofibres on the fracture toughness of the epoxy resin. The goal of this level is to get a fundamental understanding of the toughening mechanisms acting in nanotoughened epoxy similarly to what has previously been done for rubber/thermoplastic epoxy toughening methods. This will allow to have better insights into the effect of the nanofibres on the delamination/damage resistance of nanotoughened composites. Indeed, the

interlaminar fracture toughness of composites with a nanotoughened interlayer will be dependent on the fracture toughness of the nanotoughened epoxy.

At the level of a nanotoughened interlayer, other factors such as the delamination path will come into play and it is therefore a very important level to analyse. Typically, this is done by determining the interlaminar fracture toughness of interleaved laminates using typical delamination tests such as the double cantilever beam or end notched flexure method. The delamination path and fracture surfaces are subsequently investigated using microscopy to determine the toughening micromechanisms and analysing the interaction between the delamination path, the reinforcing fibres and the nanotoughened interlayer.

Although Level 1 and Level 2 both provide essential insights into the toughening micromechanisms, both are investigated using test methods in which crack/delamination growth is carefully initiated and controlled. Therefore, fully interleaved laminates are considered at Level 3. These laminates are still tested using coupon specimens, but are more closely related to the lay-up and loading conditions which can be expected in real-life applications. By subjecting these specimens for example to impact, a natural occurrence of delamination and cracks is allowed to occur. In contrast to the other levels, the initiation and growth of delaminations and cracks is not really controlled or known a priori. Therefore, the results of this level will provide the link between the previous levels and the mechanical response that can be expected in real-life situations.

Performing the analysis of these novel materials at different levels simultaneously is one of the major milestones of this PhD work. Such analysis had not been performed in published literature and provided much better insights into the behaviour of nanotoughened composites. It led to a significant advancement of the understanding of these materials in a more structured and general sense. Such a generic understanding is – in our opinion – crucial to be able to select the right type of nanofibre structure for designing novel toughened composites.

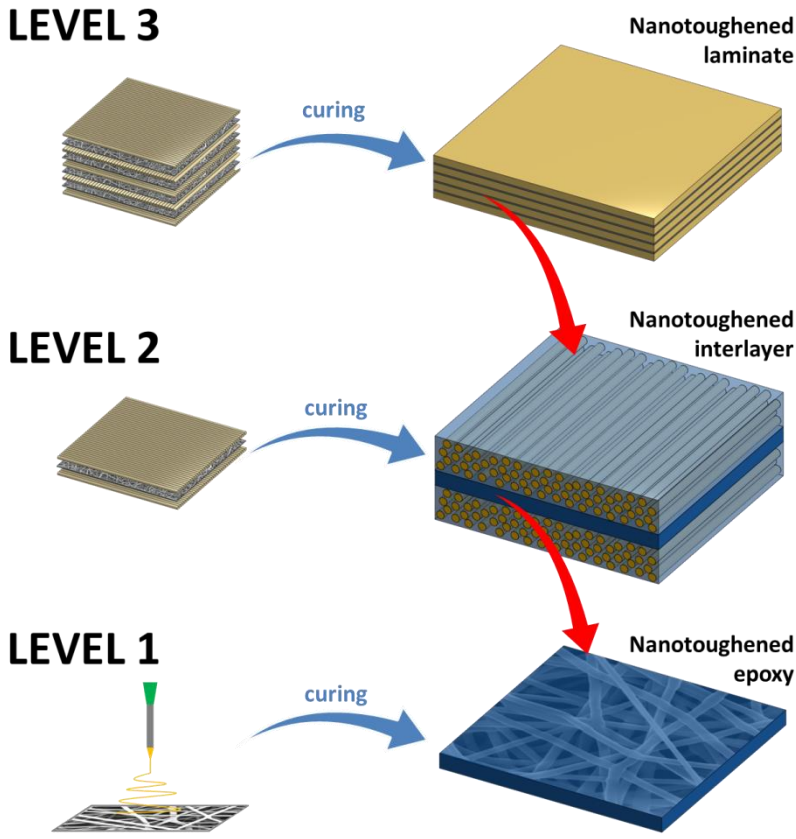

Figure 14 – Multiscale nature of nanofibre interleaved composite laminates.

1.6 OBJECTIVES AND OUTLINE

The previous sections have shown that delamination failure is still a major problem for many composite laminate applications. Although previous published research has shown that using electrospun nanofibres could be an excellent way of increasing the delamination resistance of composites, there is still a lot of scatter in experimental results. As such, the primary goal of this PhD is to develop highly toughened nanofibre enhanced composite laminates while at the same time, getting a thorough understanding of the micromechanisms and generic parameters of this novel toughening method. This will be done by a broad mechanical investigation concerned with not only fundamental loading cases, but also includes real-life loading cases such as impact. Furthermore, the toughening micromechanisms are analysed on three levels simultaneously. Attention is paid to the production route of the composites by focussing on infusion as well as prepreg-based techniques. The effect of parameters such as the veil areal density, type of nanofibre, loading mode, reinforcing fabric architecture, precracking method, adhesion strength, veil morphology and tensile properties of the electrospun fibres are investigated.

Chapter 2 explains the experimental methodology followed throughout the work. This includes the electrospinning of several nanofibre types on a relatively large scale, as necessary for the development of nanofibre enhanced composites, as well as a brief description of the main test methods that were used.

Chapter 3 presents the major research results that were obtained during this PhD work. These are arranged according to the three different levels which are present in nanofibre interleaved composites: nanotoughened epoxy, nanotoughened interlayer and fully interleaved laminates. Most of the reported results are based on own published and draft papers and more details can be found in **Paper I - VIII**, which are appended in the second part of this book. Chapter 3 begins with an analysis of the toughening mechanisms acting in nanofibre toughened epoxy (Level 1; Section 3.1). The effect of nanofibre type, strain rate and nanofibre orientation on the obtained fracture toughness are determined. This is followed by an investigation into the toughening mechanisms acting in a nanofibre interleaved interlayer of a composite laminate

in Section 3.2 and Section 3.3 (Level 2). The link between nanofibre toughened epoxy and the interlayer is made, as well as an analysis of the effect of the nanofibre veil areal density, loading mode, interleaving method, nanofibre orientation, adhesion strength, veil morphology and electrospun fibre tensile properties on the obtained delamination resistance. The chapter ends with an experimental investigation of fully interleaved laminates in which all the interlayers are toughened with electrospun nanofibrous veils (Level 3). General tensile properties as well as the low velocity impact and post impact residual compressive properties are analysed in Section 3.4.

Chapter 4 concludes the major research results obtained in this work and gives some perspective on the future of these materials. This chapter ends the first part of this PhD book which provides a general description of the work performed during the PhD.

The second part of this PhD book consists of an appendix with all the articles that were published – or are in consideration for publishing – during the PhD. These full articles provide more detail than given in the main text of this PhD book. However, the PhD is written in such a way that reading the full articles is not a necessity for a reader to comprehend the performed work.

2

METHODOLOGY

A broad experimental investigation was performed to elucidate the toughening mechanisms and principles of nanofibre interleaved fibre reinforced composite laminates. This chapter gives a brief overview of the materials and test methods used in this investigation. First, the production of nanofibres by electrospinning and their integration into composite laminates is described. This is followed by an overview of the most important mechanical test methods that were employed to determine the effect of the nanofibres on the properties of the composites.

2.1 ELECTROSPINNING OF NANOFIBRES

The general setup of an electrospinning apparatus was treated in Chapter 1. The mononozzle setup consists out of an infusion pump (KD Scientific Syringe Pump Series 100) which feeds polymer solution using PP/PE syringes through 18 gauge stainless steel disposable hollow needles with a blunted tip. The voltage is applied on the needle using a high voltage source (Glassman High Voltage Series WK125P5). A similar setup is used to produce the nanofibrous veils mentioned throughout this PhD. The main difference is that the veils needed for composite production are relatively large and thick in comparison with those that can be produced on a mononozzle electrospinning apparatus. Therefore, a different system is used to scale up the production of the nanofibres. An array of 2 – 8 nozzles is used to allow a larger throughput of nanofibres. The collector is a moving conveyor belt out of aluminium foil (grounded) to continuously produce sheets of fixed thickness and size. The array of needles travels back and forth in a linear motion, while the collector moves perpendicular to the needle movement at constant speed. The speed of the collector will determine the amount of nanofibres deposited per square meter. The setup is illustrated in Figure 15a. In essence, the same electrospinning conditions can be used as on a mononozzle setup. However, the multinozzle setup typically requires some fine-tuning to produce nanofibres in a stable manner in larger quantities. The electrospinning conditions given beneath are representative of those used, but small modifications to voltage or tip-to-collector distance (TCD) were sometimes made during manufacturing to ensure stable electrospinning conditions. These changes did not influence the obtained nanofibre morphology which was validated using SEM images taken from the nanofibrous veils at different positions. Furthermore, the quality of nanofibre formation was regularly checked by shortly placing a glass slide on the collector and observing the nanofibres with an optical microscope. Although the magnification is not enough to determine nanofibre diameters in a reliable manner, it allows for a quick and simple way of in-line quality control as bead formation and nanofibre orientation are easily observed. This ensures that the whole nanofibrous veil is of good quality and that there is no gradient in properties over time.

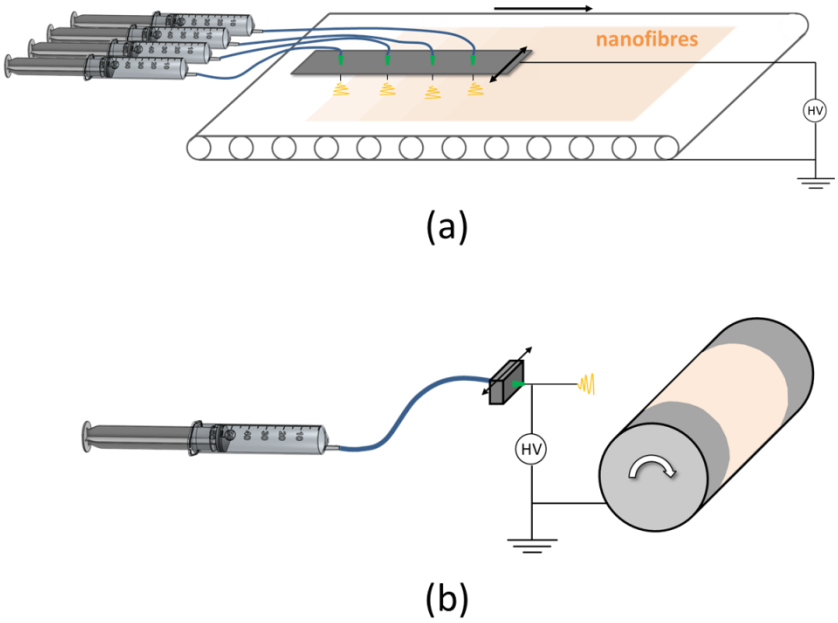

Figure 15 – Schematic illustration of the multinozzle (a) and rotating drum collector electrospinning setup (b) which are used to scale up the production of nanofibres.

For the series of polyamide 6.9 (PA6.9) nanofibrous veils mentioned in Section 3.3.5, a rotating drum collector was used. The nanofibres are deposited on the grounded rotating drum and the veil is removed as soon as it has the preferred areal density. The setup is shown in Figure 15b. This type of collector allows to change the orientation of the nanofibres in the veil by changing the frequency at which the drum rotates. At low frequencies, the nanofibres are still deposited in a random non-woven manner on the collector, but at higher frequencies the nanofibres are aligned on the drum due to the high rotational velocity at the drum surface[127,128]. The rotating drum is made of a hollow aluminium tube with an outside diameter of 120 mm and a useable length of 400 – 500 mm. Random nanofibres were produced at a frequency of 2 – 3 Hz resulting in a rotational speed of approximately 150 rpm. Oriented nanofibrous veils were produced using a frequency of 65 Hz or about 4000 rpm which results in a tangential speed at the collector's surface of approximately 41 m/s. The

high rotational velocity of the rotating drum collector induces a preferred orientation in the nanofibrous veil resulting in aligned nanofibres, see Figure 16.

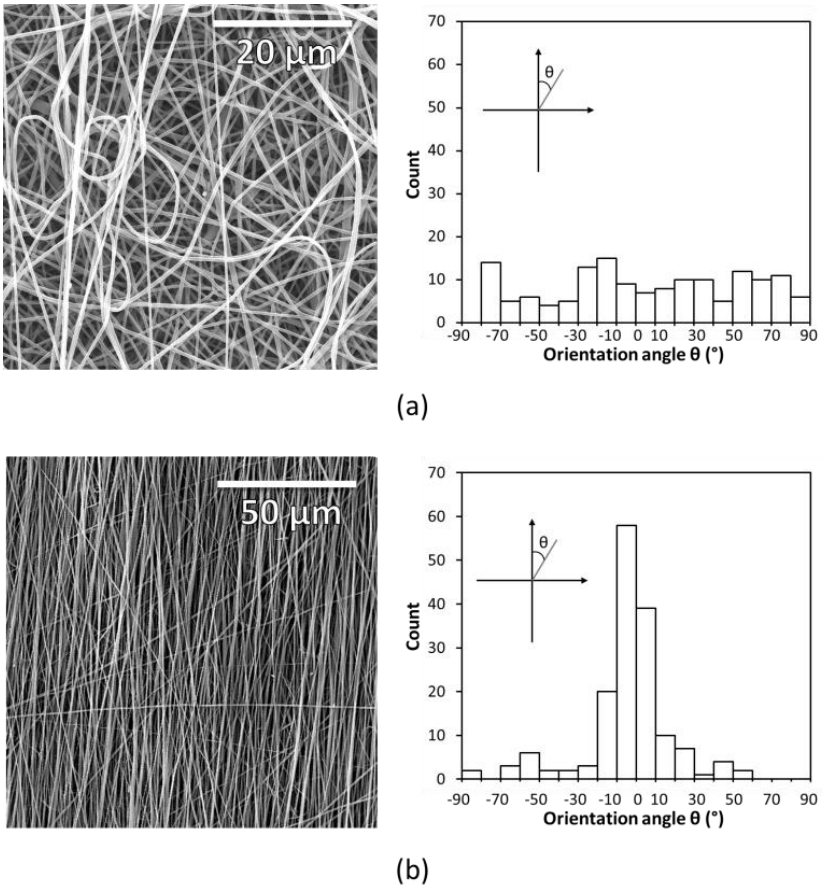

Figure 16 - Illustration of orientation induced by the high rotational velocity of a rotating drum collector. At low rpm, veils with a random deposition of nanofibres are produced (a); while at high rpm, veils with a preferred orientation of the nanofibres are obtained (b).

Several different electrospinning systems, i.e. the set of polymer solution and electrospinning parameters, have been used to produce nanofibres. All of these systems were selected based on previous research[81–84].

Table 1 gives an overview of the different electrospinning systems. A representative SEM image for each system is given in Figure 17. All stated nanofibre diameters were measured on dry specimens (before any resin infusion) as the average of at least 50 fibres using the image analysis software package ImageJ. PA6.6 (M_W 60 000 g/mol), PA6 (M_W 51 000 g/mol) and PCL (M_N 80 000) pellets were purchased from Sigma Aldrich; PA6.9 (M_W 58 000 g/mol) and PCL (M_W 100 000 g/mol) pellets were purchased from Scientific Polymer Products. Styrene-butadiene-styrene (SBS) copolymer pellets (Kraton D1101) were kindly provided by Kraton Polymers LLC. Formic acid (98%-100%), acetic acid (98%) and butyl acetate (99.5%) were purchased from Sigma Aldrich for electrospinning solvents and used as received. All electrospinning systems were spun using a hollow needle as a nozzle. The internal diameter of the needle was 1.024 mm for system #1, system #2 and system #8 and 0.84 mm for the other systems.

The areal density of the nanofibrous veils is determined by carefully cutting squares of known size, typically 5 x 5 cm², 10 x 10 cm² or 20 x 20 cm², out of the veil and determining their mass. This measurement is performed at several instances of the nanofibrous veil to make sure that the areal density is not changing in time which could indicate a faulty nozzle or unstable electrospinning. For standalone nanofibrous veils, the specimens were removed from the collector after the desired specimen length is reached. In other cases, the nanofibres were directly deposited onto the reinforcing fibre fabrics/mats during electrospinning. The areal weight of these coated structures was determined by measuring the areal density of the veil by the aforementioned method directly in front of and just behind the reinforcing fabric specimen. The addition of reinforcing fibres onto the collector did not influence the electrospinning process significantly.

Table 1 – Overview of the electrospinning systems used throughout this PhD work.

System		Flow rate per nozzle (ml/h)	TCD (cm)	Voltage (kV)	Areal density (g/m²)	Nanofibre diameter (nm)
#1	**PA6.9** **20 wt%, 1:1 FA/AA**	1.5	6	20 – 25	11	460 ± 55
#2	**PA6.9 (oriented)** **20 wt%, 1:1 FA/AA**	1.5	6	20 – 25	11	465 ± 110
#3	**PA6.9** **16 wt%, 1:1 FA/AA**	1	6	35	3, 14, 18	245 ± 30
		1.5			6, 12	200 ± 25
#4	**PA6.6** **14 wt%, 7:3 FA/AA**	1	9	35	3, 18	160 ± 20
#5	**PA6** **16 wt%, 1:1 FA/AA**	1	8	35	5, 10, 14, 15, 20, 40	195 ± 35
		1.5			6, 12	150 ± 20
#6	**PCL (M_N 80 000)** **14 wt%, 1:1 FA/AA**	2	30	35	5, 10, 14	650 ± 150
		1.5			15, 20, 40	345 ± 150
#7	**PCL (M_W 100 000)** **23 wt%, 3:7 FA/AA**	2	23	25 – 30	5, 6, 12	370 ± 200
#8	**SBS** **13 wt%, BU** **(MDI-TAD, LiBr)**	1	21	20 – 25	12, 22	2100 ± 400

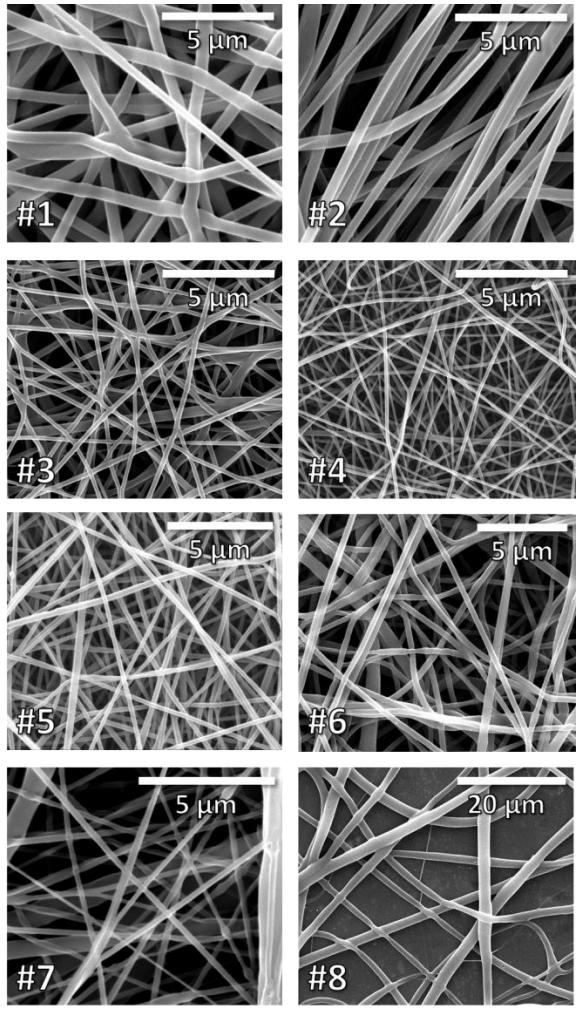

Figure 17 – Representative SEM images of the nanofibres produced using the different electrospinning systems.

2.2 PRODUCTION OF INTERLEAVED COMPOSITE LAMINATES

Throughout the PhD, two different kinds of composite laminates were produced. Glass fibre composite laminates are produced by vacuum assisted resin transfer moulding (VARTM) with unidirectional E-glass plies (either UDO ES500 manufactured by SGL group, or, Roviglas R17/475 manufactured by Syncoglas) and a high toughness epoxy/amine thermoset resin system typically used for wind turbine blades (EPIKOTE MGS RIMR135 and EPIKURE MGS RIMH137 supplied by Momentive). The in-house developed VARTM setup consists of a two-piece flat mould with internal dimensions of 3 x 300 x 300 mm³. The manufacturer's recommended curing cycle is used to cure the laminates: curing for 24 hours at 20°C and 65% RH (ambient conditions) followed by a post-cure at 80°C for 15 hours. The nominal thickness of the final laminates is 3 mm. The overall glass fibre volume fraction (52 vol%) did not change when nanofibrous veils were interleaved as a two-piece mould with a fixed thickness was used to produce the laminates. The nanofibres had no measurable influence on the infusion process and the final quality of the laminates. The infusion resin impregnated the nanofibrous veils in the interlayers. Visual inspection and microscopic images of the interlayers showed no dry spots in the final laminates (transparent epoxy resin) indicating that the porosity did not increase. Nanofibrous veils were either interleaved as standalone layers or by using reinforcing plies with nanofibres deposited on them, see Figure 18. For delamination tests like the double cantilever beam experiment, nanofibres were only placed in the midplane of the laminate, while for other tests such as the impact experiments, nanofibres were placed at each interface of two dissimilar plies, e.g. between a 0°- and 90°-oriented ply.

Another series of virgin and nanofibre interleaved composite laminates were produced by stacking layers of carbon fibre prepreg plies. The plies were cut to size before stacking. Unidirectional laminates were produced with M10R/T300 UD prepregs, while woven laminates were produced with MTM49-3/T800 2 x 2 twill weave prepregs. For the nanofibre interleaved laminates, the nanofibrous veils were first placed on the prepreg surface after which the aluminium foil was carefully peeled off. Since the nanofibres do not adhere to the aluminium foil, the nanofibrous veil can be easily transferred onto the tacky prepreg surface. The advantage of this method compared to electrospinning onto the prepreg

surface directly, is that there is no interaction between the electrospinning solvents and the prepreg material which could affect its properties. The laminates were cured in an autoclave according to the resin's prescribed curing cycle. There was no measurable difference in thickness between virgin and nanofibre interleaved laminates. Transversal cross-section images showed good quality of the impregnation with the relatively viscous prepreg epoxy, see Figure 19.

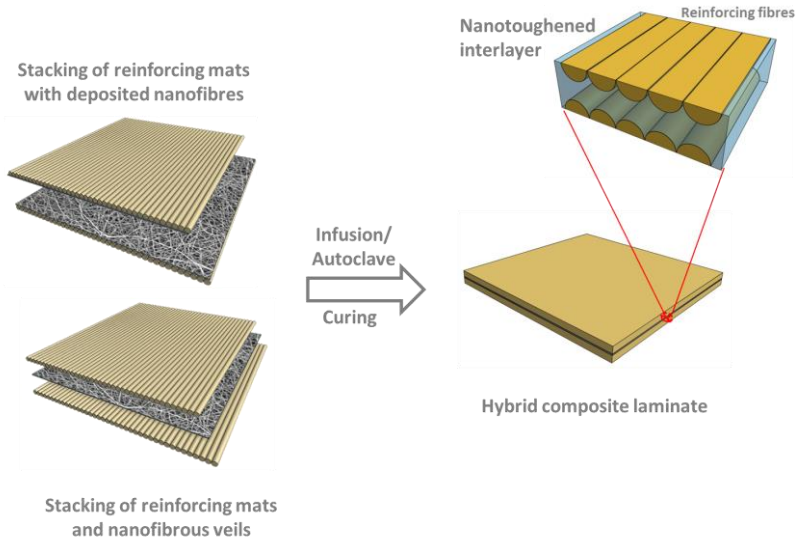

Figure 18 – Integration of nanofibres in composite laminates resulting in a hybrid composite laminate with nanotoughened interlayers.

The integration of the electrospun nanofibrous veils results in a nano-engineered interlayer. The non-woven mat morphology is maintained within the interlayer, i.e. the nanofibres do not migrate between the reinforcing fibres due to the resin flow. Therefore, the interlayer thickness increases with increasing areal density of the nanofibrous veils, see Figure 20. There is a linear relationship between interlayer thickness and areal density indicating that the veils – which are compressible due to their porosity – are "fully" compressed due to the pressure exerted during the composite production process. Indeed, the relationship seems relatively independent of the production process:

VARTM, autoclave or even filament wound composites nanofibre interleaved composites all have similar interlayer thicknesses.

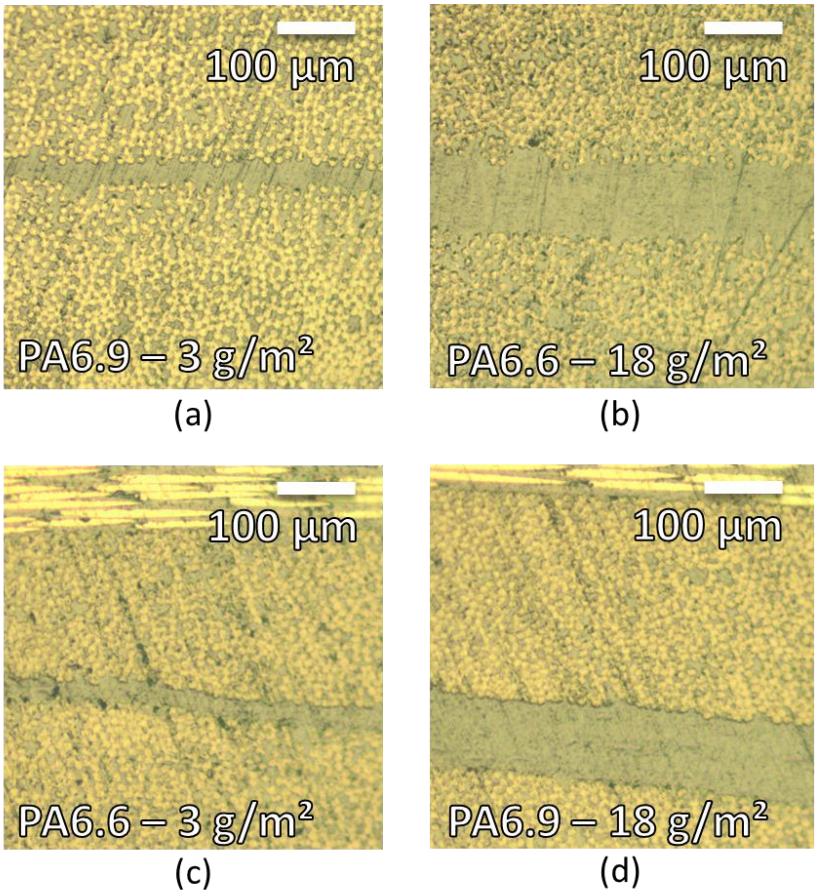

Figure 19 – Polished cross-section images of PA6.6 and PA6.9 nanofibre interleaved prepreg-based composites showing good impregnation of the nanofibrous veils during autoclaving.

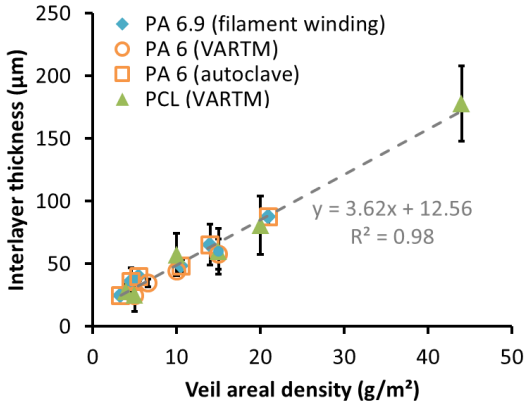

Figure 20 – Interlayer thickness in function of the nanofibrous veil's areal density show that the relationship is relatively independent of nanofibre type as well as processing method.

It is worth remarking that the integration of the nanofibrous veils does not really alter the production process of the composites. The veils can be handled relatively easily and placed at the required position. The dry veils are a bit more damage sensitive than mats/fabrics of reinforcing fibres. Nevertheless, as they come as a sheet material, they can be integrated using the same methods as are currently used in industry, e.g. manual lay-up or automated placement. Furthermore, there is no risk of small particles emanating from the veils which could be hazardous. As the nanofibres are not mixed in the resin itself, they pose no problem for the viscosity. However, the wetting of the nanofibrous veils might be affected by the resin's viscosity and the compatibility between the nanofibre polymer and the epoxy resin. Such problems were not encountered during this PhD work, but might present themselves when much larger components have to be produced or other types of nanofibres are used. Simple wetting experiments that consist out of placing sheets of nanofibres on a layer of liquid epoxy, showed that the veils impregnated without the necessity of an external pressure. However, the resin flow was mainly limited to the through-thickness direction and the resin did spread out less in the in-plane direction. Therefore, it is expected that even on large-scale production, the wetting of the veils will not pose a problem if there is sufficient through-thickness resin flow. This is usually the case as the same physical mechanism of wetting also has to

happen for the reinforcing fibre mats. Typically, distribution meshes are used in many processes to allow this through-thickness flow[129].

2.3 MAIN TEST METHODS

2.3.1 Fracture toughness of nanotoughened epoxy resin

Nanofiber/epoxy nanocomposites were made by an in-house developed VARTM setup. This setup consisted out of a two-piece flat steel mould with inner dimensions of 300 x 150 x 7 mm^3. In order to make the nanocomposites, a stacking of thick nanofibrous veils with dimensions of 300 x 150 mm^2 was used. The amount of nanofibrous veils was selected to have approximately 17 vol% of nanofibers in the final nanocomposite. This is representative for the amount of nanofibers present in the interlayer between reinforcing plies of the nanofiber interleaved laminates[107]. Several layers of breather fabric and resin flow meshes were added at the bottom and the top of the mould to facilitate through-thickness flow. Prior to infusion, the epoxy resin (EPIKOTE MGS RIMR135) and hardener (EPIKURE MGS RIMH137) were mixed in a 100:30 mass ratio using a mechanical stirrer. The mixture was placed under vacuum for 15 minutes in order to remove any trapped air introduced during mixing. After infusion of the nanofibrous veils, the mould was cured at 20°C and 65% RH for 24 hours, followed by a second curing step at 80°C for 15 hours according to the manufacturer's recommended cure cycle. Virgin epoxy plates (without nanofibers) were made by casting the epoxy resin in an empty mould. It is worth remarking, that this is the first work in which such thick nanocomposites are made using electrospun fibres. It allowed to accurately determine the fracture toughness using standardised testing methods.

The strain energy release rate, or fracture toughness, of the unmodified and modified bulk epoxy was determined using Single Edge Notched Bending (SENB) experiments according to ASTM D5045[130]. The experiment consists of a notched rectangular specimen subjected to three point bending, see Figure 21. At a certain load, the specimens will crack and the energy required per unit fracture surface is determined from the load-displacement data. Specimens with a nominal thickness of 5 mm were sectioned from the epoxy plates with a water-

cooled precision diamond cutting machine. A sharp natural precrack was produced by milling a starter notch in the specimens, followed by tapping a fresh razor blade in the milled notch with a dynamic precracking drop tower apparatus[28]. The specimens were placed in the three point bending fixture and a travelling microscope was used to align the precrack with the loading roller. The experiments were performed on an electromechanical Instron 3369 with a load cell of 500 N; load and crosshead displacement were recorded. The loading was displacement controlled at a rate of 10 mm/min.

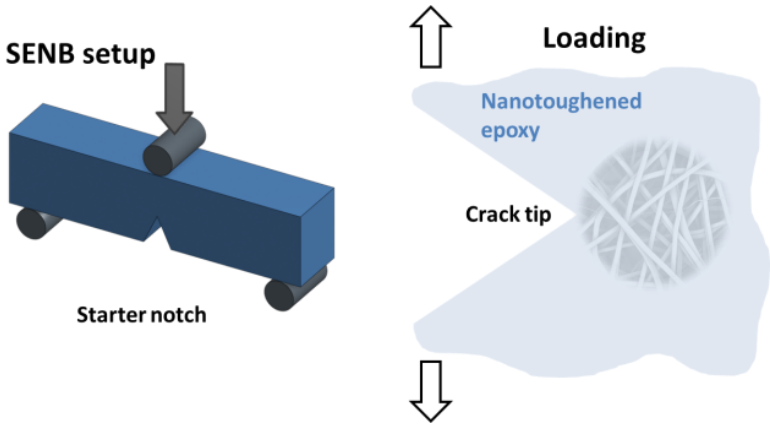

Figure 21 – Illustration of the SENB fracture toughness experiments showing the specimen in a three point bending fixture and the loading applied at the crack tip.

A second method to investigate the nanofibre toughening effect was performed by considering thin epoxy specimens (thickness around 100 µm). These specimens were made by compression moulding of nanofibrous veils and epoxy resin. The major advantage of this method was that it reduced the amount of nanofibres per specimen considerably, while advanced imaging techniques (in-situ microscopy and digital image correlation measurements) could be used, see Figure 22. The disadvantage is that a correct plane strain SERR cannot be determined due to the plane stress state induced by the small thickness of the specimens. The specimens consisted out of rectangular film specimens with a notch at one side tested in uniaxial tension. This is often referred to as the Single Edge Notched Tension (SENT) method and is rather similar to the SENB method although it is not standardised. Notches were produced by clamping the

specimens in a specially designed holder with a machined notch of fixed length and tapping a fresh razor blade in this notch. The specimens were tested on a TA Instruments Q800 Dynamic Mechanical Analyser using a tensile fixture in strain control mode. A long working distance USB microscope with polarised light was placed to visualise crack growth in the specimens. A speckle pattern was applied to several specimens using an airbrush with black ink to measure the strain fields around the crack tip using Digital Image Correlation (DIC) measurements.

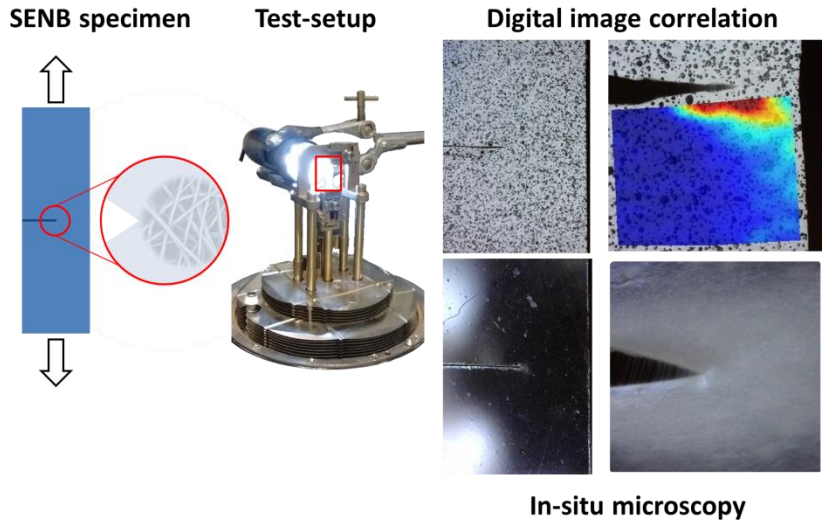

Figure 22 – SENB specimen design and test setup showing the possibility of in-situ microscopy and digital image correlation measurements.

2.3.2 Delamination resistance of interleaved laminates

The interlaminar fracture toughness expresses the amount of energy required to produce a delamination of unit area in a composite laminate. Although it is also referred to as the delamination resistance or delamination strain energy release rate, the term interlaminar fracture toughness is more often used and will also be used throughout this PhD work. The interlaminar fracture toughness will be evaluated for the two most common fracture loading conditions which occur in laminated composites: Mode I delamination (opening/tension mode) and Mode II delamination (shearing mode). These tests allow for a thorough study of

the crack and toughening behaviour under two controlled loading conditions. Understanding the effect of nanofibres in these fundamental loadings, will allow an understanding of the toughening effect in more realistic loading cases such as encountered during impact.

Virgin and nanofibre interleaved unidirectional composite laminates were made according to the previously reported procedure. An ETFE-based release film of 15 µm thickness is placed in the midplane of the stacking in order to serve as an initial delamination for the Double Cantilever Beam (DCB) and End Notched Flexure (ENF) experiments. For the nanofibre interleaved laminates, the reinforcing fibre plies facing the midplane had nanofibres electrospun on the sides facing the midplane or the nanofibres were interleaved as a self-supporting veil at the midplane. The composites were processed by infusion or autoclave and then demoulded. Specimens for DCB and ENF experiments were sectioned from the laminates with a water-cooled precision diamond cutting machine. At least three specimens were tested for each configuration. A schematic of the specimens and the loading conditions is given in Figure 23.

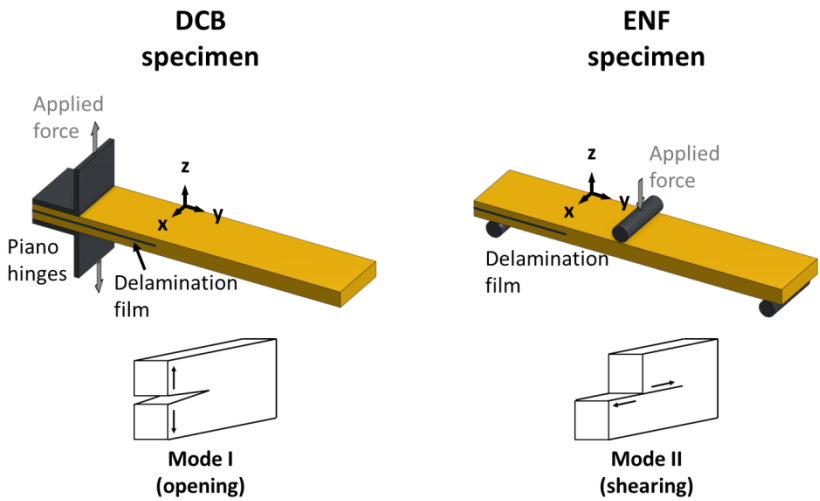

Figure 23 – Illustration of the DCB and ENF specimen for determining the Mode I and Mode II interlaminar fracture toughness of composite laminates.

The Mode I interlaminar fracture toughness G_{Ic} was determined according to the Modified Beam Theory method in ASTM D5528[131]:

$$G_{Ic} = \frac{3P_c\delta_c}{2b(a+|\Delta|)}F \quad (1)$$

where: P_c is the critical load at which crack advance occurs, δ_c is the critical displacement, b is the width, a is the delamination length, |Δ| corrects for crack front rotations and F corrects for large displacement effects. Specimens were cut to 150 x 20 mm and had a nominal thickness of 3 mm. An initial delamination length of 50 mm was used. The load was introduced to the specimens by glued piano hinges. A natural Mode I precrack was attained by loading the specimens to crack initiation and unloading them. The DCB specimens were opened at 2 mm/min while the crack front propagation was followed by a travelling microscope. The experiment was performed on an Instron 3369 equipped with a 500 N load cell.

Three different fracture toughness values are used to describe the Mode I delamination behaviour of these laminates. In order to exclude any reinforcing fibre bridging (e.g. glass or carbon fibres), $G_{Ic,NL}$ is determined by the point of non-linearity during the precracking cycle where the delamination growth starts from the initiation film. The initiation fracture toughness $G_{Ic,ini}$ is determined by the 5%/max point in the load-displacement curve after precracking as recommended by the ASTM standard, while the propagation fracture toughness $G_{Ic,prop}$ is determined as the mean G_I value once the R-curve stabilizes after the reinforcing fibre bridging zone has formed. A typical load-displacement curve and the resulting R-curve is shown in Figure 24 for a unidirectional DCB specimen. It can be seen that there is a relatively large increase in G_I with increasing delamination growth which is due to reinforcing fibres bridging the DCB specimen halves. This fibre bridging, which mainly affects $G_{Ic,prop}$ is considered to be an artefact of the DCB experiment on UD laminates[131]. Hence, $G_{Ic,prop}$ is of lesser importance as most delaminations in realistic laminates form between plies of dissimilar orientation or between woven plies where fibre bridging is minimal or occurs differently. Nevertheless, it is taken into account as its value does provide extra information about the toughening mechanisms in the nanofibre interleaved composites.

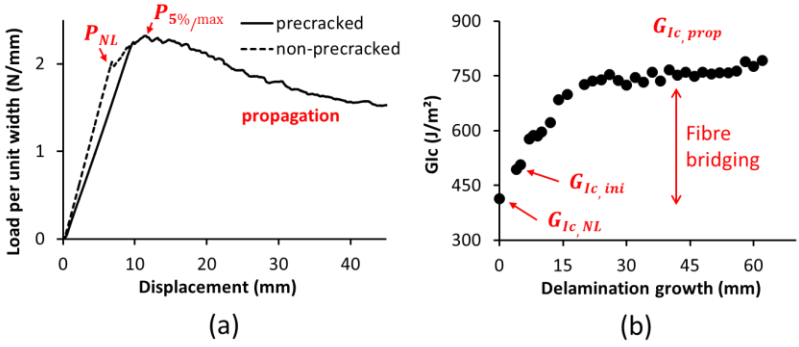

Figure 24 – Typical load-displacement curve obtained in a DCB-experiment (a) and the resulting $\boldsymbol{R}$-curve (b). The different $\boldsymbol{G_{Ic}}$-values used to discuss the Mode I interlaminar fracture toughness are indicated in red.

The Mode II interlaminar fracture toughness G_{IIc} was determined using ENF specimens according to the Compliance Based Beam Method (CBBM) including Bending Rotations[132]:

$$G_{IIc} = \frac{9P_c^2 a_{eq}^2}{2E_f b^2 (2h)^3}[1-\chi] \qquad (2)$$

where: P_c is the critical load at which delamination advance occurs, a_{eq} is an equivalent delamination length calculated from the actual compliance of the specimen, b is the width, E_f is the flexural modulus, $2h$ is the thickness and $[1-\chi]$ corrects for bending rotations. Specimens were cut to 130 x 20 mm and a span length ($2L$) of 100 mm was used. In order to establish stable crack growth in the specimens[133], the ratio of initial delamination length on the half-span length was selected to be higher than 0.7, i.e. $a_0/L > 0.7$: the initial delamination a_0 was 37.5 mm unless otherwise stated. Loading of the specimens was displacement controlled and the crosshead movement was set to 1 mm/min. The experiment was performed on an Instron 3369 equipped with a 2 kN load cell.

Although the ASTM standardization institute recently published a standardised test method for determining the Mode II interlaminar fracture toughness by ENF specimens[134], their method is not only more time consuming due to a necessity for compliance calibrating each specimen, it neglects any sub-critical crack

growth by assuming that the initial delamination length has not changed when $P = P_{max}$. Throughout the experimental campaign of this PhD, it was found that the effect of sub-critical crack growth cannot be neglected for tough resin systems such as the used infusion resin or for specimens containing electrospun nanofibres due to added plasticity at the crack tip (Section 3.2.2). The CBBM data reduction method has several advantages over the one proposed in the ASTM standard: (1) an R-curve is obtained without the need to visually measure the delamination length during the experiment by plotting (2) as a function of a_{eq}, (2) the flexural stiffness is calculated for each specimen separately using the initial compliance[133] and (3) it takes sub-critical crack growth into account as an equivalent delamination length is obtained at each point during the test. Indeed, the Mode II delamination front is difficult to define and an equivalent delamination length calculated from the compliance of the specimen is often more representative for the actual delamination length[135]. This equivalent delamination length is thus calculated during the ENF experiment using the compliance C_i at each recorded load-displacement point, i.e. $a_{eq,i} = f(C_i = \delta_i/P_i)$. It represents the delamination length required to have an imaginary ENF specimen with a perfect delamination front that has the same compliance as the actual specimen.

Two Mode II interlaminar fracture toughness values will be used throughout this PhD to describe the Mode II delamination behaviour of the composite laminates, see Figure 25. The most conservative value, $G_{IIc,NL}$ is obtained at the point where the load-displacement curve starts to deviate from linearity ($P_c = P_{NL}$, where NL stands for non-linearity). At this point, tensile microcracks are initiated in front of the delamination tip due to the shear loading conditions, but no macroscopic delamination growth occurs. Yet, the microcracks will increase the compliance of the specimen and the equivalent delamination length increases, resulting in delamination growth ($\Delta a_{eq} > 0$). The value of $G_{IIc,NL}$ thus corresponds to the energy required for the initiation of these microcracks and is the first point on the R-curve ($\Delta a_{eq} = 0$). The second fracture toughness value that will be used, $G_{IIc,ini}$, corresponds to the point at which macroscopic delamination advance occurs. In comparison to DCB experiments, the macroscopic delamination advance in ENF experiments often propagates up to the center loading point immediately (about 12.5 mm for the specimens under consideration). This results in a maximum load P_{max} followed by a steep

decrease in load in the load-displacement curve, after which the experiment is stopped. The Mode II initiation interlaminar fracture toughness $G_{IIc,ini}$ is thus defined as the G_{II} value at the maximum load during the experiment ($P_c = P_{max}$). This is the most commonly used Mode II interlaminar fracture toughness parameter and is also recommended by the ASTM D7905 standard, as it is related to the point at which macroscopic delamination growth occurs. Note that there can be some equivalent delamination growth before P_{max} is reached, especially in the case of tough laminates. Since these delamination lengths are not critical and do not result in sudden macroscopic delamination advance, this region is referred to as sub-critical crack growth. Hence, $G_{IIc,NL}$ represents the energy required to initiate sub-critical crack growth, while $G_{IIc,ini}$ represents the transition from sub-critical crack growth to macroscopic delamination advance. Section 3.2.2 goes into more detail about the micromechanisms of damage encountered during Mode II delamination.

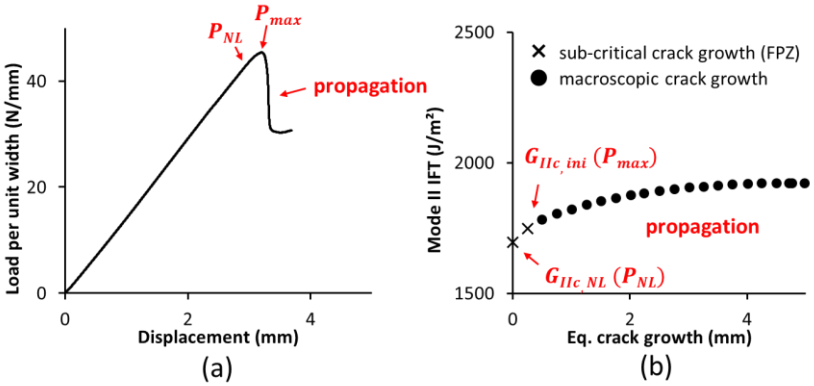

Figure 25 – Typical load-displacement curve obtained from an ENF experiment (a) and the resulting $\boldsymbol{R}$-curve (b). The different $\boldsymbol{G_{IIc}}$-values used to discuss the Mode II interlaminar fracture toughness are indicated in red.

All experiments were performed at 20 ± 2°C and 65 ± 4% RH. At least three specimens were tested for each configuration. A Jeol Quanta 200F Field Emission Gun SEM, a Phenom ProX SEM and an Olympus BX51 optical microscope with an Olympus UC30 camera were used to examine the fracture surface of the specimens.

2.3.3 Impact resistance of interleaved laminates

Low velocity impact tests were conducted according to ASTM D7136[136]. The specimens were cut from the produced composite laminates at a nominal size of 100 x 150 mm^2 by using a water-cooled diamond cutter. The test was executed on an in-house developed impact test machine. The test machine is equipped with a Gen. 5I oscilloscope to record acceleration, load and displacement data of the impactor. Two Photron SA4 high-speed cameras were used to observe the upper and lower face of the specimens during impact. A third AP-XRS high-speed camera was used to measure displacement, velocity and acceleration of the impactor by the use of a specific line pattern stuck on the impactor. The three cameras were synchronized by triggering them at the moment a force of 200 N was detected by the oscilloscope. Images were recorded at 10 000–15 000 fps. The impact test machine comprised a drop tower with an impactor. The impactor had a weight of 8.17 kg with a hemispherical nose diameter of 16 mm as recommended by the ASTM standard. It was guided through two smooth guide columns and impact occurred on the centre of the specimen. The specimen was firmly fastened by four clamps at the corners of the specimen. The initial height of the impactor could be varied in order to obtain various impact energies. Six different heights were set: 20, 40, 60, 80, 100 and 120 cm. They correspond to impact energies of 14, 28, 41, 54, 67, 79 J respectively. The impact energy was calculated as the kinetic energy of the impactor using its velocity measured at the moment a force of 200 N was detected by the oscilloscope. To start an experiment, the impactor was set to the desired height. Subsequently, the impactor was released by an electro-magnet, fell freely and struck the specimen. An anti-rebound device was used to avoid a second strike. The setup is illustrated in Figure 26.

Cross-ply $[0°/90°]_{2S}$ specimens with a nominal thickness of 3 mm were used. Electrospun nanofibrous veils were interleaved on each 0°/90°-interface. For each type of composite and for each impact energy, the drop weight impact test was repeated at least three times. The damage area after impact was measured optically due to the translucence of the laminates. The impacted specimens were tested for their residual compressive strength, i.e. the compression after impact (CAI) strength, according to ASTM D7137[137]. An anti-buckling device was used to prevent buckling of the specimens during compression. The CAI experiments were performed by A. Cohades of the Laboratory for Processing of

Advanced Composites (EPFL, Switzerland) due to his experience with the test method.

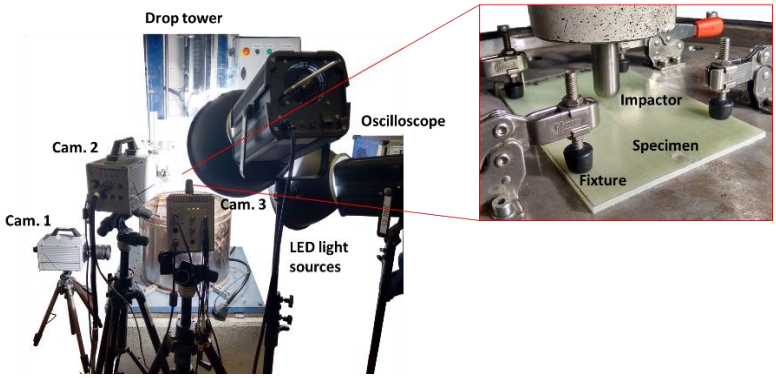

Figure 26 – Image of the drop tower impact setup used.

3

MAJOR RESEARCH RESULTS

This chapter is dedicated to the major research results that were obtained during the PhD work. The chapter is divided according to the three different levels which are present in nanofibre interleaved composites: nanotoughened epoxy, nanotoughened interlayer and fully interleaved laminate. Most of the reported results are based on own published papers, which can be found in full in the Appendix. In each (sub)section, a reference is given to the associated paper(s).

3.1 TOUGHENING MECHANISMS IN NANOTOUGHENED EPOXY

To understand the toughened response of nanofibre interleaved composite laminates, one must first understand the fundamental mechanisms through which nanofibres affect the fracture toughness of the surrounding epoxy resin. This is done by analysing fracture experiments on nanofibre toughened epoxy resin. Single Edge Notch Bending (SENB) specimens are used to determine the intrinsic and extrinsic toughening mechanisms related to nanofibres in Section 3.1.1 (**Paper I**). A further analysis of the fracture behaviour using Single Edge Notch Tension (SENT) specimens in Section 3.1.2 concludes the major research results on nanotoughened epoxy. The results reflect the major insights obtained on Level 1 of the multiscale analysis.

3.1.1 Intrinsic and extrinsic toughening mechanisms

PCL (system #6) and PA6 (system #5) nanofibres were selected as model systems as both have a high toughness compared to the epoxy matrix[28], but different mechanical properties (Figure 27a). The PA6 nanofibres show a relatively high E-modulus (960 ± 30 MPa) and tensile strength (101 ± 9 MPa). Their response is fairly elastic with relatively low strain at failure compared to the PCL nanofibres which have a lower E-modulus (391 ± 54 MPa) as well as tensile strength (79 ± 3 MPa). The electrospinning process often results in a superior mechanical response of electrospun nanofibres compared to the bulk material due to the molecular alignment of polymer chains[138,139], e.g. bulk PCL polymer has an even lower E-modulus (195 ± 10 MPa) as well as tensile strength (11.3 ± 0.3 MPa) compared to the PCL nanofibres and deforms by extensive yielding. The tensile properties of the embedded PCL nanofibres are expected to be in between the bulk and the electrospun properties due to the curing cycle of the epoxy resin. Indeed, the resin is first cured at room temperature followed by a second curing step at an elevated temperature of 80°C. The second curing stage results in (partial) melting and resolidifying of the PCL nanofibres (melting point approx. 60°C) in a confined region with the same size as the initial nanofibre.

The SENB experiments show that while the matrix resin exhibits brittle failure, i.e. sudden and complete failure at the point of crack initiation, both PCL and PA6 nanotoughened epoxy fail by extensive plastic failure (Figure 27b). This results in an increased fracture toughness of the nanotoughened epoxy

compared to the bulk epoxy resin. Additionally, the crack propagation energy increases tremendously, as can be noted from the rising R-curve obtained for nanotoughened specimens (Figure 27c). Basically, more and more energy is required to extend the crack in nanotoughened epoxy, while the brittle unmodified epoxy immediately fails when the critical load is reached.

The larger amount of energy required to initiate cracks in the nanotoughened epoxy indicates that the nanofibres result in intrinsic toughening, i.e. toughening mechanisms acting in the fracture processing zone in front of the crack tip (Figure 28). These toughening mechanisms are most likely related to yielding of the nanofibres since the effect is most pronounced in the PCL nanotoughened specimens where about 30% more energy was required for crack initiation. Note that the yield strength of bulk PCL is much less than that of the epoxy itself as opposed to PA6 nanofibres. The increase in propagation fracture toughness can be related to the extrinsic toughening mechanism of *nanofibre bridging* (Figure 28): upon crack extension, nanofibres will bridge the newly formed crack surfaces and take up energy by straining, yielding and fracture. Hence, the fracture toughness of the nanotoughened epoxy increases with increasing crack growth as the zone of bridging nanofibres becomes larger.

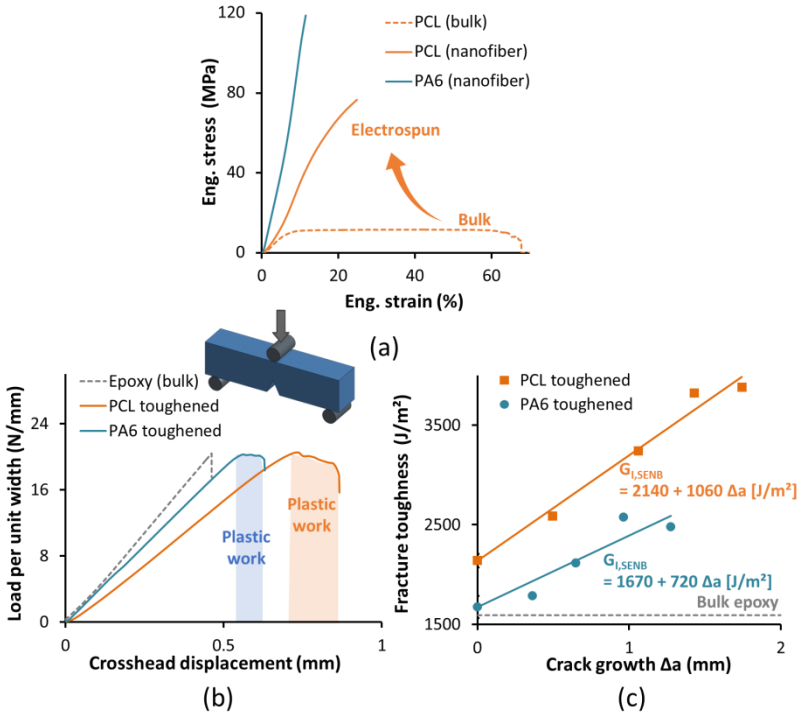

Figure 27 – Stress-strain curves of the PCL and PA6 nanofibres illustrating the difference in tensile properties. The bulk properties of PCL are also shown as the embedded PCL nanofibres (partially) melt during the post-curing of the epoxy (a). Load-displacement curves of SENB specimens show that, while the epoxy resin exhibits brittle fracture, PCL and PA6 nanotoughened epoxy fails by extensive plastic fracture (b). The nanotoughened epoxy has a higher fracture toughness than the unmodified bulk epoxy resin. Furthermore, its fracture toughness increases substantially with increasing crack growth (c).

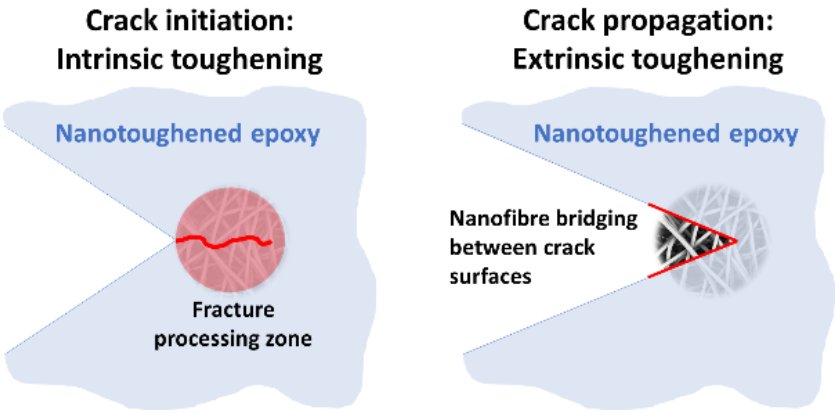

Figure 28 – Crack initiation and propagation toughening mechanisms in a nanofibre toughened epoxy. During crack initiation, nanofibres will yield in the fracture processing zone, while the nanofibres will bridge the crack surfaces during crack propagation.

The proposed mechanism of nanofibre bridging was confirmed by SEM analysis on the fracture surface of broken SENB specimens. The three main mechanisms acting in nanofibre bridging zones observed from the SEM images are schematically illustrated in Figure 29, i.e. straining of the nanofibre without debonding, straining of the nanofibre with partial debonding and full debonding/peeling of the nanofibres. The SEM images showed a highly irregular crack surface and plastically deformed nanofibres protruding from the epoxy as opposed to the flat mirror-like fracture surface of neat epoxy specimens (Figure 30). In order for the bridging nanofibres to increase the fracture toughness, it is important they take up more energy by bridging than the energy that would be required to fracture neat epoxy resin in that area. Furthermore, the nanofibre/matrix adhesion is of crucial importance for a good load transfer to the nanofibres. Although the high surface area to volume ratio of nanofibres allows for sufficient adhesion strength under shear forces, the adhesion strength rapidly declines when the nanofibres are subjected to peeling forces (normal forces)[140]. SEM images of the SENB fracture surface indicate that the PCL/epoxy adhesion is good, whereas it seems rather low for PA6 nanofibres. The good interfacial adhesion of PCL nanofibres can be explained by the occurrence of partial diffusion of PCL into the epoxy resin (see Section 3.3.7 for more details). The adhesion of PA6 nanofibres and the epoxy resin will however be mainly

governed by fairly weak Van der Waals forces. Peeling of nanofibres is seen on SEM images of broken PA6 nanotoughened epoxy specimens. These nanofibres are not likely to take up much energy as they do not deform but rather peel from the matrix, and therefore they have no significant contribution to the fracture toughness of the nanotoughened epoxy. As such, the difference in nanofibre/epoxy adhesion for PA6 and PCL, combined with the higher amount of yielding and the overall higher work of rupture of the PCL nanofibres, can explain why the PCL nanocomposites showed the best improvements in fracture toughness.

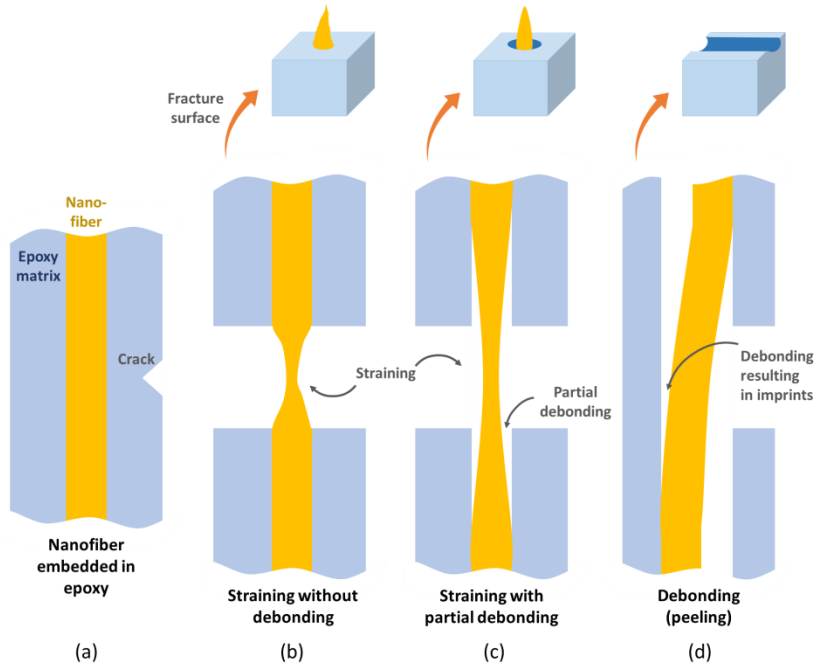

Figure 29 – Interaction of a bridging nanofibre with the crack front (a) resulting in straining of the nanofibre without debonding (b), straining of the nanofibre with partial debonding from the epoxy (c), or complete debonding of the nanofibre (peeling) (d).

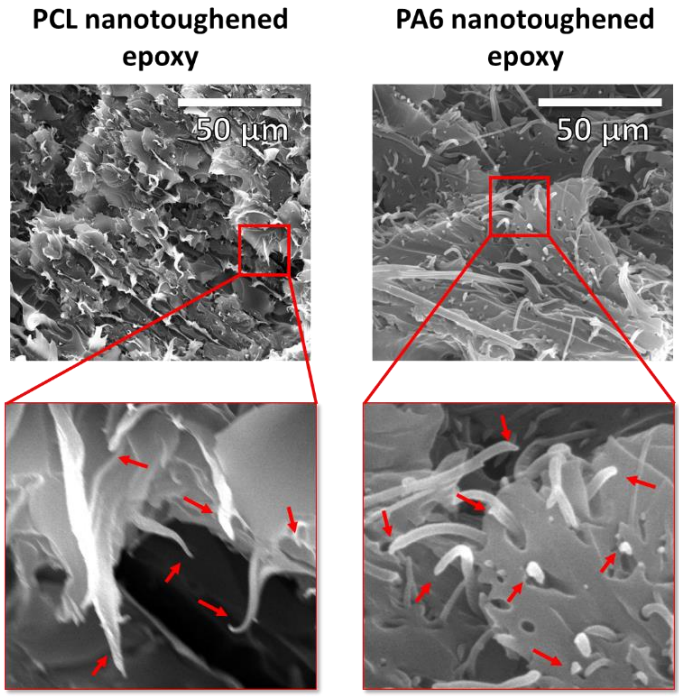

Figure 30 – SEM images of the fracture surface of PCL and PA6 nanotoughened epoxy. The PCL nanofibres are strained without debonding from the epoxy indicating good adhesion. In contrast, the adhesion between epoxy and PA6 nanofibres was poor as indicated by the smooth surface of the PA6 nanofibres and imprints left in the epoxy. Protruding nanofibres are indicated by red arrows.

3.1.2 Analysis of fracture behaviour using SENT specimens

Although SENB specimens allow accurate determination of the (plane strain) fracture toughness of the epoxy resin, they are difficult to produce due to the amount of nanofibres required for such thick specimens. As such, SENT film specimens, which had a thickness around 100 µm, provide a simpler method for analysing the fracture mechanisms due to their ease of manufacture. Furthermore, the crack plane was lying completely in the focal zone of the microscope which allows for in-situ microscopy measurements during crack formation and propagation. This resulted in a better understanding of the development of the fracture processing zone and the nanofibre bridging zone.

Figure 31 shows the development of the fracture processing zone in front of the crack tip and the stable crack propagation zone before abrupt failure of a virgin epoxy and a PCL (system #6) nanotoughened epoxy specimen. Two clear differences can be observed: (i) the fracture processing zone in nanotoughened specimens shows stress whitening, and, (ii) the length of stable crack propagation is much larger in the nanotoughened specimen. The stress whitening phenomenon is most likely due to yielding and (micro)debonding of the nanofibres near the stress concentration at the crack tip. Both effects will change the refractive index locally, resulting in a cloudy, whitened appearance in the translucent epoxy. The fracture processing zone is also less defined than in the virgin specimen and it gradually fades away further from the stress concentration. The same mechanism of yielding and debonding – both causing macroscopic plasticity at the crack tip – was also associated to the increase in initiation fracture toughness measured using SENB specimens in Section 3.1.1. During stable crack propagation, a nanofibre bridging zone develops. These bridging nanofibres cause closing tractions on both crack halves which reliefs the stresses at the crack tip. Furthermore, the nanofibres keep on bridging the crack surfaces until they break by tensile failure adding to the energy absorption, and thus toughness, of the nanotoughened epoxy. This mechanism of nanofibre bridging formation causing closing tractions was verified using in-situ microscopy combined with DIC (Figure 32). The possibility of visualising the nanofibre bridging zone during testing allows quantitative measurements of the bridging zone such as its length. Since it is this bridging effect that will cause the largest increases in fracture toughness, direct visualisation of the bridging zone allows for a better understanding of how it develops in different nanotoughened epoxy specimens.

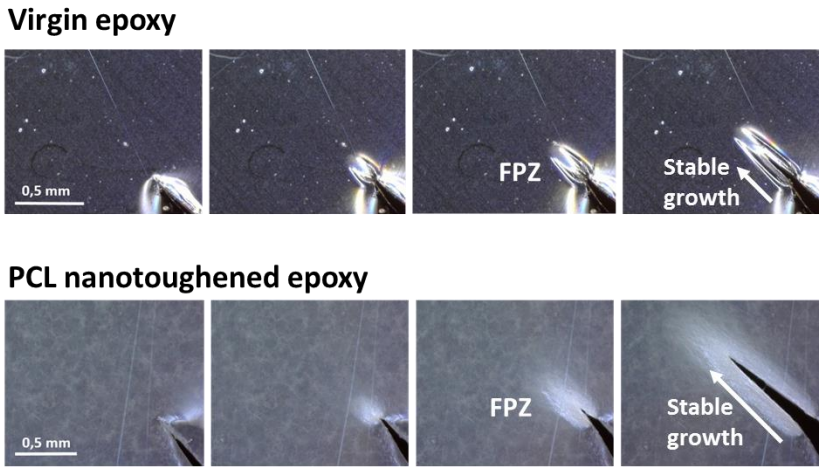

Figure 31 – Development of the fracture processing zone (FPZ) and stable crack propagation in virgin and PCL nanotoughened epoxy specimens. Nanotoughened specimens have a different FPZ with stress whitening and show a larger amount of stable crack growth.

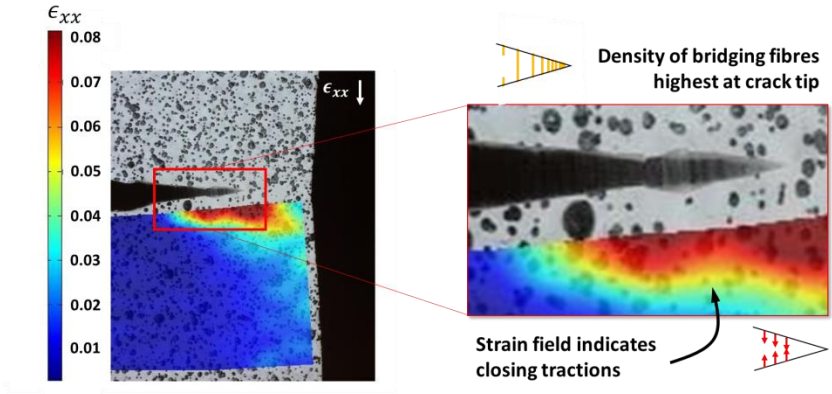

Figure 32 – In-situ microscopy on a nanotoughened SENT specimen showing the development of a nanofibre bridging zone behind the crack tip, while closing tractions can be visualised using DIC.

Similar to the SENB specimens, the plastic work necessary to break a SENT specimen relates to the toughening potential of the nanofibres (Figure 27b). Integration of the load-displacement curve of an SENT specimen up to the point of crack initiation yields the elastic energy take-up, while integration from the crack initiation point till the point of break yields the plastic energy take-up. Figure 33 shows the plastic energy take-up for virgin epoxy and PA6.9 (system #1) and PCL nanotoughened epoxy for a test performed at different strain rates. PCL nanofibres show the highest increases in plastic energy take-up resulting in almost twice the energy required to break a PCL nanotoughened epoxy compared to virgin epoxy. Indeed, the elastic energy take-up was similar for both materials. At the lowest strain rate, PA6.9 nanofibres perform slightly less than PCL nanofibres, but the increase is still considerable. However, this changes at higher strain rates: while PCL nanofibres result in a significant toughness increase relatively independent of the deformation speed, the increase in plastic energy take-up of PA6.9 nanofibres quickly decreases. This indicates that there is a strain-rate dependent behaviour causing a ductile-to-brittle transition in the PA6.9 nanofibres which decreases their toughening potential. Such effects become important when the nanofibres will experience dynamic loadings such as those encountered during impact damage. It is interesting to note that the virgin epoxy resin also becomes more brittle with increasing deformation speed.

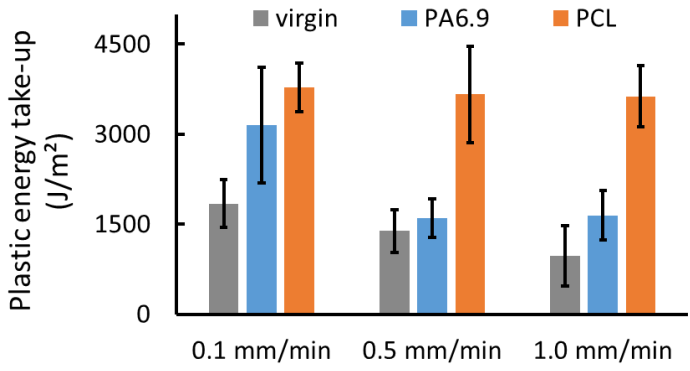

Figure 33 – Plastic energy take-up during fracture of virgin, PA6.9 toughened and PCL toughened epoxy at different strain rates.

The SEM analysis in Section 3.1.1 indicated a better adhesion between PCL and epoxy than between PA6 and epoxy as was evidenced by imprints left by peeled PA6 nanofibres. Although these imprints do provide indirect evidence of the lack of interfacial strength, a direct measurement of the interfacial quality between nanofibres and matrix resin is preferable. The SENT film specimen design allows for a relatively simple determination of the interfacial quality using aligned nanofibrous veils. Similar to test methods for regular fibre reinforced composites on $[0°]_n$ and $[90°]_n$ laminates[141], a loading direction perpendicular to the nanofibre direction stresses the interface much more than loading parallel to the nanofibre direction. SENT specimens with nanofibres aligned parallel and perpendicular to the loading direction are thus a good measure for the interfacial strength (Figure 34). PCL nanofibres show only a slight decrease when loaded perpendicular to the nanofibre direction due to a good interfacial strength. The small reduction in energy take-up is mainly due to much less nanofibre bridging occurring by an orientation of the nanofibres not promoting bridging. PA6.9 nanofibres on the other hand show a drastic decrease in plastic energy take-up as the crack easily propagates along the nanofibre/epoxy interface without much resistance due to the lack of interfacial strength. As such, this method provides the means for analysing the interfacial strength in nanofibre toughened epoxy. Due to its generality, this method can also be useful for characterising other nanocomposite systems as there is currently no method available which allows to test the interface between electrospun nanofibres and matrix resin.

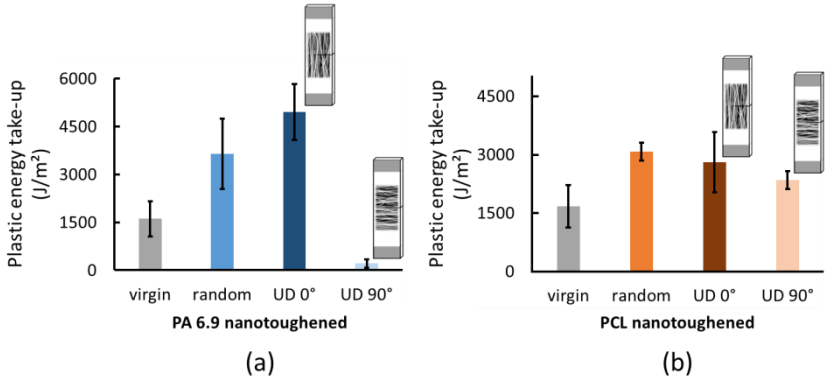

Figure 34 – The plastic energy take-up decreases drastically in SENT specimens tested perpendicular to the nanofibre direction if there is a lack of interfacial strength between the nanofibres and the epoxy resin. This is clearly illustrated for PA6.9 nanofibres (a), as opposed to the slight decrease in energy take-up measured for PCL nanofibres which have good adhesion with epoxy (b).

3.2 NANOFIBRE BRIDGING IN INTERLEAVED COMPOSITES

This section deals with the development of nanofibre bridging zones in interleaved composites at Level 2. As opposed to nanofibre bridging in nanotoughened epoxy, the development of nanofibre bridging in interleaved composites is dependent on the interaction between the delamination and the nanotoughened interlayer (Subsection 3.2.1). Furthermore, the effect of loading mode on the development of nanofibre bridging is analysed in Subsection 3.2.2 as delaminations usually occur under Mode I or Mode II loading. The represented data highlights the major results, further detailed in **Paper I**, **Paper II**, **Paper III**, **Paper IV** and **Paper V**, which consider the delamination resistance of nanofibre interleaved composites using Mode I and Mode II delamination experiments.

3.2.1 Development of nanofibre bridging zones

Delamination in composites is typically associated to the formation of a plane crack front in the (resin rich) interlayer between reinforcing plies. This is correct from a macroscopic viewpoint. However at the microscopic level of an interlayer, the delamination will progress by fracturing the resin material, debonding of the reinforcing fibres (i.e. fracture along the fibre/matrix interface) or by a combination of both mechanisms. Simplified, the delamination will progress through the weakest zones as less energy is required. If the amount of energy required for fracturing the epoxy resin is similar to that necessary for debonding the reinforcing fibres, a combination of both mechanisms is present. For the resin systems used in this PhD (EPIKOTE RIMR135, HexPly M10R and MTM49-3), microscopy showed that delaminations in virgin composites progress almost exclusively at the reinforcing fibre/epoxy interface. The energy required for such interfacial failure will depend on the adhesion of the reinforcing fibres with the matrix resin and forms the major contribution to the Mode I and Mode II interlaminar fracture toughness, G_{Ic} and G_{IIc} respectively, of virgin laminates. The delaminations in nanofibre interleaved composites show the same reinforcing fibre/epoxy interfacial failure, but additionally show crossings of the interlaminar region through the nanotoughened interlayer (Figure 35). The amount of reinforcing fibre/epoxy interfacial failure remains similar to that in virgin laminates as the interlaminar crossings are oriented transversely to the

macroscopic delamination plane. However, the interlaminar crossings result in a crack through the nanotoughened epoxy which causes nanofibre bridging.

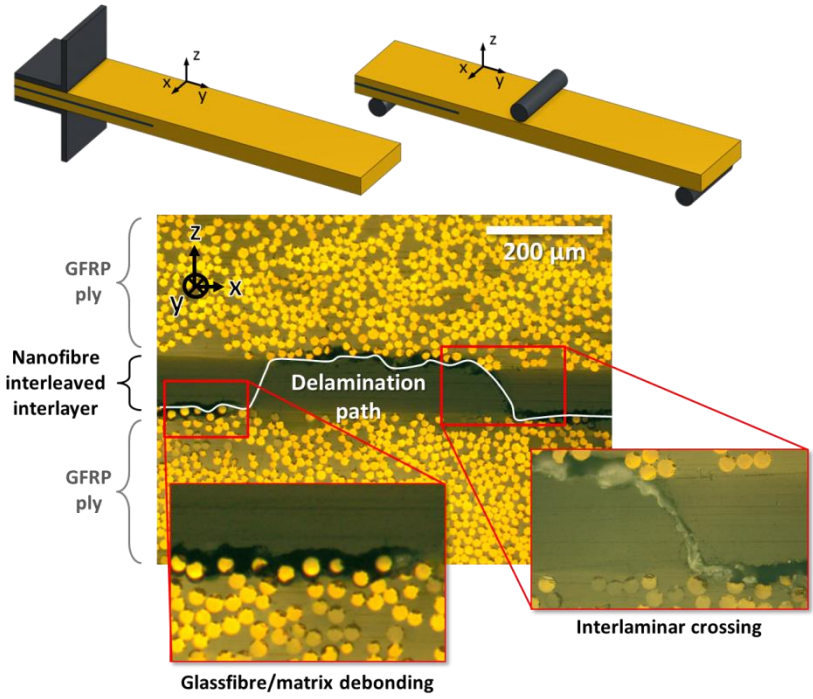

Figure 35 – Delaminated nanofibre interleaved DCB and ENF specimens show regular interlaminar crossings besides reinforcing fibre/matrix debonding. Nanofibre bridging zones will mainly develop in the interlaminar crossings where there is a lot of interaction between the delamination path and the nanotoughened interlayer.

The occurrence of interlaminar crossings results in a very distinct fracture surface topology consisting of classical interfacial failure (fibre/matrix debonding) similar to the virgin laminates and interlaminar failure at points where the crack passes from one side of the interlayer to the other (Figure 36). Furthermore, it can be seen that the interlaminar failure mainly propagates parallel to the crack growth direction resulting in a "banded" structure on the fracture surface. The delamination path and fracture surface morphology are often not reported in publications, but do reveal a substantial amount of information about the different micromechanisms which affect the

delamination resistance of an interleaved composite. In case the delamination is completely deflected towards the reinforcing fibre/epoxy interface, no nanofibre bridging can occur at all, and the delamination resistance will thus hardly be affected. The deflection towards the intralaminar zone can be caused by the nanofibres themselves due to an increased toughness, but can also be dependent on the exact layup of the composite. For example, it is known that delamination between 0°/90°-interfaces typically causes a deflection in the 90°-oriented ply[142]. On the other hand, if the delamination goes completely through the nanofibre interleaved interlayer, one might expect a very high delamination resistance due to excessive nanofibre bridging. This does not necessarily has to be the case as it can also indicate that the adhesion between the nanofibres and the epoxy is so low that it requires less energy to propagate along the nanofibre/epoxy interface. During this PhD work, the best improvements in interlaminar fracture toughness were almost always obtained for specimens which had regular occurrences of interlaminar crossings besides the classical interfacial failure.

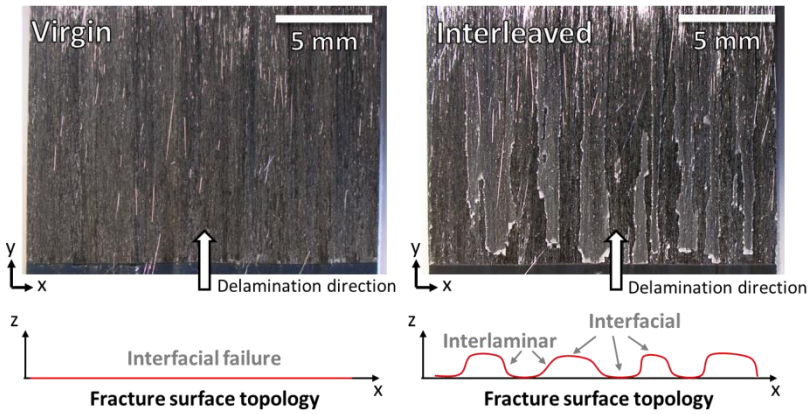

Figure 36 – Nanofibre interleaved specimens show a banded morphology due to the occurrence of interlaminar crossings besides reinforcing fibre/matrix debonding at the ply interface (interfacial failure). The pictures show the fracture surfaces of a Mode II delaminated CFRP interleaved with PA6.9 (#1) nanofibres.

3.2.2 Loading mode effects

Figure 37 illustrates the delamination mechanisms that are present in a composite laminate under Mode I loading conditions. Nanofibre bridging will only occur at the interlaminar crossings in interleaved laminates due to an interaction between the delamination path and the nanotoughened interlayer. Each interlaminar crossing corresponds to a crack through nanotoughened epoxy similar to the material studied in Section 3.1. Note that although the delamination plane is parallel to the nanofibrous veil, the interlaminar cracks go in the through-thickness direction similar to the crack studied with SENB and SENT specimens. Hence, the increase in Mode I interlaminar fracture toughness of the nanofibre interleaved specimens, $\Delta G_I = G_{Ic,interleaved} - G_{Ic,virgin}$, can be attributed to the total amount of interlaminar crossing fracture surface area and the fracture toughness of the nanotoughened epoxy, $G_{Ic,SENB}$:

$$\Delta G_I \approx G_{Ic,SENB}\left(\frac{nt}{\sin\theta}\right) \tag{3}$$

where n is the amount of crossings per unit delamination width, t is the thickness of the interlayer and θ defines the angle of the interlaminar crossings with the delamination plane. Microscopy images of tested DCB specimens near the initiation point allow for measuring the total amount of interlaminar crossing fracture surface area (n, t and θ). In combination with the $G_{Ic,SENB}$ values determined in Section 3.1.1, this allows for the calculation of ΔG_I according to (3). Good agreement with ΔG_I determined from DCB experiments on PCL (system #6) interleaved laminates was found, thus validating the proposed equation (Table 2). The correlation between $G_{Ic,SENB}$ and $G_{Ic,interleaved}$ is further confirmed by SEM analysis of the interlaminar crossings in DCB laminate specimens which showed extensive nanofibre bridging with a similar morphology as the fracture surface of the nanotoughened epoxy specimens of Section 3.1.1 (Figure 38).

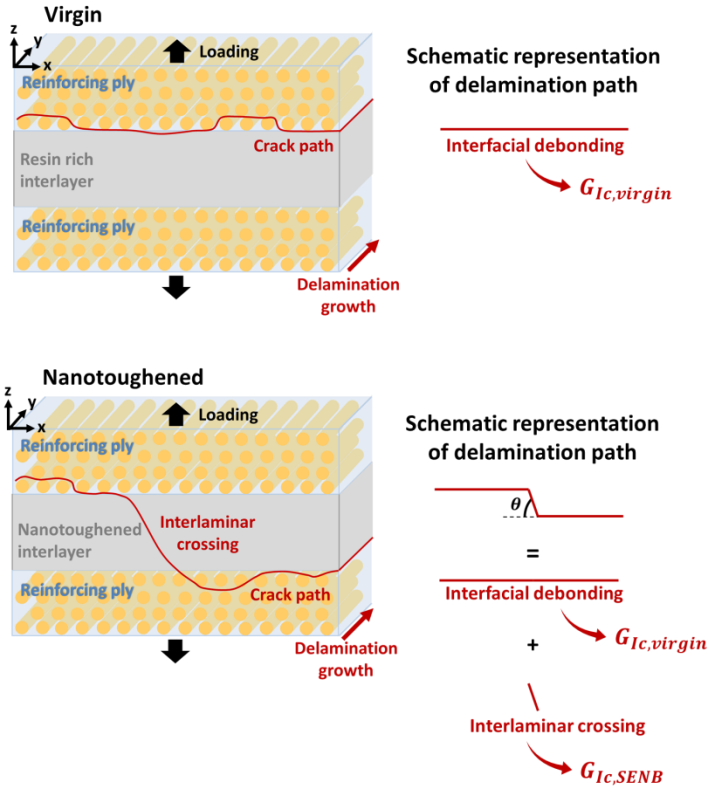

Figure 37 – Illustration of the delamination path in virgin and nanofibre interleaved composite laminates under Mode I loading. The virgin laminates show almost exclusively reinforcing fibre/matrix debonding, while in interleaved laminates, interlaminar crossings are observed as well.

Table 2 – Values of ΔG_{Ic} obtained from DCB experiments and from (3) for several PCL nanofibre interleaved specimen showing good agreement.

Specimen	Interlayer thickness (µm)	Amount of crossings per specimen (-)	ΔG_{Ic} (J/m²)	
			Experiment	Eq. (3)
PCL 44 g/m² specimen #1	178	4	175	145
PCL 44 g/m² specimen #2	178	6	215	218
PCL 15 g/m² specimen #1	59.9	17	253	207
PCL 10 g/m² specimen #2	57.4	14	176	164

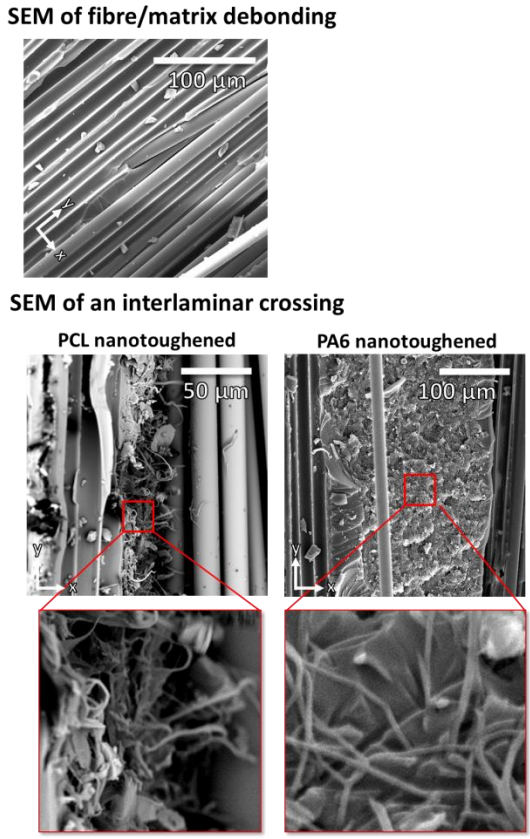

Figure 38 – SEM images of intralaminar failure and interlaminar crossings. Nanofibre bridging zones developed at the interlaminar crossings in interleaved laminates. The fracture surface morphology of the bridging zones resembles that of the nanotoughened epoxy specimens of Section 3.1.

The delamination mechanism under Mode II loadings is more complex and consists out of tensile microcrack formation in front of the crack tip in the interlaminar region at 45° relative to the macroscopic delamination growth direction (development of the fracture processing zone)[143,144]. As detailed in Section 2.3.2, the initiation of these microcracks is represented by $G_{IIc,NL}$. After the initiation of the microcracks, sub-critical crack growth continues by the formation and growth of more microcracks. The coalescence of these microcracks results in macroscopic delamination advance at P_{max}, represented by $G_{IIc,ini}$. The resulting delaminated fracture surface has hackles which are

typical for Mode II loadings. Figure 39 illustrates the delamination mechanism under Mode II loading.

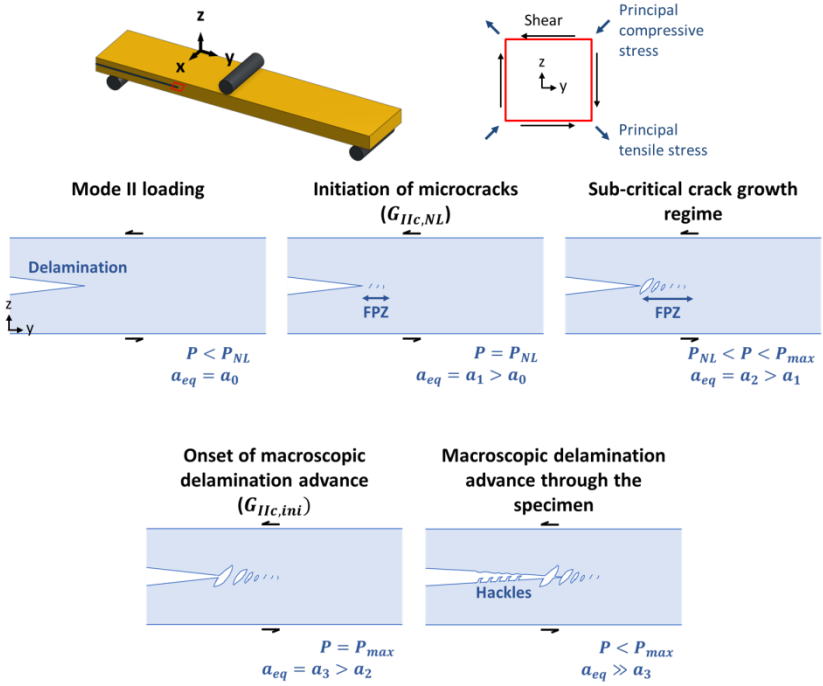

Figure 39 – Illustration of the Mode II delamination mechanism. Shear stresses at the crack tip generate (principal) tensile stresses which cause microcrack formation in front of the crack tip at 45 ° to the shear loading direction. This is followed by sub-critical crack growth. The maximum load is reached when the microcracks start to coalesce and macroscopic delamination advance is observed.

The improvement in Mode II interlaminar fracture toughness ΔG_{II} is a combination of the development of nanofibre bridging zones in interlaminar crossings as well as in the microcracks and hackles which form in the interlaminar region (Figure 40). The nanofibres will not only increase the energy required for microcrack initiation $G_{IIc,NL}$, but also take up more energy during the sub-critical crack growth regime. Indeed, more energy is required for the growth and coalescence of microcracks due to the development of nanofibre bridging zones. At the same time, regular interlaminar crossings also improve

the delamination resistance similar to their effect under Mode I loading. Both mechanisms of nanofibre bridging development will improve the energy required for macroscopic delamination resistance $G_{IIc,ini}$ considerably and will typically cause longer regimes of sub-critical crack growth. As such it is not possible to define a simple relationship between ΔG_{II} and $G_{Ic,SENB}$ as the amount of microcrack surface can hardly be measured. However, since microcrack initiation under Mode II loadings is governed by the formation of tensile microcracks in the interlaminar region, the increase in energy required to initiate these microcracks – represented by $G_{IIc,NL}$ – is similar to the increase in initiation fracture toughness of the nanotoughened epoxy itself (Figure 41). This proves again that there is a strong link between the nanotoughened epoxy level and the nanotoughened interlayer level. It is worth remarking that the amount of interlaminar crossings was generally found to be higher in Mode II delaminated specimens compared to Mode I delaminated specimens. There occurrence is facilitated by the shear loading conditions which generate (principal) tensile stresses in the interlayer.

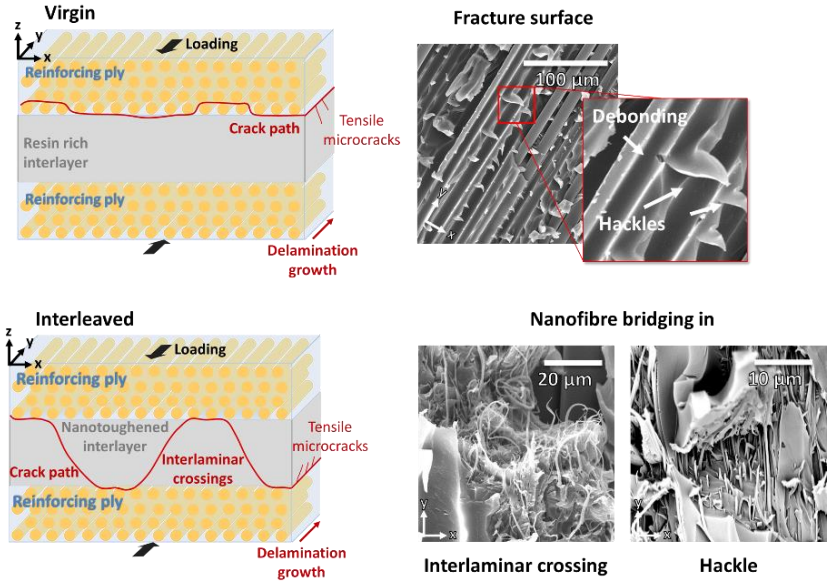

Figure 40 – Illustration of the delamination path in virgin and nanofibre interleaved composite laminates under Mode II loading. Nanofibre bridging zones develop at the

interlaminar crossings, but also at microcracks in the nanotoughened interlayer (hackles).

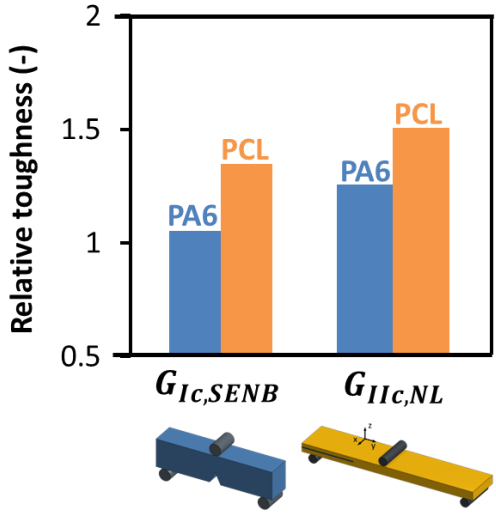

Figure 41 – The increase in initiation fracture toughness of nanofibre toughened epoxy is similar to the increase in Mode II microcrack initiation energy as the microcracks form under tensile stress in the nanotoughened interlayer.

Besides the difference in crack mechanisms, the (macroscopic) delamination loading mode will also affect the way in which the nanofibres are loaded on the microscopic level. The improvement in initiation interlaminar fracture toughness for PA6 (system #5) and PCL (system #6) interleaved composites with identical nanofibrous veil areal density, reinforcing ply architecture and interleaving method is shown in Figure 42a. Both PCL and PA6 nanofibres show an extraordinary increase in $G_{IIc,ini}$ (energy required to initiate macroscopic delamination failure). This result is in accordance with the results obtained in Section 3.1 where both PA6 and PCL nanotoughened epoxy had an increased fracture toughness. PCL nanofibres also increased $G_{Ic,ini}$ substantially, whereas PA6 nanofibres seemed to have hardly any effect on $G_{Ic,ini}$. Based only on the results obtained on nanotoughened epoxy, one would not expect such a different behaviour between Mode I and Mode II loading conditions. However, under Mode I loading, crack growth subjects the nanofibres to normal forces. When the nanofibre/matrix adhesion is low, as is the case for polyamide

nanofibres (see Section 3.1.2), this causes extensive peeling of the nanofibres (Figure 42b). Hence, the adhesion between nanofibre and epoxy resin becomes very important under Mode I delamination growth as low interfacial strength results in low energy take-up by the nanofibres. This mechanism results in minor to no improvements in $G_{Ic,ini}$ for PA6 interleaved laminates. Under Mode II loading conditions, adhesion between nanofibre and epoxy resin poses less of a problem as the shear adhesion strength of all nanofibres is relatively high due to their high surface area to volume ratio[140]. Furthermore, the formation of tensile microcracks at 45° relative to the delamination direction also results in stretching of the nanofibres that bridge these cracks (Figure 42b). As a result, high improvements in $G_{IIc,ini}$ are obtained for PCL as well as PA6 nanofibre toughened composites.

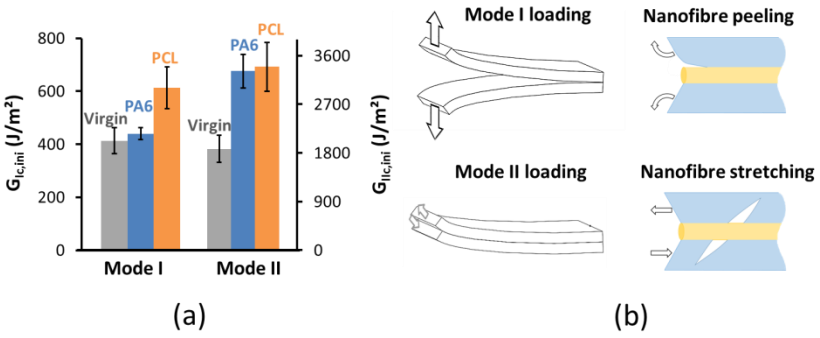

Figure 42 – Mode I and Mode II interlaminar fracture toughness for a virgin, PA6 interleaved and PCL interleaved composite laminate (a). Schematic illustration of the loading exerted on the laminate and the loading experienced by the nanofibres (b).

3.3 PARAMETERS AFFECTING NANOFIBRE BRIDGING IN INTERLEAVED COMPOSITES

The previous section showed that interlaminar crossings are very important in order to obtain highly toughened composites as they are the main cause of nanofibre bridging on the interlaminar level. Further analysis at Level 2 showed that the occurrence of interlaminar crossings was found to be dependent on parameters related to the nanofibres themselves, the veil morphology, the interleaving technique, the reinforcing fabric architecture and even the way in which the delamination experiment is performed. It is therefore of crucial importance that these effects are understood and taken into account when discussing the toughening potential of a certain nanofibre system. Indeed, while one type of nanofibrous veil might result in good improvements for one type of composite laminates, it does not necessarily result in the same improvements for other types of laminates. This was especially clear in several publications in which the same nanofibre system is used, but completely different results of interlaminar fracture toughness are recorded, see also Section 1.4. Generally, in order to increase the fracture toughness on the interlaminar level, the interaction between the delamination path (interlaminar crossings and microcrack formation) and the nanotoughened interlayer characteristics (fracture toughness, nanofibre properties, adhesion, …) are of crucial importance and should be considered in order to design damage resistant composite materials.

This section is divided in several subsections which each treat one parameter that affects the nanofibre bridging in an interleaved composite. The results highlight the results from several of our published papers.

3.3.1 Areal density of nanofibrous veils

One important and simple parameter which can drastically affect the obtained interlaminar fracture toughness is the nanofibrous veil areal density. This was analysed in **Paper I** and **Paper II**.

The interlaminar thickness increases linearly with the veil density (Figure 20). On the one hand, the interlaminar fracture toughness thus increases with increasing veil density as each interlaminar crossing becomes larger. On the other hand, we

found that the amount of interlaminar crossings under Mode I loadings typically declines quickly with increasing nanofibrous veil density, resulting in an optimum ΔG_I at intermediate veil densities. For PCL (system #6) nanotoughened GFRP composites, an optimum veil density was found to be around 10 g/m² (Figure 43). At higher veil densities, the improvements in $G_{Ic,ini}$ started to level off and even declined at very high veil densities of > 40 g/m². For polyamide nanofibres (PA6, PA6.6 and PA6.9) the trend was less clear as there is hardly an increase in $G_{Ic,ini}$ due to extensive peeling of the polyamide nanofibres.

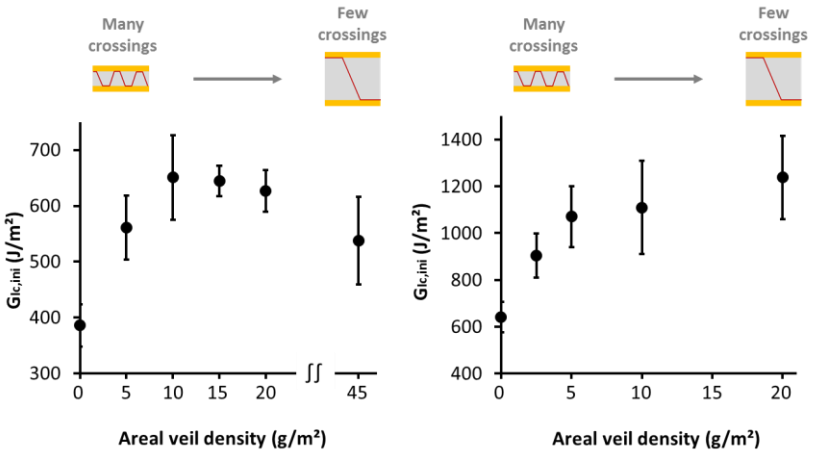

Figure 43 – The increase in $G_{Ic,ini}$ levels off and even decreases with increasing areal density of the (PCL) nanofibrous veil. The results are obtained on GFRP UD laminates with UDO ES500 (left) and Roviglas R17/475 (right) reinforcing plies.

Under Mode II loadings, the amount of interlaminar crossings is much less affected and ΔG_{II} increases with increasing nanofibre veil density after which it starts to level off (Figure 44a). However, compared to Mode I loadings, no decrease in $G_{IIc,ini}$ is found at very high veil densities. The Mode II interlaminar fracture toughness is still very high for veil densities of > 40 g/m². However, the flexural properties of the composite laminate will probably start to decline due to the creation of a very thick unreinforced interlayer. The fact that regular interlaminar crossings still occur at these higher veil densities in comparison with Mode I delamination is related to the shear loading conditions at the crack tip under Mode II delamination. This results in a tensile stress component

through the interlayer which can promote crack formation through the interlayer (Figure 44b). Note that this is similar to the way tensile microcracks form in front of the crack tip during Mode II delamination as explained in Section 3.2.2.

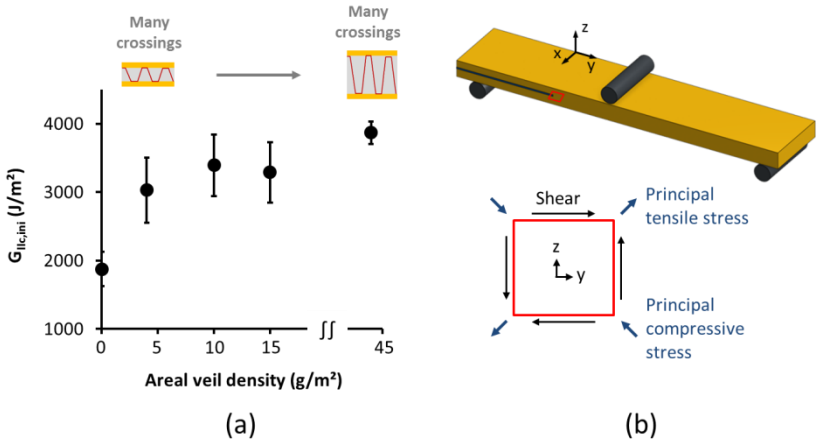

Figure 44 – The Mode II interlaminar fracture toughness increases with increasing areal veil density and starts to level of for very high veil densities (a). The generation of tensile stresses through the interlayer due to the Mode II shear loading (b).

3.3.2 Interleaving method

There are three different ways in which nanofibrous veils can be integrated in a composite laminate that are relevant for practical applications: (i) using reinforcing plies coated on both sides with electrospun nanofibres, (ii) using reinforcing plies only coated on one side, or (iii) interleaving a self-supporting nanofibrous veil. The effect of the integration method on the Mode I interlaminar fracture toughness was analysed in **Paper II**.

When using reinforcing plies coated on both sides with electrospun nanofibres, referred to as the Double Layer Coated (DLC) configuration, the interlayer between reinforcing plies will contain two nanofibrous layers. In the other cases, the Single Layer Coated (SLC) and Self-Supporting Interlayer (SSI) configuration, only one nanofibrous layer is present. If the areal density of the nanofibres in the interlayer is mentioned for the DLC configuration, it is always the total

amount, e.g. interleaving 5 g/m² of nanofibres in DLC configuration is done by using two reinforcing plies coated with 2.5 g/m² of nanofibres on each side. It was found that these methods of interleaving can affect the improvement in Mode I interlaminar fracture toughness due to a change in interlaminar crossing occurrence. DCB experiments were performed on GFRP composite laminates interleaved with the same amount of PCL (system #6) nanofibres. Two different reinforcing ply types were used. Both were unidirectional E-glass fibres, but had a different architecture. Ply Type A (Roviglas 17/475) consisted of unidirectional warp yarns held together by a very low amount of (E-glass) weft yarns. Ply Type B (UDO ES500) on the other hand consisted out of unidirectional fibre plies held together by a polyester scrim at its surface. While Type A plies had a very bundled morphology and "rough" surface morphology, Type B plies were much flatter and represented the ideal case of unidirectional fibre plies better (Figure 45).

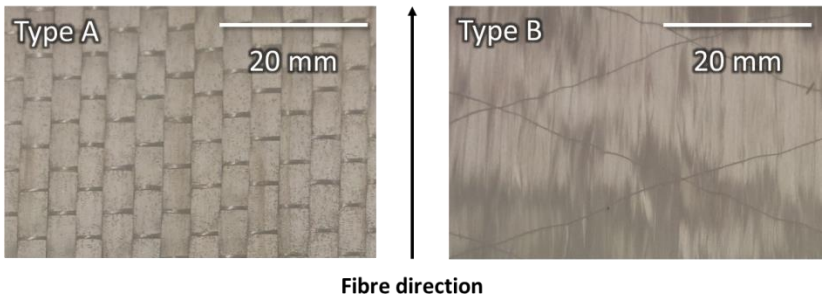

Figure 45 – Although both reinforcing ply types are considered to be unidirectional, there is a distinct difference in surface morphology from bundled for Type A to flat for Type B.

In the case of ply Type A, there was a significant difference between the obtained Mode I interlaminar fracture toughness and the way in which the nanofibres were interleaved. Figure 46a shows the R-curve obtained for representative DCB specimens containing 5 g/m² of PCL nanofibres. The DLC configuration of the nanofibres resulted in very large increases of G_I over the whole delamination length. On the contrary, the SLC and SSI configuration hardly increased G_I. Microscopic analysis of the delaminated specimens showed

that these differences were due to much more interlaminar crossings present in the DLC configuration. Although this may be unexpected as the same amount of nanofibres was present in the interlayer, the "lay-up" of the interlayer differs depending on the interleaving method. Indeed, when nanofibres are directly spun onto the reinforcing fibres, there is much more interaction between the nanofibres and the reinforcing fibres. Furthermore, the nanofibres are deposited according to the morphology of the reinforcing ply. As the delamination is often deflected towards the reinforcing fibre/matrix interface, toughening this interface with nanofibres is beneficial for the delamination resistance. A DLC configuration has this toughening effect at both sides of the interlayer, while a SLC only has one side of the interlayer toughened (the side on which the nanofibres were spun). In the case of an SSI configuration, it is highly unlikely that the self-supporting veil will perfectly deform according to the reinforcing ply morphology at both sides. Therefore, in the case of an SSI or SLC configuration, the delamination is more likely to be deflected towards the untoughened reinforcing fibre/matrix interface resulting in minimal improvements of the delamination resistance (Figure 46b).

In the case of ply Type B, the interleaving technique affected the improvements in Mode I interlaminar fracture toughness much less. A series of composites was produced with different amounts of PCL nanofibres in either a DLC or an SSI configuration. Microscopic analysis of the delaminated specimens showed regular occurrences of interlaminar crossings in both configurations. In contrast to ply Type A, ply Type B had a much flatter topology. As such, the interaction between the nanofibres and the reinforcing plies was much better in the SSI configuration and both interleaving techniques resulted in similar improvements of $G_{Ic,ini}$ (Figure 47).

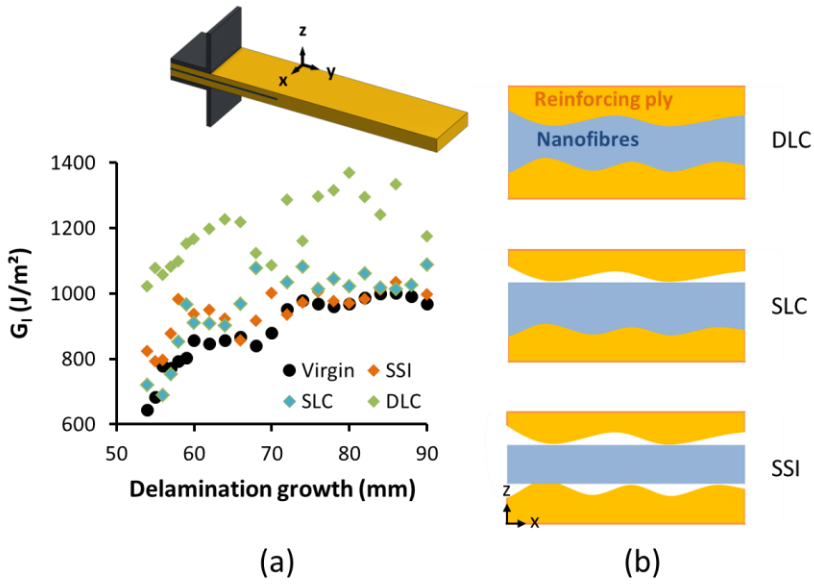

Figure 46 – A DLC configuration results in the highest improvements in G_I compared to a SLC or a SSI configuration of the nanofibres for Type A plies (a). Illustration of the interaction between the interleaving technique and the Type A ply morphology (b).

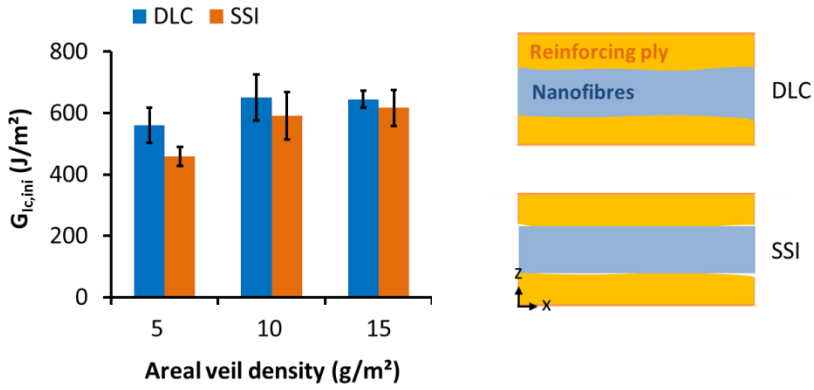

Figure 47 – The interleaving technique does not affect the $G_{Ic,ini}$ substantially for Type B reinforcing plies due to the flat morphology of the reinforcing plies.

The results show that it is often better to use a DLC configuration for interleaving nanofibrous veils in a composite laminate. Especially if the reinforcing plies have a rough topology, which is for example encountered when using woven fabrics, directly coating both sides of the reinforcing plies with nanofibres results in much better improvements of the Mode I interlaminar fracture toughness. It should be noted however that this can only be done when working with dry fabrics. In the case of prepreg materials where the reinforcing fibres are already surrounded by (partially reacted) epoxy resin, electrospinning nanofibres directly on the prepreg surface makes less sense. It could even initiate a harmful reaction between the electrospinning solvents and the uncured prepreg resin. Many prepreg materials are however unidirectional and have a near perfect arrangement of fibres resulting in a very flat morphology. As such, the added value of directly spinning the nanofibres on their surface would probably be negligible.

3.3.3 Position of the initiation film

In a DCB or ENF experiment, a release film is used to initiate the delamination in between the central plies of the laminate. With regard to the materials studied in the previous subsection (Section 3.3.2), this means that the initiation film is on top of the nanofibrous veils for SLC configurations, while it is sandwiched between two nanofibrous veils for the DLC configuration. In order to assess the influence of this difference in position of the initiation film, modified DCB specimens were produced in which there was a gap of 1 mm between the nanofibrous veil and the tip of the release film, see Figure 48 (**Paper II**). Hence, the delamination initiated in front of the nanofibrous veil and the deflection towards either side of the nanotoughened interlayer only happened after 1 mm of delamination growth. Nevertheless, no difference in Mode I interlaminar fracture toughness was found for these modified specimens. The DLC configuration still resulted in much better improvements due to more occurrences of interlaminar crossings.

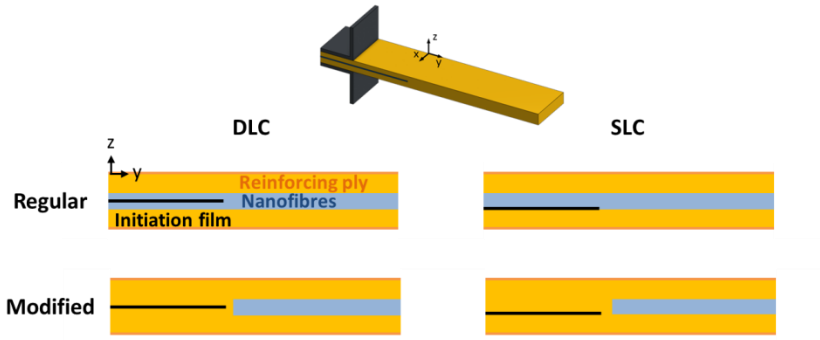

Figure 48 – Schematic illustration of the position of the initiation film in regular and modified DCB specimens.

The effect of the position of the initiation film was also investigated for prepreg-based CFRP unidirectional composite laminates interleaved with PA6.9 (system #3) nanofibrous veils in **Paper III**. In this case, the veils were interleaved using an SSI configuration to prevent any interaction between the prepreg resin and the electrospinning solvents as discussed in Section 3.3.2. In comparison to PCL nanofibres, the PA6.9 nanofibres typically have a low adhesion with the epoxy matrix (Section 3.1.2). A microscopic analysis of delaminated DCB specimens showed that the Mode I delamination propagated preferably at the nanofibre/epoxy interface due to excessive peeling of the nanofibres. This did not positively influence the Mode I delamination resistance. However, when there was a gap of 3 mm between the tip of the initiation film and the nanofibrous veil, the obtained G_I increased considerably. The DCB fracture surface changed from one with nanofibre peeling to one with interlaminar crossings and intralaminar failure (Figure 49). This effect is attributed to the development of a natural crack front with bridging carbon fibres in the first 3 mm of delamination growth. This might have resulted in small zones where the local crack growth was not purely Mode I or where the crack growth direction was not parallel with the plane of the interlayer resulting in a better load transfer to the nanofibres (less peeling). Furthermore, when a zone of bridging (carbon) fibres develops, these fibres need to tear through the nanofibre toughened interlaminar region. Consequently, zones of plastically deformed PA6.9 nanofibres were visible on the fracture surface and this tearing of the nanofibres takes up energy leading to a higher interlaminar fracture

toughness. As compared to the results obtained in Mode I delamination growth, no difference in delamination behaviour was observed for Mode II delamination growth using modified ENF specimens.

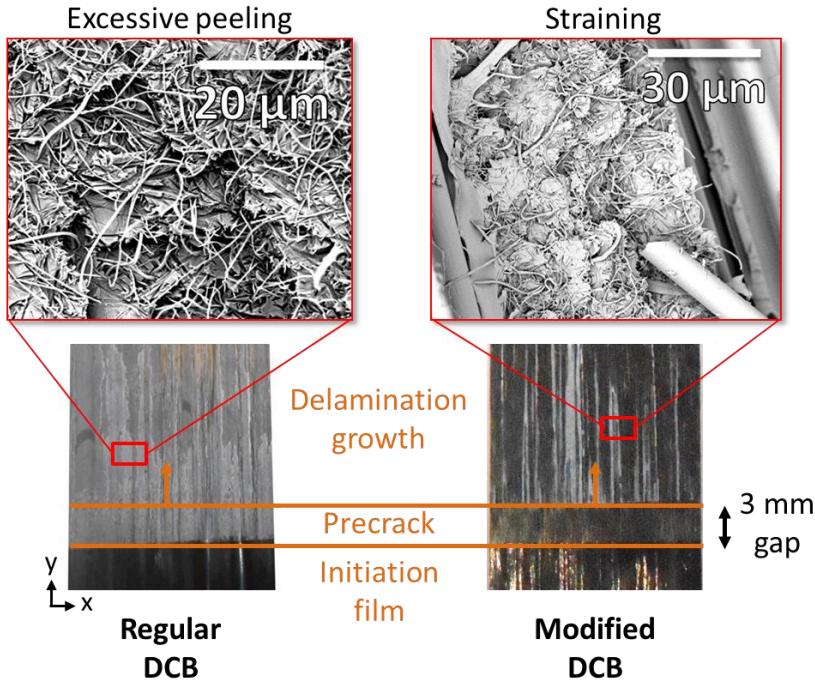

Figure 49 – A gap of 3 mm between the tip of the initiation foil and the nanofibrous interleaf resulted in the change of delamination path from one with nanofibre peeling to one with regular interlaminar crossings and nanofibre straining. This resulted in significant increases in obtained G_{Ic} for the modified DCB experiment.

It is clear that a small difference in crack initiation geometry can have a big influence on the resulting G_I, especially in the case of polyamide nanofibres which have a low adhesion with the matrix. In a third modified geometry, nanofibrous strips with a length of 15 mm were placed at 15 mm and at 45 mm ahead of the initiation film. Hence, a relatively large zone of carbon fibre bridging is allowed to develop before the delamination encounters the nanofibres. This resulted in a significant increase in G_I in the zones where nanofibres were present (Figure 50).

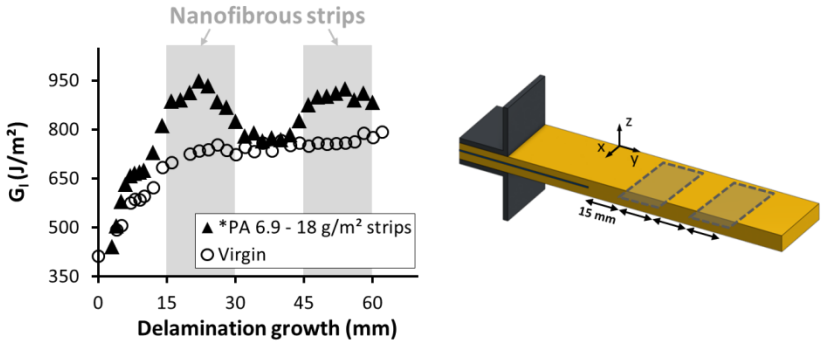

Figure 50 – A modified DCB setup with strips of nanofibrous veils in front of the delamination showed that the G_I increased due to the presence of PA6.9 nanofibres.

The polyamide nanofibre interleaved laminates with a modified initiation geometry described above showed large increases in Mode I interlaminar fracture toughness compared to specimens where the initiation film was placed on top of the nanofibrous veils. This mechanism can be of use to toughen laminates where the delamination will start from a known region, e.g. around (drilled) holes, free edges or inserts. If the nanofibrous veils are placed several millimetres away from these regions in order for a fibre bridge zone to develop, they can act as "delamination-stoppers". More importantly however, in order to interpret the DCB data of nanofibrous interleaved composites it is very important that the interleaving of the nanofibres is done carefully and reported in detail since a small gap between initiation film and nanofibres can have a large effect on the fracture behaviour. This effect may not always be representative of the actual behaviour of the material. For the determination of the generic Mode I delamination resistance for example, there should be no gap between the initiation film and the nanofibrous veil to prevent any artificial increases in interlaminar fracture toughness as it is expected that in real-life, delaminations will initiate from the weakest spot, possible the nanofibre/matrix interface, and not from an initiation film.

3.3.4 Ply reinforcement architecture

Section 3.3.2 already showed that the interaction between the ply reinforcement architecture and the nanofibre interleaving method can affect the obtained delamination resistance of nanotoughened composite laminates. Those results were however based on composites made from unidirectional reinforcing plies. This section deals with the effect of the ply reinforcement architecture on the obtained Mode I and Mode II delamination resistance. More precisely, the difference between unidirectional ply based and woven fabric based composites was analysed in **Paper III**. The materials under consideration are unidirectional and 2x2 twill woven prepreg-based CFRP laminates interleaved with PA6.9 (system #3) nanofibres (SSI configuration).

The main difference in Mode I delamination between a UD and a woven composite is the occurrence of reinforcing fibre bridging. While woven composites typically result in flat R-curves with some scatter associated to local differences in toughness due to the woven architecture and resin pockets, UD composites show a clear increase in interlaminar fracture toughness with increasing delamination growth due to bridging of the reinforcing fibres (Figure 51). This means that the propagation toughness $G_{Ic,prop}$ is actually artificially affected by the reinforcing plies as bridging will occur differently in real-life multidirectional composite laminates. Therefore, when discussing the improvements in Mode I interlaminar fracture toughness in this PhD, the initiation value – either $G_{Ic,NL}$ or G_{Ic} – is mainly used (see also Section 2.3.2). Yet, the propagation value reveals information about how nanofibres can affect the occurrence of reinforcing fibre bridging.

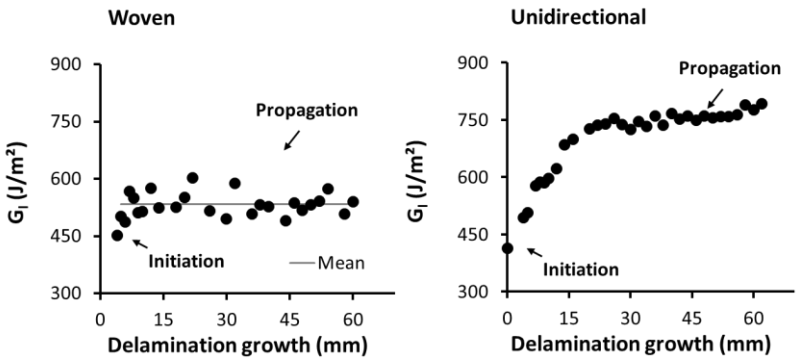

Figure 51 – Woven specimens result in a relatively flat $\boldsymbol{R}$-curve, while unidirectional specimen have an increase in $\boldsymbol{G_I}$ with increasing delamination length due to the development of a reinforcing fibre bridging zone.

Figure 52 illustrates the initiation and propagation Mode I interlaminar fracture toughness of nanofibre interleaved unidirectional and woven composite laminates. For the woven composites, it is clear that adding nanofibres results in an improvement of the delamination resistance. Furthermore, as compared to the virgin material, the propagation fracture toughness is much higher than the initiation fracture toughness in the nanofibre interleaved woven laminates. This is a result of the formation of a nanofibre bridging zone at the delamination surface which took up significant amounts of energy by plastic failure of the nanofibres. On the other hand, the initiation and propagation fracture toughness are hardly improved and even decrease in unidirectional laminates. As compared to the virgin material, the difference between the initiation and propagation fracture toughness is much less and even negligible in the nanofibre interleaved composites indicating that there was no nanofibre bridging zone which took up energy. The bridging of the reinforcing fibres was also prohibited by the nanofibres. This resulted in decreases of $G_{Ic,prop}$ compared to the virgin material. SEM analysis of the fracture surface showed plastically deformed and teared PA6.9 nanofibres in the woven laminates, but peeled off nanofibres without much deformation for the unidirectional laminates due to a lack of adhesion with the matrix. This indicates that the load transfer to the nanofibres was more efficient in woven laminates. The woven architecture probably resulted in small zones where the local crack growth was not purely Mode I or

where the crack growth direction was not parallel with the plane of the interlayer resulting in a better load transfer to the nanofibres.

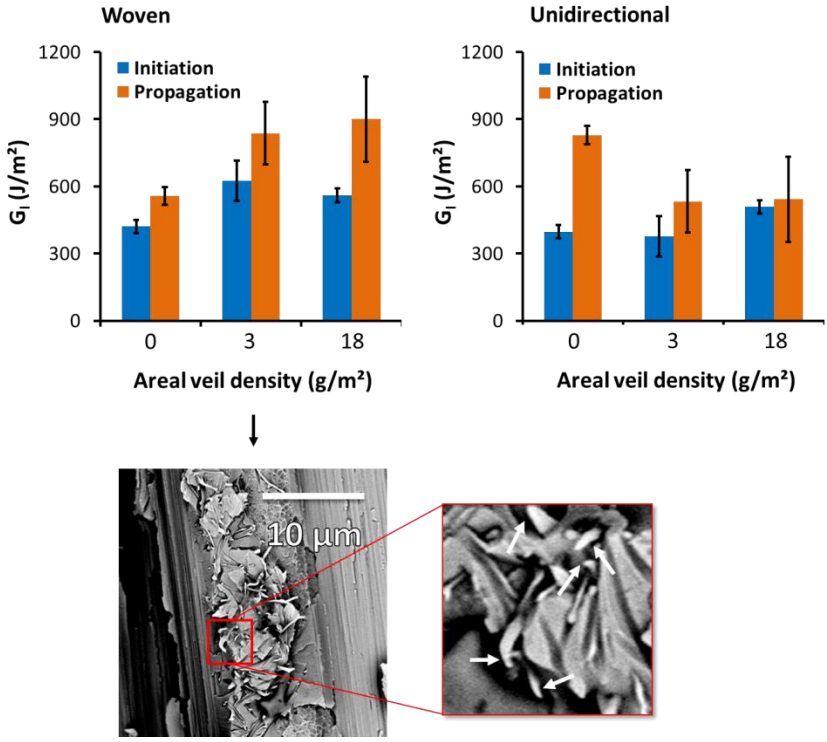

Figure 52 – PA6.9 nanofibres increase both initiation as well as propagation Mode I delamination resistance in woven laminates, but not in unidirectional laminates.

For Mode II loading conditions, the amount of bridging reinforcing fibres is much less due to the propagation mechanism of microcrack formation and coalescence in the interlayer. As such the R-curves are flat and the difference between macroscopic delamination initiation $G_{IIc,ini}$ and propagation $G_{IIc,prop}$ is often negligible. Indeed, for the reference UD material, experiments showed that $G_{IIc,ini} = 1580 \pm 50$ J/m² and $G_{IIc,prop} = 1610 \pm 60$ J/m². However, the energy required for the initiation of microcracks, $G_{IIc,NL}$, is lower than $G_{IIc,ini}$, especially in nanofibre interleaved laminates. This is clearly visible in the R-curves in Figure 53. The difference between both energies, i.e. $\Delta G_{II,SCG} =$

$G_{IIc,ini} - G_{IIc,NL}$, is a measure for the amount of energy taken up during sub-critical crack growth (Figure 53). Indeed, the nanofibres affect both the energy required for microcrack initiation $G_{IIc,NL}$ as well as the energy required for major delamination advance $G_{IIc,ini}$. However, their effect on $G_{IIc,NL}$ is relatively small as the nanofibre bridging effect is still very low at crack initiation (Section 3.1.1). During sub-critical crack growth, more microcracks will form and propagate, thus causing more nanofibre bridging. This results in a much higher improvement in $G_{IIc,ini}$. Note that the (equivalent) delamination length during sub-critical crack growth can be several millimetres long due to the added toughness of the nanotoughened interlayer. This means that $G_{IIc,ini}$ should be regarded as the energy required to initiate major delamination advance and not as an energy required to initiate damage. Furthermore, as the adhesion between the nanofibres and the matrix poses less of a problem under Mode II delamination (see also Section 3.2.2), the same trend in improvements is found for UD as well as woven composites. Indeed, the nanofibres on the fracture surface show a high degree of plastic deformation indicating good load transfer to the nanofibres.

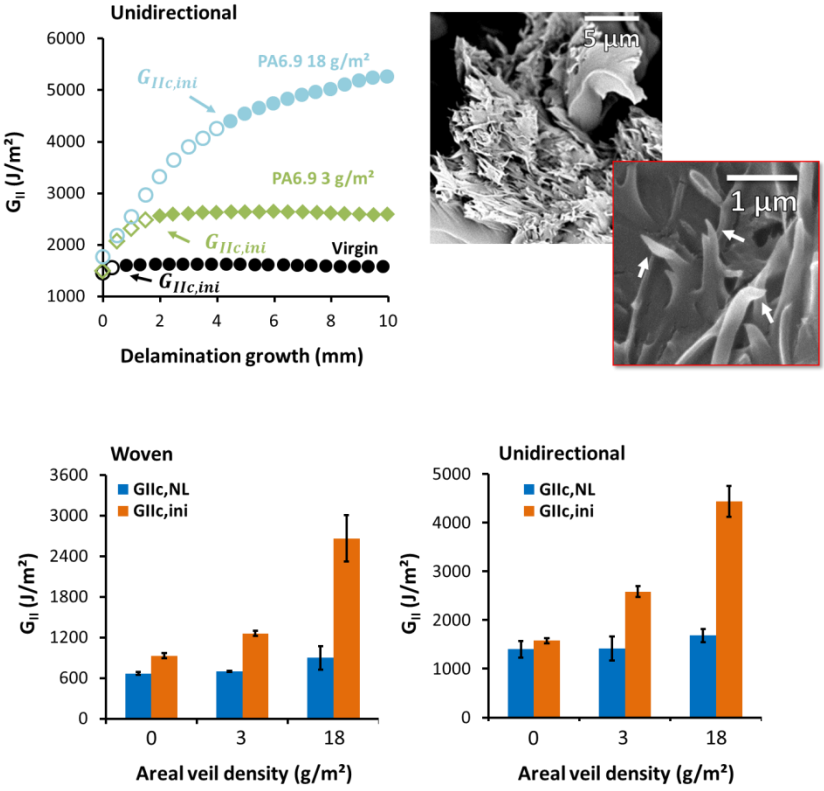

Figure 53 – The development of nanofibre bridging causes a large increase in energy take-up during sub-critical crack growth as visualised by a rising $\boldsymbol{R}$-curve (sub-critical crack growth is indicated by a hollow symbol). The $\boldsymbol{G_{IIc,ini}}$ increases substantially compared to virgin specimens in both unidirectional as well as woven composite laminates as nanofibre/matrix adhesion poses less of a problem under Mode II loading.

3.3.5 Nanofibre orientation

Throughout the previous sections good load transfer to the nanofibres has proven to be essential for improving the delamination resistance. Just as with regular fibre reinforced composite where the fibre orientation determines the stiffness and strength, the nanofibre orientation can have a profound effect on the development and effectiveness of nanofibre bridging zones in nanotoughened composite laminates. This was analysed using ENF experiments on PA6.9 (system #1 and system #2) toughened prepreg-based CFRP UD laminates in **Paper IV**. Mode II delamination was selected as it results in microcrack formation (hackles) besides interlaminar crossings and nanofibre bridging can develop at both regions (Section 3.2.2). Furthermore, there is no nanofibre peeling which could obscure the toughening mechanisms due to a lack of adhesion between the nanofibres and the matrix. The ENF specimens in this section were slightly different from the other ENF specimens as they were performed according to the ASTM D7905 standard ($a_0/L = 0.6; 0.5$ mm/min). The raw data was however processed using the method described in Section 2.3.2.

Three nanofibrous veil morphologies were used to study the effect of the nanofibre orientation distribution on the Mode II interlaminar fracture toughness (Figure 54a): (1) a random deposition of nanofibres (RNDM), (2) nanofibres oriented parallel to the delamination growth direction (PAR), and (3) nanofibres oriented transversely to the delamination growth direction (TRANS). There was a clear effect of nanofibrous veil orientation on the $G_{IIc,ini}$ (Figure 54b). The Mode II interlaminar fracture toughness increased by approximately 50% for specimens in which the nanofibres were parallel to the delamination growth direction, by 75% for nanofibres oriented transversely to the delamination growth direction and even by 100% when a random deposition of nanofibres was used. Since there was a difference in observed $G_{IIc,ini}$ between PAR and TRANS interleaved specimens, indicating that both orientations induced a different toughening of the interleaved laminates, it can be expected that, in extremum, a RNDM interleaved laminate combines both effects of PAR and TRANS interleaved laminates. Indeed, the random oriented nanofibrous veil is composed of both nanofibres more or less parallel and more or less transversely oriented to the delamination growth direction. Hence, the

toughening effect of both parallel and transversely oriented nanofibres can be associated to the RNDM interleaved laminates.

The increase in toughness during sub-critical crack growth $\Delta G_{II,SCG}$ is a measure for the effectiveness, or "size", of the nanofibre bridging zone. A larger $\Delta G_{II,SCG}$ indicates a more effective nanofibre bridging zone which takes up more energy. It should be noted however that $\Delta G_{II,SCG}$ is not purely a measure of nanofibre bridging, but is associated to the complex crack growth mechanism under Mode II loading (Section 3.2.2) and it can be non-zero for virgin laminates. The R-curves in Figure 54c show that while $G_{IIc,NL}$ remained similar for all nanofibre interleaved configurations, $G_{IIc,ini}$ was dependent on the nanofibre orientation. Hence, there was a significant effect of nanofibre orientation on $\Delta G_{II,SCG}$. The effectiveness of the toughening mechanism characteristic to PAR interleaved specimens was less effective compared to the toughening mechanism in TRANS interleaved specimens. The RNDM interleaved laminates showed the largest $\Delta G_{II,SCG}$ values, indicating that the nanofibre bridging zone in this configuration was the most effective – or the "largest" – compared to PAR and TRANS configurations (Figure 54d).

Analysis of the fracture surface of delaminated specimens showed that there were differences in the nanofibre bridging zones developed at hackles near the ply interface failure region and at interlaminar crossings depending on the orientation of the nanofibres. For PAR interleaved specimens, severe nanofibre bridging and deformed nanofibres were mainly visible at the ply interface regions (Figure 56). As the interlaminar crossing failure plane (yz-plane) was parallel to the nanofibres, the delamination could advance through the nanofibre/epoxy interface and only limited bridging occurred in these regions (Figure 55). At the ply interface region, the microcracks and hackles formed in the interlayer were oriented perpendicular to the nanofibre direction and thus promoted severe nanofibre bridging. Nevertheless, it only resulted in the bridging of nanofibres near the surface of the nanofibrous veil. Hence, the total amount of bridging nanofibres was relatively low in both regions and the induced toughening effect will also be relatively low.

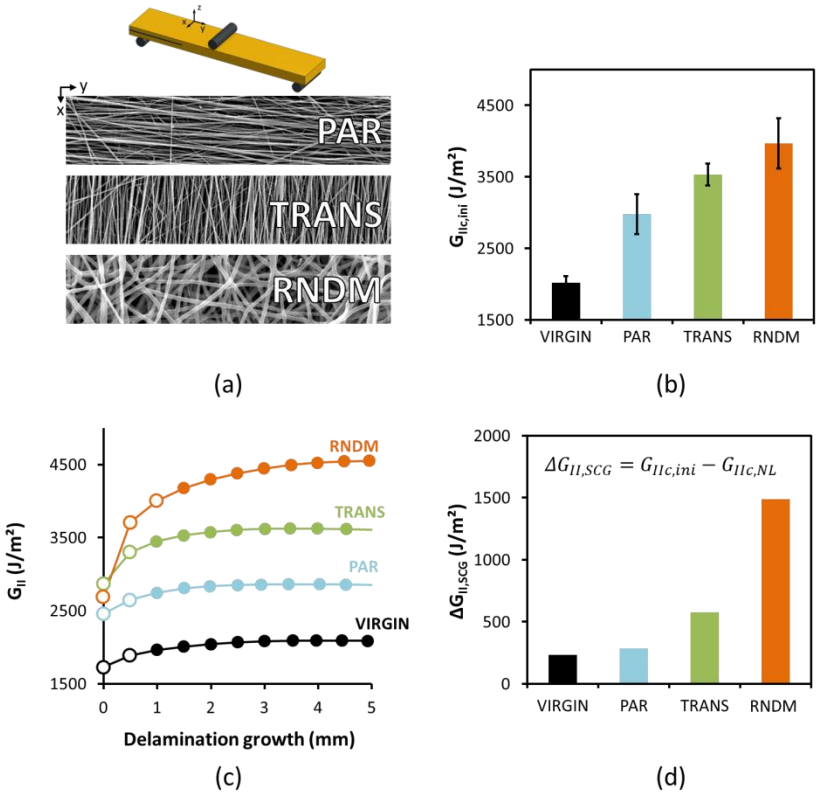

Figure 54 – Illustration of the nanofibre orientation for PAR, TRANS and RNDM interleaved specimens (a). The $\boldsymbol{G_{IIc,ini}}$ increases substantially for the nanofibre interleaved specimens and there is a clear difference between PAR, TRANS and RNDM (b). While $\boldsymbol{G_{IIc,NL}}$ remains similar for all nanofibre interleaved specimens, $\boldsymbol{G_{IIc,ini}}$ (first datapoint represented as a full circle on the $\boldsymbol{R}$-curves) increases more for TRANS and RNDM laminates indicating a more effective nanofibre bridging zone (sub-critical crack growth is indicated by hollow circles) (c – d).

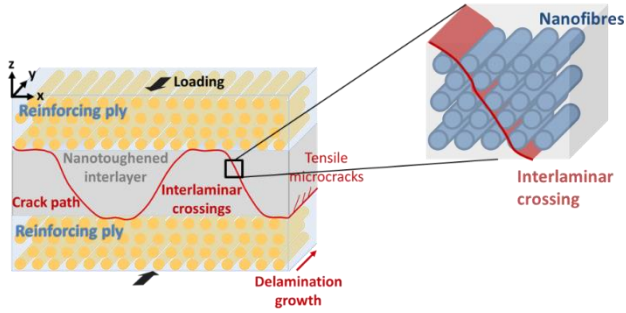

Figure 55 – The failure plane of the interlaminar crossings is parallel to the nanofibres and the delamination can progress along the nanofibre/matrix interface resulting in limited bridging in PAR interleaved specimens.

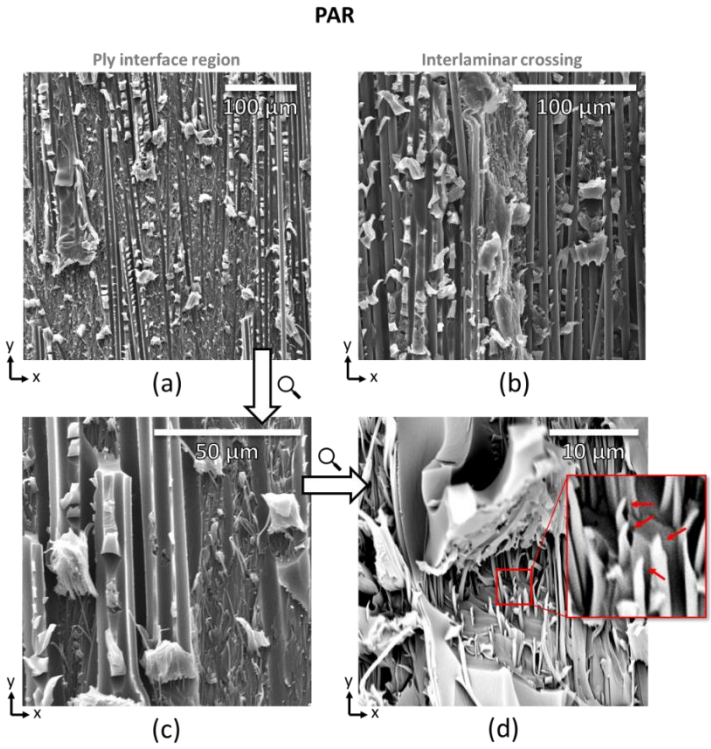

Figure 56 – View of the fracture surface of a Mode II delaminated PAR interleaved specimen at the ply interface (a) and at the interlaminar crossing (b) regions. Nanofibre bridging zones mainly develop at the microcracks and hackles near the ply interface region (c – d).

The opposite effect was found for TRANS interleaved specimens where severe nanofibre bridging zones were mainly visible at interlaminar crossings and not at the microcracks and hackles at the ply interface region (Figure 58). Again this can be attributed due to the advantageous orientation of the nanofibres compared to the failure plane of interlaminar crossings (Figure 57), while their orientation is disadvantageous for bridging microcracks and hackles since those cracks can occur along the nanofibre/matrix interface without resulting in bridging nanofibres. The effectiveness of the nanofibre bridging zones in TRANS interleaved specimens is thus much higher than in PAR interleaved specimens as each interlaminar crossing resulted in the failure of almost all the nanofibres present in the nanotoughened interlayer. This was indeed reflected by the higher $\Delta G_{II,SCG}$.

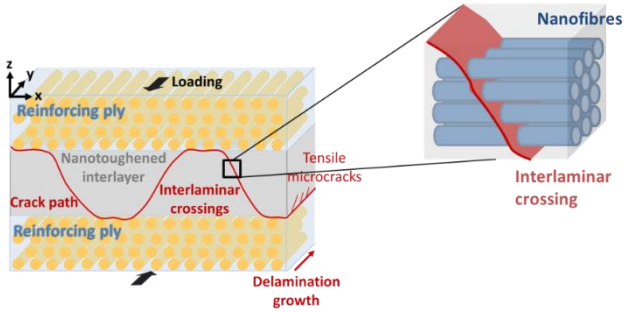

Figure 57 – The failure plane of the interlaminar crossings is perpendicular to the nanofibres and the delamination has to go through the nanofibres resulting in many bridging nanofibres in TRANS interleaved specimens.

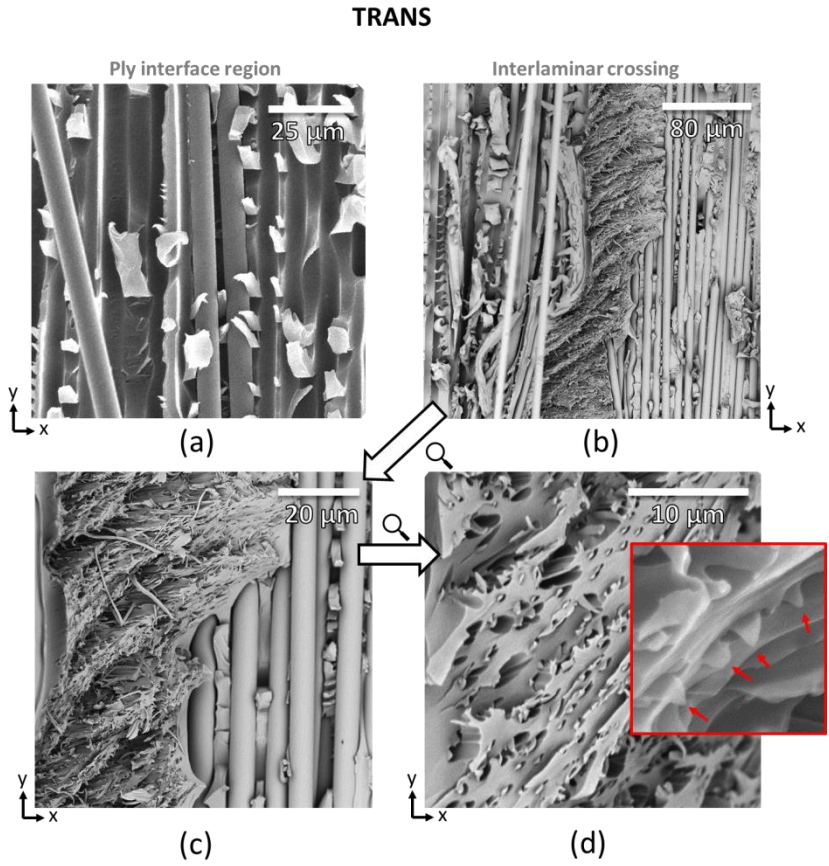

Figure 58 – View of the fracture surface of a Mode II delaminated TRANS interleaved specimen at the ply interface (a) and at the interlaminar crossing (b) regions. Nanofibre bridging zones mainly develop at the interlaminar crossings and almost all nanofibres in the interlayer have been broken (c – d).

Since both nanofibre bridging zones develop independently of each other in different failure regions, their effect in a RNDM interleaved laminate can be seen as a superposition of both mechanisms, each resulting in an increased delamination resistance. Indeed, severe nanofibre bridging was visible at both the ply interface region as well as at interlaminar crossings for the RNDM interleaved laminates (Figure 59). This indicated that each failure mode requires a certain orientation distribution of the nanofibres. Nanofibre bridging zones develop during hackle formation when the nanofibres are oriented more or less

parallel to the delamination growth direction. Similarly, they develop at interlaminar crossings when the nanofibres are oriented more or less perpendicular to the delamination growth direction. Hence, a random distribution of nanofibres results in the initiation of both toughening mechanisms. This resulted in the highest improvements of the Mode II interlaminar fracture toughness for RNDM interleaved laminates of approximately 2000 J/m². The PAR and TRANS interleaved specimens resulted in an increase in $G_{IIc,ini}$ compared to the virgin laminates of approximately 1000 J/m² and 1500 J/m² respectively. Hence, for RNDM interleaved laminates where both mechanisms of nanofibre bridging are present, the increase in $G_{IIc,ini}$ can be approximated as the sum of 1000 J/m² and 1500 J/m². This is an overestimation of course as only a certain fraction of the randomly distributed nanofibres will develop nanofibre bridging zones related to PAR and TRANS mechanisms.

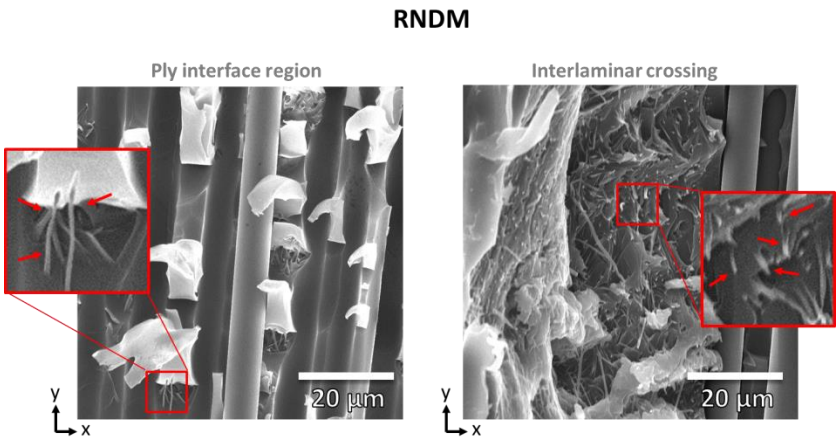

Figure 59 – In RNDM interleaved laminates, nanofibre bridging zones develop in the microcracks and hackles near the intralaminar region as well as at the interlaminar crossings.

3.3.6 Fatigue loading conditions

Composite components will often experience repeated loading during their life-time, for example wind turbine blades experience fluctuating loadings depending on the wind conditions. These repeated loadings can cause a weakening of the material due to the formation of micro-sized damage which in the end can lead to failure of the component at stresses much lower than the static strength of the material. Hence, besides analysing the static delamination resistance of nanofibre interleaved composites, it is also important to understand and consider delamination under cyclic/fatigue loading in these materials. Indeed, it is known that the delamination behaviour in (toughened) composite laminates might differ substantially between static and fatigue loadings[143,145,146]. The focus of this section is on the Mode II delamination behaviour as delamination growth during service often occurs under Mode II dominated loadings. The Mode II fatigue behaviour of nanofibre interleaved laminates was analysed in **Paper V**. The Central Cut-Ply (CCP) method[147] was used to determine the delamination growth rate under cyclic loading as this method is representative for delamination initiation encountered in structural applications, where, for example, delaminations initiate from terminated plies, near free edges or in tapered sections. GFRP (UDO ES500) composites produced by VARTM interleaved with PCL (system #6) and PA6.9 (system #3) nanofibres (SSI configuration) were used for this purpose. More details about the CCP specimen design and experimental setup can be found in **Paper V**. The specimens were subjected to cyclic loads of a certain load level, defined as the ratio of the maximum applied energy release rate during the cyclic experiment to the statically determined interlaminar fracture toughness of the virgin material $G_{IImax}/G_{IIc,virgin}$, while the delamination length was monitored. This allowed the calculation of the delamination growth rate da/dN, which is a measure for the resistance against delamination under cyclic loading. A low delamination growth rate means that the material will be able to withstand more loading cycles before the delaminations will reach a certain (critical) length.

The (Mode II) delamination was found to grow linearly with the amount of loading cycles independent of the applied load level for the virgin material. However, for nanofibre interleaved specimens a distinct transition in delamination growth rate was often observed after a few millimetres of

delamination growth. Initially, the delamination grew relatively slowly for several millimetres at a constant rate after which the delamination growth rate increased to values similar to those of virgin specimens. This is schematically represented in Figure 60. Microscopic images of the cross-section of delaminated specimens taken near the initiation region showed the same delamination behaviour as observed in the static experiments with regular occurrences of interlaminar crossings. At several millimetres away from the initiation region, however, some specimens showed almost complete glass fibre/epoxy debonding with none or only very few interlaminar crossings. Hence, at these points, the delamination growth rate starts to approach that of the virgin non-interleaved specimens as the amount of interlaminar crossings, and thus the amount of bridging nanofibres, is minimal. Observation of the fracture surface indicated that the distance between two neighbouring interlaminar crossings becomes smaller with increasing delamination growth. Eventually, both crossings combined at a certain point of delamination growth after which the delamination grows by glass fibre/epoxy debonding without crossing the interlayer (Figure 61). The transition from a delamination path with interlaminar crossings (Region I delamination growth) to one without (Region II delamination growth) was not instantaneous, but spanned a certain amount of cycles and a certain amount of delamination growth, as it is associated with the disappearance of individual interlaminar crossings. Indeed, analysis of the fracture surface showed that these crossings do not all disappear at the same time (same point of delamination growth).

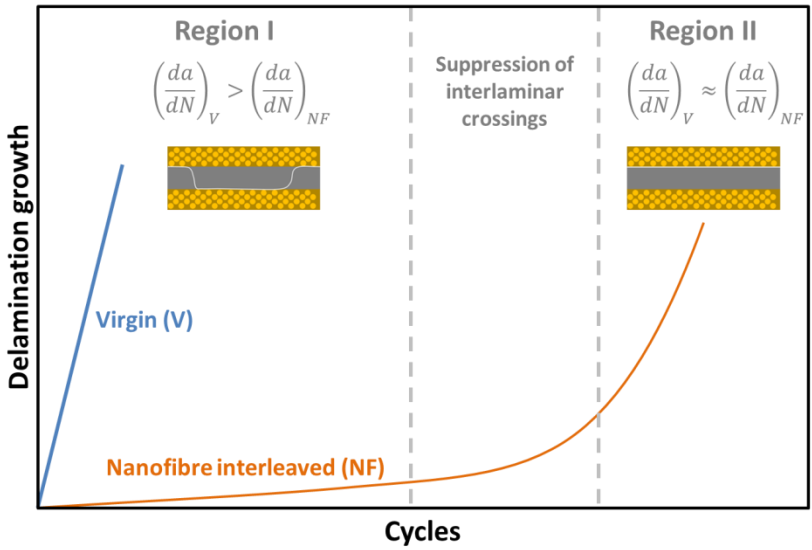

Figure 60 – The Mode II delamination growth of nanofibre interleaved specimens exhibits three regions during fatigue testing: (i) relatively constant delamination growth rate smaller than that of the non-interleaved material (Region I), (ii) rapidly increasing delamination growth rate due to suppression of interlaminar crossings (transition zone), and (iii) delamination growth rate similar to that of the non-interleaved material (Region II).

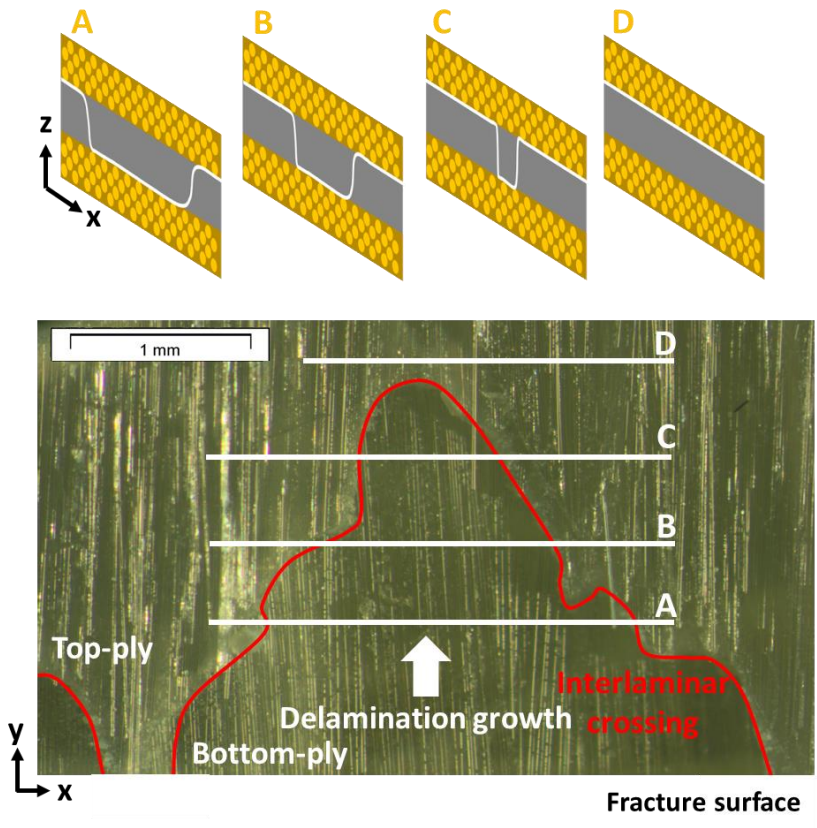

Figure 61 – Illustration of the suppression of an interlaminar crossing resulting in complete reinforcing fibre/matrix debonding after a certain distance of delamination growth.

The transition from Region I to Region II delamination growth in nanofibre interleaved specimens seemed to be predominantly present at low load levels, while a constant delamination growth rate was more often observed at high load levels (Figure 62). Inspection of the fracture surface of delaminated specimens showed that the suppression mechanism is still present at high load levels, but takes place after a longer length of delamination. As such, the transition from Region I to Region II delamination growth was not always visible on the delamination growth data as it happened at delamination lengths higher than the maximum measurable delamination length in the experiment. Particularly at the lower load levels, the driving force for the suppression of

interlaminar crossings seemed to be high, which results in complete glass fibre/epoxy interfacial failure without crossings after several millimetres. As the amount of delamination growth per cycle decreases substantially at lower load levels, the delamination has more time (i.e. more cycles) to realign itself in a more energetic favourable position outside of the toughened interlayer (i.e. at the glass fibre/epoxy interface) after only a few millimetres. Furthermore, the plasticity of the epoxy matrix increases at lower strain rates (Section 3.1.2) which adds to the driving force for the suppression of interlaminar crossings at low load levels as the increased plasticity also has a toughening effect. The interlaminar crossing suppression was also observed on the fracture surfaces of specimens tested under static conditions, but there it took several centimetres before all the interlaminar crossings disappeared. Hence, the mechanism of interlaminar crossing suppression seems to always be present in nanofibre interleaved specimens, but the length at which all the crossings disappear depends on the type of loading (high load level, low load level, static) and on the type of nanofibre system (Figure 62).

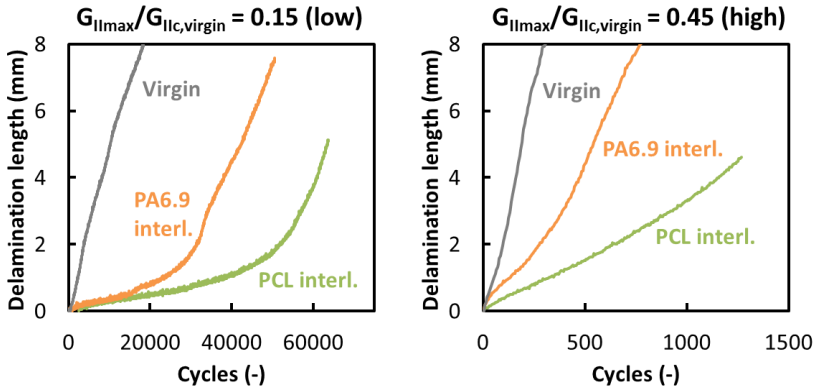

Figure 62 – At low load levels, nanofibre interleaved specimens show a substantial reduction in delamination growth rate compared to virgin specimens during Region I delamination growth. At higher load levels, a constant delamination growth rate (but also lower than that of virgin specimens) is more often observed.

The delamination growth rate as a function of load level for the nanofibre interleaved laminates is given in Figure 63. The plotted delamination growth rates are those obtained during Region I delamination growth. Both PCL and

PA6.9 nanofibre interleaved specimens showed an overall decrease in da/dN as compared to the virgin specimens, indicating an improved delamination resistance under fatigue loading. Improvements in delamination growth rate up to 15 times compared to the virgin material were obtained for individual specimens. It is worth noting that the PCL nanofibre interleaved specimens performed best over the range of load levels tested. SEM analysis of the fracture surface confirmed the existence of nanofibre bridging zones at interlaminar crossings and interlaminar microcracks similar to static tested specimens.

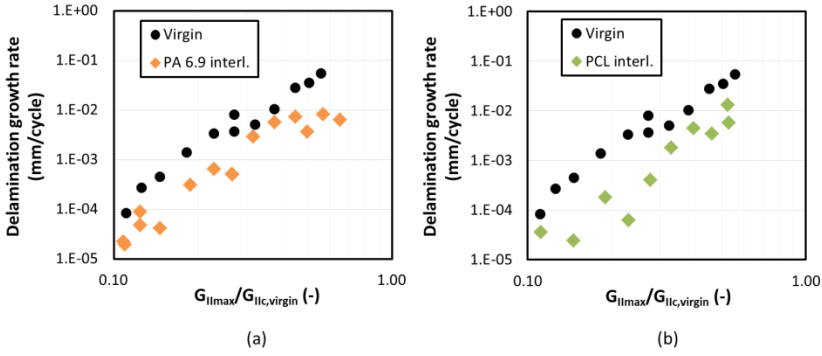

Figure 63 – The delamination growth rate decreases for laminates interleaved with PA6.9 (a) and PCL (b) nanofibrous veils (each point represents an individual specimen). Overall improvements up to one order of magnitude are obtained for the nanofibre interleaved laminates. The PCL interleaved specimens show the best improvements over the whole load severity range considered.

3.3.7 Nanofibre/matrix adhesion strength

It is clear from the results mentioned in Section 3.2.2 for PA6 and PCL nanotoughened laminates that the nanofibre/matrix adhesion is important for toughness improvements, especially under Mode I loading conditions. Yet, it is still a comparison between systems interleaved with chemically and mechanically different nanofibres making it difficult to really quantify the adhesion effect. Therefore, the influence of adhesion was analysed in **Paper VI** using only PCL (system #6) nanofibres interleaved (DLC configuration) in GFRP (UDO ES500) composites produced with VARTM. Due to the interaction between PCL polymer and the epoxy resin, the adhesion between the nanofibres and the matrix can be varied. Earlier studies have already shown that a PCL/epoxy blend can result in a single homogeneous amorphous phase with a glass transition temperature intermediate between those of both single components, i.e. $T_{g,PCL} < T_{g,blend} < T_{g,epoxy}$[148,149]. Hence, the PCL and epoxy are miscible at the molecular level and form a single phase in which there is no macroscopic distinction between both components. This mechanism can be exploited to create a strong interfacial bond between an epoxy resin and a solid PCL polymer. Indeed, as a solid PCL phase is brought into contact with the uncured liquid epoxy resin, the PCL/epoxy miscibility can result in the formation of a blended structure at the interface. This creates molecular diffusion/mixing between the PCL and epoxy which, upon curing, can result in better interfacial strength between both polymers due to molecular interlocking. The formation of this blend interface will of course depend on the mobility of both PCL and epoxy molecules, the contact time, the temperature and the affinity between both polymers. During curing of the epoxy resin – which is performed at temperatures well above $T_{g,PCL}$ (-60°C) – the mobility of the epoxy resin will quickly decline after gelation or vitrification. Hence, the contact time in which PCL and epoxy can blend, is limited by the curing reaction itself. The temperature at which the curing occurs thus has a direct influence on the available contact time for blending. The temperature also affects the mobility of the PCL polymer, especially when the temperature reaches the melting onset. As such, the curing cycle that is used will evoke a cure-induced self-fusion or not. The proposed mechanism is illustrated in Figure 64.

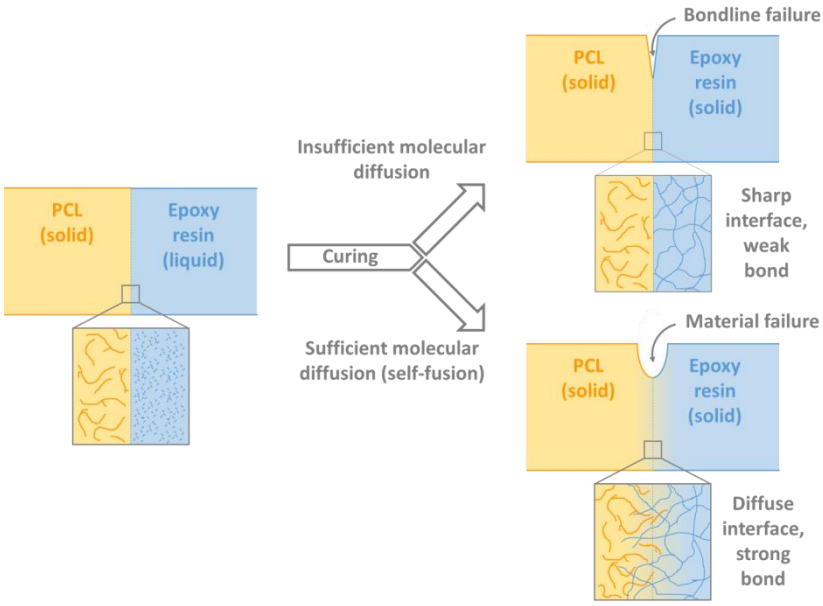

Figure 64 – Mechanism of cure-induced self-fusion resulting in a strong bond between PCL and epoxy.

Using double butt-jointed tensile specimens with controlled PCL/epoxy interfaces, the effect of curing cycle temperature on the bond strength was evaluated. The results of the tensile tests are illustrated in Figure 65 and showed a clear trend in increasing bond strength with increasing cure temperature. For cure temperatures between 25°C and 35°C, the failure of the tensile specimens was at one of the PCL/epoxy interfaces due to limited bond strength between PCL and epoxy. Nevertheless, the bond strength increased from 2 MPa at a cure temperature of 25°C to 6 MPa at a cure temperature of 35°C which is three times higher. At cure temperatures equal to or above 40°C, the bond strength became higher than the bulk PCL yield strength. The tensile specimens showed yielding of the PCL near one of the interfaces at a stress equal to the bulk PCL yield stress and failed by extensive elongation of the bulk PCL phase instead of the clear interfacial fracture in the specimens cured below 40°C. This shows that cure cycles above 40°C resulted in enough molecular mixing between PCL and epoxy near the interface, resulting in a diffuse boundary which increased the bond strength above the bulk PCL strength.

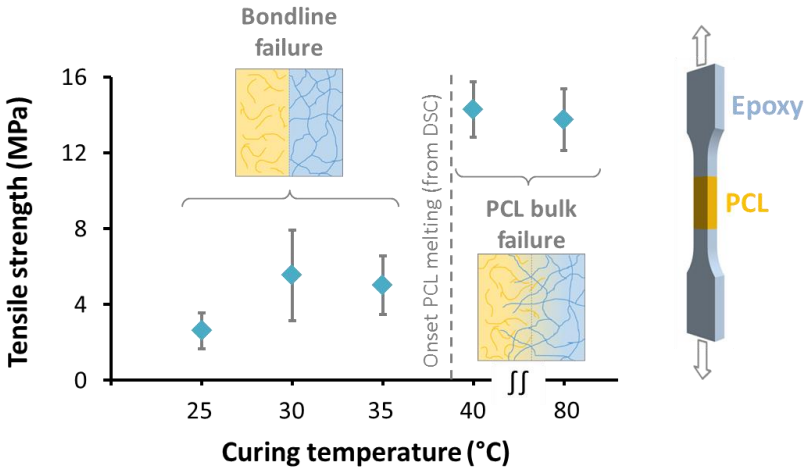

Figure 65 – Tensile strength of the double butt-jointed specimens at different isothermal cure temperatures show an increased bond strength at higher curing temperatures (specimens in which no self-fusing occurred had a bond strength of essentially zero).

The principle of the cure-induced fusing mechanism was used to produce nanotoughened composite laminates with different degrees of PCL nanofibre/matrix bond strength by isothermally curing them at a fixed temperature of 30°C, 40°C, 50°C or 80°C. Unmodified virgin composite laminates were produced in the same manner for comparison. These laminates were then tested for their Mode I and Mode II interlaminar fracture toughness (Figure 66). Note that for the virgin specimens both the Mode I as well as Mode II interlaminar fracture toughness were independent of the cure cycle as its delamination resistance was mainly determined by glass fibre/matrix debonding.

Under Mode I loading of the specimens, which promotes debonding of the nanofibres, the delamination propagated by interfacial debonding of the nanofibres and the delamination resistance was hardly improved at low curing temperatures (30°C and 40°C). However, when the bonding between the nanofibres and the epoxy was improved by the self-fusion mechanism, the energy take-up of the nanofibres increased, resulting in an improvement of the Mode I interlaminar fracture toughness at higher cure temperatures (> 50°C).

Note that the morphology of the nanofibres was lost when the composite was cured at 80°C as this temperature is above the melting point of PCL resulting in a blended zone larger than the nanofibres themselves. The highest improvements were found for cure cycles of 50°C and above. Analysis of the delaminated fracture surfaces with SEM confirmed that the adhesion between the nanofibres and epoxy improves with increasing cure temperature while their nanofibrous morphology disappears, see Figure 67. At low curing temperatures (30°C and 40°C), clearly outlined nanofibres are visible on the fracture surface. Furthermore, the nanofibres of the Mode I loaded specimens showed a high degree of debonding which was visible on the SEM images as imprints left by peeled nanofibres. The specimens cured at 50°C showed better bonding, but the morphology of the nanofibres became less clear. For the specimens cured at 80°C, no clear nanofibres were observed anymore and the interlayer is comprised of a single homogeneous phase.

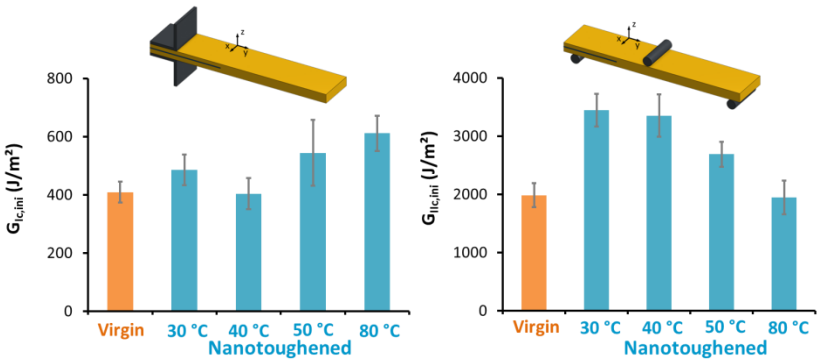

Figure 66 – Mode I and Mode II interlaminar fracture toughness for virgin and hybrid laminates cured at different temperatures. Increasing the curing temperature results in a better Mode I delamination resistance, but a lower Mode II delamination resistance.

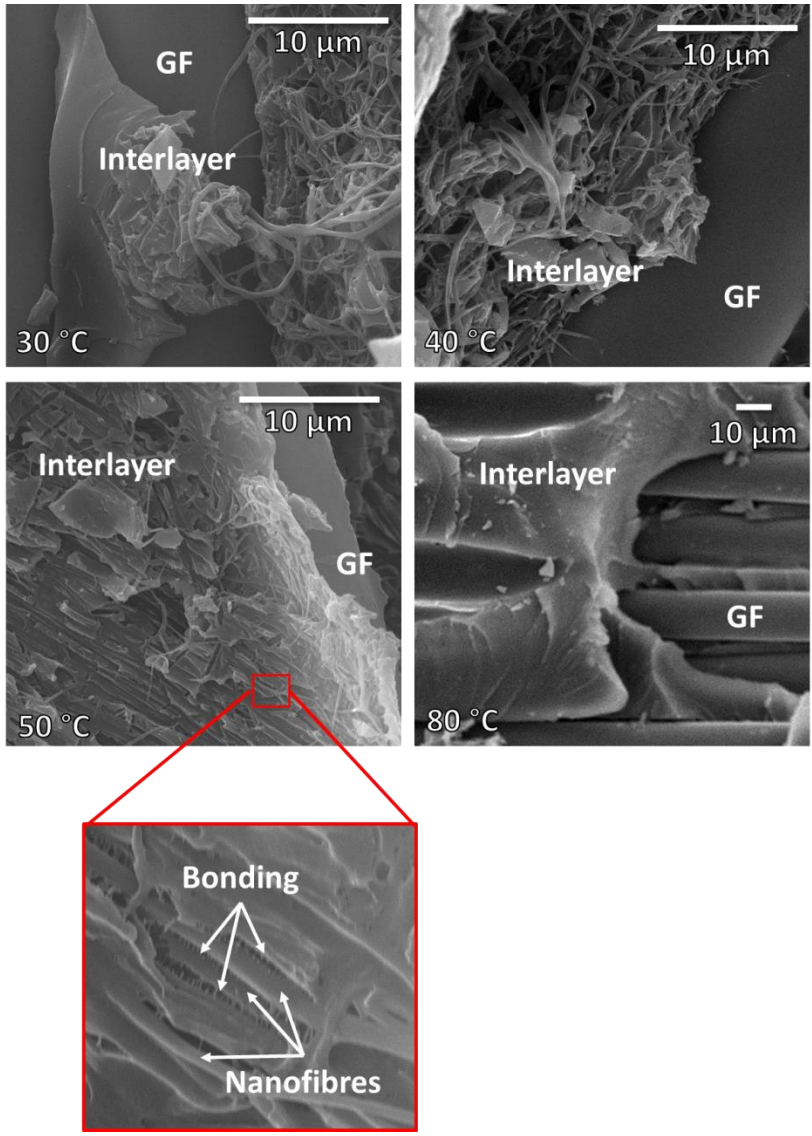

Figure 67 – For cure cycles of 30°C to 50°C, increased bonding is observed between the nanofibres and the epoxy matrix, while the nanofibre morphology becomes less clear. At 80°C, the interlayer is a homogeneous phase indicating that the nanofibres completely dissolved into the epoxy resin. (SEM images taken from Mode I delaminated specimens)

Under Mode II loading conditions, one would expect a relatively stable Mode II interlaminar fracture toughness independent of the isothermal curing temperature. However, there was a clear decreasing trend visible with increasing cure temperature which is opposite to the trend observed under Mode I loading. This trend cannot be associated with a difference in interfacial strength, but instead, reveals that the Mode II toughness improvement is dependent on the nanofibrous morphology itself. Indeed, with increasing cure temperature, a more diffuse interface is created and the morphology of the nanofibres starts to differ from their initial morphology. At 80°C, the nanofibrous morphology is completely lost which resulted in a decrease of the Mode II fracture toughness compared to the virgin material. These results indicate the importance and duality of both adhesion and morphology aspects to optimize the nanotoughened composites. From a practical aspect, the best overall damage resistance is obtained when a significant increase in both Mode I and Mode II delamination resistance occurs at the same time.

Next, a two-step curing cycle was investigated in order to optimize the interfacial bond strength while maintaining the morphology of the nanofibres. More specifically, a low temperature ($T < T_{m,PCL}$) curing step fixed the nanofibre morphology as the diffusion of PCL will be limited while the epoxy resin reacts. A second curing step at elevated temperature ($T > T_{m,PCL}$) allowed enough diffusion of the PCL into the partially reacted epoxy to have substantial self-fusing. Of course, this implies that diffusion of the PCL in the epoxy can still happen. Therefore, it is important that the time and temperature of the first curing step is chosen such that the epoxy is viscous/solid enough to maintain the nanofibre morphology (as a sort of self-formed mould), while still be "open" enough to allow sufficient mixing between PCL and epoxy molecules. A two-step curing procedure was used with a curing step at 25°C for 24 hours followed by a curing step at 80°C for 15 hours. The results show that both Mode I and Mode II interlaminar fracture toughness were significantly increased at the same time, something which was not possible using a single curing step (Figure 68). The Mode I interlaminar fracture toughness was even higher than all the ones obtained for single step curing. The Mode II interlaminar fracture toughness was similar to those of the laminates isothermally cured at 30°C and 40°C and significantly higher than those obtained with a single curing step at 50°C or 80°C. Analysis of the fracture surface with SEM showed the duality between the bond

strength and morphology of the nanofibres. The specimens showed no real signs of bad bonding such as imprints or peeled nanofibres, but rather showed a lot of deformation due to a good load transfer at the epoxy/PCL interface. The morphology of the nanofibres was in between a complete dissolution (as observed during a single curing step at 80 °C) and the non-dissolved morphology (as observed during a single curing step at low temperature).

Another interesting approach to obtain good bonding and maintain the nanofibre morphology is the use of electrospun core-shell nanofibres. The technique of coaxial electrospinning allows the production of core-shell structured nanofibres for which there is a wide variety in core and shell polymer possible. Apart from the requirement of a coaxial needle, this technique does not differ that much from regular electrospinning and is thus also capable of producing nanofibrous veils for nanotoughened composites. The coaxial electrospinning technique was used to produce 70/30 m% PA6/PCL core-shell nanofibres. While the morphology of the PA6 core will not be affected by the curing temperature, the PCL shell which surrounds the core will be able to bond with the epoxy matrix. It is expected that there was also some interdiffusion, and thus adhesion, between the PA6 core and PCL shell as both solutions were spun from the same solvent and came into contact in the coaxial needle. The specimens were made with a single curing step at 80°C to have a high conversion of the epoxy resin and limit the curing time. The Mode I and Mode II interlaminar fracture toughness values of virgin laminates and nanotoughened laminates containing PCL nanofibres, PA6 nanofibres and PA6/PCL core-shell nanofibres are shown in Figure 69. All specimens underwent the same curing conditions and had the same amount of nanofibres inside. Compared to the single component nanofibre systems, the core-shell structured nanofibres resulted in toughness improvements under both Mode I and Mode II loading conditions. This indicates that the bonding was improved due to the PCL shell, while the nanofibre morphology remained due to the PA6 core. Analysis of the fracture surface with SEM indeed showed clearly distinguishable nanofibres that bridge cracks without much debonding/peeling.

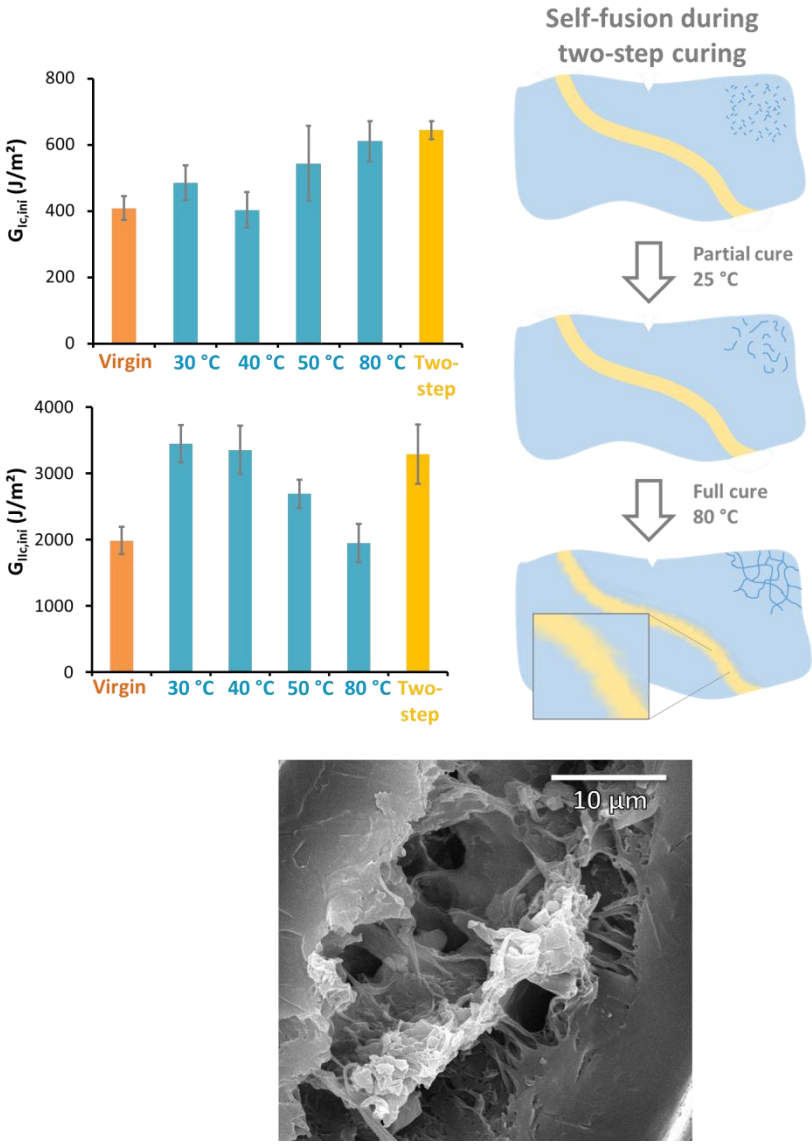

Figure 68 – Using a two-step curing cycle results in good improvements of both Mode I and Mode II interlaminar fracture toughness.

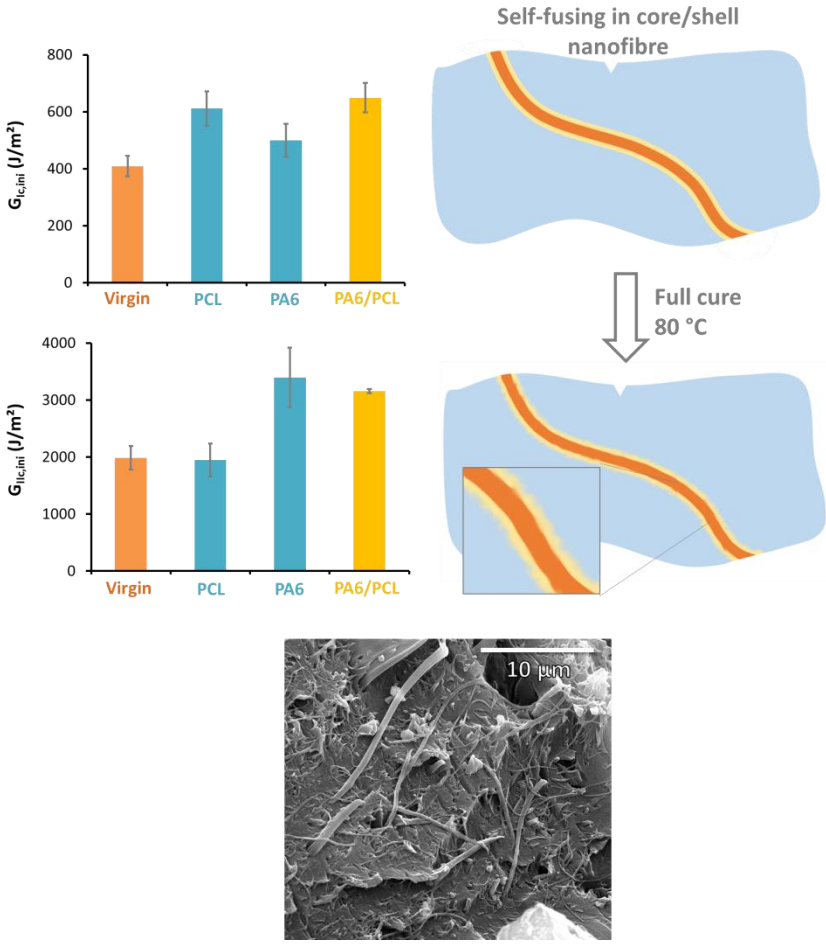

Figure 69 – Self-fusion with PA6/PCL core-shell nanofibres results in a synergetic effect between bond strength and nanofibre morphology. The core/shell nanofibre based interleaved laminates have a better delamination resistance under both loading conditions than those using single component nanofibres.

3.3.8 Precracking effects under Mixed Mode loading

The delamination resistance of virgin and PCL (system #6) nanofibre interleaved GFRP (UDO ES500) laminates was also assessed under Mixed Mode loading conditions using Single Leg Bend (SLB) experiments. The SLB test is similar to an ENF test, but the lower delaminated leg of the specimen is removed. This causes opening as well as shearing stresses at the crack tip resulting in delamination propagation under a Mixed Mode loading (Figure 70). The specimen design was the same as used for the ENF test. The Mixed Mode initiation interlaminar fracture toughness $G_{I/IIc}$ was calculated according to the Compliance Based Beam Method[150]:

$$G_{I/IIc,ini} = \frac{21P_c^2 a_e^2}{16E_f B^2 h^3} + \frac{3P_c^2}{40G_{13}B^2 h} \quad (4)$$

where P_c is the load at delamination initiation, a_e is the effective delamination length, E_f is the flexural modulus, B is the specimen width, $2h$ is the specimen thickness and G_{13} is the shear modulus. The Mixed Mode loading had a 57% Mode I component and 43% Mode II component.

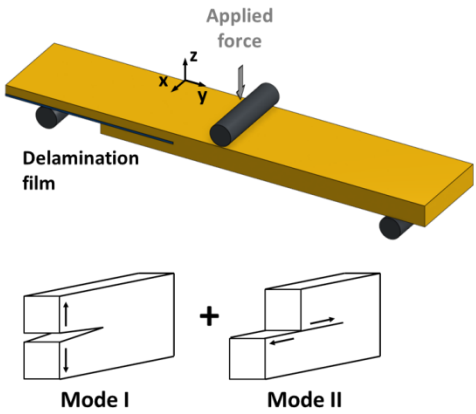

Figure 70 – Illustration of the SLB specimen to determine the Mixed Mode interlaminar fracture toughness.

To assure that the delamination initiates from a natural flaw and not from the initiation film, delamination specimens (DCB, ENF, SLB, …) are usually precracked in the same loading mode as they are tested, i.e. DCB specimens are precracked under Mode I, ENF specimens under Mode II and SLB specimens under Mixed Mode conditions. However, when considering realistic damage events such as those that occur during low velocity impact, the way in which delaminations initiate and grow is much more complex and not as well controlled as in a delamination test. For example, delaminations can initiate under Mode II conditions and grow further under Mode I or Mixed conditions or the other way around. Regarding the low velocity impact experiments performed in Section 3.4.3, it was interesting to test the nanofibre interleaved specimens under Mixed Mode loading, but precracking them in different modes to determine if this influenced the delamination resistance of the nanofibre interleaved composite laminates.

The Mixed Mode interlaminar fracture toughness of virgin and PCL nanotoughened composite laminates is shown in Figure 71. The interlaminar fracture toughness of the virgin specimens was not affected by the precrack mode. On the other hand, a Mode II precrack induces a significant toughening effect in the nanofibre interleaved specimens. Analysis of the fracture surface of the delaminated specimens showed that Mode II precracking resulted in the initiation of more interlaminar crossings than the other loading modes (see also Section 3.3.1). Upon subsequent Mixed Mode loading, this resulted in more nanofibre bridging zones which increased the delamination resistance. If these results are generalised, the best improvements in interlaminar fracture toughness – regardless of the delamination mode – can be attained if the delamination is initiated under a Mode II loading regime that promotes the occurrence of many interlaminar crossings. Such insights can be of importance in applications because nanotoughened regions where delaminations initiate under Mode II conditions will benefit more from nanofibre addition than regions where delaminations initiate under Mode I loading conditions. Hence, different delamination regions might require different types of nanofibres.

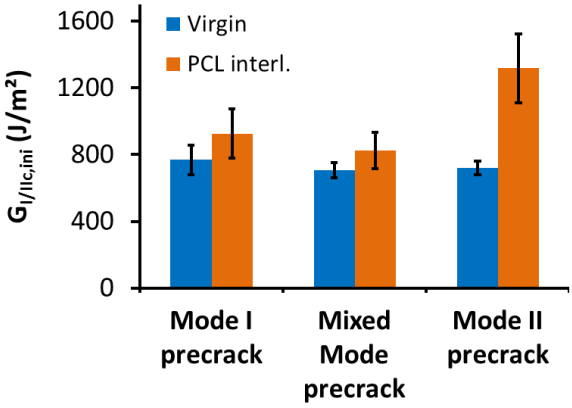

Figure 71 – The $G_{I/IIc,ini}$ obtained for virgin and PCL nanofibre interleaved specimens using different precracking modes shows that a Mode II precrack promotes the occurrence of interlaminar crossings resulting in a substantial increase in $G_{I/IIc,ini}$ compared to the virgin material.

3.3.9 Tensile properties of the electrospun fibres

During nanofibre bridging, nanofibres experience tensile stresses which take up (plastic) energy (Section 3.1.1). The tensile properties of the nanofibres will thus likely have an effect on the effectiveness and even development of nanofibre bridging. This effect was analysed in **Paper VII** using mechanically tuneable SBS (system #8) electrospun fibres which were developed within our research group[81]. These were interleaved (SSI configuration) in GFRP (UDO ES500) laminates produced with VARTM. Note that although the SBS fibres have diameters of approximately 2 µm and cannot be classified as nanofibres, they still have a diameter about 1/10th lower than the reinforcing fibres. Using a MDI-TAD cross-linker post-treatment, it was shown that the mechanical properties of individual electrospun SBS fibres can be varied from very stretchable to stiff (Figure 72)[81]. The cross-linking degree is quantified by the ratio of the number of MDI-TAD to the number of double bonds (both expressed in mole). The unmodified and low cross-linked SBS fibres had a low E-modulus and high elongation at break, around 10 – 30 MPa and 400 – 600% respectively. The highly cross-linked specimens on the other hand, had a higher E-modulus but lower elongations at break up to 140 MPa and 100% respectively. The difference in tensile properties also caused a distinct difference in energy take-up during straining, i.e. the area underneath the stress-strain curve (Figure 73). The energy take-up of unmodified and low cross-linked SBS fibres only becomes significant when the SBS fibres were elongated up to high strains (> 300%), whereas in the low strain region (< 100%) their energy take-up is very limited. For the SBS fibres with relatively high amounts of cross-linking, the total work of rupture (10 – 15 MPa) was lower, but these fibres did absorb significantly more energy in the low strain region.

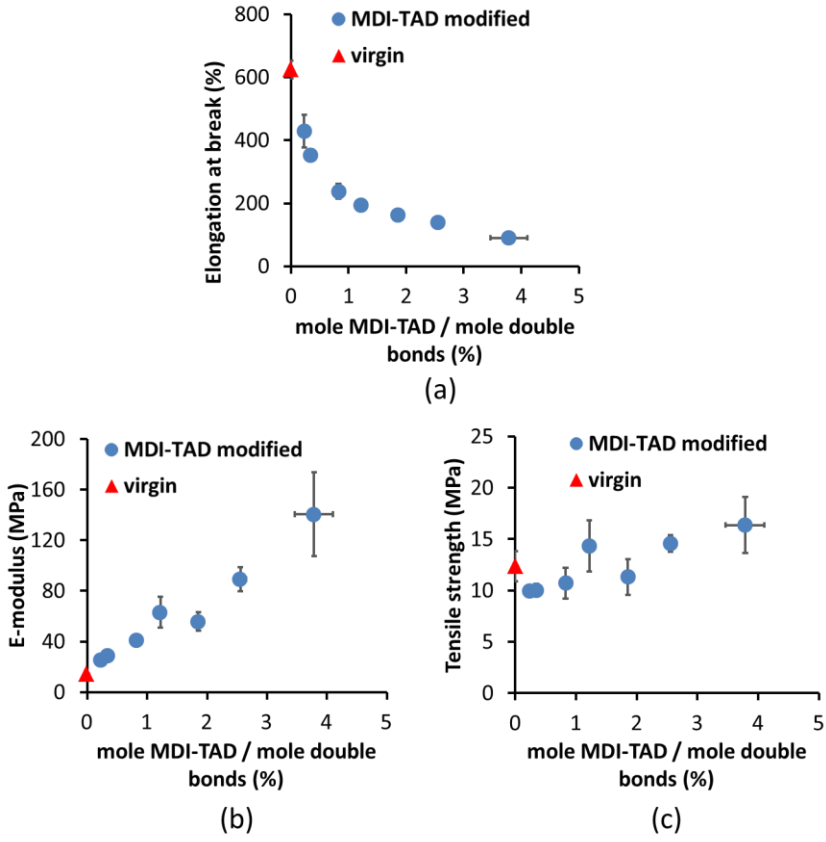

Figure 72 – Influence of the MDI-TAD cross-linking on the elongation at break (a), the E-modulus (b) and the tensile strength (c) of SBS fibres[81].

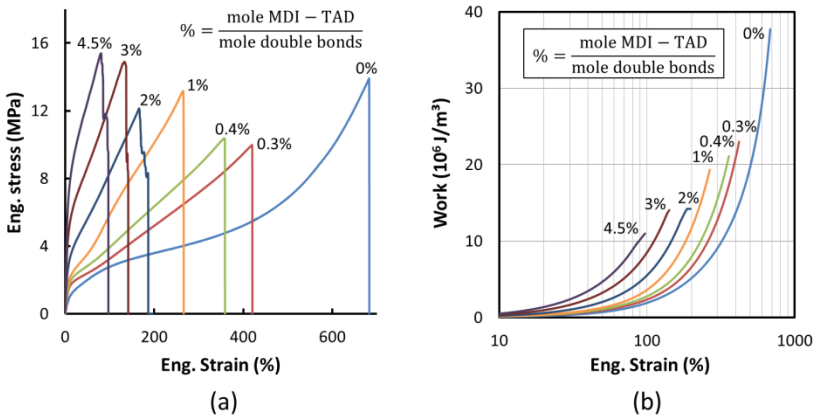

Figure 73 – Representative stress-strain curves for SBS fibres cross-linked with different amounts of MDI-TAD (a) and the resulting work in function of strain as calculated from the area beneath the stress-strain curve (b).

Fibrous veils of SBS were electrospun, post-treated to change their mechanical properties and interleaved (SSI configuration) in GFRP composite laminates produced by VARTM. The laminates were subsequently tested for their Mode I and Mode II delamination resistance. Microscopic analysis of the delaminated specimens showed a strong dependency of the fibres' tensile properties on the delamination path behaviour (Figure 74).

- → The low cross-linked SBS fibres (0 – 0.5%) provided little to no resistance to crack growth and the delamination progressed completely through the SBS fibre modified interlayer. Due to the low stiffness of these SBS fibres, the interlayer becomes the weakest zone and the delamination path thus stays within the interlayer.
- → For intermediate cross-linked SBS fibres (0.5 – 2%), the delamination path was deflected towards the reinforcing fibre/matrix interface due to an increased stiffness of the SBS fibres. Both Mode I and Mode II delaminated specimens showed regular occurrences of interlaminar crossings.
- → At high cross-linking (> 2%), the delamination was completely deflected towards the reinforcing fibre/matrix interface and almost no

interlaminar crossings occurred under Mode I loading, while regular crossings were still observed for Mode II delaminated specimens.

These results show that the tensile properties of the electrospun fibres will affect the way in which the delaminations propagate in an interleaved composite laminate.

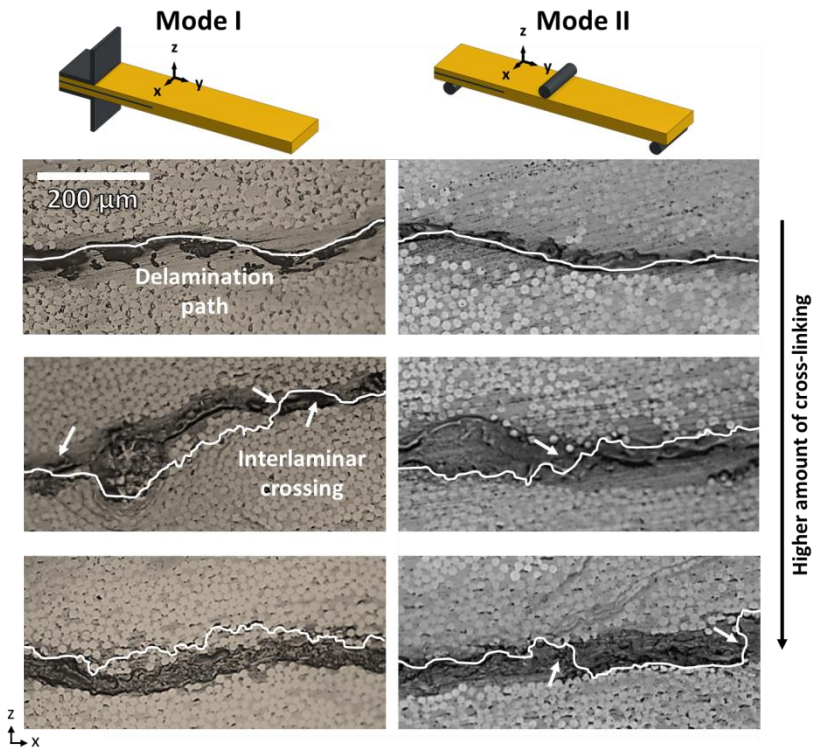

Figure 74 – The delamination path is deflected towards the reinforcing fibre/matrix interface for higher cross-linked SBS fibre modified interlayers. Under Mode I loading almost no interlaminar crossings are observed at very high cross-linking, while under Mode II loading regular crossings can still be observed.

As the low cross-linked SBS fibres resulted in delamination growth through the modified interlayer, one would expect the highest increases in delamination resistance for these laminates as the amount of nanofibre bridging will be much higher. Yet, the Mode I and Mode II interlaminar fracture toughness were found

to be better for intermediate and high cross-linked SBS fibres respectively where only regular interlaminar crossings occur (Figure 75). Although this might seem contradictory, one should consider the amount of energy take-up by the nanofibres. The low cross-linked SBS fibres need to be strained to more than 400 – 500% before they have the same energy take-up as the higher cross-linked fibres. Such high strains are not encountered during the initiation of a delamination. Indeed, the displacement between the delaminated halves is much lower in the ENF experiment than in the DCB experiment. As such, the low cross-linked SBS fibres even decrease $G_{IIc,ini}$, while a small increase in $G_{Ic,ini}$ is recorded. At higher cross-linking, the SBS fibres are able to take up more energy for the same strain level and both $G_{Ic,ini}$ and $G_{IIc,ini}$ increase substantially. This effect resulted in the highest improvements in $G_{IIc,ini}$ at the highest cross-link levels. However, the disappearance of interlaminar crossings at high cross-linking in the Mode I delaminated specimens resulted in an optimum $G_{Ic,ini}$ at intermediate levels of cross-linking around 0.7%.

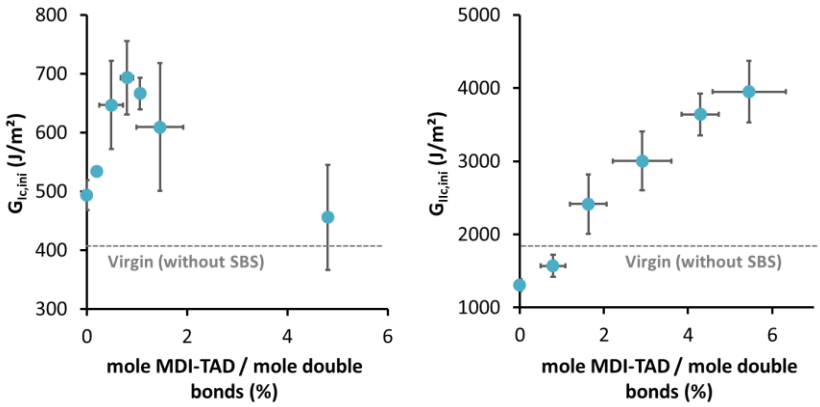

Figure 75 – The Mode I and Mode II interlaminar fracture toughness depend on the tensile properties of the SBS fibres. An optimum $\boldsymbol{G_{Ic,ini}}$ is found at intermediate cross-linking levels, while $\boldsymbol{G_{IIc,ini}}$ increases with increases cross-linking.

3.4 PROPERTIES AND DAMAGE RESISTANCE OF FULLY INTERLEAVED LAMINATES

Section 3.2 and Section 3.3 already clearly illustrated the potential of nanofibrous interleaves to increase the delamination resistance. The test methods used in these sections, however, all used a controlled delamination initiation and propagation. Furthermore, the delamination specimens typically have a unidirectional layup. To provide a further link between the *interlaminar level* and the mechanical response that can be expected in real-life situations, multi-directional fully interleaved composite laminates – Level 3 – are considered in this section. These laminates are still tested using coupon specimens, but are more closely related to the lay-up and loading conditions which can be expected in real-life applications. Three different aspects of fully interleaved cross-ply laminates are highlighted in this section: (i) the general mechanical response (tensile, shear and flexure), (ii) the open-hole tension strength, and (iii) the (post) low-velocity impact properties. All the laminates considered in this section were GFRP cross-ply $[0°/90°]_{2s}$ laminates produced by VARTM. The nanofibres were only interleaved between plies of 0° and 90° orientation. The effect of the nanofibres on the general mechanical properties and the open hole strength was analysed in **Paper II**, while the impact properties of nanofibre interleaved laminates are analysed in **Paper VIII**.

3.4.1 General mechanical properties

The laminates under consideration were interleaved (DLC configuration) with 10 g/m² of PCL (system #6) nanofibres. The choice for this nanofibre system is justified as it provided the best increases in delamination resistance under both Mode I and Mode II loading conditions. Furthermore, PCL also has low mechanical properties and a low glass transition temperature compared to polyamide nanofibres. As such, if the PCL nanofibrous interleaves would affect the mechanical properties other than delamination resistance negatively (e.g. stiffness), this is expected to be worse for PCL nanofibres than for polyamide nanofibres.

The tensile properties were determined according to ASTM D3039[151] using $[0°/90]_{2s}$ specimens with nominal dimensions of 250 x 30 x 3 mm³ (0°-direction is the loading direction). A clip-on extensometer was used to measure the

longitudinal strain. The test was displacement-controlled using a deformation rate of 2 mm/min. At least three specimens were tested for each configuration. The (in-plane) shear response was measured according to ASTM D3518[152] on $[+45°/-45°]_{2s}$ tensile specimens of 250 x 30 x 3 mm³ instrumented with two perpendicular strain gauges to determine the shear. The test was performed similar to the tensile tests on $[0°/90°]_{2s}$ specimens. The flexural properties were determined according to ASTM D7264[153] using $[0°/90°]_{2s}$ specimens (0°-direction is the length direction). A support span-to-thickness ratio of 32:1 was used and the nominal width of the specimens was 13 mm. The flexural properties were determined from the load-crosshead displacement curve. Note that these specimens were made using the UDO ES500 reinforcement, while the tensile specimens were made using the Roviglas R17/R430 reinforcement.

The mechanical response under each loading is given in Table 3. These show that the presence of the nanotoughened interlayers does not really affect – be it positively or negatively – the general mechanical properties of the interleaved laminates. The tensile and flexural modulus are maintained, but a slight decrease in the in-plane shear modulus can however be observed. This is most likely due to the in-plane shear loading which mainly stresses the resin rich interlayers and to lesser extent the complete laminate. From the results of Section 3.1.1, it is known that the PCL nanofibres result in a lower stiffness of the nanotoughened epoxy, and it can thus be expected that this is reflected in the in-plane shear modulus. The tensile, shear and flexural strength are all maintained.

The glass transition temperature of the nanofibre interleaved composite laminate was determined according to ASTM D7028[154] on $[0°/90°]_{2s}$ and $[\pm45°]_{2s}$ specimens using a single cantilever bending fixture. The experiments were performed on a Q800 DTMA analyser from TA Instruments. A displacement amplitude of 20 µm was imposed with a frequency of 1 Hz while the temperature was ramped up to 150°C with a heating rate of 2.5°C/min. The T_g of the virgin and nanofibre interleaved specimens – determined from the step in the storage modulus – was 82 ± 2°C and 80 ± 2°C respectively. Due to the presence of the PCL nanofibres ($T_g = -60$°C) only in the interlayers, the T_g of the bulk composite laminate is maintained. This shows that even polymers with

a much lower T_g than the epoxy resin itself can be used for toughening purposes.

Table 3 – Overview of the tensile, shear and flexural properties for a virgin and PCL nanofibre interleaved laminate.

Property	Virgin	Nanofibre interleaved
Tensile modulus (GPa)	25 ± 1	24 ±1
Tensile strength (MPa)	574 ± 50	596 ± 50
Shear modulus (GPa)	4.4 ± 0.2	3.9 ± 0.2
Shear strength (MPa)	62 ± 2	59 ± 2
Flexural modulus (GPa)	29 ± 2	30 ± 1
Flexural strength (MPa)	311 ± 35	346 ± 10

3.4.2 Open hole tensile strength

The open hole tensile test is used to determine the stress required to break a composite specimen with a centrally located hole. The hole results in stress concentrations inside the material and a reduced net cross-section which both lower the tensile strength compared to pristine material. This test method is commonly used in the aerospace industry to evaluate the strength in a notched component, for example when fasteners are used. As such it can be a limiting design parameter for many composite structures. Open hole tensile tests were performed on $[0°/90°]_{2s}$ specimens (Roviglas R17/475) with a size of 300 x 36 x 3 mm³ according to ASTM D5766[155]. The specimens had a central hole of 8 ± 0.1 mm in diameter. The nanofibre interleaved laminates contained 10 g/m² of PCL (#6) nanofibres in a DLC configuration.

The open hole strength increased from 360 ± 7 MPa for the virgin material to 387 ± 19 MPa for the nanofibre interleaved laminates. As opposed to tensile failure in the pristine $[0°/90°]_{2s}$ material, the failure mode in the open hole specimens was heavily delamination dominant. Figure 76 shows images of an open hole tensile specimen during failure. The stress concentrations located near the hole caused delamination initiation between the 0°/90° plies. With

increasing tensile load, the delaminations propagated further towards the sides of the specimen. This reduced the effective cross-section of the laminate which is able to take up the tensile stress, resulting in faster delamination growth up till failure of the specimen. When nanofibres are interleaved, the resistance against delamination initiation and propagation is increased. This allowed more stress take-up by the 0°-plies in the nanofibre toughened specimen laminates before the delamination reached a critical length and the specimen abruptly failed. Failed open hole tensile specimens are shown in Figure 77. Nanofibre interleaved specimens showed significantly less delamination which resulted in the improvement of the open hole tensile strength. This is a clear illustration of the link between the nanotoughened interlayer and its effect on the mechanical behaviour of a fully interleaved laminate. Failure modes in which delaminations occur, such as encountered at stress concentrators, are improved by the presence of the nanotoughened interlayers due to an increased delamination resistance.

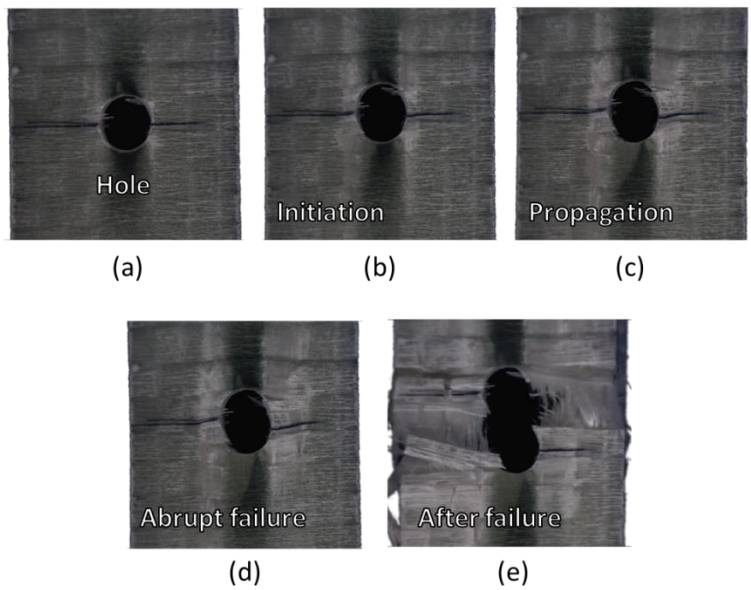

Figure 76 – Damage sequence during failure of an open hole tensile specimen (a – e). The stress concentrations initiate delaminations between 0°/90° plies which propagate and result in abrupt failure of the specimen.

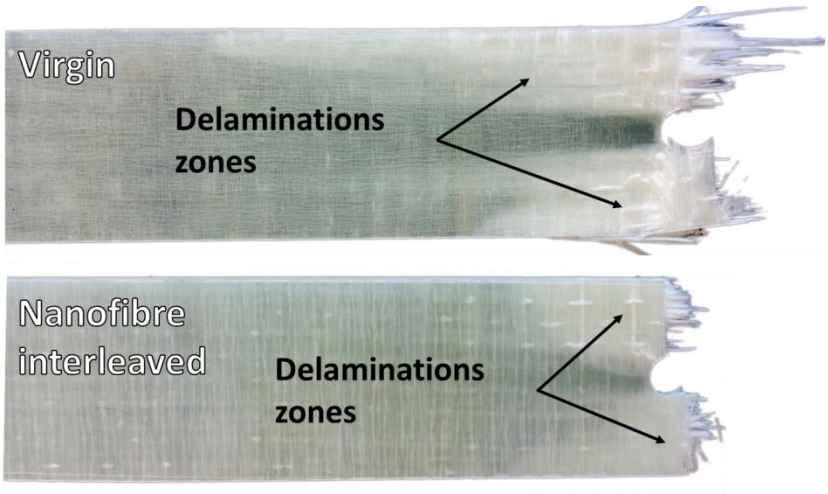

Figure 77 – Nanofibre interleaved open hole tensile specimen show significantly less delamination damage due to an increase in the delamination resistance.

3.4.3 Low velocity impact resistance

Low velocity impact (LVI) experiments were performed on virgin and nanofibre interleaved cross-ply laminates (UDO ES500). PA6.9 (system #3) and PCL (system #7) nanofibrous veils of 6 g/m² and 12 g/m² were investigated. More experimental details can be found in Chapter 2.

An example of the load exerted by the specimen on the impactor during the impact event is shown in Figure 78. The curve is characterised by four (time) regions which relate to the mechanical response of the composite specimen. Time t_1 and t_5 correspond to the beginning, i.e. impactor contacts specimen, and the end of an impact event, i.e. impactor rebounds from the specimen. Region $t_1 - t_2$ represents elastic bending of the specimen. At this point, no major damage occurs although initiation of sub-critical matrix cracks and delaminations can already occur[136]. Region $t_2 - t_3$ is characterised by a small load drop at t_2 and a change in slope of the load-time curve indicating a first decrease of the stiffness of the specimen due to (more pronounced) matrix cracking and delamination onset[156]. At t_3, the velocity of the impactor is zero and its kinetic energy has been transferred completely to the specimen. A certain fraction of the energy will be transferred back to the impactor (elastic energy) causing the impactor to be accelerated upwards, while the other fraction is absorbed in the specimen (dissipated energy). Region $t_3 - t_4$ shows a drop in the load due to major damage propagation in the specimen. The final stage, $t_4 - t_5$, corresponds to the residual stiffness and strength of the specimen causing the impactor to be rebounded from the specimen. Figure 79 shows the impact event as recorded by high speed cameras during the different regions.

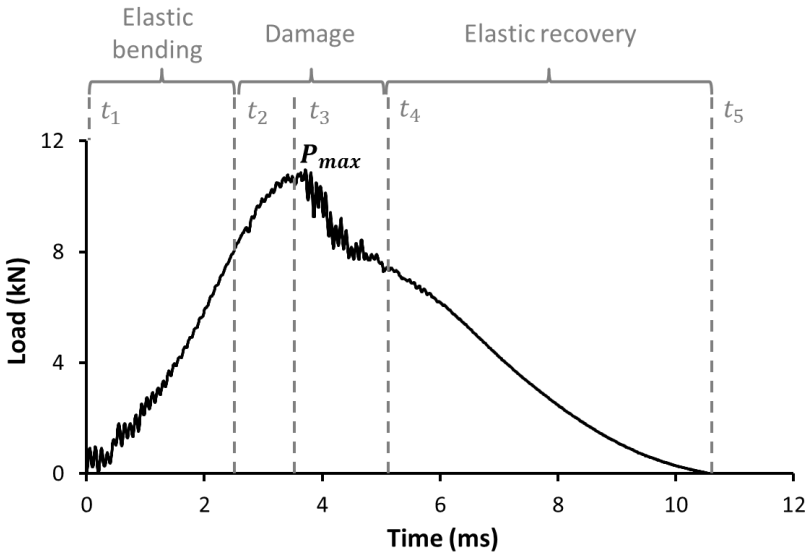

Figure 78 – Load versus time recorded during an impact event shows four regions: elastic bending ($t_1 - t_2$), (minor) damage initiation ($t_2 - t_3$), major damage ($t_3 - t_4$) and elastic recovery ($t_4 - t_5$).

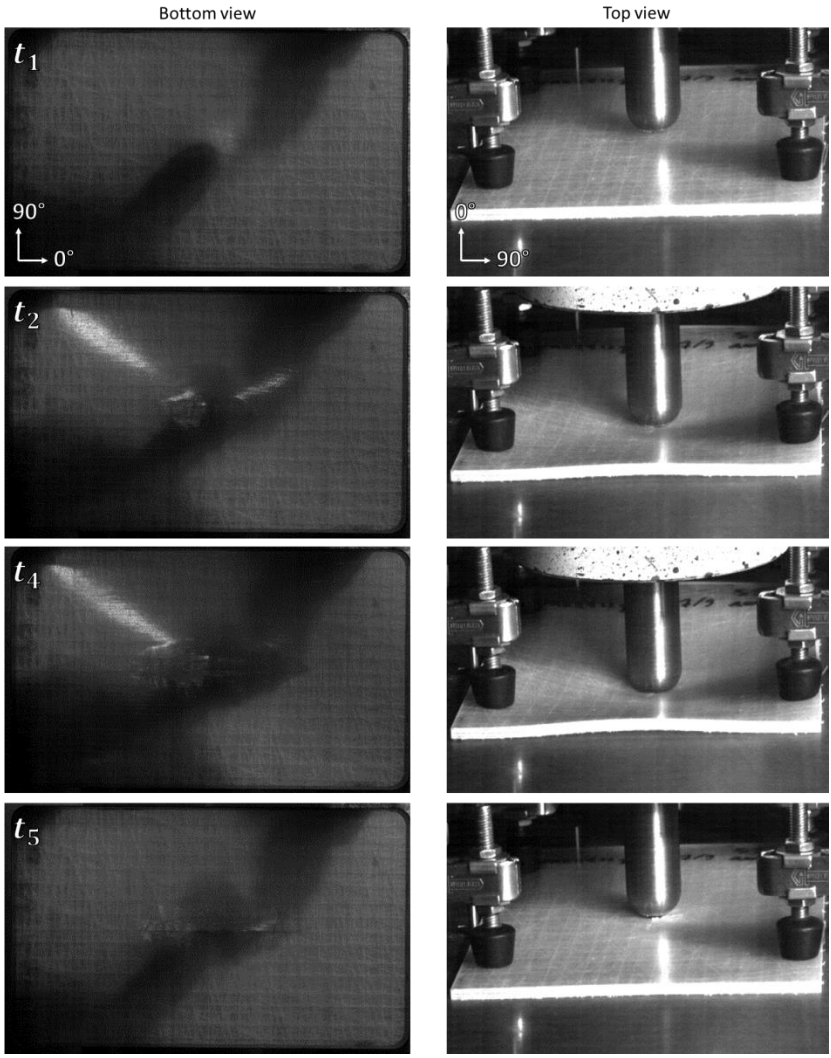

Figure 79 – Images obtained from high-speed camera during an impact event giving a bottom and top view of the specimen at times t_1, t_2, t_4 and t_5.

Representative load-time curves for virgin and nanofibre interleaved specimens at low, intermediate and high impact energies are given in Figure 80. The results show that the $t_1 - t_2$ and $t_2 - t_3$ regions did not differ much for the virgin or nanofibre interleaved material. This indicates that the addition of the nanofibrous interleaves did not affect the elastic behaviour of the laminates in agreement with results of Section 3.4.1. The maximum load P_{max} encountered at t_3 increased for the nanofibre interleaved laminates compared to the virgin material at higher impact energies. This means that the nanofibre interleaved laminates can withstand more load before the sub-critical cracks reach the limit where major damage will occur. Such an effect was also encountered during Mode II delamination of nanofibre interleaved specimens where the energy for sub-critical crack growth increased due to nanofibre bridging (Section 3.3.4 and Section 3.3.5). The major difference between virgin and nanofibre interleaved specimens was however encountered in the $t_3 - t_4$ region for impact energies of 41 J and higher. At this stage, major delamination and interlaminar crack formation between plies took place. The resistance against these damage mechanisms is readily improved by the nanotoughened interlayers. The effect was most visible for the PCL interleaved specimens for which the load-time curve still remained predominantly elastic at impact energies of 67 J. Since the damage was more limited in the nanofibre interleaved specimens, their residual stiffness and strength is higher compared to the virgin specimens and the impactor was rebounded faster as for example visible in the $t_4 - t_5$ region of the specimens subjected to 67 J.

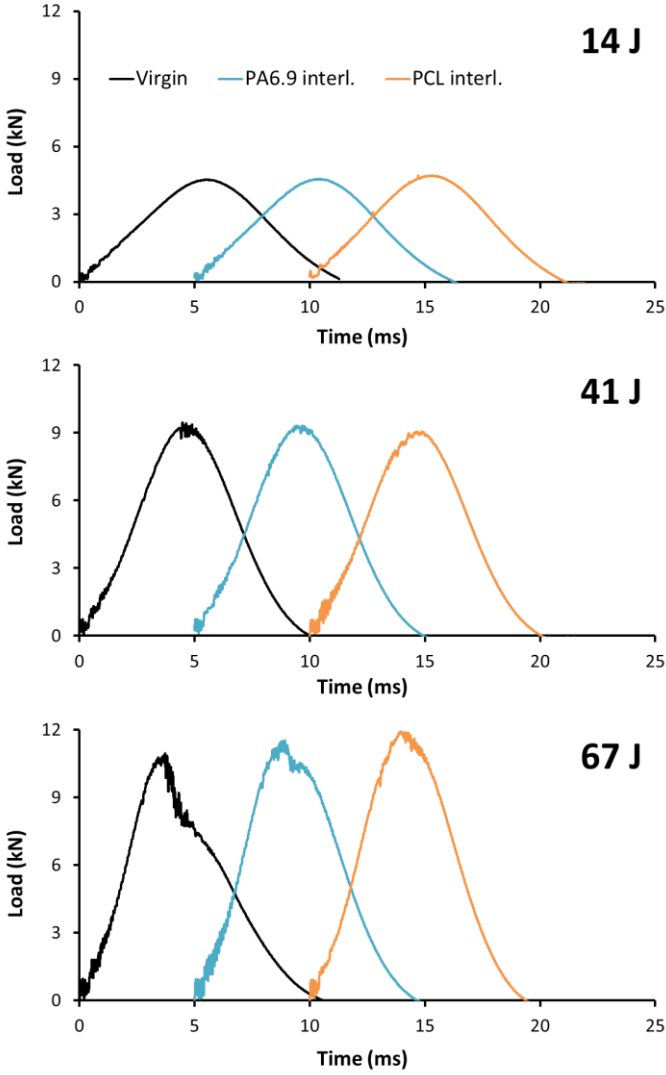

Figure 80 – Load-time curves for virgin, PA6.9 (12 g/m²) interleaved and PCL (12 g/m²) interleaved specimens at impact energies of 14 J, 41 J and 67 J. $\boldsymbol{P_{max}}$ increases with increasing impact energy while the impact events become shorter and more damage occurs in the $\boldsymbol{t_2 - t_4}$ region. Nanofibre interleaved specimens showed less signs of damage development in this region. Curves of PA6.9 and PCL are shifted 5 ms and 10 ms for clarity.

The (projected) damage area after impact was determined by measuring the delaminated area on impacted specimens which was clearly visible due to translucency of the specimens. A series of C-scans on impacted specimens showed that the agreement between the damage area measured by both methods was good. This is illustrated in Figure 81 for three specimens subjected to an impact energy of 67 J. Nanofibre interleaved specimens had a reduction in (projected) damage area and the smallest damage area was obtained with PCL nanofibrous veils. The shape of the damage area was rhombus-like for all tested impact energies. It showed a larger damage growth in the 0°-direction compared to the 90°-direction, most likely caused by the rectangular shaped specimen fixture[136] used in the LVI experiments and the cross-ply layup. Hence, the reduction in damage area is mainly attributed due to a reduction in damage length in the 0°-direction.

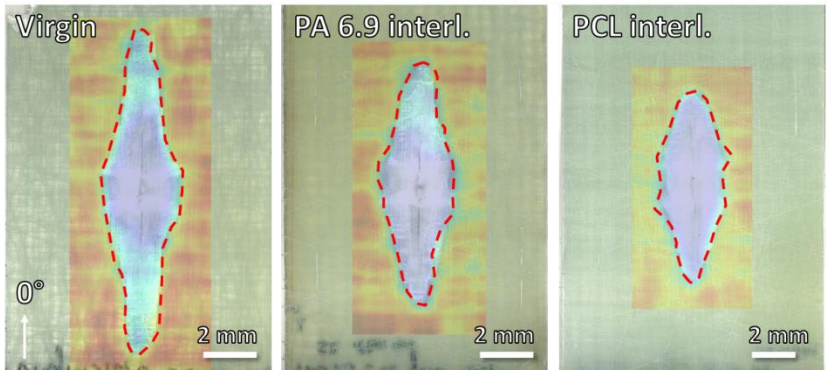

Figure 81 – Optical measured damage area corresponded with the C-scan results. Nanofibre interleaved specimens showed a smaller damage area (mainly by a reduction in damage length). PCL nanofibres resulted in the best improvements.

The (projected) damage area in function of the impact energy is given in Figure 82. The toughening effect of the nanofibres was relatively small at low impact energies, especially for PA6.9 interleaved specimens, but increased significantly at impact energies higher than 40J. Overall, specimens interleaved with PCL nanofibres again showed the highest reductions in damage area. The damage area reduced up to 60% for PCL nanofibre interleaved specimens. The veil

density of the nanofibres did not influence the results and similar improvements are obtained at densities of 6 g/m² and 12 g/m².

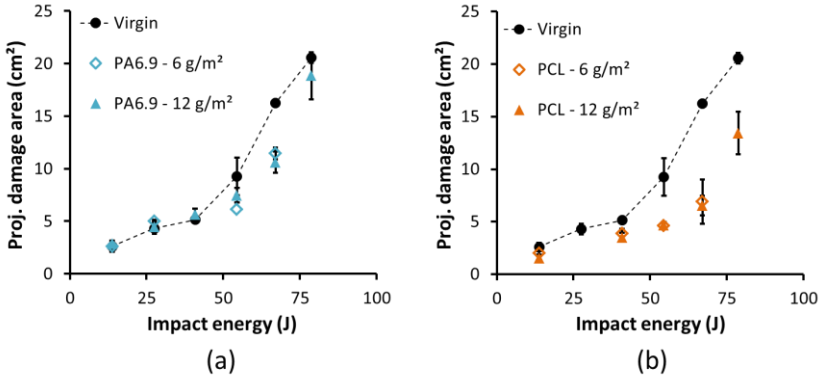

Figure 82 – Projected damage area versus impact energy for PA6.9 (a) and PCL (b) interleaved composite laminates. The damage area decreases compared to the virgin material, especially at impact energies higher than 50 J. PCL nanofibre interleaved specimens showed the best improvements. The veil density had no effect for both nanofibre types.

The depth of the permanent indentation after impact was measured using a micrometre and is illustrated in Figure 83. A change in damage mechanism is clearly visible by a sudden increase of the indentation depth above impact energies of 50 J. The virgin specimens showed very large dent formation at these impact energies caused by severe splitting of the plies and almost full penetration of the impactor in the specimen. The dent formation in the nanofibre interleaved specimens was less severe, resulting in a relatively smooth surface of the specimens after impact. This indicates that a significant portion of the impact energy was absorbed by the nanofibres resulting in a decrease in projected damage area as well as dent damage. Contrary to the damage area however, the difference between PCL and PA6.9 nanofibres is relatively small.

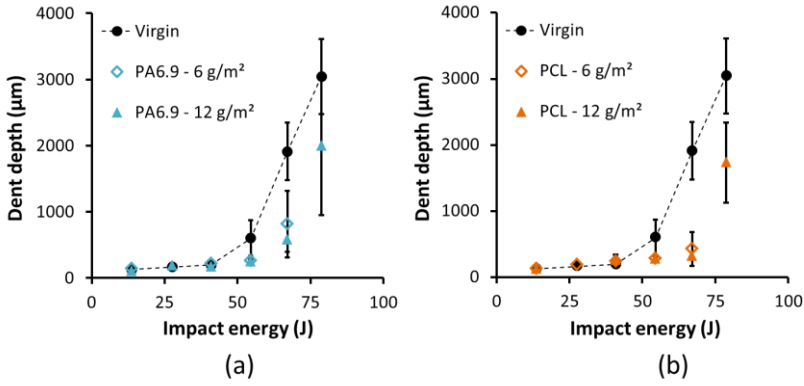

Figure 83 – Dent depth versus impact energy for PA6.9 (a) and PCL (b) interleaved composite laminates. Macroscopic dent formation occurs at energies higher than 50 J. The nanofibre interleaved specimens showed much lower dent depths due to better damage resistance. The veil density had no effect for both nanofibre types.

A microscopic investigation of the damage mechanisms was performed by analysing cross-sectional images taken at the impact point along the transversal direction, i.e. along the 90° direction (Figure 84). As expected, the damage region increased as the impact energy increased. At 14 J, few intralaminar cracks and delaminations were present, resembling the typical pine tree pattern. Intralaminar tensile cracks can be seen in the lowest reinforcing ply due to the bending of the specimens during impact. At an intermediate impact energy of 41 J, more intralaminar cracks are observed while the delaminations were longer. The lower plies also started to show signs of glass fibre failure. At this point, the indentation was still limited and thus the material beneath the impact point is still able to take up the load induced by the impact event. At higher energies of 67 J however, the specimens were severely damaged. Many cracks and delaminations are observed at further distances away from the impact point. Pulled-out glass fibres were also visible. In the virgin specimens, the material beneath the impact point showed failure throughout the thickness of the specimen. On the contrary, the nanofibre toughened specimens, especially PCL interleaved specimens, showed much less cracks and smaller delaminations. Furthermore, they maintained the structural integrity of the material underneath the impact point much better.

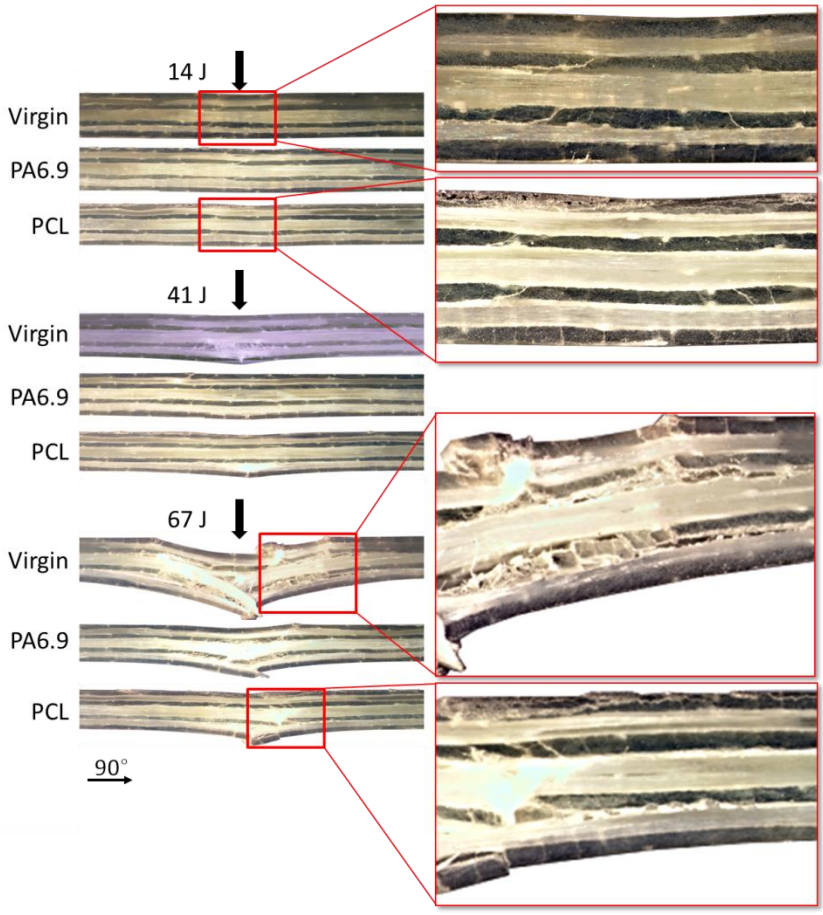

Figure 84 – Cross-section view of impacted specimens. The amount of interlaminar cracks and delaminations was found to be lower in the nanofibre interleaved laminates. At impact energies of 67 J, severe dent formation is visible for the virgin specimens due to complete ply failure underneath the impact, while much less damage and smaller dents are observed for the nanofibre interleaved specimens. (External light sources were used to produce a high contrast between the cracks/delaminations and the 0°-oriented plies.)

Similar to results obtained by delamination testing, the nanofibre interleaved impacted specimens showed regular occurrences of interlaminar crossings, while the majority of the delamination is found at the reinforcing ply interface. (Figure 85a). Furthermore, interlaminar cracks through the nanotoughened interlayers were also observed in regions without delaminations (Figure 85b). Sections of the delaminated area were analysed with SEM. These images confirmed that nanofibre bridging zones also developed during impact events (Figure 86). Both PA6.9 and PCL nanofibres showed signs of plastic deformation indicating good load/energy take-up which resulted in the improved impact resistance. However, a certain fraction of PA6.9 nanofibres was also peeled from the matrix resin. Hence, the fracture surface showed signs of both Mode I (peeling) and Mode II (straining) conditions. Such Mixed Mode behaviour is to be expected for relatively thin composite laminates as (tensile) failure of the bottom plies allows an opening mode deformation between delaminated plies. Indeed, the delaminations in Figure 84 were "open" indicating (partial) Mode I conditions. The results obtained through delamination tests – which showed poor performance of polyamide nanofibres due to low adhesion with the matrix compared to PCL nanofibres under Mode I delamination growth (Section 3.2 and Section 3.3) – thus agree well with the low velocity impact results. PCL interleaved laminates perform better due to an increased delamination resistance under both Mode I and Mode II loading. Furthermore, the strain rate dependence of the PA6.9 nanofibres (see Section 3.1.2) might also have reduced their toughening potential during impact, which is typically a high strain-rate event.

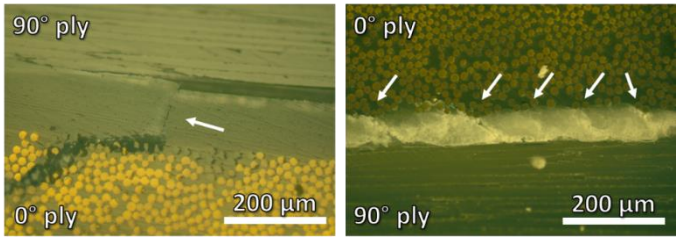

Figure 85 – Interlaminar crossing of the nanotoughened interlayer by a delamination which jumps from the 0°-interface to the 90°-interface (a). Interlaminar cracks formed between plies with different orientation due to shear stresses (b).

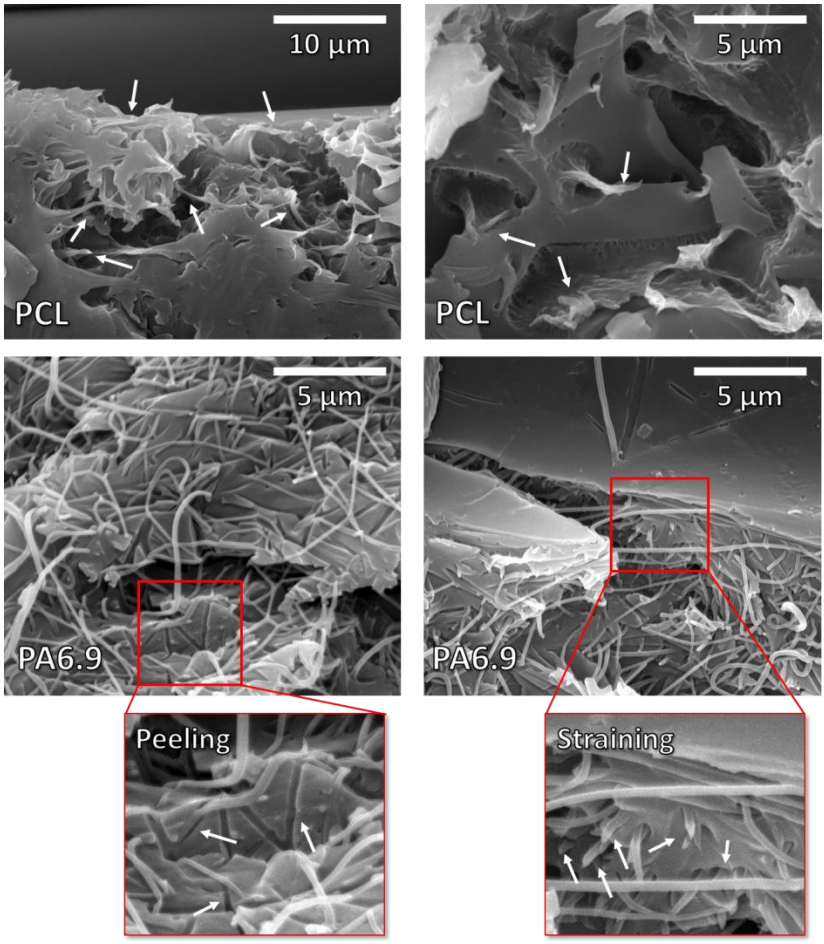

Figure 86 – SEM analysis of the fracture surface showed nanofibre bridging zones. The PCL nanofibres were severely deformed without signs of a weak interface thus indicating good load transfer and energy take-up by the nanofibres. The PA6.9 nanofibres also showed plastic deformation (straining), but many peeled off nanofibres were also visible due to the low interfacial strength.

3.4.4 Post-impact residual compressive strength

The impacted specimens of Section 3.4.3 were tested for their residual compressive strength according to ASTM D7137[137], often referred to as the Compression After Impact (CAI) strength. The CAI strength is a very important parameter since it is a measure for the anticipated damage tolerance of a composite material. Indeed, many structural applications will face an impact event at some point during their use (hail stones, pebbles, tool drops). This induces damage in the material which lowers the mechanical properties. Especially the compressive strength reduces greatly and may lower up to 60% of that of the undamaged material[160]. Delaminations will cause the internal plies to behave as sub-laminates with a much lower thickness than that of the complete laminate. Under compression, these sub-laminates will buckle out at lower loads causing the material to fail at a lower compressive stress. The failure mechanism is typically triggered by the initiation of delaminations due to buckling of sub-laminates. In turn, this will cause the sub-laminates to grow and buckle out more easily resulting in abrupt compressive failure of the specimens. Therefore, nanofibre toughened interlayers could increase the CAI strength by increasing the load before delamination initiation. Furthermore, the delaminated area is also smaller in these specimens which also increases the CAI strength. The failure mechanism is schematically represented in Figure 87.

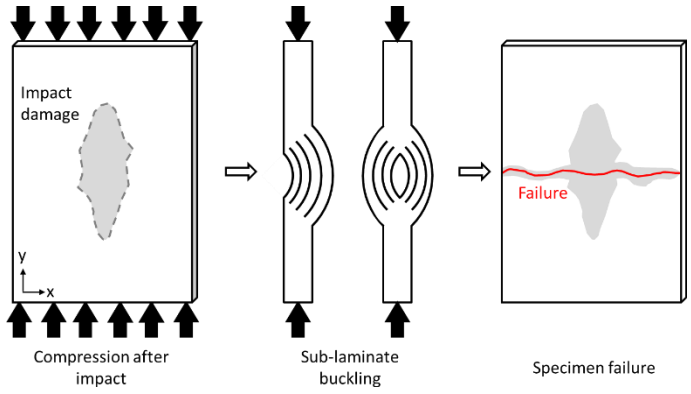

Figure 87 – Schematic illustration of compression after impact testing: compressive loading of an impacted specimen causing sub-laminate buckling and failure of the specimen at lower stresses than the pristine material.

The results of the CAI experiments are given in Figure 88. The individual measurements are plotted for the nanofibre interleaved laminates as it was not always possible to obtain multiple valid measurements. As the specimens were relatively thin, they tended to fail in an invalid manner in which the failure was initiated near the edges of the fixture and not by compression through the impact zone. For the same reason, no valid measurements were obtained at the lowest energy level for the virgin material. On average, the nanotoughened interlayers did not improve the CAI strength although the damage area was considerably smaller. However, the damage area was mainly reduced in length and not in width for the interleaved specimens. This means that the effective cross-section that experiences the compressive load is more or less similar for virgin and nanofibre interleaved specimens. The stiffness in the compression direction will thus hardly be affected by the difference in damage length. Furthermore, the impact energies considered were quite high and induced major damage. As such, the material under the impact point degraded to that extent that it likely acted as a local failure initiation point before the delaminated sub-laminates could buckle out. Indeed, glass fibre failure already occurred at impact energies of 40 J. Therefore, it is unlikely that at energies higher than 40 J, the failure event is governed by delamination and the toughened interlayers will not affect the CAI strength.

Impact and post-impact studies often focus on the Barely Visible Impact Damage (BVID) energy range, which is defined as those energies that cause a permanent indentation smaller than 0.3 mm[161]. For the specimens under consideration, the BVID range had an upper impact energy limit of approximately 50 J (Figure 83). In this range, the average CAI strength of the nanofibre interleaved specimens was still comparable to that of the virgin material. Yet several specimens showed a CAI strength which could be considered to be relatively high based on the trend visible in Figure 88. Especially some of the specimens interleaved with PCL nanofibres and subjected to an impact of 14 J had a high CAI strength. At this energy level, damage was still limited to – relatively small – matrix cracks and delamination. For the three specimens interleaved with 6 g/m² PCL nanofibres, the bottom surfaces before and after CAI testing are shown in Figure 89. The lowest CAI strength was recorded for specimen #1 which showed the largest delaminated area after CAI testing, while the highest CAI strength was recorded for specimen #3 which had the smallest delamination area. A possible

explanation for this behaviour is that the onset of delamination induced by sub-laminate buckling in specimen #3 had more interlaminar crossings. Hence, it could take up more load before the damage reached a critical size and abrupt compressive failure occurred. Similarly, the PA6.9 interleaved specimens subjected to an impact energy of 14 J also showed relatively large scatter on their CAI strength.

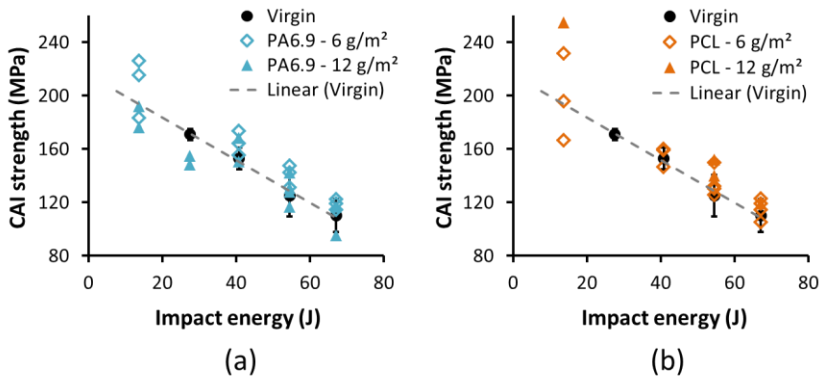

Figure 88 – CAI strength for PA6.9 (a) and PCL (b) interleaved composite laminates. Individual measurements are plotted for the nanofibre interleaved specimens, while the average and standard deviation is plotted for the virgin material (including a linear fit). The CAI strength decreases with increasing impact energy. On average, the nanofibres do not differ significantly from the virgin material.

The results of Section 3.4.3 and Section 3.4.4 show that the nanofibres have a lot of potential to improve the impact resistance and the residual compressive strength. However, the use of relatively thin GFRP cross-ply specimens resulted in a damage mechanism in which major delamination failure only occurred at higher impact energies. Therefore, the highest improvements in impact resistance were also obtained at higher impact energies above the BVID range. This caused severe reinforcing fibre failure underneath the impact point. Furthermore, the delamination area was mainly reduced due to a decrease in the delamination length, but not the delamination width. Whereas the CAI experiment is usually very sensitive to the delaminated area, the fact that the delamination width remained similar and severe fibre/ply damage already occurred limited the dependence of the CAI strength on the delaminated area.

This resulted in comparable CAI values for the virgin and nanofibre interleaved material. In order to better analyse the potential of nanofibrous interleaves for impact toughening, future studies should consider impact energies near the BVID region and possibly use thicker quasi-isotropic laminates as recommended by ASTM D7136. This will result in a more delamination dominant failure mode during impact. This will also be more relevant for applications as the main concern in industry is to improve the BVID resistance.

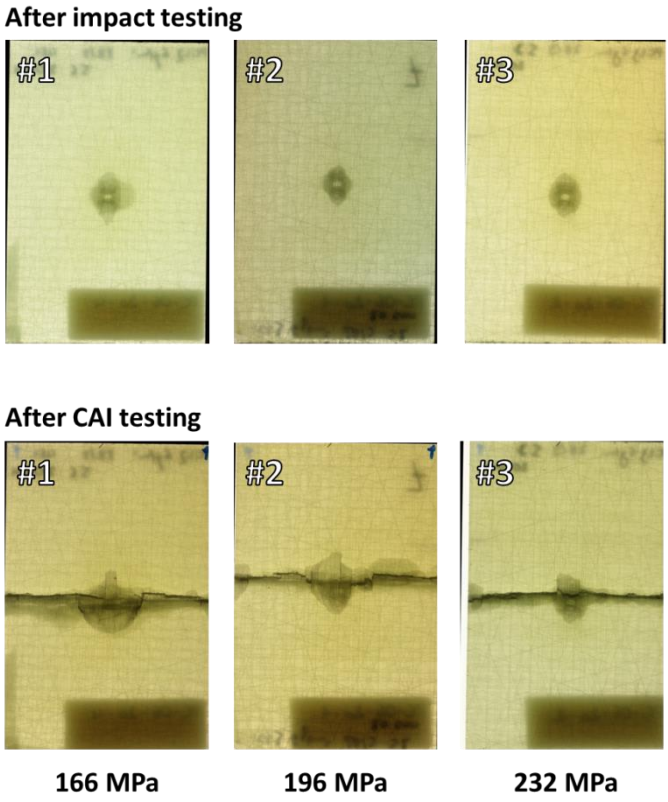

Figure 89 – Images of the specimens interleaved with 6 g/m² of PCL nanofibres subjected to an impact energy of 14 J before and after CAI testing. When a lower CAI strength was recorded, a larger delaminated area can be seen on the failed specimens.

4

CONCLUDING REMARKS

This PhD shows that electrospun nanofibrous veils are a viable option to design advanced composite materials with a very high delamination and damage resistance. As opposed to many traditional toughening techniques, the electrospun nanofibres are easily integrated into a composite laminate either by directly electrospinning onto the reinforcing ply surface or by interleaving self-supporting veils in between the reinforcing plies. Furthermore, the high porosity and relative small thickness of these veils allows easy wetting of the epoxy resin and regular composite production processes, like autoclaving and infusion, can be used without any modifications. Combine these advantages with the fact that the delamination resistance can be increased up to two or three times that of the virgin material without significant mass increase, and it should be clear that electrospun nanofibrous veils have the potential to improve the performance of many composite structures and applications.

The electrospinning process is relatively simple, scalable, and can be used to produce nanofibers from a whole set of polymers. The macroscopic length and sub-micron diameter of nanofibres removes many of the health risks often associated to nanomaterials in an industrial setting such as particles that are easily airborne and inhaled. Currently, there are already industrial producers who can deliver electrospun nanofibrous veils or electrospinning systems on the scale necessary for composite applications such as Revolution Fibres, Bioinicia, ElectrospinTech and Elmarco. It is expected that many more producers will follow as the demand of nanofibrous veils in other sectors such as in filtration or medicine is also growing.

Thus it seems that it is not a question of if, but when these materials find their way into structural composite applications. Yet, before that can happen, the exact toughening mechanisms need to be understood. At the beginning of this PhD this was perhaps the major shortcoming in the state-of-the-art literature. Although, within the few publications available, there were results showing improved delamination resistance, there were just as many publications which obtained opposite results without giving an apparent reason for these discrepancies. Clearly, a deeper understanding of the behaviour of nanofibre interleaved composites was necessary. Therefore, in this PhD, we performed a multiscale analysis of the toughening micromechanisms that are present in these materials. Such an analysis had not been performed before and provided

much better insights into the behaviour of nanotoughened composites. It led to a significant advancement of the understanding of these materials in a more structured and general sense.

The interleaved composites can be thought to have three different levels at which the nanofibres affect the properties. These coincide with the hierarchical nature of the laminate itself: (i) the nanotoughened epoxy resin, (ii) the nanotoughened interlayer and (iii) the nanotoughened laminate.

At the nanotoughened epoxy level (Section 3.1), the effect of electrospun nanofibres on the fracture toughness of the epoxy resin was analysed. The main goal of this level was to get a fundamental understanding of the toughening mechanisms acting in nanotoughened epoxy similarly to what has been done previously for rubber/thermoplastic toughened epoxies. Using SENB experiments on relatively thick nanotoughened epoxy specimens, we found that there are two distinct mechanisms causing an increased fracture toughness compared to neat epoxy resin. The first one is the yielding of nanofibres in the fracture processing zone in front of the crack tip (intrinsic toughening) which caused an increase in the initiation fracture toughness of about 20 – 30 % for PCL nanofibre toughened epoxy. However, the main increase in fracture toughness was due to the extrinsic toughening mechanism of nanofibre bridging. If the crack propagates, nanofibres will bridge the newly formed crack surfaces and take up energy by straining, yielding and eventually (tensile) fracture. At the same time, they provide closing tractions on the crack which relieves the stress at the crack tip. Both effects will cause an increase in the fracture toughness. Furthermore, the nanofibre bridging zone increases in size during crack growth, thus causing an even higher fracture toughness of the nanotoughened epoxy during crack growth. Using modified specimens, we found that the adhesion between the nanofibre and the matrix is very important to have good load transfer to the nanofibres and thus effective nanofibre bridging. While the adhesion with polyamide nanofibres was quite low resulting in peeling of the nanofibres, PCL nanofibres did result in a good interface. For the PCL nanotoughened epoxy, fracture toughness values up to 4000 J/m² were recorded, values far higher than the 1500 J/m² of the neat epoxy resin. The insights gained on this level were quintessential for understanding the

behaviour of toughened composite laminates, especially since no such experiments or insights had been reported before.

At the level of the nanotoughened interlayer (Section 3.2), other factors such as the delamination path will come into play. Microscopic analysis of delaminated specimens showed that the delamination did not progress solely through the nanotoughened interlayer. Thus, nanofibre bridging zones did not just develop over the whole delamination plane. Rather the delamination was deflected towards the reinforcing ply boundary where it progressed by "classical" interfacial failure of the reinforcing fibres. Regular crossings of the nanotoughened interlayer by the delamination path however occurred and it was mainly at these interlaminar crossings that nanofibre bridging zones developed. SEM analysis of the fracture surface of delaminated specimens showed the same fracture morphology of the nanofibre bridging zones with protruding, plastically deformed nanofibres visible. An equation was derived which related the improvement in Mode I delamination resistance to the results obtained from the SENB experiments on the nanotoughened epoxy. Good agreement with the experimental data was obtained, proving a strong link between both levels. Similarly, there was also a link between the improvements of the Mode II delamination resistance and the fracture toughness of the epoxy resin. It was found that the delamination mode affects the development of nanofibre bridging zones. Not only did a Mode I loading mode typically result in less interlaminar crossings, it also exerted peeling forces to the nanofibres, making their adhesion with the epoxy become very important. Indeed, while PCL nanofibres readily improved G_I, PA nanofibres hardly had a positive effect due their lack of adhesion causing extensive peeling. Mode II loadings on the other hand typically resulted in a higher amount of interlaminar crossings while exerting straining forces to the nanofibres. As such, both PA and PCL nanofibres were able to increase the Mode II delamination resistance to almost twice the value of the virgin material.

The interaction between the delamination path and the nanotoughened interlayers – which determines the amount of nanofibre bridging zones – was found to be dependent on parameters related to the nanofibres themselves, the veil morphology, the interleaving technique, the reinforcing fabric architecture and even the way in which the delamination experiment is performed. Especially

under Mode I loading conditions, the amount of interlaminar crossings depended for example on the areal density of the veils (higher densities resulted in less crossings) and the interleaving method (directly electrospinning on the reinforcing plies provided the most crossings). The analysis of delamination experiments with different parameters was performed in Section 3.3. While one type of nanofibrous veil might result in good improvements for one type of composite laminates, it does not necessarily result in the same improvements for other types of laminates. Generally, in order to increase the fracture toughness on the interlaminar level, the interaction between the delamination path and the nanotoughened interlayer characteristics are of crucial importance and should all be considered in order to design damage resistant composite materials.

Although Section 3.1 – Section 3.3 provided the essential insights into the toughening micromechanisms acting in nanotoughened epoxy and nanotoughened interlayers, the crack and delamination growth were always carefully initiated and controlled. Furthermore, the delamination specimens typically had a unidirectional layup, something which is often not encountered in applications. To provide a link between the fundamental insights and the mechanical response that can be expected in real-life situations, fully interleaved cross-ply composite laminates were analysed in Section 3.4. While the (in-plane) tensile, shear and flexural stiffness and strength were retained, the open-hole strength of interleaved laminates even increased about 8% compared to the virgin material. Since the failure mechanism of notched laminates, such as the open hole tensile specimen, is typically delamination dominant, the nanofibres "delay" the delamination progression due to an increase in the interlaminar fracture toughness. This results in notched laminates which can bear a higher load before failure.

The low velocity impact resistance of fully interleaved laminates increased considerably compared to the virgin material. The (projected) damage decreased substantially up to 50 – 60 %, especially at higher impact energies where the virgin material showed much delamination. PCL nanofibre interleaved laminates performed better than PA6.9 nanofibre interleaved ones. This was attributed to the strain rate sensitivity of PA6.9 and its low adhesion strength with the epoxy matrix. The interleaved laminates also showed much less

indentation for the same impact energy than the virgin material. As more energy was absorbed in the interleaved laminates due to delamination and interlaminar cracks through the nanotoughened interlayers, less damage was inflicted to reinforcing fibres and matrix resin. Analysis of the fracture surface of impacted specimens showed the development of nanofibre bridging zones again providing the link between the three levels. The PCL nanofibre bridging zones were more effective as much more plastic deformation and no peeling was observed compared to the PA6.9 bridging zones. The residual compressive strength of the impacted specimens was not influenced much by the presence of the nanotoughened interlayers. Although a decrease in damage area was obtained during impact testing, the decrease was mainly attributed to a decrease in length of the damage zone while the width remained similar. Furthermore, the applied impact energies were relatively high and caused reinforcing fibre failure near the impact point. This might explain why no substantial improvements in CAI strength were recorded for the nanofibre interleaved laminates.

The primary goal of this PhD work was to develop highly toughened nanofibre enhanced composite laminates and to gain fundamental insights into the toughening mechanisms and generic parameters of these novel materials. This was successfully accomplished by analysing the material using a multilevel approach. Nanofibre interleaved composites with excellent delamination resistance were designed, while obtaining a lot more fundamental knowledge about the prerequisites for effective nanofibre toughening. The improvements are in-line and often even better than those for traditional toughening methods.

Currently, the most critical aspect is to develop/optimize a temperature stable nanofibre system with good adherence to the epoxy matrix. Indeed, PCL nanofibres often outperformed the polyamide equivalents due to better adhesion, but cannot be processed or used at temperatures above their melting point of 60°C limiting their application for higher temperature production methods and applications. Yet, the multistep curing procedure and core-shell structured nanofibres described in Section 3.3 already show that the solution for this problem will be within reach of the current electrospinning community. Other possibilities might include the electrospinning of other types of polymer or the use of surface treatments and sizings. Furthermore, even smaller nanofibres can be produced with a higher surface area to volume ratio to

increase the bonding with the matrix resin. Another future aspect is the construction of a roadmap and/or model which engineers can use to design the nanofibre interleaved composites in an optimal way. Depending on the desired improvement in delamination resistance, the roadmap/model will output for example which nanofibre to use, how thick the veils should be, the best configuration to integrate them in the composite and so on. Lastly, using the insights obtained in this PhD, an experimental campaign focussed on improving some real-life composite structures can be initiated. This would bridge the gap between the lab environment and the industrial application. These aspects are for sure attainable in a relatively short timeframe. Clearly, there is a bright future for these materials in structural composite applications, a future which is hopefully facilitated by this PhD.

5

BIBLIOGRAPHY

(1) Campbell, F. C. *Structural Composite*; ASM International, 2010.

(2) Hull, D.; Clyne, T. W. *An Introduction to Composite Materials*; Cambridge University Press, 1996.

(3) Kaw, A. K. *Mechanics of Composite Materials*; Taylor & Francis, 2006.

(4) Evans, K. E.; Gibson, A. G. Prediction of the Maximum Packing Fraction Achievable in Randomly Oriented Short-Fibre Composites. *Composites Science and Technology* **1986**, *25* (2), 149–162.

(5) Gibson, R. F. *Principles of Composite Material Mechanics*; CRC Press, 2016.

(6) Scida, D.; Aboura, Z.; Benzeggagh, M. L.; Bocherens, E. A Micromechanics Model for 3D Elasticity and Failure of Woven-Fibre Composite Materials. *Composites Science and Technology* **1999**, *59* (4), 505–517.

(7) Hsiao, H. M.; Daniel, I. M. Effect of Fiber Waviness on Stiffness and Strength Reduction of Unidirectional Composites under Compressive Loading. *Composites Science and Technology* **1996**, *56* (5), 581–593.

(8) Witten, E. Composites Market Report 2016:Market Developments, Trends, Outlook and Challenges. AVK (Industrievereinigung Verstärkte Kunststoffe) 2016.

(9) Hoa, S. V. (Suong V. . *Principles of the Manufacturing of Composite Materials*; DEStech Publications, 2009.

(10) Cantwell, W. J.; Morton, J. The Impact Resistance of Composite Materials — a Review. *Composites* **1991**, *22* (5), 347–362.

(11) Sela, N.; Ishai, O. Interlaminar Fracture Toughness and Toughening of Laminated Composite Materials: A Review. *Composites* **1989**, *20* (5), 423–435.

(12) Herrera-Franco, P. J.; Drzal, L. T. Comparison of Methods for the Measurement of Fibre/matrix Adhesion in Composites. *Composites* **1992**, *23* (1), 2–27.

(13) Drzal, L. T.; Madhukar, M. Fibre-Matrix Adhesion and Its Relationship to Composite Mechanical Properties. *Journal of Materials Science* **1993**, *28* (3), 569–610.

(14) Kim, J.-K.; Sham, M.-L. Impact and Delamination Failure of Woven-Fabric Composites. *Composites Science and Technology* **2000**, *60* (5), 745–761.

(15) Wisnom, M. R. The Role of Delamination in Failure of Fibre-Reinforced Composites. *Philosophical transactions. Series A, Mathematical, physical, and engineering sciences* **2012**, *370* (1965), 1850–1870.

(16) Sridharan, S. *Delamination Behaviour of Composites*; Woodhead Pub, 2008.

(17) Abrate, S. Impact on Laminated Composite Materials. *Applied Mechanics Reviews* **1991**, *44* (4), 155.

(18) Richardson, M. O. W.; Wisheart, M. J. Review of Low-Velocity Impact Properties of Composite Materials. *Composites Part A: Applied Science and Manufacturing* **1996**, *27* (12), 1123–1131.

(19) Symons, D. D.; Davis, G. Fatigue Testing of Impact-Damaged T300/914 Carbon-Fibre-Reinforced Plastic. *Composites Science and Technology* **2000**, *60* (3), 379–389.

(20) Sanchez-Saez, S.; Barbero, E.; Zaera, R.; Navarro, C. Compression after Impact of Thin Composite Laminates. *Composites Science and Technology* **2005**, *65* (13), 1911–1919.

(21) Prichard, J. C.; Hogg, P. J. The Role of Impact Damage in Post-Impact Compression Testing. *Composites* **1990**, *21* (6), 503–511.

(22) Varley, R. J.; Tian, W. Toughening of an Epoxy Anhydride Resin System Using an Epoxidized Hyperbranched Polymer. *Polymer International* **2004**, *53* (1), 69–77.

(23) Ratna, D.; Varley, R.; Simon, G. P. Toughening of Trifunctional Epoxy Using an Epoxy-Functionalized Hyperbranched Polymer. *Journal of Applied Polymer Science* **2003**, *89* (9), 2339–2345.

(24) Ratna, D.; Becker, O.; Krishnamurthy, R.; Simon, G. .; Varley, R. . Nanocomposites Based on a Combination of Epoxy Resin, Hyperbranched Epoxy and a Layered Silicate. *Polymer* **2003**, *44* (24), 7449–7457.

(25) Siddhamalli, S. K.; Kyu, T. Toughening of Thermoset/thermoplastic Composites via Reaction-Induced Phase Separation: Epoxy/phenoxy Blends. *Journal of Applied Polymer Science* **2000**, *77* (6), 1257–1268.

(26) Hodgkin, J. H.; Simon, G. P.; Varley, R. J. Thermoplastic Toughening of Epoxy Resins: A Critical Review. *Polymers for Advanced Technologies* **1998**, *9* (1), 3–10.

(27) Dadfar, M. R.; Ghadami, F. Effect of Rubber Modification on Fracture Toughness Properties of Glass Reinforced Hot Cured Epoxy Composites. *Materials & Design* **2013**, *47*, 16–20.

(28) Allaer, K.; De Baere, I.; Van Paepegem, W.; Degrieck, J. Direct Fracture Toughness Determination of a Ductile Epoxy Polymer from Digital Image Correlation Measurements on a Single Edge Notched Bending Sample. *Polymer Testing* **2015**, *42*, 199–207.

(29) Ratna, D.; Banthia, A. K. Rubber Toughened Epoxy. *Macromolecular Research* **2004**, *12* (1), 11–21.

(30) Pearson, R. A.; Yee, A. F. Influence of Particle Size and Particle Size Distribution on Toughening Mechanisms in Rubber-Modified Epoxies. *Journal of Materials Science* **1991**, *26* (14), 3828–3844.

(31) De, B.; Karak, N.; He, L.; Li, X.; Wang, H.; Wu, X.; Jiang, P. Ultralow Dielectric, High Performing Hyperbranched Epoxy Thermosets: Synthesis, Characterization and Property Evaluation. *RSC Adv.* **2015**, *5* (44), 35080–35088.

(32) Willner, A. M.; McGarry, F. J. Toughening of an Epoxy Resin by an Elastomeric Second Phase. *Research Report Department of Civil Engineering, Massachusetts Institute of Technology* **1968**, *68* (8), 52.

(33) Dadfar, M. R.; Ghadami, F. Effect of Rubber Modification on Fracture Toughness Properties of Glass Reinforced Hot Cured Epoxy Composites. *Materials and Design* **2013**, *47*, 16–20.

(34) Chonkaew, W.; Sombatsompop, N.; Brostow, W. High Impact Strength and Low Wear of Epoxy Modified by a Combination of Liquid Carboxyl Terminated Poly(butadiene-Co-Acrylonitrile) Rubber and Organoclay. *European Polymer Journal* **2013**, *49* (6), 1461–1470.

(35) Yahyaie, H.; Ebrahimi, M.; Tahami, H. V.; Mafi, E. R. Toughening Mechanisms of Rubber Modified Thin Film Epoxy Resins. *Progress in Organic Coatings* **2013**, *76* (1), 286–292.

(36) Hwang, J.-F.; Manson, J. A.; Hertzberg, R. W.; Miller, G. A.; Sperling, L. H. Structure-Property Relationships in Rubber-Toughened Epoxies. *Polymer Engineering and Science* **1989**, *29* (20), 1466–1476.

(37) Sprenger, S. Epoxy Resins Modified with Elastomers and Surface-Modified Silica Nanoparticles. *Polymer* **2013**, *54* (18), 4790–4797.

(38) Bucknall, C. B.; Partridge, I. K. Addition of Polyethersulphone to Epoxy Resins. *British Polymer Journal* **1983**, *15* (1), 71–75.

(39) Alessi, S.; Conduruta, D.; Pitarresi, G.; Dispenza, C.; Spadaro, G. Accelerated Ageing due to Moisture Absorption of Thermally Cured Epoxy Resin/polyethersulphone Blends. Thermal, Mechanical and Morphological Behaviour. *Polymer Degradation and Stability* **2011**, *96* (4), 642–648.

(40) Raghava, R. S. Development and Characterization of Thermosetting-Thermoplastic Polymer Blends for Applications in Damage-Tolerant Composites. *Journal of Polymer Science Part B: Polymer Physics* **1988**, *26* (1), 65–81.

(41) Raghava, R. S. Role of Matrix-Particle Interface Adhesion on Fracture Toughness of Dual Phase Epoxy-Polyethersulfone Blend. *Journal of Polymer Science Part B: Polymer Physics* **1987**, *25* (5), 1017–1031.

(42) Siddhamalli, S. K. Toughening of Epoxy/polycaprolactone Composites via Reaction Induced Phase Separation. *Polymer Composites* **2000**, *21* (5), 846–855.

(43) Bucknall, C. B.; Gilbert, A. H. Toughening Tetrafunctional Epoxy Resins Using Polyetherimide. *Polymer* **1989**, *30* (2), 213–217.

(44) Hourston, D. .; Lane, J. . The Toughening of Epoxy Resins with Thermoplastics: 1. Trifunctional Epoxy Resin-Polyetherimide Blends. *Polymer* **1992**, *33* (7), 1379–1383.

(45) Pearson, R. A.; Yee, A. F. Toughening Mechanisms in Thermoplastic-Modified Epoxies: 1. Modification Using Poly(phenylene Oxide). *Polymer* **1993**, *34* (17), 3658–3670.

(46) Pearson, R. A.; Yee, A. F. Toughening Mechanisms in Elastomer-Modified Epoxies. *Journal of Materials Science* **1986**, *21* (7), 2475–2488.

(47) Jiao, J.; Sun, X.; Pinnavaia, T. J. Mesostructured Silica for the Reinforcement and Toughening of Rubbery and Glassy Epoxy Polymers. *Polymer* **2009**, *50* (4), 983–989.

(48) Jumahat, A.; Soutis, C.; Mahmud, J.; Ahmad, N. Compressive Properties of Nanoclay/Epoxy Nanocomposites. *Procedia*

Engineering **2012**, *41*, 1607–1613.

(49) Subramaniyan, A. K.; Sun, C. T. Toughening Polymeric Composites Using Nanoclay: Crack Tip Scale Effects on Fracture Toughness. *Composites Part A: Applied Science and Manufacturing* **2007**, *38* (1), 34–43.

(50) Gojny, F. H.; Wichmann, M. H. G.; Köpke, U.; Fiedler, B.; Schulte, K. Carbon Nanotube-Reinforced Epoxy-Composites: Enhanced Stiffness and Fracture Toughness at Low Nanotube Content. *Composites Science and Technology* **2004**, *64* (15), 2363–2371.

(51) Gojny, F.; Wichmann, M.; Fiedler, B.; Schulte, K. Influence of Different Carbon Nanotubes on the Mechanical Properties of Epoxy Matrix Composites – A Comparative Study. *Composites Science and Technology* **2005**, *65* (15–16), 2300–2313.

(52) Iwahori, Y.; Ishiwata, S.; Sumizawa, T.; Ishikawa, T. Mechanical Properties Improvements in Two-Phase and Three-Phase Composites Using Carbon Nano-Fiber Dispersed Resin. *Composites Part A: Applied Science and Manufacturing* **2005**, *36* (10), 1430–1439.

(53) Manjunatha, C. M.; Taylor, A. C.; Kinloch, A. J.; Sprenger, S. The Tensile Fatigue Behaviour of a Silica Nanoparticle-Modified Glass Fibre Reinforced Epoxy Composite. *Composites Science and Technology* **2010**, *70* (1), 193–199.

(54) Kostopoulos, V.; Baltopoulos, A.; Karapappas, P.; Vavouliotis, A.; Paipetis, A. Impact and after-Impact Properties of Carbon Fibre Reinforced Composites Enhanced with Multi-Wall Carbon Nanotubes. *Composites Science and Technology* **2010**, *70* (4), 553–563.

(55) Khan, S. U.; Iqbal, K.; Munir, A.; Kim, J.-K. Quasi-Static and Impact Fracture Behaviors of CFRPs with Nanoclay-Filled Epoxy Matrix. *Composites Part A: Applied Science and Manufacturing* **2011**, *42* (3), 253–264.

(56) Liu, L.; Wagner, H. D. Rubbery and Glassy Epoxy Resins Reinforced with Carbon Nanotubes. *Composites Science and Technology* **2005**, *65* (11–12), 1861–1868.

(57) Wang, W. X.; Takao, Y.; Matsubara, T.; Kim, H. S. Improvement of the Interlaminar Fracture Toughness of Composite Laminates by

Whisker Reinforced Interlamination. *Composites Science and Technology* **2002**, *62* (6), 767–774.

(58) Wetzel, B.; Rosso, P.; Haupert, F.; Friedrich, K. Epoxy Nanocomposites – Fracture and Toughening Mechanisms. *Engineering Fracture Mechanics* **2006**, *73* (16), 2375–2398.

(59) Zhao, S.; Schadler, L. S.; Hillborg, H.; Auletta, T. Improvements and Mechanisms of Fracture and Fatigue Properties of Well-Dispersed Alumina/epoxy Nanocomposites. *Composites Science and Technology* **2008**, *68* (14), 2976–2982.

(60) Gojny, F. H.; Wichmann, M. H. G.; Fiedler, B.; Schulte, K. Influence of Different Carbon Nanotubes on the Mechanical Properties of Epoxy Matrix Composites – A Comparative Study. *Composites Science and Technology* **2005**, *65* (15), 2300–2313.

(61) Quaresimin, M.; Schulte, K.; Zappalorto, M.; Chandrasekaran, S. Toughening Mechanisms in Polymer Nanocomposites: From Experiments to Modelling. *Composites Science and Technology* **2015**, *123*, 187–204.

(62) Johnsen, B. B.; Kinloch, A. J.; Mohammed, R. D.; Taylor, A. C.; Sprenger, S. Toughening Mechanisms of Nanoparticle-Modified Epoxy Polymers. *Polymer* **2007**, *48* (2), 530–541.

(63) Thostenson, E. T.; Ren, Z.; Chou, T.-W. Advances in the Science and Technology of Carbon Nanotubes and Their Composites: A Review. *Composites Science and Technology* **2001**, *61* (13), 1899–1912.

(64) Gojny, F. H.; Wichmann, M. H. G.; Köpke, U.; Fiedler, B.; Schulte, K. Carbon Nanotube-Reinforced Epoxy-Composites: Enhanced Stiffness and Fracture Toughness at Low Nanotube Content. *Composites Science and Technology* **2004**, *64* (15), 2363–2371.

(65) Khan, S. U.; Iqbal, K.; Munir, A.; Kim, J.-K. Quasi-Static and Impact Fracture Behaviors of CFRPs with Nanoclay-Filled Epoxy Matrix. *Composites Part A: Applied Science and Manufacturing* **2011**, *42* (3), 253–264.

(66) Bogdanovich, A. E.; Mohamed, M. H. Three-Dimensional Reinforcements for Composites. *SAMPE Journal* **2009**, *45* (6), 8–28.

(67) Wang, X.; Hu, B.; Feng, Y.; Liang, F.; Mo, J.; Xiong, J.; Qiu, Y. Low Velocity Impact Properties of 3D Woven Basalt/aramid Hybrid

Composites. *Composites Science and Technology* **2008**, *68* (2), 444–450.

(68) Callus, P. J.; Mouritz, A. P.; Bannister, M. K.; Leong, K. H. Tensile Properties and Failure Mechanisms of 3D Woven GRP Composites. *Composites Part A: Applied Science and Manufacturing* **1999**, *30* (11), 1277–1287.

(69) Gerlach, R.; Siviour, C. R.; Wiegand, J.; Petrinic, N. In-Plane and through-Thickness Properties, Failure Modes, Damage and Delamination in 3D Woven Carbon Fibre Composites Subjected to Impact Loading. *Composites Science and Technology* **2012**, *72* (3), 397–411.

(70) Massabò, R.; Mumm, D. R.; Cox, B. Characterizing Mode II Delamination Cracks in Stitched Composites. *International Journal of Fracture* **1998**, *92* (1), 1–38.

(71) Mouritz, A. P.; Leong, K. H.; Herszberg, I. A Review of the Effect of Stitching on the in-Plane Mechanical Properties of Fibre-Reinforced Polymer Composites. *Composites Part A: Applied Science and Manufacturing* **1997**, *28* (12), 979–991.

(72) Mouritz, A. P. Ballistic Impact and Explosive Blast Resistance of Stitched Composites. *Composites Part B: Engineering* **2001**, *32* (5), 431–439.

(73) Dransfield, K.; Baillie, C.; Mai, Y.-W. Improving the Delamination Resistance of CFRP by Stitching—a Review. *Composites Science and Technology* **1994**, *50* (3), 305–317.

(74) Yan, W.; Liu, H.-Y.; Mai, Y.-W. Mode II Delamination Toughness of Z-Pinned Laminates. *Composites Science and Technology* **2004**, *64* (13), 1937–1945.

(75) Cartié, D. D. R.; Troulis, M.; Partridge, I. K. Delamination of Z-Pinned Carbon Fibre Reinforced Laminates. *Composites Science and Technology* **2006**, *66* (6), 855–861.

(76) Partridge, I. K.; Cartié, D. D. R. Delamination Resistant Laminates by Z-Fiber® Pinning: Part I Manufacture and Fracture Performance. *Composites Part A: Applied Science and Manufacturing* **2005**, *36* (1), 55–64.

(77) Mouritz, A. P. Review of Z-Pinned Composite Laminates. *Composites*

Part A: Applied Science and Manufacturing **2007**, *38* (12), 2383–2397.

(78) Mouritz, A. P.; Cox, B. N. A Mechanistic Interpretation of the Comparative in-Plane Mechanical Properties of 3D Woven, Stitched and Pinned Composites. *Composites Part A: Applied Science and Manufacturing* **2010**, *41* (6), 709–728.

(79) Huang, Z.-M.; Zhang, Y.-Z.; Kotaki, M.; Ramakrishna, S. A Review on Polymer Nanofibers by Electrospinning and Their Applications in Nanocomposites. *Composites Science and Technology* **2003**, *63* (15), 2223–2253.

(80) Tian, M.; Hu, Q.; Wu, H.; Zhang, L.; Fong, H.; Zhang, L. *Formation and Morphological Stability of Polybutadiene Rubber Fibers Prepared through Combination of Electrospinning and in-Situ Photo-Crosslinking*; 2011; Vol. 65.

(81) van der Heijden, S.; De Bruycker, K.; Simal, R.; Du Prez, F.; De Clerck, K. Use of Triazolinedione Click Chemistry for Tuning the Mechanical Properties of Electrospun SBS-Fibers. *Macromolecules* **2015**, *48* (18), 6474–6481.

(82) Van der Schueren, L.; De Schoenmaker, B.; Kalaoglu, Ö. I.; De Clerck, K. An Alternative Solvent System for the Steady State Electrospinning of Polycaprolactone. *European Polymer Journal* **2011**, *47* (6), 1256–1263.

(83) De Schoenmaker, B.; Goethals, A.; Van der Schueren, L.; Rahier, H.; De Clerck, K. Polyamide 6.9 Nanofibres Electrospun under Steady State Conditions from a Solvent/non-Solvent Solution. *Journal of Materials Science* **2012**, *47* (9), 4118–4126.

(84) De Vrieze, S.; De Schoenmaker, B.; Ceylan, Ö.; Depuydt, J.; Van Landuyt, L.; Rahier, H.; Van Assche, G.; De Clerck, K. Morphologic Study of Steady State Electrospun Polyamide 6 Nanofibres. *Journal of Applied Polymer Science* **2011**, *119* (5), 2984–2990.

(85) Geltmeyer, J.; Van der Schueren, L.; Goethals, F.; De Buysser, K.; De Clerck, K. Optimum Sol Viscosity for Stable Electrospinning of Silica Nanofibres. *Journal of Sol-Gel Science and Technology* **2013**, *67* (1), 188–195.

(86) Geltmeyer, J.; De Roo, J.; Van den Broeck, F.; Martins, J. C.; De Buysser, K.; De Clerck, K. The Influence of Tetraethoxysilane Sol

Preparation on the Electrospinning of Silica Nanofibers. *Journal of Sol-Gel Science and Technology* **2016**, *77* (2), 453–462.

(87) Megelski, S.; Stephens, J. S.; Bruce Chase, D.; Rabolt, J. F. Micro- and Nanostructured Surface Morphology on Electrospun Polymer Fibers. *Macromolecules* **2002**, *35* (22), 8456–8466.

(88) Casper, C. L.; Stephens, J. S.; Tassi, N. G.; Chase, D. B.; Rabolt, J. F. Controlling Surface Morphology of Electrospun Polystyrene Fibers: Effect of Humidity and Molecular Weight in the Electrospinning Process. *Macromolecules* **2004**, *37* (2), 573–578.

(89) van der Heijden, S.; Daelemans, L.; Meireman, T.; De Baere, I.; Rahier, H.; Van Paepegem, W.; De Clerck, K. Interlaminar Toughening of Resin Transfer Molded Laminates by Electrospun Polycaprolactone Structures: Effect of the Interleave Morphology. *Composites Science and Technology* **2016**, *136*, 10–17.

(90) Persano, L.; Camposeo, A.; Tekmen, C.; Pisignano, D. Industrial Upscaling of Electrospinning and Applications of Polymer Nanofibers: A Review. *Macromolecular Materials and Engineering* **2013**, *298* (5), 504–520.

(91) Agarwal, S.; Burgard, M.; Greiner, A.; Wendorff, J. *Electrospinning: A Practical Guide to Nanofibers*; 2016.

(92) Dzenis, Y. A.; Reneker, D. H. Delamination Resistant Composites Prepared by Small Diameter Fiber Reinforcement at Ply Interfaces. United States Patent 6265333:, 2001.

(93) Kim, J.; Reneker, D. H. Mechanical Properties of Composites Using Ultrafine Electrospun Fibers. *Polymer Composites* **1999**, *20* (1), 124–131.

(94) Dzenis, Y. A.; Reneker, D. H. Delamination Resistant Composites Prepared by Small Fiber Reinforcement at Ply Interfaces, 1999.

(95) Lin, S.; Cai, Q.; Ji, J.; Sui, G.; Yu, Y.; Yang, X.; Ma, Q.; Wei, Y.; Deng, X. Electrospun Nanofiber Reinforced and Toughened Composites through in Situ Nano-Interface Formation. *Composites Science and Technology* **2008**, *68* (15–16), 3322–3329.

(96) Li, G.; Li, P.; Zhang, C.; Yu, Y.; Liu, H.; Zhang, S.; Jia, X.; Yang, X.; Xue, Z.; Ryu, S. Inhomogeneous Toughening of Carbon Fiber/epoxy Composite Using Electrospun Polysulfone Nanofibrous Membranes

by in Situ Phase Separation. *Composites Science and Technology* **2008**, *68* (3–4), 987–994.

(97) Akangah, P.; Lingaiah, S.; Shivakumar, K. Effect of Nylon-66 Nano-Fiber Interleaving on Impact Damage Resistance of Epoxy/carbon Fiber Composite Laminates. *Composite Structures* **2010**, *92* (6), 1432–1439.

(98) Zhang, J.; Lin, T.; Wang, X. Electrospun Nanofibre Toughened Carbon/epoxy Composites: Effects of Polyetherketone Cardo (PEK-C) Nanofibre Diameter and Interlayer Thickness. *Composites Science and Technology* **2010**, *70* (11), 1660–1666.

(99) Hamer, S.; Leibovich, H.; Green, A.; Intrater, R.; Avrahami, R.; Zussman, E.; Siegmann, A.; Sherman, D. Mode I Interlaminar Fracture Toughness of Nylon 66 Nanofibrilmat Interleaved Carbon/epoxy Laminates. *Polymer Composites* **2011**, *32* (11), 1781–1789.

(100) Zhang, J.; Niu, H.; Zhou, J.; Wang, X.; Lin, T. Synergistic Effects of PEK-C/VGCNF Composite Nanofibres on a Trifunctional Epoxy Resin. *Composites Science and Technology* **2011**, *71* (8), 1060–1067.

(101) Zucchelli, A.; Focarete, M. L.; Gualandi, C.; Ramakrishna, S. Electrospun Nanofibers for Enhancing Structural Performance of Composite Materials. *Polymers for Advanced Technologies* **2011**, *22* (3), 339–349.

(102) Magniez, K.; Chaffraix, T.; Fox, B. Toughening of a Carbon-Fibre Composite Using Electrospun Poly(Hydroxyether of Bisphenol A) Nanofibrous Membranes Through Inverse Phase Separation and Inter-Domain Etherification. *Materials* **2011**, *4* (12), 1967–1984.

(103) Bilge, K.; Ozden-Yenigun, E.; Simsek, E.; Menceloglu, Y. Z.; Papila, M. Structural Composites Hybridized with Epoxy Compatible polymer/MWCNT Nanofibrous Interlayers. *Composites Science and Technology* **2012**, *72* (14), 1639–1645.

(104) Palazzetti, R.; Zucchelli, A.; Gualandi, C.; Focarete, M. L.; Donati, L.; Minak, G.; Ramakrishna, S. Influence of Electrospun Nylon 6,6 Nanofibrous Mats on the Interlaminar Properties of Gr–epoxy Composite Laminates. *Composite Structures* **2012**, *94* (2), 571–579.

(105) Chen, Q.; Zhang, L.; Zhao, Y.; Wu, X.-F.; Fong, H. Hybrid Multi-Scale Composites Developed from Glass Microfiber Fabrics and Nano-

Epoxy Resins Containing Electrospun Glass Nanofibers. *Composites Part B: Engineering* **2012**, *43* (2), 309–316.

(106) Zhang, J.; Yang, T.; Lin, T.; Wang, C. H. Phase Morphology of Nanofibre Interlayers: Critical Factor for Toughening Carbon/epoxy Composites. *Composites Science and Technology* **2012**, *72* (2), 256–262.

(107) van der Heijden, S.; Daelemans, L.; De Schoenmaker, B.; De Baere, I.; Rahier, H.; Van Paepegem, W.; De Clerck, K. Interlaminar Toughening of Resin Transfer Moulded Glass Fibre Epoxy Laminates by Polycaprolactone Electrospun Nanofibres. *Composites Science and Technology* **2014**, *104*, 66–73.

(108) Daelemans, L.; van der Heijden, S.; De Baere, I.; Rahier, H.; Van Paepegem, W.; De Clerck, K. Using Aligned Nanofibres for Identifying the Toughening Micromechanisms in Nanofibre Interleaved Laminates. *Composites Science and Technology* **2015**, *124*, 17–26.

(109) Daelemans, L.; van der Heijden, S.; De Baere, I.; Rahier, H.; Van Paepegem, W.; De Clerck, K. Damage Resistant Composites Using Electrospun Nanofibers: A Multiscale Analysis of the Toughening Mechanisms. *ACS applied materials & interfaces* **2016**.

(110) Daelemans, L.; van der Heijden, S.; De Baere, I.; Rahier, H.; Van Paepegem, W.; De Clerck, K. Using Aligned Nanofibres for Identifying the Toughening Micromechanisms in Nanofibre Interleaved Laminates. *Composites Science and Technology* **2016**, *124*, 17–26.

(111) Daelemans, L.; van der Heijden, S.; De Baere, I.; Rahier, H.; Van Paepegem, W.; De Clerck, K. Nanofibre Bridging as a Toughening Mechanism in Carbon/epoxy Composite Laminates Interleaved with Electrospun Polyamide Nanofibrous Veils. *Composites Science and Technology* **2015**, *117*, 244–256.

(112) van der Heijden, S.; Daelemans, L.; De Bruycker, K.; Simal, R.; De Baere, I.; Van Paepegem, W.; Rahier, H.; De Clerck, K. Novel Composite Materials with Tunable Delamination Resistance Using Functionalizable Electrospun SBS Fibers. *Composite Structures* **2017**, *159*, 12–20.

(113) Daelemans, L.; van der Heijden, S.; De Baere, I.; Rahier, H.; Van Paepegem, W.; De Clerck, K. Improved Fatigue Delamination Behaviour of Composite Laminates with Electrospun Thermoplastic Nanofibrous Interleaves Using the Central Cut-Ply Method.

Composites Part A: Applied Science and Manufacturing **2017**, *94*, 10–20.

(114) Bilge, K.; Venkataraman, S.; Menceloglu, Y. Z.; Papila, M. Global and Local Nanofibrous Interlayer Toughened Composites for Higher in-Plane Strength. *Composites Part A: Applied Science and Manufacturing* **2014**, *58*, 73–76.

(115) Jiang, S.; Duan, G.; Schöbel, J.; Agarwal, S.; Greiner, A. Short Electrospun Polymeric Nanofibers Reinforced Polyimide Nanocomposites. *Composites Science and Technology* **2013**, *88*, 57–61.

(116) De Schoenmaker, B.; Van der Heijden, S.; De Baere, I.; Van Paepegem, W.; De Clerck, K. Effect of Electrospun Polyamide 6 Nanofibres on the Mechanical Properties of a Glass Fibre/epoxy Composite. *Polymer Testing* **2013**, *32* (8), 1495–1501.

(117) De Schoenmaker, B.; van der Heijden, S.; Moorkens, S.; Rahier, H.; van Assche, G.; De Clerck, K. Effect of Nanofibres on the Curing Characteristics of an Epoxy Matrix. *Composites Science and Technology* **2013**, *79*, 35–41.

(118) van der Heijden, S.; De Schoenmaker, B.; Rahier, H.; Van Assche, G.; De Clerck, K. The Effect of the Moisture Content on the Curing Characteristics of an Epoxy Matrix in the Presence of Nanofibrous Structures. *Polymer Testing* **2014**, *40*, 265–272.

(119) Saghafi, H.; Zucchelli, A.; Palazzetti, R.; Minak, G. The Effect of Interleaved Composite Nanofibrous Mats on Delamination Behavior of Polymeric Composite Materials. *Composite Structures* **2014**, *109*, 41–47.

(120) Beckermann, G. W.; Pickering, K. L. Mode I and Mode II Interlaminar Fracture Toughness of Composite Laminates Interleaved with Electrospun Nanofibre Veils. *Composites Part A: Applied Science and Manufacturing* **2015**, *72*, 11–21.

(121) Palazzetti, R.; Yan, X.; Zucchelli, A. Influence of Geometrical Features of Electrospun Nylon 6,6 Interleave on the CFRP Laminates Mechanical Properties. *Polymer Composites* **2014**, *35* (1), 137–150.

(122) Tsotsis, T. K. Interlayer Toughening of Composite Materials. *Polymer Composites* **2009**, *30* (1), 70–86.

(123) Ramirez, V. A.; Hogg, P. J.; Sampson, W. W. The Influence of the Nonwoven Veil Architectures on Interlaminar Fracture Toughness of Interleaved Composites. *Composites Science and Technology* **2015**, *110*, 103–110.

(124) Guo, M.; Yi, X.; Liu, G.; Liu, L. Simultaneously Increasing the Electrical Conductivity and Fracture Toughness of Carbon–fiber Composites by Using Silver Nanowires-Loaded Interleaves. *Composites Science and Technology* **2014**, *97*, 27–33.

(125) Lee, S.-H.; Lee, J.-H.; Cheong, S.-K.; Noguchi, H. A Toughening and Strengthening Technique of Hybrid Composites with Non-Woven Tissue. *Journal of Materials Processing Technology* **2008**, *207* (1–3), 21–29.

(126) Chou, I.; Inutake, T.; Namba, K. Correlation of Damage Resistance under Low Velocity Impact and Mode II Delamination Resistance in CFRP Laminates. *Advanced Composite Materials* **1999**, *8* (2), 167–176.

(127) Matthews, J. A.; Wnek, G. E.; Simpson, D. G.; Bowlin, G. L. Electrospinning of Collagen Nanofibers. *Biomacromolecules* **2002**, *3* (2), 232–238.

(128) Baji, A.; Mai, Y. W.; Wong, S. C.; Abtahi, M.; Chen, P. Electrospinning of Polymer Nanofibers: Effects on Oriented Morphology, Structures and Tensile Properties. *Composites Science and Technology*. 2010, pp 703–718.

(129) Long, A. C. (Andrew C.; Textile Institute (Manchester, E. *Design and Manufacture of Textile Composites*; Woodhead, 2005.

(130) ASTM International. ASTM D5045 - 14 Standard Test Methods for Plane-Strain Fracture Toughness and Strain Energy Release Rate of Plastic Materials. 2014.

(131) ASTM Standard D5528, Standard Test Method for Mode I Interlaminar Fracture Toughness of Unidirectional Fiber Reinforced Polymer Matrix Composites www.astm.org.

(132) Arrese, A.; Carbajal, N.; Vargas, G.; Mujika, F. A New Method for Determining Mode II R-Curve by the End-Notched Flexure Test. *Engineering Fracture Mechanics* **2010**, *77* (1), 51–70.

(133) De Baere, I.; Jacques, S.; Van Paepegem, W.; Degrieck, J. Study of the

Mode I and Mode II Interlaminar Behaviour of a Carbon Fabric Reinforced Thermoplastic. *Polymer Testing* **2012**, *31* (2), 322–332.

(134) ASTM Standard D7905-14, Standard Test Method for Determination of the Mode II Interlaminar Fracture Toughness of Unidirectional Fiber-Reinforced Polymer Matrix Composites.

(135) Blackman, B. R. K.; Kinloch, A. J.; Paraschi, M. The Determination of the Mode II Adhesive Fracture Resistance, GIIC, of Structural Adhesive Joints: An Effective Crack Length Approach. *Engineering Fracture Mechanics* **2005**, *72* (6), 877–897.

(136) ASTM International. ASTM D7136 / D7136M - 15 Standard Test Method for Measuring the Damage Resistance of a Fiber-Reinforced Polymer Matrix Composite to a Drop-Weight Impact Event.

(137) ASTM International. ASTM D7137 / D7137M - 12 Standard Test Method for Compressive Residual Strength Properties of Damaged Polymer Matrix Composite Plates.

(138) Naraghi, M.; Chasiotis, I.; Kahn, H.; Wen, Y.; Dzenis, Y. Mechanical Deformation and Failure of Electrospun Polyacrylonitrile Nanofibers as a Function of Strain Rate. *Applied Physics Letters* **2007**, *91* (15), 151901.

(139) Papkov, D.; Zou, Y.; Andalib, M. N.; Goponenko, A.; Cheng, S. Z. D.; Dzenis, Y. A. Simultaneously Strong and Tough Ultrafine Continuous Nanofibers. *ACS nano* **2013**, *7* (4), 3324–3331.

(140) Najem, J. F.; Wong, S.-C.; Ji, G. Shear Adhesion Strength of Aligned Electrospun Nanofibers. *Langmuir : the ACS journal of surfaces and colloids* **2014**, *30* (34), 10410–10418.

(141) Madhukar, M. S.; Drzal, L. T. Fiber-Matrix Adhesion and Its Effect on Composite Mechanical Properties: II. Longitudinal (0°) and Transverse (90°) Tensile and Flexure Behavior of Graphite/Epoxy Composites. *Journal of Composite Materials* **1991**, *25* (8), 958–991.

(142) Farmand-Ashtiani, E.; Alanis, D.; Cugnoni, J.; Botsis, J. Delamination in Cross-Ply Laminates: Identification of Traction–separation Relations and Cohesive Zone Modeling. *Composites Science and Technology* **2015**, *119*, 85–92.

(143) Hojo, M.; Ando, T.; Tanaka, M.; Adachi, T.; Ochiai, S.; Endo, Y. Modes I and II Interlaminar Fracture Toughness and Fatigue Delamination of

CF/epoxy Laminates with Self-Same Epoxy Interleaf. *International Journal of Fatigue* **2006**, *28* (10), 1154–1165.

(144) Xia, Z. C.; Hutchinson, J. W. Mode II Fracture Toughness of a Brittle Adhesive Layer. *International Journal of Solids and Structures* **1994**, *31* (8), 1133–1148.

(145) Hojo, M.; Matsuda, S.; Tanaka, M.; Ochiai, S.; Murakami, A. Mode I Delamination Fatigue Properties of Interlayer-Toughened CF/epoxy Laminates. *Composites Science and Technology* **2006**, *66* (5), 665–675.

(146) Knoll, J. B.; Riecken, B. T.; Kosmann, N.; Chandrasekaran, S.; Schulte, K.; Fiedler, B. The Effect of Carbon Nanoparticles on the Fatigue Performance of Carbon Fibre Reinforced Epoxy. *Composites Part A: Applied Science and Manufacturing* **2014**, *67*, 233–240.

(147) Allegri, G.; Jones, M. I.; Wisnom, M. R.; Hallett, S. R. A New Semi-Empirical Model for Stress Ratio Effect on Mode II Fatigue Delamination Growth. *Composites Part A: Applied Science and Manufacturing* **2011**, *42* (7), 733–740.

(148) Remiro, P. M.; Cortazar, M. M.; Calahorra, M. E.; Calafel, M. M. Miscibility and Crystallization of an Amine-Cured Epoxy Resin Modified with Crystalline Poly(ε-Caprolactone). *Macromolecular Chemistry and Physics* **2001**, *202* (7), 1077–1088.

(149) Chen, J.-L.; Chang, F.-C. Phase Separation Process in Poly(-Caprolactone)-Epoxy Blends. *Macromolecules* **1999**, *32*, 5348–5356.

(150) Fernández, M. V.; de Moura, M. F. S. F.; da Silva, L. F. M.; Marques, A. T. Mixed-Mode I+II Fatigue/fracture Characterization of Composite Bonded Joints Using the Single-Leg Bending Test. *Composites Part A: Applied Science and Manufacturing* **2013**, *44*, 63–69.

(151) ASTM International. ASTM D3039 / D3039M - 14 Standard Test Method for Tensile Properties of Polymer Matrix Composite Materials.

(152) ASTM International. ASTM D3518 / D3518M - 13 Standard Test Method for In-Plane Shear Response of Polymer Matrix Composite Materials by Tensile Test of a ±45° Laminate. 2013.

(153) ASTM International. ASTM D7264 / D7264M - 15 Standard Test

Method for Flexural Properties of Polymer Matrix Composite Materials. 2015.

(154) ASTM International. ASTM D7028 - 07(2015) Standard Test Method for Glass Transition Temperature (DMA Tg) of Polymer Matrix Composites by Dynamic Mechanical Analysis (DMA).

(155) ASTM International. ASTM D5766 / D5766M - 11 Standard Test Method for Open-Hole Tensile Strength of Polymer Matrix Composite Laminates https://www.astm.org/Standards/D5766.htm (accessed May 10, 2017).

(156) Denneulin, S.; Viot, P.; Leonardi, F.; Lataillade, J.-L. The Influence of Acrylate Triblock Copolymer Embedded in Matrix on Composite Structures' Responses to Low-Velocity Impacts. *Composite Structures* **2012**, *94* (4), 1471–1481.

(157) Wang, P.; Zhang, X.; Lim, G.; Neo, H.; Malcolm, A. A.; Xiang, Y.; Lu, G.; Yang, J. Improvement of Impact-Resistant Property of Glass Fiber-Reinforced Composites by Carbon Nanotube-Modified Epoxy and Pre-Stretched Fiber Fabrics. *Journal of Materials Science* **2015**, *50* (18), 5978–5992.

(158) Matadi Boumbimba, R.; Froustey, C.; Viot, P.; Gerard, P. Low Velocity Impact Response and Damage of Laminate Composite Glass Fibre/epoxy Based Tri-Block Copolymer. *Composites Part B: Engineering* **2015**, *76*, 332–342.

(159) Aktaş, M.; Atas, C.; İçten, B. M.; Karakuzu, R. An Experimental Investigation of the Impact Response of Composite Laminates. *Composite Structures* **2009**, *87* (4), 307–313.

(160) Sanchez-Saez, S.; Barbero, E.; Zaera, R.; Navarro, C. Compression after Impact of Thin Composite Laminates. *Composites Science and Technology* **2005**, *65* (13), 1911–1919.

(161) de Freitas, M.; Reis, L. Failure Mechanisms on Composite Specimens Subjected to Compression after Impact. *Composite Structures* **1998**, *42* (4), 365–373.

PART II
Publications

PAPER I

DAMAGE-RESISTANT COMPOSITES USING ELECTROSPUN NANOFIBERS: A MULTISCALE ANALYSIS OF THE TOUGHENING MECHANISMS

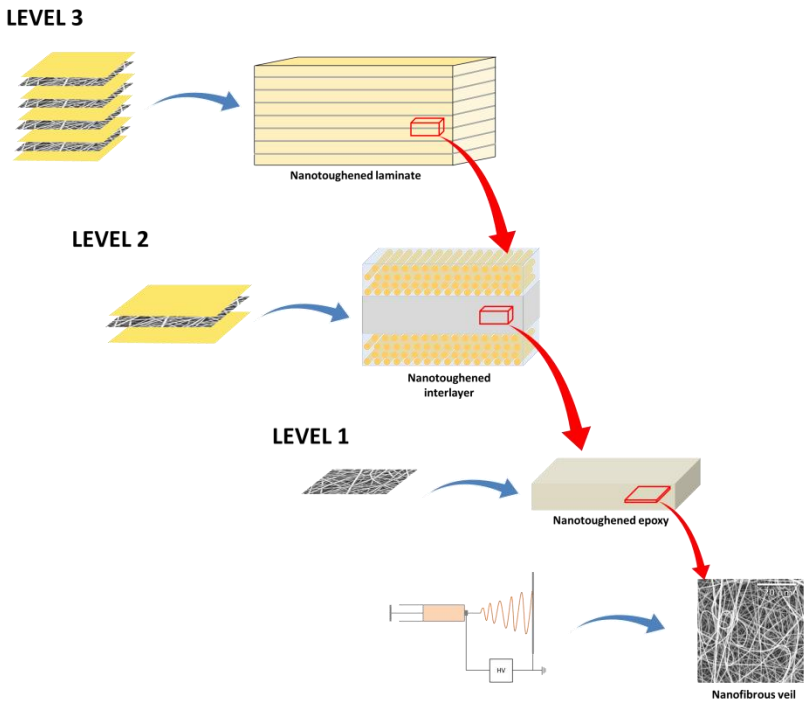

Lode Daelemans, Sam van der Heijden, Ives De Baere, Hubert Rahier, Wim Van Paepegem and Karen De Clerck

(2016) *ACS APPLIED MATERIALS & INTERFACES*. 8(18). p.111806-11818

ACS APPLIED MATERIALS & INTERFACES

Research Article

www.acsami.org

Damage-Resistant Composites Using Electrospun Nanofibers: A Multiscale Analysis of the Toughening Mechanisms

Lode Daelemans,[*,†] Sam van der Heijden,[*,†] Ives De Baere,[‡] Hubert Rahier,[§] Wim Van Paepegem,[‡] and Karen De Clerck[*,†]

[†]Department of Textiles, Ghent University, Technologiepark-Zwijnaarde 907, B-9052 Zwijnaarde, Belgium

[‡]Department of Materials Science and Engineering, Ghent University, Technologiepark-Zwijnaarde 903, B-9052 Zwijnaarde, Belgium

[§]Department Materials and Chemistry, Vrije Universiteit Brussel, Pleinlaan 2, B-1050 Brussels, Belgium

Supporting Information

ABSTRACT: Today, fiber-reinforced polymer composites are a standard material in applications where a high stiffness and strength are required at minimal weight, such as aerospace structures, ultralight vehicles, or even flywheels for highly efficient power storage systems. Although fiber-reinforced polymer composites show many advantages compared to other materials, delamination between reinforcing plies remains a major problem limiting further breakthrough. Traditional solutions that have been proposed to toughen the interlaminar region between reinforcing plies have already reached their limit or have important disadvantages such as a high cost or the need for adapted production processes. Recently, electrospun nanofibers have been suggested as a more viable interlaminar toughening method. Although the expected benefits are numerous, the research on composite laminates enhanced with electrospun nanofibrous veils is still very limited. The work that has been done so far is almost exclusively focused on interlaminar fracture toughness tests with different kinds of nanofibers, where typically a trial and error approach has been used. A thorough understanding of the micromechanical fracture mechanisms and the parameters to obtain toughened composites has not been reported as of yet, but it is crucial to advance the research and design highly damage-resistant composites. This article provides such insight by analyzing the nanofiber toughening effect on three different levels for several nanofiber types. Only by combining the results from different levels, a thorough understanding can be obtained. These levels correspond to the hierarchical nature of a composite: the laminate, the interlaminar region, and the matrix resin. It is found that each level corresponds to certain mechanisms that result in a toughening effect. The bridging of microcracks by electrospun nanofibers is the main toughening mechanism resulting in damage resistance. Nevertheless, the way in which the nanofiber bridging mechanism expresses itself is different for each scale and dependent on parameters linked to a certain scale. The multiscale analysis of the toughening mechanisms reported in this paper is therefore crucial for understanding the behavior of nanofiber toughened composites, and as such allows for designing novel, damage-resistant, nanofiber-toughened materials.

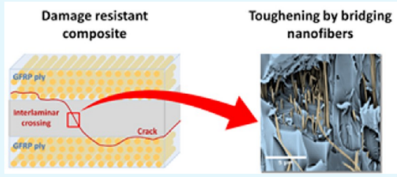

KEYWORDS: *nanocomposites, fiber reinforced polymer, electrospinning, fracture toughness, delamination, nanofiber bridging, veils*

1. INTRODUCTION

Fiber-reinforced polymer composite laminates are the material of choice for applications requiring a high stiffness and high strength with minimal density, hence, their wide use in wind turbine blades, airplanes, and many other applications over the last decades. However, because of their laminated structure, delamination between reinforcing plies and brittle matrix fracture are a major concern for fiber-reinforced composites and are among the most frequent types of failure encountered in service.[1,2] Traditional proposed solutions for this problem often involve mixing in tough thermoplastic materials, reactive rubbers, or stiff nanoparticles into the epoxy matrix.[3−8] These systems, however, significantly increase the viscosity of the uncured resin and thus have a detrimental effect on the resin flow, which is crucial to obtain high-quality laminates. Furthermore, a homogeneous dispersion of the toughening particles throughout the composite is not easily obtained.

Recently, a more viable method to increase the resistance to delamination has received a lot of attention. This method consists of interleaving the reinforcing plies with tough electrospun nanofibrous veils. As proposed by Dzenis and Reneker[9,10] and confirmed by recent literature,[11] electrospun thermoplastic nanofibrous veils have a high potential to be used as an interlaminar toughener for composite laminates.[12] These nanofibrous veils can be readily deposited between the primary reinforcing fiber layers prior to infusion or autoclaving, and

Received: February 23, 2016
Accepted: April 18, 2016

DOI: 10.1021/acsami.6b02247
ACS Appl. Mater. Interfaces XXXX, XXX, XXX−XXX

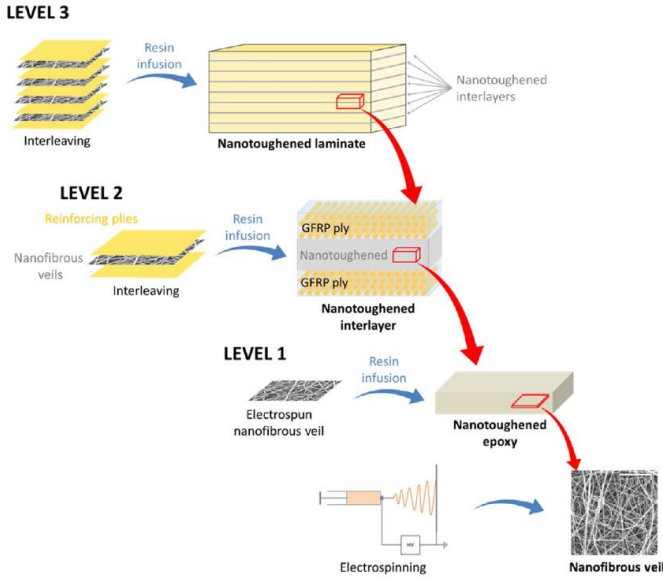

Figure 1. Multiscale approach for analyzing the toughening (micro)mechanisms in composites interleaved with electrospun nanofibrous veils.

thus, do not affect the viscosity of the epoxy resin. Furthermore, because of their high porosity, the resin flow is hardly affected. Nanofiber-toughened composites are novel for their superior performance and can be comprised of a wide variety of polymer materials, while the electrospinning process used for producing nanofibrous veils is relatively simple and scalable.[13,14] The research on composite laminates enhanced with electrospun nanofibrous veils is currently limited to interleaving a specific type of polymer nanofibers into the composites and determining the fracture toughness using standard interlaminar fracture tests under Mode I and Mode II loadings.[15−26] However, there are also a lot of (seemingly) discrepancies in these results. These discrepancies are probably related to the toughening (micro)mechanisms, which are present in nanofiber interleaved laminates. To the best of our knowledge, these micromechanical fracture mechanisms and the generic parameters to obtain toughened composites have not been reported before. Nevertheless, such more generic understanding is crucial to select the right type of nanofiber and design novel toughened composites. To do so, standard interlaminar fracture tests provide useful information on an "interlaminar" level, but in addition other approaches are needed to study the toughening effect on different scales. In this paper, we provide such insights by analyzing the nanofiber toughening effect on three different levels simultaneously (Figure 1): (i) nanotoughened epoxy, (ii) nanotoughened interlaminar region, and (iii) nanotoughened laminate. These levels coincide with the hierarchical nature of laminated composite materials.

Level 1, the nanotoughened epoxy, provides insights on the interaction between the nanofibers and the epoxy resin. The mechanical properties of the electrospun nanofibers and their effect on the resulting nanotoughened epoxy—composed of nanofibers embedded in epoxy resin—are analyzed. Similarly to regular fiber-reinforced composites, the properties of such a nanotoughened epoxy will mainly depend on the mechanical properties of the nanofibers and epoxy matrix as well as the adhesion between them. Two types of nanofibers were selected as model systems, polyamide and poly(ε-caprolactone), as both of them have a high potential in interlaminar fracture toughness improvements.[15,16,27]

The interlaminar region in laminated composites, the focus of Level 2, is considered to be a weak part of the composite, as it consists of a resin-rich layer and is exposed to stress concentrations due to a mismatch in elastic properties of adjacent plies. The interlaminar fracture toughness is often a limiting design parameter since failure on the structural level of composites is predominantly governed by delamination between plies resulting from cracks in the interlaminar region. By interleaving the composites with nanofibrous veils, the interlaminar region will consist no longer solely out of brittle epoxy resin, but rather of the nanotoughened epoxy. Hence, Level 2 investigates the effect of the nanotoughened interlayer on the delamination behavior of the interlaminar region.

DOI: 10.1021/acsami.6b02247
ACS Appl. Mater. Interfaces XXXX, XXX, XXX−XXX

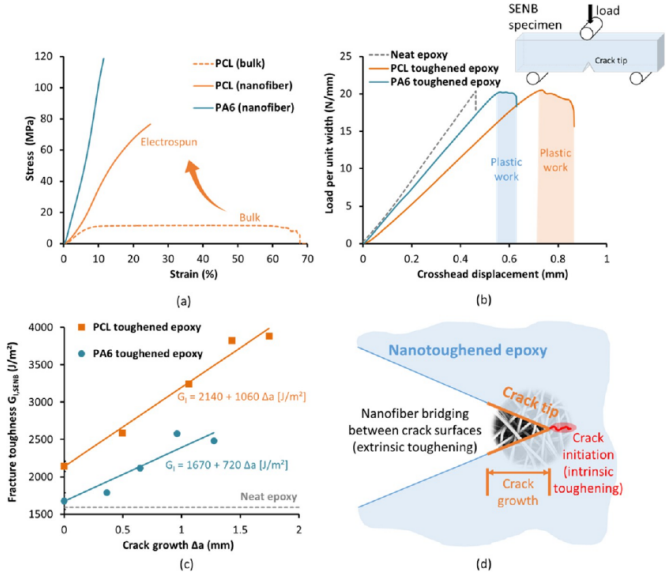

Figure 2. Toughening mechanisms in nanofiber-reinforced epoxy. (a) Stress−strain curves illustrating the different tensile properties of PCL and PA6 nanofibers. Bulk PCL properties are also shown, as the embedded PCL nanofibers will melt due to the postcuring of the epoxy resin. (b) Load−displacement curves of SENB specimens show that, while the epoxy resin exhibits brittle fracture, PCL and PA6 nanotoughened epoxy fails by extensive plastic fracture. (c) The nanotoughened epoxy has a higher fracture toughness than the unmodified bulk epoxy resin. Furthermore, its fracture toughness increases substantially with increasing crack growth. (d) Illustration of the intrinsic and extrinsic toughening mechanisms in the nanotoughened epoxy.

The final level, Level 3, is that of a nanotoughened composite laminate in which multiple interlayers have been interleaved with a nanofibrous veil. By using a realistic multidirectional stacking sequence and experiments that simulate in-service loading conditions, this level analyzes the toughening effect, which can be expected in applications. It is thus to link the insights from Level 1 and Level 2 to the damage resistance of a true life composite. This multilevel approach allows us to accurately determine the crucial parameters and toughening mechanisms through the use of electrospun nanofibers on the micro- and macroscale, which is necessary for the design of advanced composite materials.

2. RESULTS AND DISCUSSION

Level 1: Nanotoughened Epoxy. Level 1 analyzes the effect of the electrospun nanofibers' properties on the fracture toughness of bulk epoxy (Figure 1) to determine the toughening mechanism of nanofibers. Two types of nanofibers were selected as model systems, that is, polyamide 6 (PA6) and poly(ε-caprolactone) (PCL), both of which have a high toughness compared to the epoxy matrix[28] but different mechanical properties (Figure 2a). The PA6 nanofibers show a relatively high E-modulus (960 ± 30 MPa) and tensile strength (101 ± 9 MPa). Their response is fairly elastic with relatively low strain at failure compared to the PCL nanofibers, which have a lower E-modulus (391 ± 54 MPa) as well as tensile strength (79 ± 3 MPa). The electrospinning process often results in a superior mechanical response of electrospun nanofibers compared to the bulk material due to the molecular alignment of polymer chains;[29,30] for example, bulk PCL polymer has a lower E-modulus (195 ± 10 MPa) as well as tensile strength (11.3 ± 0.3 MPa) compared to the PCL nanofibers and deforms by extensive yielding (Figure 2a). The tensile properties of the embedded PCL nanofibers are expected to be between the bulk and the electrospun properties due to the curing cycle of the epoxy resin. The resin is first cured at room temperature followed by a second curing step at an elevated temperature of 80 °C according to the manufacturer's recommended cure cycle. The second curing stage results in melting and resolidifying of the PCL nanofibers (melting point ∼60 °C) in a confined region with the same size as the initial nanofiber. The tensile properties of the embedded PA6 nanofibers, however, are expected to be close to the electrospun properties due to their relatively high melting point (∼220 °C).

The PA6 and PCL nanofibers were used to produce relatively thick (7 mm) nanotoughened epoxy plates by infusing a stacking of nanofibrous veils with epoxy resin under vacuum.

DOI: 10.1021/acsami.6b02247
ACS Appl. Mater. Interfaces XXXX, XXX, XXX−XXX

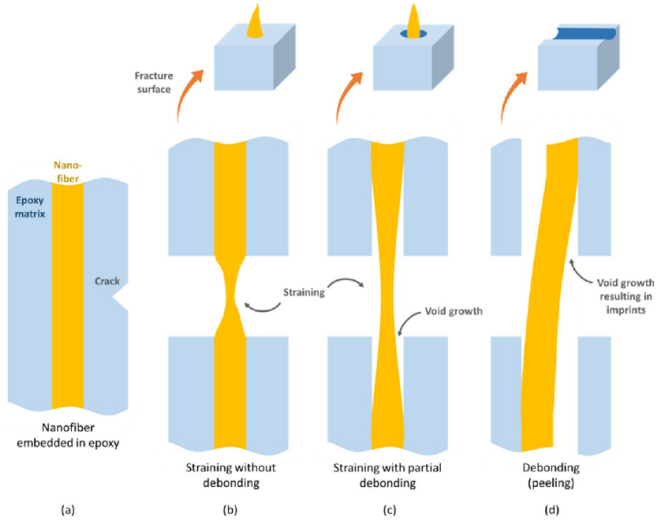

Figure 3. Interaction of a bridging nanofiber with the crack front. (a) Schematic view of an embedded nanofiber interacting with the crack front, which can result in (b) straining of the nanofiber without debonding, (c) straining of the nanofiber with partial debonding from the epoxy, or (d) complete debonding of the nanofiber (peeling).

The volume fraction of nanofibers was controlled to be similar to the volume fraction of nanofibers in the interlaminar region (Section 4). To the best of our knowledge, such thick nanotoughened epoxy plates have never been characterized or even produced before. It allowed us to accurately determine the fracture toughness via the standardized single edge notched bending (SENB) method. The SENB experiments show that, while the matrix resin exhibits brittle failure, that is, sudden and complete failure at the point of crack initiation, both PCL and PA6 nanotoughened epoxy fail by extensive plastic failure (Figure 2b). This results in an increased fracture toughness of the nanotoughened epoxy compared to the bulk epoxy resin (Figure 2c). The larger amount of energy required to initiate cracks in the nanotoughened epoxy indicates that the nanofibers result in intrinsic toughening, that is, toughening mechanisms acting in the fracture processing zone in front of the crack tip (Figure 2d). These toughening mechanisms are most likely related to yielding of the nanofibers. Since the embedded PCL nanofibers will exhibit excessive yielding when loaded, this effect is especially evident in the PCL nanotoughened epoxy where ~30% more energy is required for crack initiation. Additionally, the crack propagation energy increases tremendously, as can be noted from the sustained loading capability of the nanotoughened epoxy specimens after crack initiation. Basically, more and more energy is required to extend the crack in nanotoughened epoxy (Figure 2c), while the brittle unmodified epoxy immediately fails when the critical load is reached. This increase in propagation fracture toughness can be related to the extrinsic toughening mechanism of *nanofiber bridging* (Figure 2d): upon crack extension, nanofibers will bridge the newly formed crack surfaces and take up energy by straining, yielding, and fracture. Hence, the fracture toughness of the nanotoughened epoxy increases with increasing crack growth as the zone of bridging nanofibers becomes larger.

The proposed mechanism of nanofiber bridging was confirmed by scanning electron microscopy (SEM) analysis on the fracture surface of broken SENB specimens. The three main mechanisms acting in nanofiber bridging zones observed from the SEM images are schematically illustrated in Figure 3, that is, straining of the nanofiber without debonding, straining of the nanofiber with partial debonding, and full debonding/peeling of the nanofibers. The SEM images showed a high degree of irregularity and plastically deformed nanofibers protruding from the epoxy as opposed to the flat mirrorlike fracture surface of neat epoxy specimens (Figure 4). For the bridging nanofibers to increase the fracture toughness, it is important they take up more energy by bridging than the energy that would be required to fracture neat epoxy resin in that area. Furthermore, the nanofiber-matrix adhesion is also of crucial importance for a good load transfer to the nanofibers. Zoomed in SEM images of the SENB fracture surface reveal that the PCL-epoxy adhesion is very good, whereas it seems rather low for PA6 nanofibers. Earlier experiments show that PCL can dissolve into uncured epoxy resin, especially at high temperatures.[31] However, because of the first curing step at room temperature where minor diffusion at the PCL-epoxy interface already occurs, the diameter of the PCL nanofibers is retained in the final nanotoughened epoxy. Indeed, after the first curing stage, the epoxy resin has already reacted to such

DOI: 10.1021/acsami.6b02247
ACS Appl. Mater. Interfaces XXXX, XXX, XXX−XXX

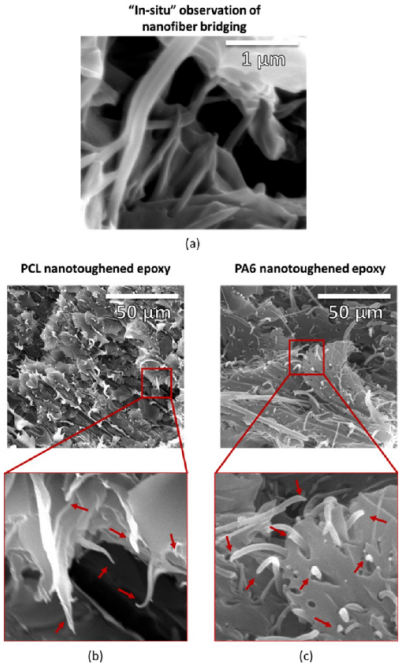

Figure 4. (a) In situ observation of nanofibers bridging a microcrack in a tested specimen. (b) SEM images of SENB fracture surface of PCL nanotoughened epoxy showing good adhesion between epoxy and PCL nanofibers. The PCL nanofibers are strained without debonding from the epoxy. (c) In contrast, the adhesion between epoxy and PA6 nanofibers was rather low as indicated by the smooth surface of the PA6 nanofibers and imprints left in the epoxy.

extent that complete dissolution of the PCL is prevented during the second curing stage.[15] These curing stages result in a diffuse boundary between PCL and epoxy in which there is some mechanical interlocking on the molecular level. The good interfacial adhesion of PCL nanofibers can be explained by this partial diffusion of PCL into the epoxy resin. It results in a diffuse interfacial region with no distinct transition between PCL and epoxy, which leads to a good adhesion between both polymers.[32,33] PA6 nanofibers, however, do not dissolve into the epoxy resin and have very limited chemical interaction with it.[34,35] The adhesion of PA6 nanofibers and the epoxy resin will mainly be governed by fairly weak van der Waals forces. Although the high surface area to volume ratio of the PA6 nanofibers allows for sufficient adhesion strength under shear forces, the adhesion strength rapidly declines when the nanofibers are subjected to peeling forces (normal forces).[36] This mechanism is also observed on the SEM images of broken PA6 nanotoughened epoxy specimens where a certain fraction of nanofibers seemed to be peeled from the epoxy resin without much deformation (Figure 4c). These nanofibers are not likely to take up much energy as they do not deform but rather peel from the matrix, and therefore they have no significant contribution to the fracture toughness of the nanotoughened epoxy. As such, the difference in nanofiber-epoxy adhesion for PA6 and PCL, combined with the higher amount of yielding and the overall higher work of rupture of the PCL nanofibers, can explain why the PCL nanocomposites showed the best improvements in fracture toughness.

Level 2: Nanotoughened Interlaminar Region. Level 2 analyses the interlaminar region of nanofiber interleaved composites, which consists of the nanofiber toughened epoxy of Level 1 between reinforcing plies (Figure 1). The interlaminar fracture toughness is analyzed under both Mode I and Mode II loading, G_{Ic} and G_{IIc} by the double cantilever beam (DCB) and end nnotch flexure (ENF) methods, respectively, for an extensive set of composites interleaved with PCL and PA6 nanofibers. The improvement in interlaminar fracture toughness for PA6 and PCL interleaved composites with identical nanofibrous veil areal density, reinforcing ply architecture and interleaving method, is shown in Figure 5a. The G_{Ic} and G_{IIc} values were both obtained at the point of macroscopic delamination initiation. Both PCL and PA6 nanofibers show an extraordinary increase in G_{IIc}. This result is in accordance with the results obtained in Level 1, where both PA6 and PCL nanocomposites had an increased fracture toughness. The increase in G_{Ic} is slightly lower than the increase in G_{IIc} for the PCL-toughened laminates, whereas PA6 nanofibers seemed to have hardly any effect on G_{Ic}. Based only on the results of the Level 1, one would not expect such a different behavior between Mode I and Mode II loading conditions. However, under Mode I loading, crack growth subjects the nanofibers to normal forces. When the nanofiber-matrix adhesion is low, for example, in case of PA6 nanofibers (see Level 1), this causes extensive peeling of the nanofibers. Hence, the adhesion between nanofiber and epoxy resin becomes very important under Mode I delamination growth, as low interfacial strength results in low-energy uptake by the nanofibers and thus low toughening. This mechanism results in minor to no improvements in G_{Ic} for PA6 interleaved laminates. Under Mode II loading conditions, adhesion between nanofiber and epoxy resin poses less of a problem as the shear adhesion strength of all nanofibers is relatively high due to their high surface area to volume ratio.[36] As a result, high improvements in G_{IIc} are obtained for PCL as well as PA6 nanofiber-toughened composites.

Microscopic analysis of tested DCB and ENF specimens showed the presence of additional micromechanisms related to the interlaminar region, which affect the fracture toughness of the nanofiber toughened composites. Figure 6 and Figure 7 schematically present the observed delamination path for Mode I and Mode II loadings (actual microscopic images are given in Figure S1 and Figure S2). Contrary to the common assumption that delaminations propagate in the middle of the interlaminar region, microscopy showed that delaminations in virgin composites progress almost exclusively at the glass fiber-epoxy interface. The energy required for such interfacial failure will depend on the adhesion of the glass fibers with the matrix resin and forms the major contribution to G_{Ic} and G_{IIc} of virgin laminates. The delaminations in nanofiber interleaved composites show the same glass fiber-epoxy interfacial failure, but they additionally show regular crossings of the interlaminar region

DOI: 10.1021/acsami.6b02247
ACS Appl. Mater. Interfaces XXXX, XXX, XXX−XXX

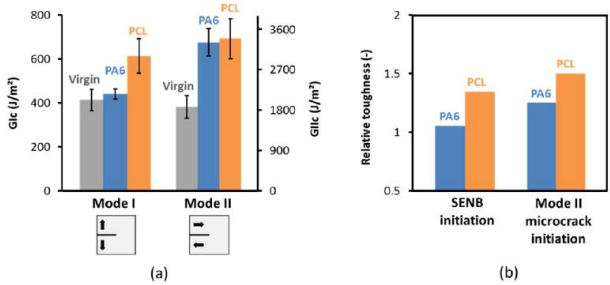

Figure 5. (a) Mode I and Mode II interlaminar fracture toughness for nanofiber interleaved composite laminates increases substantially compared to virgin (noninterleaved) laminates. (b) Relative fracture toughness (compared to reference material without nanofibers) of SENB results (Level 1) and Mode II microcrack initiation (Level 2) is similar, since Mode II initiation is governed by tensile microcracks in the nanocomposite interlayer material.

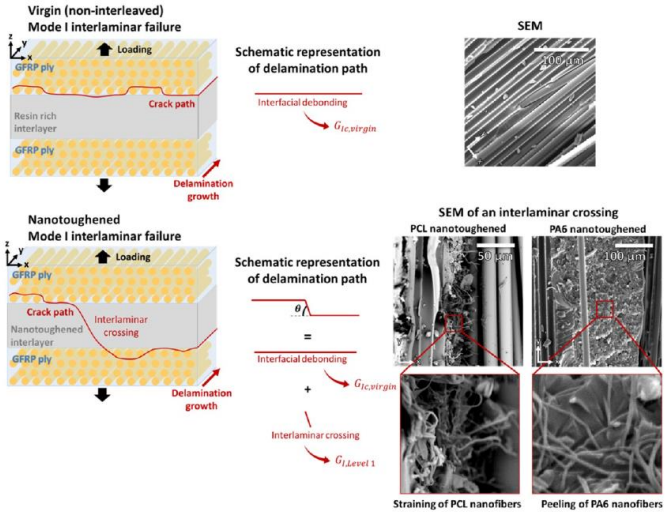

Figure 6. Schematic view of the delamination path in virgin (noninterleaved) and interleaved composite laminates under Mode I loading. Noninterleaved laminates show almost exclusively glass fiber-epoxy debonding. In interleaved composite laminates, sporadic interlaminar crossings are observed besides glass fiber-epoxy debonding. Analysis of the fracture surface with SEM showed that nanofiber bridging zones develop in these interlaminar crossings. Adhesion between PCL and epoxy was relatively compared to the low adhesion between PA6 and epoxy, which resulted in extensive peeling of the PA6 nanofibers.

through the nanotoughened interlayer. The amount of glass fiber-epoxy interfacial failure remains similar to that in virgin laminates as the interlaminar crossings are oriented transversely to the macroscopic delamination plane (Figure 6). However, the interlaminar crossings result in a crack through the nanotoughened epoxy, which causes nanofiber bridging. Each interlaminar crossing corresponds to a crack through nanotoughened epoxy similar to the material studied in Level 1. Hence, the increase in Mode I interlaminar fracture toughness of the nanofiber interleaved specimens, $\Delta G_{Ic,Level\ 2} = G_{Ic,interleaved} - G_{Ic,virgin}$, can be attributed to the total amount of interlaminar crossing fracture surface area and the fracture toughness of the nanotoughened epoxy, $G_{I,Level\ 1}$, obtained in Level 1:

$$\Delta G_{Ic,Level2} \approx G_{I,Level1}\left[\frac{nt}{\sin\theta}\right] \quad (1)$$

DOI: 10.1021/acsami.6b02247
ACS Appl. Mater. Interfaces XXXX, XXX, XXX−XXX

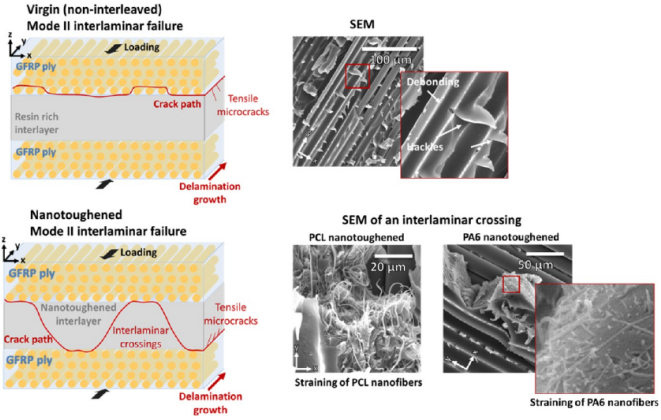

Figure 7. Schematic view of the delamination path in virgin (noninterleaved) and interleaved composite laminates under Mode II loading. Noninterleaved laminates show almost exclusively glass fiber-epoxy debonding combined with hackle formation. The hackles develop due to the formation of tensile microcracks in front of the crack tip. In nanofiber interleaved laminates, sporadic interlaminar crossings are observed besides glass fiber-epoxy debonding and hackle formation. More interlaminar crossings are observed under Mode II loading than under Mode I loading. Analysis of the fracture surface with SEM showed that nanofiber bridging zones also develop in the interlaminar crossings where both PCL and PA6 nanofibers are strained.

where n is the amount of crossings per unit delamination width, t is the thickness of the interlayer, and θ defines the angle of the interlaminar crossings with the delamination plane (Figure 6). Microscopy images of tested DCB specimens near the initiation point allow for measuring the total amount of interlaminar crossing fracture surface area (n, t, and θ). In combination with the $G_{I,Level\ 1}$ values determined under Level 1, this allows for the calculation of $\Delta G_{Ic,Level\ 2}$ according to eq 1. This resulted in a very good agreement with $\Delta G_{Ic,Level\ 2}$ determined from DCB experiments, thus validating the proposed equation. The correlation between $G_{I,Level\ 1}$ and $\Delta G_{Ic,Level\ 2}$ is further confirmed by SEM analysis. Images of the fracture surface around interlaminar crossing of tested DCB specimens are shown in Figure 6. It can be observed that nanofibers are protruding from the fracture surface and have been strained until failure or have been peeled off in the case of PA6 nanofibers. Furthermore, a "mirror-image" is obtained by studying both fracture surface halves. This indicates that extensive nanofiber bridging occurred in these interlaminar crossings during delamination.

In case of Mode II loading, the virgin laminates show glass fiber-epoxy debonding as well as typical hackle formation due to shearing of microcracks (Figure 7). The fracture mechanism under Mode II loadings is more complex and consists of tensile (Mode I) microcrack formation in front of the crack tip in the interlaminar region followed by microcrack coalescence and hackle formation due to shear stresses.[37,38] The coalescence of microcracks in turn results in macroscopic delamination advance. Hence, the improvement in Mode II interlaminar fracture toughness ΔG_{IIc} is a combination of the development of nanofiber bridging zones in microcracks—which form in the interlaminar region—as well as in interlaminar crossings. Previous work has shown that the contribution of interlaminar crossings is higher than that of microcrack formation.[27] Just as for Mode I loading, the interlaminar crossings are related to the improved fracture toughness of the nanotoughened epoxy on Level 1. In addition, since microcrack initiation under Mode II loadings is governed by the formation of tensile microcracks in the interlaminar region, the increase in energy required to form these microcracks in the nanotoughened interlayer is similar to the increase in fracture toughness of the nanotoughened epoxy itself (Figure 5b).

The interlaminar crossings are very important to obtain highly toughened composites, as they are the main cause of nanofiber bridging on the interlaminar level as observed from the Level 2 testing. One important parameter that can drastically affect the obtained interlaminar fracture toughness is the nanofibrous veil areal density. On the one hand, the interlaminar fracture toughness increases with increasing nanofibrous veil areal density as the interlaminar thickness t increases linearly with veil density (Figure 8a). On the other hand, the amount of interlaminar crossings n under Mode I loadings quickly declines with increasing nanofibrous veil density, resulting in an optimum ΔG_{Ic} at intermediate veil densities of ∼10 g/m^2 for PCL nanotoughened composites (Figure 8b). For PA6 nanotoughened composites, only minor improvements in G_{Ic} independent of the veil density were obtained due to excessive peeling of the PA6 nanofibers in the interlaminar crossings (Figure 8b). Under Mode II loadings, the amount of interlaminar crossings is much less affected, and ΔG_{IIc} increases with increasing nanofiber veil density (Figure 8c). In addition, we have previously shown that the interleaving method as well as the nanofibers' mechanical properties affect the amount of interlaminar crossings and, thus, the resulting interlaminar fracture toughness. An analysis of the interleaving methodology demonstrated that electrospinning nanofibers

DOI: 10.1021/acsami.6b02247
ACS Appl. Mater. Interfaces XXXX, XXX, XXX−XXX

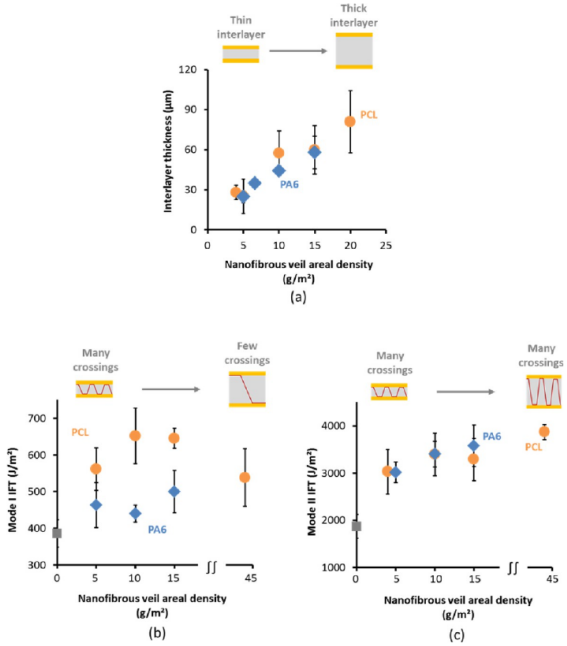

Figure 8. (a) The interlayer thickness of interleaved composite laminates increases linearly with nanofibrous veil areal density and is similar for PA6 and PCL nanotoughened laminates. (b) The Mode I interlaminar fracture toughness of PCL interleaved laminates shows an optimum at 10−15 g/m^2 veil density as the amount of interlaminar crossings decreases with increasing veil density. The improvement in Mode I interlaminar fracture toughness of PA6 interleaved laminates is relatively low and independent of the veil density, since excessive peeling of the PA6 nanofibers occurs in the interlaminar crossings, which does not take much energy. (c) The Mode II interlaminar fracture toughness increases with increasing veil density for PCL and PA6 interleaved laminates, as the amount of interlaminar crossings is relatively independent of the veil density, and no peeling occurs.

directly onto the reinforcing plies facing the interlaminar region results in a higher amount of interlaminar crossings.[15] The effect of nanofibers' mechanical properties was studied using mechanically tunable electrospun styrene−butadiene−styrene (SBS) fibers, which showed that the amount of interlaminar crossings is linked to the tensile properties of the SBS fibers. This again confirms that the obtained interlaminar fracture toughness of a nanofiber-interleaved laminate depends on the micromechanisms and the delamination path in the interlaminar region. As such, seeming discrepancies can be observed in literature, since interleaving a specific type of polymer nanofibers into a composite laminate will not always result in the same toughening effect. For example, while several researchers report relatively high improvements in interlaminar fracture toughness on introducing polyamide nanofibrous veils,[16,18,23] other researchers only report small to no improvements for polyamide interleaved laminates.[26,39] Indeed, although the same nanofiber type is used, different results will be obtained depending on parameters such as the used interleaving method, the nanofibrous veil areal density, or the nanofibers' mechanical properties. Hence, it is important to take these effects into account and perform delamination crack path studies such as done in this work to interpret the obtained results and compare different studies to each other for future studies.

Generally, to increase the fracture toughness on the interlaminar level, the interaction between the delamination path (interlaminar crossings, microcrack formation) and the nanocomposite interlayer characteristics (fracture toughness, nanofiber properties, adhesion) are of crucial importance and should be considered to design damage-resistant composite materials.

Level 3: Nanotoughened Laminate. Finally for Level 3, the toughening capability of electrospun nanofibers is shown on a large-scale laminate with a true life realistic stacking sequence, which is subjected to a low-velocity impact (m = 8.17 kg, v = 4 m/s, E = 67 J). Crossply $[0°/90°]_{2S}$ composite laminates were produced with PA6 or PCL nanofibrous veils placed between reinforcing plies on every 0°/90° interface. The effect of nanofiber toughening can clearly be noted from looking at the

DOI: 10.1021/acsami.6b02247
ACS Appl. Mater. Interfaces XXXX, XXX, XXX−XXX

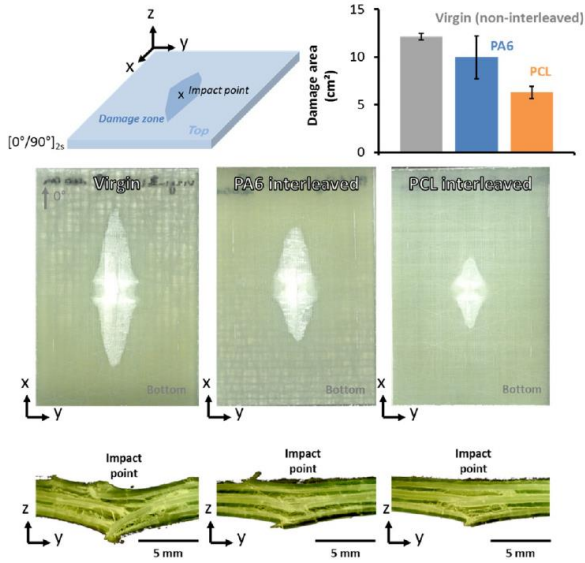

Figure 9. Damage decreases for nanofiber interleaved composite laminates indicating a higher impact resistance. The damage area decreases up to 50% for PCL interleaved laminates. A cross-sectional view underneath the impact point shows that the amount of damage is severely reduced for nanofiber-interleaved laminates resulting in a small dent with relatively low amount of internal damage compared to the virgin (noninterleaved) material.

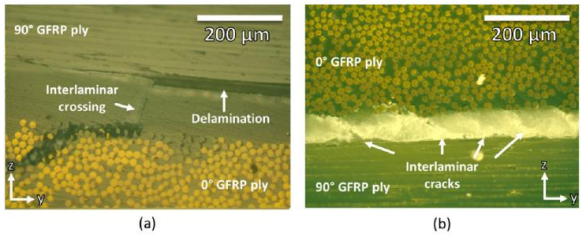

Figure 10. (a) The damage mechanisms under impact show similarities with the interlaminar fracture tests of Level 2 such as delaminations with sporadic interlaminar crossings. (b) However, more damage mechanisms are present under impact loading conditions, and interlaminar cracks, not related to delamination, are also observed.

damage area as it decreases dramatically for nanofiber interleaved composites (Figure 9). Furthermore, the virgin composites showed large indentations at the point of impaction due to excessive failure of the composite, while this indentation and associated damage are limited for nanofiber interleaved composites. Hence, the nanofibers effectively toughen the composites when subjected to impact loadings. This is especially evident in composites interleaved with PCL nanofibers where a reduction in damage area of ~50% is obtained.

Structural composite laminates are typically made of reinforcing plies with different ply orientation to have high mechanical properties in several directions. As opposed to the standard DCB and ENF methods, which are optimized to measure interlaminar fracture toughness between 0°/0° interfaces in unidirectional specimens, delaminations will naturally occur at interfaces with dissimilar orientation during impact due to the mismatch in elastic properties. Hence, the delamination mechanism of a nanofiber-interleaved laminate

DOI: 10.1021/acsami.6b02247
ACS Appl. Mater. Interfaces XXXX, XXX, XXX−XXX

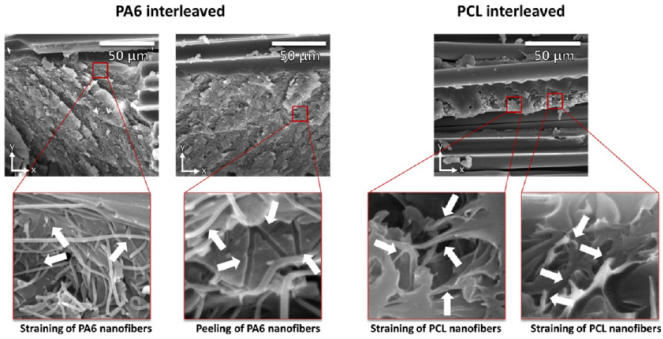

Figure 11. SEM images of the interlaminar cracks/crossings of impacted specimens show nanofiber bridging zones with strained and fractured nanofibers (see arrows). Because of the low adhesion between PA6 nanofibers and epoxy, peeling of the PA6 nanofibers (see arrows) is also observed due to local Mode I loading conditions. In comparison, this is not observed for the PCL nanofibers do to their good adhesion with the epoxy.

can be affected by the reinforcing ply orientation at the delamination interface. Microscopy on impacted specimens and SEM images of the fracture surfaces in the delamination region show a mixed mode delamination behavior, exhibiting fracture mechanisms that are typical for Mode I as well as for Mode II loadings like extensive peeling of PA6 nanofibers and hackle formation. There are many similarities with the results obtained in Level 2 such as sporadic interlaminar crossings in which nanofiber bridging zones develop (Figure 10a). In accordance with Level 2, SEM analysis of the fracture surfaces after impact showed nanofiber bridging zones with plastically deformed PCL nanofibers indicating good load transfer due to good adhesion, while many PA6 nanofibers showed signs of interfacial failure (Figure 11). As such, PCL nanofiber-interleaved laminates also perform better at the laminate level due to their good adhesion and large amount of interlaminar crossings, resulting in a highly toughened response.

Although a large analogy exists between the fracture mechanisms in Level 2 and those observed on the laminate level, not all damage mechanisms can be directly extrapolated from the DCB and ENF experiments. This is most evident when looking at the damage zone directly under the point of impact, where damage mechanisms such as matrix cracking and reinforcing fiber failure are present besides delamination. These damage mechanisms can also result in interlaminar cracks that are not due to delamination but also result in a toughened response, as the interlaminar cracks can be related to the improvement in fracture toughness of the nanotoughened epoxy studied in Level 1 (Figure 10b). Another important difference between both levels is related to the 0°/90° delamination interface at Level 3, which is representative for delaminations in real applications as compared to the controlled delamination growth at a 0°/0° delamination interface in DCB and ENF specimens. Indeed, the latter may lead to values that are not representative for the true life material. Hence, experiments done at the laminate level are advantageous as they provide additional information on how the nanoreinforcements affect the toughness of a laminate subjected to more realistic loading conditions. This stage is especially important to elucidate the full potential of these novel damage-resistant composite materials.

3. CONCLUSION

This paper shows that electrospun nanofibrous veils are a viable option to design advanced composite materials with a very high damage resistance. The electrospinning process is relatively simple, scalable, and can be used to produce nanofibers from a whole set of polymers ranging from traditional polymers like polyamides to specially designed polymers for toughening purposes. Their effect is shown to be significant, not only on a microscopic level in nanotoughened epoxy, as is the case for most other nanotougheners, but also on an interlaminar and laminate level. We performed a multiscale analysis of the toughening micromechanisms that are present in nanofiber toughened composites for two distinct nanofiber types (PCL and PA6). This allowed us to gain insight and uncover the crucial parameters that are necessary to design highly damage-resistant materials.

On Level 1, that of the nanotoughened epoxy resin, yielding of nanofibers in the fracture processing zone as well as nanofiber bridging increases the fracture toughness substantially. The effect is mainly determined by the mechanical properties of the nanofibers and their interaction with the matrix resin. The fracture behavior of the nanotoughened epoxy is representative for cracks in the interlaminar region on the parent levels (Level 2 and Level 3).

On Level 2, that of the nanotoughened interlaminar region, careful analysis of the delamination path was found to be crucial for understanding and optimizing the interlaminar toughening effect of electrospun nanofibers. More specifically, it was shown that crossings of the interlaminar region are the main contributors to the increase in interlaminar fracture toughness as nanofiber bridging zones develop in them. The amount of these interlaminar crossings can depend on numerous parameters such as the delamination mode, the nanofibrous veil areal density, reinforcing ply architecture, interleaving method, and mechanical poperies of the nanofibers. To obtain damage-resistant materials, it is important to consider these

DOI: 10.1021/acsami.6b02247
ACS Appl. Mater. Interfaces XXXX, XXX, XXX−XXX

effects, as they will affect the interlaminar fracture toughness of the nanotoughened composite materials.

At Level 3, that of a fully interleaved composite laminate with a realistic stacking sequence, fracture mechanisms similar to Level 2 are observed in every interlayer. Delamination growth in the interlaminar regions is hindered due to the formation of nanofiber bridging zones in the interlaminar crossings. Additionally, interlaminar cracks through the nanotoughened interlayer not related to delaminations cause an added toughening effect besides the increased delamination resistance. These interlaminar cracks will also develop nanofiber bridging zones and result in a locally increased fracture toughness.

The insight gained throughout the multiscale analysis is crucial to advance the research for these novel materials. It allows for optimizing and designing highly toughened advanced composite applications. Furthermore, uncovering the important parameters through the multiscale analysis allows more dedicated future research on specific parameters.

4. MATERIALS AND METHODS

Nanofiber Veil Preparation. PCL (Sigma-Aldrich, M_N 80 000) and PA6 nanofibers (Sigma-Aldrich, M_W 51 000 g/mol) were electrospun from a formic acid (Sigma-Aldrich, 98%)/acetic acid (Sigma-Aldrich, 98%) solution according to previously reported procedures.[40,41] An in-house developed multinozzle electrospinning machine was used.[42] The PCL and PA6 nanofibers had a diameter of 343 ± 150 nm and 195 ± 35 nm, respectively. Representative SEM images are shown in Figure 12. All stated nanofiber diameters were measured on dry samples prior to resin infusion. This allowed for the best sample handling and reproducible measurements. In addition, multiple SEM images were also taken to study the fracture surface of loaded specimens (SENB, DCB, ENF, and impact) showing the embedded nanofibers in the epoxy resin. Although the nanofibers have already been deformed in these specimens, the image analysis confirmed that the dry nanofiber diameters are indeed a good measure for the embedded nanofibers.

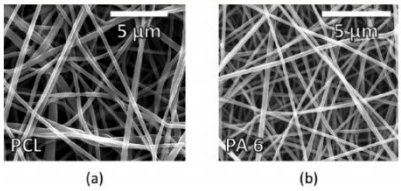

Figure 12. Representative SEM images of (a) PCL and (b) PA6 electrospun nanofibers.

Tensile Properties of Nanofibers. PA6 tensile properties were measured on a bundle of aligned nanofibers, whereas the tensile properties of the PCL inside the cured composite was approximated by the bulk properties of PCL films. The tensile experiments were performed according to a previously reported procedure.[43]

Nanotoughened Epoxy Production. Nanofiber/epoxy nanocomposites were made by an in-house developed VARTM setup. This setup consisted out of a two-piece flat steel mold with inner dimensions of 300 × 150 × 7 mm^3. To make the nanocomposites, a stacking of nanofibrous veils (±68 g/m^2) with dimensions of 300 × 150 mm^2 was used. The amount of nanofibrous veils was selected to have ∼17 vol % of nanofibers in the final nanocomposite. This is representative for the amount of nanofibers present in the interlayer between reinforcing plies of the nanofiber interleaved laminates. Prior to infusion, the epoxy resin (EPIKOTE MGS RIMR135) and hardener (EPIKURE MGS RIMH137) were mixed in a 100:30 mass ratio using a mechanical stirrer. The mixture was placed under vacuum for 15 min to remove any trapped air introduced during mixing. After infusion of the nanofibrous veils, the mold was cured at 23.2 °C and 50% relative humidity for 24 h, followed by a second curing step at 80 °C for 15 h according to the manufacturer's recommended cure cycle. Virgin epoxy plates (without nanofibers) were made by casting the epoxy resin in an empty mold.

Fracture Toughness of Nanotoughened Epoxy. SENB experiments were performed according to ASTM D5045. The samples had a thickness of 5 mm. A sharp natural precrack was produced by milling a starter notch in the specimens, followed by tapping a fresh razor blade in the milled notch with a dynamic precracking drop tower apparatus.[28] The experiments were performed on an electromechanical Instron 3369 with a load cell of 500 N.

Interlaminar Fracture Toughness. Unidirectional $[0°]_8$ laminates with PCL or PA6 nanofibers in the tested interlayer and were manufactured according to previously reported procedure by VARTM using UDO ES500 unidirectional glass fiber plies.[15] The laminates had a nominal thickness of 3 mm. The nanofibers were directly spun onto the reinforcing plies facing the midplane. The interlaminar fracture toughness was evaluated using DCB[15,44] as well as ENF[27] experiments.

Low-Velocity Impact. Low-velocity impact tests were performed according to ASTM D7136 at an impact energy of 67 J (drop height of 1 m and impactor mass of 8.17 kg). The tests were executed on an in-house developed impact test machine. The test machine was equipped with a Gen 5I oscilloscope to record acceleration, load, and displacement data of the impactor. Two Photron SA4 high-speed cameras were used to observe the upper and lower faces of the specimens during impact. A third AP-XRS high-speed camera was used to measure displacement, velocity, and acceleration of the impactor by the use of a specific line pattern stuck on the impactor. Crossply [0°/90°]2S specimens with a nominal thickness of 3 mm were used. Electrospun nanofibrous veils were interleaved on each 0°/90° interface. The damage area after impact was measured optically.

■ ASSOCIATED CONTENT

Supporting Information

This material is available free of charge online at The Supporting Information is available free of charge on the ACS Publications website at DOI: 10.1021/acsami.6b02247.

Microscopic images of delamination paths and values of ΔG_{Ic} calculated according to eq 1. (PDF)

■ AUTHOR INFORMATION

Corresponding Author

*E-mail: Karen.DeClerck@UGent.be. Phone: +32 9 264 57 40. Fax: +32 9 264 58 46.

Author Contributions

*Both authors contributed equally to this work

Notes

The authors declare no competing financial interest.

■ ACKNOWLEDGMENTS

Financial support from the Agency for Innovation by Science and Technology of Flanders (IWT) is gratefully acknowledged. Results in this paper were obtained within the framework of the IWT Strategic Basic Research Grant 141344 and Strategic Basic Research Grant 121156.

■ REFERENCES

(1) Sridharan, S. *Delamination Behaviour of Composites*, 1st ed.; Woodhead Publishing, 2008.

DOI: 10.1021/acsami.6b02247
ACS Appl. Mater. Interfaces XXXX, XXX, XXX−XXX

(2) Wisnom, M. R. The Role of Delamination in Failure of Fibre-Reinforced Composites. *Philos. Trans. R. Soc., A* **2012**, *370* (1965), 1850−1870.
(3) Chen, L.; Chai, S.; Liu, K.; Ning, N.; Gao, J.; Liu, Q.; Chen, F.; Fu, Q. Enhanced Epoxy/silica Composites Mechanical Properties by Introducing Graphene Oxide to the Interface. *ACS Appl. Mater. Interfaces* **2012**, *4* (8), 4398−4404.
(4) Yavari, F.; Rafiee, M. A.; Rafiee, J.; Yu, Z.-Z.; Koratkar, N. Dramatic Increase in Fatigue Life in Hierarchical Graphene Composites. *ACS Appl. Mater. Interfaces* **2010**, *2* (10), 2738−2743.
(5) Martinez-Rubi, Y.; Ashrafi, B.; Guan, J.; Kingston, C.; Johnston, A.; Simard, B.; Mirjalili, V.; Hubert, P.; Deng, L.; Young, R. J. Toughening of Epoxy Matrices with Reduced Single-Walled Carbon Nanotubes. *ACS Appl. Mater. Interfaces* **2011**, *3* (7), 2309−2317.
(6) Chen, S.; Chen, B.; Fan, J.; Feng, J. Exploring the Application of Sustainable Poly(propylene Carbonate) Copolymer in Toughening Epoxy Thermosets. *ACS Sustainable Chem. Eng.* **2015**, *3* (9), 2077−2083.
(7) Choi, J.; Yee, A. F.; Laine, R. M. Toughening of Cubic Silsesquioxane Epoxy Nanocomposites Using Core−Shell Rubber Particles: A Three-Component Hybrid System. *Macromolecules* **2004**, *37* (9), 3267−3276.
(8) Knoll, J. B.; Riecken, B. T.; Kosmann, N.; Chandrasekaran, S.; Schulte, K.; Fiedler, B. The Effect of Carbon Nanoparticles on the Fatigue Performance of Carbon Fibre Reinforced Epoxy. *Composites, Part A* **2014**, *67*, 233−240.
(9) Kim, J.; Reneker, D. H. Mechanical Properties of Composites Using Ultrafine Electrospun Fibers. *Polym. Compos.* **1999**, *20* (1), 124−131.
(10) Dzenis, Y. A.; Reneker, D. H. Delamination Resistant Composites Prepared by Small Diameter Fiber Reinforcement at Ply Interfaces. United States Patent 6265333, 2001.
(11) Dzenis, Y. Structural Nanocomposites. *Science (Washington, DC, U. S.)* **2008**, *319* (5862), 419−420.
(12) Zucchelli, A.; Focarete, M. L.; Gualandi, C.; Ramakrishna, S. Electrospun Nanofibers for Enhancing Structural Performance of Composite Materials. *Polym. Adv. Technol.* **2011**, *22* (3), 339−349.
(13) Greiner, A.; Wendorff, J. H. Electrospinning: A Fascinating Method for the Preparation of Ultrathin Fibers. *Angew. Chem., Int. Ed.* **2007**, *46* (30), 5670−5703.
(14) Huang, Z.-M.; Zhang, Y.-Z.; Kotaki, M.; Ramakrishna, S. A Review on Polymer Nanofibers by Electrospinning and Their Applications in Nanocomposites. *Compos. Sci. Technol.* **2003**, *63* (15), 2223−2253.
(15) van der Heijden, S.; Daelemans, L.; De Schoenmaker, B.; De Baere, I.; Rahier, H.; Van Paepegem, W.; De Clerck, K. Interlaminar Toughening of Resin Transfer Moulded Glass Fibre Epoxy Laminates by Polycaprolactone Electrospun Nanofibres. *Compos. Sci. Technol.* **2014**, *104*, 66−73.
(16) Daelemans, L.; van der Heijden, S.; De Baere, I.; Rahier, H.; Van Paepegem, W.; De Clerck, K. Nanofibre Bridging as a Toughening Mechanism in Carbon/epoxy Composite Laminates Interleaved with Electrospun Polyamide Nanofibrous Veils. *Compos. Sci. Technol.* **2015**, *117*, 244−256.
(17) Chen, Q.; Zhang, L.; Zhao, Y.; Wu, X.-F.; Fong, H. Hybrid Multi-Scale Composites Developed from Glass Microfiber Fabrics and Nano-Epoxy Resins Containing Electrospun Glass Nanofibers. *Composites, Part B* **2012**, *43* (2), 309−316.
(18) Beckermann, G. W.; Pickering, K. L. Mode I and Mode II Interlaminar Fracture Toughness of Composite Laminates Interleaved with Electrospun Nanofibre Veils. *Composites, Part A* **2015**, *72*, 11−21.
(19) Bilge, K.; Venkataraman, S.; Menceloglu, Y. Z.; Papila, M. Global and Local Nanofibrous Interlayer Toughened Composites for Higher in-Plane Strength. *Composites, Part A* **2014**, *58*, 73−76.
(20) Hamer, S.; Leibovich, H.; Green, A.; Avrahami, R.; Zussman, E.; Siegmann, A.; Sherman, D. Mode I and Mode II Fracture Energy of MWCNT Reinforced Nanofibrilmats Interleaved Carbon/epoxy Laminates. *Compos. Sci. Technol.* **2014**, *90*, 48−56.
(21) Li, G.; Li, P.; Zhang, C.; Yu, Y.; Liu, H.; Zhang, S.; Jia, X.; Yang, X.; Xue, Z.; Ryu, S. Inhomogeneous Toughening of Carbon Fiber/epoxy Composite Using Electrospun Polysulfone Nanofibrous Membranes by in Situ Phase Separation. *Compos. Sci. Technol.* **2008**, *68* (3−4), 987−994.
(22) Magniez, K.; Chaffraix, T.; Fox, B. Toughening of a Carbon-Fibre Composite Using Electrospun Poly(Hydroxyether of Bisphenol A) Nanofibrous Membranes Through Inverse Phase Separation and Inter-Domain Etherification. *Materials* **2011**, *4* (12), 1967−1984.
(23) Saghafi, H.; Zucchelli, A.; Palazzetti, R.; Minak, G. The Effect of Interleaved Composite Nanofibrous Mats on Delamination Behavior of Polymeric Composite Materials. *Compos. Struct.* **2014**, *109*, 41−47.
(24) Zhang, J.; Lin, T.; Wang, X. Electrospun Nanofibre Toughened Carbon/epoxy Composites: Effects of Polyetherketone Cardo (PEK-C) Nanofibre Diameter and Interlayer Thickness. *Compos. Sci. Technol.* **2010**, *70* (11), 1660−1666.
(25) Zhang, J.; Yang, T.; Lin, T.; Wang, C. H. Phase Morphology of Nanofibre Interlayers: Critical Factor for Toughening Carbon/epoxy Composites. *Compos. Sci. Technol.* **2012**, *72* (2), 256−262.
(26) Palazzetti, R.; Zucchelli, A.; Gualandi, C.; Focarete, M. L.; Donati, L.; Minak, G.; Ramakrishna, S. Influence of Electrospun Nylon 6,6 Nanofibrous Mats on the Interlaminar Properties of Gr−epoxy Composite Laminates. *Compos. Struct.* **2012**, *94* (2), 571−579.
(27) Daelemans, L.; van der Heijden, S.; De Baere, I.; Rahier, H.; Van Paepegem, W.; De Clerck, K. Using Aligned Nanofibres for Identifying the Toughening Micromechanisms in Nanofibre Interleaved Laminates. *Compos. Sci. Technol.* **2016**, *124*, 17−26.
(28) Allaer, K.; De Baere, I.; Van Paepegem, W.; Degrieck, J. Direct Fracture Toughness Determination of a Ductile Epoxy Polymer from Digital Image Correlation Measurements on a Single Edge Notched Bending Sample. *Polym. Test.* **2015**, *42*, 199−207.
(29) Naraghi, M.; Chasiotis, I.; Kahn, H.; Wen, Y.; Dzenis, Y. Mechanical Deformation and Failure of Electrospun Polyacrylonitrile Nanofibers as a Function of Strain Rate. *Appl. Phys. Lett.* **2007**, *91* (15), 151901.
(30) Papkov, D.; Zou, Y.; Andalib, M. N.; Goponenko, A.; Cheng, S. Z. D.; Dzenis, Y. A. Simultaneously Strong and Tough Ultrafine Continuous Nanofibers. *ACS Nano* **2013**, *7* (4), 3324−3331.
(31) Ni, Y.; Zheng, S. Influence of Intramolecular Specific Interactions on Phase Behavior of Epoxy Resin and Poly(ε-Caprolactone) Blends Cured with Aromatic Amines. *Polymer* **2005**, *46* (15), 5828−5839.
(32) Wang, Y.; Winnik, M. A. Polymer Diffusion across Interfaces in Latex Films. *J. Phys. Chem.* **1993**, *97* (11), 2507−2515.
(33) Schreiber, H. P.; Ouhlal, A. Polymer Diffusion and the Evolution of Adhesive Bond Strength. *J. Adhes.* **2003**, *79* (2), 141−153.
(34) van der Heijden, S.; De Schoenmaker, B.; Rahier, H.; Van Assche, G.; De Clerck, K. The Effect of the Moisture Content on the Curing Characteristics of an Epoxy Matrix in the Presence of Nanofibrous Structures. *Polym. Test.* **2014**, *40*, 265−272.
(35) De Schoenmaker, B.; van der Heijden, S.; Moorkens, S.; Rahier, H.; van Assche, G.; De Clerck, K. Effect of Nanofibres on the Curing Characteristics of an Epoxy Matrix. *Compos. Sci. Technol.* **2013**, *79*, 35−41.
(36) Najem, J. F.; Wong, S.-C.; Ji, G. Shear Adhesion Strength of Aligned Electrospun Nanofibers. *Langmuir* **2014**, *30* (34), 10410−10418.
(37) Hojo, M.; Ando, T.; Tanaka, M.; Adachi, T.; Ochiai, S.; Endo, Y. Modes I and II Interlaminar Fracture Toughness and Fatigue Delamination of CF/epoxy Laminates with Self-Same Epoxy Interleaf. *Int. J. Fatigue* **2006**, *28* (10), 1154−1165.
(38) Xia, Z. C.; Hutchinson, J. W. Mode II Fracture Toughness of a Brittle Adhesive Layer. *Int. J. Solids Struct.* **1994**, *31* (8), 1133−1148.
(39) Palazzetti, R.; Yan, X.; Zucchelli, A. Influence of Geometrical Features of Electrospun Nylon 6,6 Interleave on the CFRP Laminates Mechanical Properties. *Polym. Compos.* **2014**, *35* (1), 137−150.
(40) Van der Schueren, L.; De Schoenmaker, B.; Kalaoglu, Ö. I.; De Clerck, K. An Alternative Solvent System for the Steady State

DOI: 10.1021/acsami.6b02247
ACS Appl. Mater. Interfaces XXXX, XXX, XXX−XXX

Electrospinning of Polycaprolactone. *Eur. Polym. J.* **2011**, *47* (6), 1256−1263.
(41) De Schoenmaker, B.; Van der Heijden, S.; De Baere, I.; Van Paepegem, W.; De Clerck, K. Effect of Electrospun Polyamide 6 Nanofibres on the Mechanical Properties of a Glass Fibre/epoxy Composite. *Polym. Test.* **2013**, *32* (8), 1495−1501.
(42) Westbroek, P.; Van Camp, T.; De Vrieze, S.; De Clerck, K. Production and Use of Laminated Nanofibrous Structures. Patent 2687563, November 28, 2008.
(43) van der Heijden, S.; De Bruycker, K.; Simal, R.; Du Prez, F.; De Clerck, K. Use of Triazolinedione Click Chemistry for Tuning the Mechanical Properties of Electrospun SBS-Fibers. *Macromolecules* **2015**, *48* (18), 6474−6481.
(44) ASTM Standard D5528, Standard Test Method for Mode I Interlaminar Fracture Toughness of Unidirectional Fiber Reinforced Polymer Matrix Composites www.astm.org.

DOI: 10.1021/acsami.6b02247
ACS Appl. Mater. Interfaces XXXX, XXX, XXX−XXX

PAPER II

INTERLAMINAR TOUGHENING OF RESIN TRANSFER MOULDED GLASS FIBRE EPOXY LAMINATES BY POLYCAPROLACTONE ELECTROSPUN NANOFIBRES

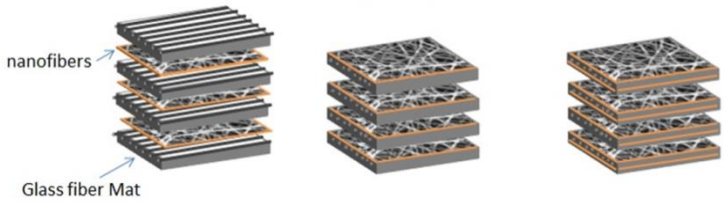

Sam van der Heijden, Lode Daelemans, Bert De Schoenmaker, Ives De Baere, Hubert Rahier, Wim Van Paepegem and Karen De Clerck

(2014) *COMPOSITES SCIENCE AND TECHNOLOGY*. 104. p.66-73

L. Daelemans assisted in the experimental work and interpretation of the results.

Composites Science and Technology 104 (2014) 66–73

Contents lists available at ScienceDirect

Composites Science and Technology

journal homepage: www.elsevier.com/locate/compscitech

Interlaminar toughening of resin transfer moulded glass fibre epoxy laminates by polycaprolactone electrospun nanofibres

Sam van der Heijden [a], Lode Daelemans [a], Bert De Schoenmaker [a], Ives De Baere [b], Hubert Rahier [c], Wim Van Paepegem [b], Karen De Clerck [a,*]

[a] Ghent University, Department of Textiles, Technologiepark-Zwijnaarde 907, B-9052 Zwijnaarde, Belgium
[b] Ghent University, Department of Materials Science and Engineering, Technologiepark-Zwijnaarde 903, B-9052 Zwijnaarde, Belgium
[c] Vrije Universiteit Brussel, Department Materials and Chemistry, Pleinlaan 2, B-1050 Brussels, Belgium

ARTICLE INFO

Article history:
Received 25 April 2014
Received in revised form 5 September 2014
Accepted 6 September 2014
Available online 16 September 2014

Keywords:
A. Nano composites
E. Resin transfer moulding (RTM)
B. Delamination
B. Fracture toughness

ABSTRACT

Delamination and brittle matrix fracture has since long been a problem of fibre reinforced composites. This paper investigates if polycaprolactone (PCL) nanofibre nonwovens can increase the interlaminar fracture toughness of resin transfer moulded glass fibre/epoxy laminates, without causing problems during impregnation and without negatively affecting other (mechanical) properties.

The mode I fracture toughness was shown to be dependent on both the nanofibre content as well as on how the nanofibres were introduced into the laminates. Almost 100% improvement in fracture toughness could be achieved by electrospinning the PCL nanofibres on both sides of the glass fibre mats prior to impregnation. This led to a mode I fracture toughness of over 1200 J/m^2. Tensile and dynamic mechanical properties of the toughened laminates were not affected by the PCL nanofibres. It could be concluded that even state of the art infusion resins with a high intrinsic fracture toughness can benefit significantly from nanofibre toughening.

1. Introduction

Delamination and brittle matrix fracture has since long been a problem of fibre reinforced composites [1–3]. A lot of research has been devoted to prevent delamination by modifying the epoxy matrix, either by chemically modifying the resin and hardener components, e.g. by using dendritic hyper branched polymers [4], or by adding additional components to the epoxy resin, e.g. mixing in rubber particles or creating specific thermoplastic phase morphologies in the matrix [5–12]. Although creating a rubbery phase inside of the epoxy matrix often increases the fracture toughness of the laminates, this increase is often accompanied with a decrease in other mechanical properties such as stiffness and strength. In the research of Dadfar et al. the mode I interlaminar fracture toughness (G_{Ic}) of the glass epoxy laminates increased from 220 J/m^2 to about 500 J/m^2 whereas the elastic modulus and tensile strength went down from 28.4 GPa to 17.8 GPa and 584 MPa to 489 MPa respectively [12]. More recently, the effect of nanoparticles such as nanoclay, carbon nanotubes, nanowhiskers and vapour grown carbon nanofibres on the toughness of the epoxy matrix has been studied [13–15]. Although an increase in bulk fracture toughness could often be accomplished by adding these additional components to the epoxy matrix, the absolute increase in interlaminar fracture toughness of the composite laminates remains moderate at best [16–18]. For example, Arai et al. could improve the mode I initiation interlaminar fracture toughness ($G_{Ic,ini}$) of carbon fibre epoxy laminates from 200 J/m^2 to approximately 300 J/m^2 whereas the propagation fracture toughness (G_{Icprop}) increased form 500 J/m^2 to 650 J/m^2. Wang et al. obtained an increase in G_{IC} from 140 J/m^2 to 220 J/m^2 using nanowhiskers [17,18]. In addition, all the toughening systems mentioned above have two common disadvantages: (1) it is difficult to get a homogeneous dispersion of extra phases into the epoxy matrix and final laminate, and (2) the resin viscosity increases tremendously when these phases are mixed into the resin prior to moulding. These problems are of course very problematic for all infusion applications, such as resin transfer moulding (RTM).

Thermoplastic nanofibrous structures could offer a solution for the increased viscosity and the inhomogeneous dispersion, as nanofibre nonwovens can be readily deposited in between the primary reinforcing fibre layers prior to infusion. Thus, the viscosity of the epoxy resin is not affected. Although the idea of using electrospun nanofibres as a secondary reinforcement in composite

* Corresponding author. Tel.: +32 9 264 57 40; fax: +32 9 264 58 46.
E-mail address: Karen.DeClerck@ugent.be (K. De Clerck).

http://dx.doi.org/10.1016/j.compscitech.2014.09.005
0266-3538/

structures has already been proposed by Dzenis and Reneker in 1999 [19], it is only since the last few years that the interlaminar toughening effects of thermoplastic nanofibres are being reported. Bilge et al. showed that P(St-co-GMA) nanofibrous interlayers can improve the open hole strength of carbon/epoxy laminates [20]. Palazetti et al. reported about the use of nylon 6.6 nanofibrous mats to increase the interlaminar properties and impact resistance of composites. The G_{Ic} increased from 473 J/m^2 to 496 J/m^2 [21,22]. Zhang et al. showed that G_{Ic} of a carbon fibre epoxy laminate could be increased from 175 J/m^2 to about 320 J/m^2 (depending on nanofibre diameter and interlayer thickness) using polyetherketone cardo nanofibres [23]. Li et al. used polysulfone (PSF) nanofibres to increase the G_{Ic} of carbon fibre epoxy laminates from 310 J/m^2 up to 870 J/m^2. Furthermore, it was shown that the use of PSF nanofibrous nonwovens leads to a more efficient toughening than the use of PSF films of equal weight [24].

All research papers mentioned above used prepreg material on which the nanofibres were deposited. Although prepreg materials are often used in industry, e.g. aerospace industry almost exclusively uses prepreg materials, resin infusion has substantially gained importance for the production of big composite parts such as windmill blades and yacht parts. Modern infusion moulded laminates make use of low viscosity and high toughness epoxy resins. The mode I interlaminar fracture toughness of these laminates is typically higher than 600 J/m^2. This fracture toughness is much higher than that of the prepreg materials studied so far in literature [20–24]. This paper aims to investigate if high toughness polycaprolactone (PCL) nanofibre nonwovens can increase the interlaminar fracture toughness of these infusion moulded laminates even more, without causing problems during infusion and without negatively affecting other (mechanical) properties of the laminates.

2. Materials and methods

2.1. Materials

All composite laminates were reinforced with unidirectional E-glass fabric (Roviglas R17/475). The reinforcement had a weight of 475 g/m^2 in the fibre direction and a weight of 17 g/m^2 in the perpendicular direction.

The epoxy resin was composed of EPIKOTE resin MGS RIMR 135 with EPIKURE curing agent MGS RIMH 137 (Momentive). This is an infusion resin designed for windmill applications and it has a low viscosity and a high toughness.

Polycaprolactone pellets and solvents 98 v% formic acid and 99.8 v% acetic acid were supplied by Sigma–Aldrich and used as received.

2.2. Electrospinning

Prior to electrospinning, an appropriate solvent system was selected to allow for the production of nanofibre nonwovens in a stable and reproducible way. Furthermore the toxicity of the solvent system should be low, in order to make the system relevant for industrial application.

PCL can be electrospun in a stable and reproducible manner from a 1:1 formic acid/acetic acid solution which has a relatively low toxicity [25,26]. Therefore, 14 wt% of PCL was dissolved in a 1:1 solution of formic acid and acetic acid. To obtain large uniform nanofibrous nonwovens, the nanofibres were produced using a multi-nozzle electrospinning set-up. This multi-nozzle method, an in house developed technology [22], diverges from a mono-nozzle set-up mainly by the number of nozzles, the general methodology itself is identical. It consists out of 32 nozzles, each fed by 16 syringes. The nozzles are placed in 4 alternating rows which have a movement in the transverse direction to ensure uniform deposition of nanofibres. In the meantime, a grounded collector is moving in the longitudinal or production direction. The speed of the ground-collector is adjusted to obtain the required areal density of the nanofibrous nonwovens. All nanofibrous nonwovens were spun in a conditioned room at 23 ± 2 °C and 50 ± 5% RH. The tip-to-collector distance was 12.5 cm and the flow rate was set at 1 ml/h (per nozzle). The voltage was set between 20 kV and 25 kV until a stable process was achieved. Nanofibrous structures were both produced as stand-alone structures as well as deposited structures. The stand-alone nanofibrous nonwovens were electrospun on an aluminium foil, and were peeled off afterwards. The deposited structures were directly electrospun onto glass fibre mats. In both cases the fibre diameter of the nanofibrous structures was 400 ± 100 nm.

2.3. Vacuum assisted resin transfer moulding and preparation of PCL toughened laminates

The composite laminates were manufactured by vacuum assisted resin transfer moulding (VARTM). The glass fibre mats were stacked into a steel mould, either in a $[0°]_8$ or in a $[0°/90°]_{2s}$ configuration. All laminates consisted out of 8 layers of glass fibres and had a total thickness of 3 ± 0.1 mm. Three different configurations were used to introduce the nanofibres into the laminates. In addition to these three configurations, reference samples were produced containing only glass fibres.

In the first configuration a single layer of nanofibres was directly electrospun on one side of the glass fibre mats. These mats are stacked on top of each other. Hence, the interlayer of two neighbouring plies contains a single layer of nanofibre nonwoven. This configuration will be referred to as the single layer deposited configuration (SLD).

The second configuration, referred to as the double layer deposited configuration (DLD), consists out of one layer of nanofibres electrospun on each side of the glassfibre mats. Therefore, the interlayer of two neighbouring plies contained two layers of nanofibres on top of each other.

The third configuration was named the interlayered configuration (IL). This configuration consists of standalone nanofibre nonwovens placed in between the glass fibre mats. Therefore, the interlayer contains one layer of nanofibrous nonwoven, but that layer is not directly electrospun onto the glass fibre mats.

The samples prepared for the tensile tests contained nanofibrous nonwoven, according to the above configurations, in each interlayer. For the double cantilever beam samples (DCB), the nanofibrous nonwoven was incorporated in the tested interlayer.

Prior to infusion, the resin and hardener were mixed in a 100:30 mass ratio. A mechanical stirrer was used to ensure good mixing of resin and hardener. After mixing, the epoxy resin was placed under vacuum for 15 min to remove any air introduced during mixing.

After injection, the glass–epoxy laminate is first cured at room temperature for 24 h and then post-cured for 15 h at 80 °C. It should be noted that although the temperature in the post curing step is above the melting region of PCL (approximately at 60 °C) the curing at room temperature is well below the melting region [27].

2.4. Characterisation

Scanning electron microscopy (SEM, Joel Quanta 200 F FE-SEM) was used to investigate the fibre diameter of the electrospun nanofibres as well as the delamination fracture surface of the laminates. Prior to the SEM-measurements, the specimens were coated by a gold sputter coater (Balzers Union SCD 030). An optical microscope, an Olympus BX51 with an Olympus UC30 camera, was used to visualise delamination cracks in the cross section of the composite

laminates as well as to determine the thickness of the interlayer between two neighbouring plies.

Mode I delamination fracture toughness was measured by DCB experiments on an electromechanical Instron 5800R machine following the ASTM D 5528 (2013) standard. Five samples were tested for each configuration. All DCB experiments were performed on unidirectional laminates and piano hinges were used to transfer the load to the sample. The dimensions of the DCB samples were $20 \times 160 \times 3$ mm and the initial delamination length was 50 mm and was created using a release film with a thickness of 30 μm. The crack propagation in the DCB samples was followed using a traveling microscope. Throughout this paper, different cross sections of these DCB samples will be shown, a coordinate system is used to indicate the glass fibre direction (X), the direction perpendicular to the unidirectional glass fibres (Y) and the thickness direction (Z).

Tensile tests and open hole strength tests on the composites were performed on an electromechanical Instron 5800R machine with a load cell of 100 kN following the ASTM D3039/D3039 M standard. The tests were displacement controlled with a speed of 2 mm/min and both displacement and load were recorded.

The $[0°/90°]_{2s}$ tensile specimens were instrumented with an extensometer to measure the longitudinal strain. The $[+45°/-45°]_{2s}$ tensile specimens were instrumented with two strain gauges to measure shear. All signals were sampled on the same time basis. The nanofibre containing tensile specimens had a DLD configuration and contained 10 g/m^2 or 20 g/m^2 of PCL nanofibres in each interlayer. Four samples were tested for each of these configurations.

The $[0°/90°]_{2s}$ open hole strength specimens had a width of 36 ± 0.5 mm and a central hole of 8 ± 0.1 mm in diameter. Three samples were tested for each configuration. The nanofibre containing open hole specimens had a DLD configuration and contained 5 g/m^2 or 20 g/m^2 of PCL nanofibres in each interlayer.

The dynamic mechanical analysis (DMA) was executed on a Q800 from TA Instruments. Before the start of the DMA experiments, a complete calibration was carried out; the temperature calibration was performed using an indium standard. Due to the high modulus of the samples, the experiments were carried out with a single cantilever clamp. The frequency was kept constant at 1 Hz and the displacement amplitude was set to 20 μm. The experiments started with bringing the DMA-temperature to 30 °C followed by an equilibration time of 15 min, after which the temperature was raised at 2.5 °C/min to 150 °C. At least 3 samples were tested for each configuration.

3. Results and discussion

3.1. Expressing the nanofibre content

In composite materials, the fibre content is seen as a very important material parameter. There are different ways in which the nanofibre content can be expressed. In this paper, the areal density of the nanofibre nonwovens is used as a main parameter to indicate the nanofibre content. This has several advantages over other parameters such as the weight fraction to the total composite weight or to the resin weight. Areal density allows for easy comparison independent of the resin or primary reinforcing fibre density. In addition, a nanofibre weight fraction to the matrix weight does not take the positioning of the nanofibres in the interlayers into account. Indeed, the nanofibres are mainly present in the interlayers and not, or at least to a much lesser extent, in between the reinforcing fibres. Therefore, properties of a pure epoxy/nanofibre bulk material with the same weight fraction to resin content as in the laminate cannot be compared to what is present in the interlayer. To avoid this problem, the weight fraction of the nanofibres compared to the resin present in the interlayer may be used. Table 1 shows the different areal densities used and their corresponding calculated fibre fractions in the interlayer as well as the fraction of the nanofibres to the resin weight and to the total weight of the laminates for the SLD and DLD configuration.

3.2. Effect of PCL nanofibres on the resin infusion process

All laminates were produced using vacuum assisted resin transfer moulding. The viscosity and reactivity of the epoxy resin are of major importance for all infusion moulded parts. The PCL nanofibres had no measurable influence on this infusion process. The low viscosity infusion resin could easily impregnate all nanofibrous nonwovens in the interlayers. Visual examination and microscopic images showed no dry spots in the final laminates (the epoxy resin is transparent), see Section 3.4.

3.3. The effect of nanofibre nonwoven placement on the interlaminar fracture toughness

Three different configurations (single layer deposited (SLD), double layer deposited (DLD) and interlayered (IL) were tested in comparison to the reference configuration without nanofibres

Fig. 1A shows the mode I fracture toughness for the three different nanofibre stacking configurations as a function of the crack length. These values were calculated according to ASTM D 5528 from the load displacement curve (Fig. 1B) and the measured crack length recorded by a traveling microscope. The nanofibre content in the interlayer was 5 g/m^2 for each configuration implying that the DLD samples had 2.5 g/m^2 of nanofibres in each deposited nanofibre layer. It can be noted that both the IL configuration as well as the SLD configuration only show a marginal improvement over the reference laminates. In contrast the DLD configuration showed a substantial improvement. Both the initiation fracture toughness ($G_{Ic,ini}$) and the propagation fracture toughness ($G_{Ic,prop}$) were increased by about 430 J/m^2 and 280 J/m^2 respectively compared to the reference laminate. Taking into account that due to the selection of a high toughness infusion resin, the reference material already had a $G_{Ic,ini}$ of 640 ± 60 J/m^2, the mode I initiation fracture toughness of the DLD configuration was found to be as high as 1070 ± 130 J/m^2.

An explanation for the remarkable difference between these configurations is found by visually examining the fracture surface of the DCB samples. Fig. 2 shows a comparison between a SLD configuration and a DLD configuration. For the SLD configuration, the PCL nanofiber layer can be found on the fractured sample half that contained the glass fibre mat on which the PCL nanofibres were deposited. Therefore, the delamination crack propagated between the embedded nanofibrous layer and the glass fibre mat directly above it. The microscopic analysis also supports this hypothesis, see Section 3.4. It is assumed that a better adhesion/interaction of the nanofibres with the glass fibres in case the nanofibres are directly deposited on top of the glass fibres during the electrospinning process is the reason for the crack propagating above the toughened nanofibre layer. As such, the delamination crack did not go through the toughened interlayer. Hence, only marginal improvement compared to the reference was found.

In contrast, for the DLD configuration, parts of the embedded nanofibrous layer can be found on both halves of the fractured sample. This indicates that the delamination crack propagated, at least partially, through the toughened interlayer. Therefore, in the DLD configuration, more energy was required for the delamination crack to propagate through the nanofibre toughened interlayer, and hence, the fracture toughness of the DLD configuration is significantly higher than the SLD configuration.

Table 1
Different ways of expressing the nanofibre content of the glass–epoxy laminates.

	Areal density in interlayer (g/m^2)	Thickness interlayer (μm)	wt% to resin (%)	wt% to resin in interlayer (%)	wt% to laminate (%)
Single layer deposited configuration	2.5 ± 0.2	30 ± 5	0.92 ± 0.07	7 ± 2	0.26 ± 0.02
	10 ± 0.5	67 ± 7	3.69 ± 0.18	13 ± 2	1.05 ± 0.05
	40 ± 0.5	176 ± 12	14.77 ± 0.18	19 ± 2	4.21 ± 0.05
Double layer deposited configuration	2.5 ± 0.2	17 ± 5	0.92 ± 0.07	13 ± 5	0.26 ± 0.02
	5 ± 0.5	43 ± 7	1.85 ± 0.18	10 ± 3	0.53 ± 0.05
	10 ± 0.6	53 ± 15	3.69 ± 0.22	16 ± 6	1.05 ± 0.06
	20 ± 0.5	89 ± 15	7.39 ± 0.18	19 ± 4	2.11 ± 0.05

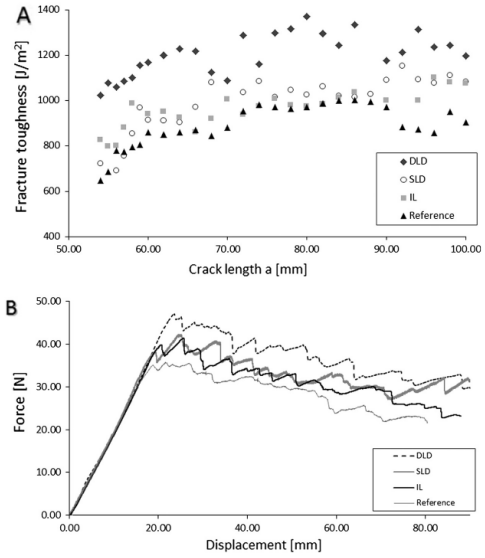

Fig. 1. Mode I fracture toughness as a function of crack length (A) and load–displacement curves (B), showing significant increases when a double layer deposited (DLD) configuration is used as compared to a single layer deposited configuration (SLD) or interlayered configuration (IL).

In a DCB experiment, a release film is used to initiate the delamination in between the central plies of the laminate. Thus the film was on top of the nanofibrous nonwoven for the SLD configuration, whereas for the DLD configuration, the film was in between two nanofibrous layers. To verify the film placement had no effect on the observed differences between the SLD and DLD configurations, modified DCB specimens were designed in which there was a 1 mm gap between the nanofibrous reinforcement and the release film. Thus the delamination crack started in front of the nanofibrous reinforcement. No difference in mode I fracture toughness was found for these modified specimens compared to the standard designed specimens. Again a substantial improvement for the DLD configuration was observed compared to the other configurations.

3.4. Microscopic analysis of the fracture behaviour

SEM images were taken from the fracture surfaces of the DCB samples, see Figs. 3 and 4. In addition, optical microscopy was used to analyse the cross section of these samples. The images were taken just before the tip of the crack path and perpendicular to the glass fibre orientation and crack propagation direction, Fig. 5.

Fig. 3 illustrates imprints of the PCL nanofibres, indicating the nanofibrous structure is at least partially maintained during the impregnation and curing process. The room temperature curing step is assumed to be crucial in this perspective. During this step, a solid matrix is formed, which prevents the PCL nanofibres to mix with the epoxy matrix during the post-curing step at 80 °C, which is above the melting point of PCL.

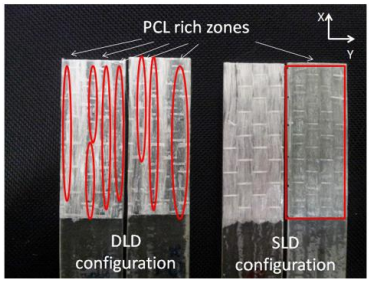

Fig. 2. Fracture surface of DCB samples showing how the impregnated nanofibrous PCL nonwoven is distributed over the two sample halves after fracture in case of the DLD (left) and SLD (right) configuration.

Comparing the images of the fracture surface of a nanofibre toughened laminate, Fig. 4B, to the reference laminate, Fig. 4A, PCL rich zones can clearly be noted. On a macroscopic level, it is assumed that these zones represent spots where the glass fibres were strongly attached to the PCL nanofibrous web. These glass fibres in turn microscopically bridge the crack front until they are finally broken or completely pulled out of the PCL rich zone. On a nano scale level, these zones contain the plastically deformed PCL and PCL nanofibres bridging matrix particles, as shown in Fig. 4B. This effect is present both in the case of a DLD as well as a SLD configuration. This phenomenon could therefore explain the slightly higher fracture toughness of the single layer configuration as compared to the reference. For the DLD configuration, it is suggested that a crack path deflection during initiation has an even more important role. This is indeed illustrated in Fig. 5, showing the crack front alternatingly propagates above and below the nanofibre toughened interlayer when a DLD configuration is used. In case of the SLD configuration, the crack path stays preferably above the nanofibrous layer. The toughening effect is also illustrated through the visual examination of the crack surface. Fig. 2

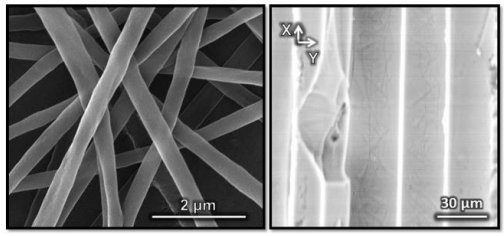

Fig. 3. SEM image of PCL nanofibres (left) and a fracture surface of a DLD configuration DCB specimen showing imprints of PCL nanofibres (right).

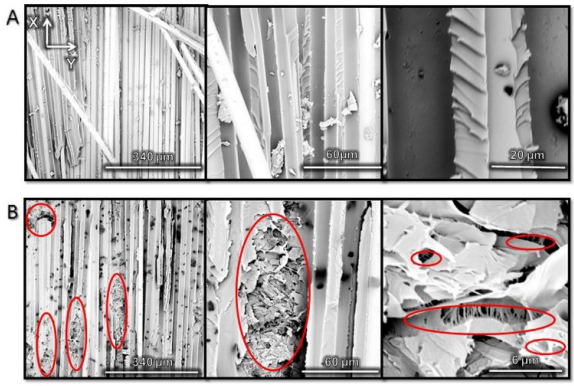

Fig. 4. SEM image of reference (A) and DLD PCL nanofibre containing (B) DCB fracture surfaces. High amounts of plastic deformation and fractured pieces of epoxy matrix held together by PCL rich zones can be observed in (B).

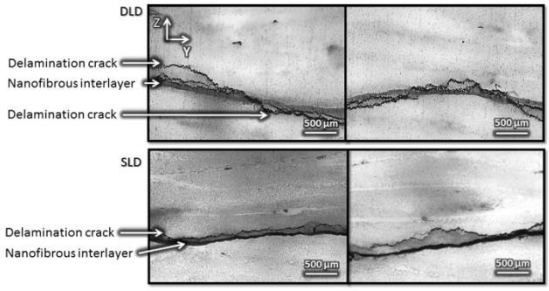

Fig. 5. Cross-sectional optical microscopy images of double layer deposited configuration (DLD) and single layer deposited configuration (SLD). The crack path is perpendicular to the image plane and goes above and below the nanofibre toughened interlayer when a DLD configuration is used.

shows that the PCL rich layer distribution over the two sample halves is more or less constant in the fibre direction and fluctuates mainly in the direction perpendicular to the glass fibres. It is this fluctuation that can be seen in the macroscopic images in Fig. 5, where the crack goes through the nanofibrous layer at several locations, after which it continues on the other side of the toughened interlayer until a next jump through the interlayer occurs. From the crack surface, Fig. 2, it can be noted that most of these jumps were initiated at the start of the experiment, during the initiation of the delamination crack. When the delamination crack is initiated, it will meet the PCL toughened interlayer. At this point, a crack path deflection effect is likely to occur since it requires more energy to go through the toughened interlayer than to propagate below or above it. For the SLD configuration, the delamination crack went above the toughened interlayer across the whole width of the sample. As explained in Section 3.3, this is most likely due to a better interaction between the nanofibres and the glass fibre mat on which they were deposited as opposed to the glass fibre mat above it. For the DLD configuration, it can be assumed that the interaction between the nanofibrous interlayer and the top and bottom glass fibre mat is similar. As a result, the crack front does not go above the toughened interlayer across the whole width of the sample. Instead, the crack front went below or above the toughened interlayer at specific positions, depending on small variations in nanofibre to glass fibre interactions across the width of the sample. Thus the crack front had to pass through the toughened interlayer to go from one side to the other.

3.5. The effect of nanofibre content on the interlaminar fracture toughness

The nanofibre content is varied from 2.5 g/m^2 to 40 g/m^2 of PCL nanofibres in the interlayer. Fig. 6 illustrates the mode I interlaminar fracture toughness of the resin transfer moulded laminates, both for the SLD and the DLD configuration.

For the SLD configuration the fracture toughness shows no important variation with nanofibre content and has a value of around 765 ± 100 J/m^2 for initiation and 1060 ± 100 J/m^2 for propagation. These values are slightly better than the 640 J/m^2 and 950 J/m^2 obtained for the reference laminates without nanofibres in the interlayer. It should also be noted that even though the thickness of the interlayer increases significantly when high amounts of PCL nanofibres are added to the laminate, the interlaminar fracture toughness remains almost constant. This observation supports the

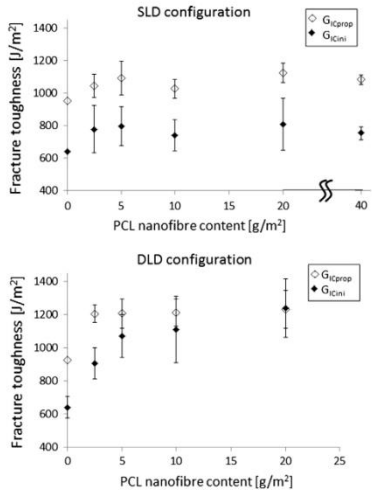

Fig. 6. Effect of PCL nanofibre content on $G_{IC,ini}$ and $G_{IC,prop}$ for single and double layer deposited configurations.

hypothesis that in case of a SLD configuration, the crack mainly propagates above the nanofibre layer. Hence, the obtained fracture toughness is less dependent on the nanofibre content.

For the DLD configuration, the initiation fracture toughness increases rapidly with increasing nanofibre content up to a value of 1070 ± 130 J/m^2 when 5 g/m^2 of nanofibres are added in the interlayer. When more than 5 g/m^2 of nanofibres are added to the interlayer, the initiation facture toughness still increases although at a much slower rate. For the maximum value of 20 g/m^2 the initiation fracture toughness increased up to 1240 ± 170 J/

Table 2
Tensile properties of composite laminates show no decrease when PCL nanofibres are added (DLD configuration).

	Nanofibre content (g/m^2)	σ_{xx} (MPa)	E_{xx} (GPa)
Ref $[0°/90°]_{2S}$	0	574 ± 50	25 ± 1
Nf $[0°/90°]_{2S}$	10	596 ± 50	24 ± 1
Nf $[0°/90°]_{2S}$	20	603 ± 20	25 ± 1
		τ max (MPa)	G_{xy} (GPa)
Ref $[+45°/-45°]_{2S}$	0	62 ± 2	4.4 ± 0.2
Nf $[+45°/-45°]_{2S}$	10	59 ± 2	3.9 ± 0.2
Nf $[+45°/-45°]_{2S}$	20	60 ± 1	4.2 ± 0.2

m^2. This is an increase of almost 100% compared to the reference laminates. As opposed to the initiation fracture toughness, the propagation fracture toughness is shown to be relatively independent of the nanofibre content. The propagation fracture toughness is approximately 1200 J/m^2 for all nanofibre contents. This is around 250 J/m^2 higher compared to the reference laminates. Overall it is clear the fracture toughness of the laminate increased significantly when a DLD configuration is used.

3.6. Effect of PCL nanofibre toughening on tensile properties and open hole strength

The tensile properties and open hole strength of the DLD laminate were also evaluated and compared to the reference. Tensile tests were performed on $[0°/90°]_{2S}$ and $[+45°/-45°]_{2S}$ laminates. From these tests an elastic modulus, shear modulus, tensile strength and shear strength were calculated.

It can be noted, Table 2, that the tensile properties of the laminates where hardly affected by the presence of the nanofibres, both the tensile strength and Young's modulus are maintained. In addition an improvement in open hole strength from 360 ± 7 MPa to 387 ± 19 MPa for the 5 g/m^2 DLD configuration and to 383 ± 14 MPa for the 20 g/m^2 DLD configuration can be observed.

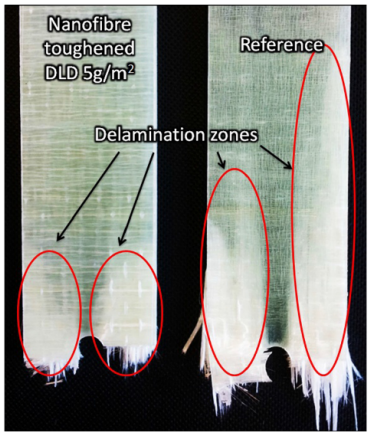

Fig. 7. Open hole specimens show significantly less delamination when 5 g/m^2 of nanofibres are present in each interlayer using a DLD configuration.

This improvement is attributed to the fact that nanofibre toughened laminates show less delamination during the open hole test. This is clearly illustrated in Fig. 7 showing two open hole samples after testing (5 g/m^2 DLD configuration). The nanofibre toughened specimen clearly shows less delamination compared to the reference sample.

3.7. Dynamic mechanical properties

Dynamic mechanical analysis verified the PCL nanofibres had no negative effect on the modulus of the glass epoxy laminates above room temperature. The DMA curves of the nanofibre containing samples are overlapping with the reference. Thus, even above the melting point of PCL (60 °C) the modulus of the nanofibre containing samples is nearly identical to the reference.

In addition the glass transition temperature of the nanofibre containing laminate, which can be evaluated from the step in the storage modulus at 77 °C is identical to that of the neat glass epoxy laminate.

4. Conclusion

The effect of PCL nanofibres on the interlaminar fracture toughness of resin transfer moulded glass fibre epoxy laminates was studied. The infusion process is not negatively influenced by the presence of the PCL nanofibres. The way in which the nanofibres are arranged into the laminate has a major effect on the mode I fracture toughness of the laminates. A DLD configuration in which the nanofibres were directly electrospun on both sides of the unidirectional glass fibre mats is clearly superior over the other tested configurations. More specifically, the obtained improvement was a function of the nanofibre content in the DLD samples. For a nanofibre content of 20 g/m^2 in the interlayers, an improvement in initiation interlaminar fracture toughness of almost 100% was obtained. The initiation fracture toughness increased from 640 J/m^2 for the reference laminates to 1230 J/m^2 for the nanofibre toughened laminates. The improved fracture toughness of the DLD configuration was also confirmed in the open hole strength tests, where the nanofibre containing samples showed significantly less delamination around the central hole.

It can be concluded that even state-of-the-art infusion resins can benefit from nanofibre toughening. This toughening effect was attributed to a good adhesion of deposited nanofibres onto the glass fibre mats, as well as to the inherent tough and ductile properties of the PCL nanofibres themselves. It is assumed that these properties resulted in glass fibre bridging as well as a crack path deflection effect during initiation of the delamination. Due to this crack path deflection, the delamination crack propagated partially through the nanofibre toughened interlayer (in case of a DLD configuration) resulting in a significant increase in fracture toughness. The tensile, shear and dynamic mechanical properties were not significantly influenced by the presence of PCL nanofibres in the interlayers.

Acknowledgement

Financial support from The Agency for Innovation by Science and Technology of Flanders (IWT) is gratefully acknowledged. Results in this paper were obtained within the framework of the IWT Strategic Basic Research Grant 121156.

References

[1] Ye L. Role of matrix resin in delamination onset and growth in composite laminates. Compos Sci Technol 1988;33(4):257–77.
[2] Garg AC. Delamination – a damage mode in composite structures. Eng Fract Mech 1988;29(5):557–84.

[3] Salpekar SA, Raju IS, Obrien TK. Strain-energy-release rate analysis of delamination in a tapered laminate subjected to tension load. J Compos Mater 1991;25(2):118–41.
[4] Mezzenga R, Boogh L, Manson JAE. A review of dendritic hyperbranched polymer as modifiers in epoxy composites. Compos Sci Technol 2001;61(5):787–95.
[5] Garg AC, Mai YW. Failure mechanisms in toughened epoxy-resins – a review. Compos Sci Technol 1988;31(3):179–223.
[6] Bascom WD, Hunston DL. Fracture of elastomer-modified epoxy polymers. Adv Chem Ser 1989;222:135–72.
[7] Hedrick JL, Yilgor I, Jurek M, Hedrick JC, Wilkes GL, Mcgrath JE. Chemical modification of matrix resin networks with engineering thermoplastics. 1. synthesis, morphology, physical behavior and toughening mechanisms of poly(arylene ether sulfone) modified epoxy networks. Polymer 1991;32(11):2020–32.
[8] Wilkinson SP, Ward TC, Mcgrath JE. Effect of thermoplastic modifier variables on toughening a bismaleimide matrix resin for high-performance composite-materials. Polymer 1993;34(4):870–84.
[9] Kunz SC, Sayre JA, Assink RA. Morphology and toughness characterization of epoxy-resins modified with amine and carboxyl terminated rubbers. Polymer 1982;23(13):1897–906.
[10] Riew CK, Siebert AR, Smith RW, Fernando M, Kinloch AJ. Toughened epoxy resins: preformed particles as tougheners for adhesives and matrices. Toughened Plastics Ii 1996;252:33–44.
[11] Pearson RA, Yee AF. Toughening mechanisms in thermoplastic-modified epoxies. 1. modification using poly(phenylene oxide). Polymer 1993;34(17):3658–70.
[12] Dadfar MR, Ghadami F. Effect of rubber modification on fracture toughness properties of glass reinforced hot cured epoxy composites. Mater Des 2013;47:16–20.
[13] Barber AH, Cohen SR, Kenig S, Wagner HD. Interfacial fracture energy measurements for multi-walled carbon nanotubes pulled from a polymer matrix. Compos Sci Technol 2004;64(15):2283–9.
[14] Desai AV, Haque MA. Mechanics of the interface for carbon nanotube-polymer composites. Thin Wall Struct 2005;43(11):1787–803.
[15] Coleman JN, Khan U, Blau WJ, Gun'ko YK. Small but strong: a review of the mechanical properties of carbon nanotube-polymer composites. Carbon 2006;44(9):1624–52.
[16] Zhu J, Imam A, Crane R, Lozano K, Khabashesku VN, Barrera EV. Processing a glass fiber reinforced vinyl ester composite with nanotube enhancement of interlaminar shear strength. Compos Sci Technol 2007;67(7–8):1509–17.
[17] Wang WX, Takao Y, Matsubara T, Kim HS. Improvement of the interlaminar fracture toughness of composite laminates by whisker reinforced interlamination. Compos Sci Technol 2002;62(6):767–74.
[18] Arai M, Noro Y, Sugimoto KI, Endo M. Mode I and mode II interlaminar fracture toughness of CFRP laminates toughened by carbon nanofiber interlayer. Compos Sci Technol 2008;68(2):516–25.
[19] Kim JS, Reneker DH. Mechanical properties of composites using ultrafine electrospun fibers. Polym Compos 1999;20(1):124–31.
[20] Bilge K, Venkataraman S, Menceloglu YZ, Papila M. Global and local nanofibrous interlayer toughened composites for higher in-plane strength. Compos Part A: Appl Sci Manuf 2014;58:73–6.
[21] Palazzetti R, Zucchelli A, Gualandi C, Focarete ML, Donati L, Minak G, et al. Influence of electrospun Nylon 6,6 nanofibrous mats on the interlaminar properties of Gr–epoxy composite laminates. Compos Struct 2012;94(2):571–9.
[22] Palazzetti R, Zucchelli A, Trendafilova I. The self-reinforcing effect of Nylon 6,6 nano-fibres on CFRP laminates subjected to low velocity impact. Compos Struct 2013;106:661–71.
[23] Zhang J, Lin T, Wang XG. Electrospun nanofibre toughened carbon/epoxy composites: effects of polyetherketone cardo (PEK-C) nanofibre diameter and interlayer thickness. Compos Sci Technol 2010;70(11):1660–6.
[24] Li G, Li P, Zhang C, Yu YH, Liu HY, Zhang S, et al. Inhomogeneous toughening of carbon fiber/epoxy composite using electrospun polysulfone nanofibrous membranes by in situ phase separation. Compos Sci Technol 2008;68(3–4):987–94.
[25] Van der Schueren L, De Schoenmaker B, Kalaoglu OI, De Clerck K. An alternative solvent system for the steady state electrospinning of polycaprolactone. Eur Polym J 2011;47(6):1256–63.
[26] Lavielle N, Popa AM, de Geus M, Hebraud A, Schlatter G, Thony-Meyer L, et al. Controlled formation of poly(epsilon-caprolactone) ultrathin electrospun nanofibers in a hydrolytic degradation-assisted process. Eur Polym J 2013;49(6):1331–6.
[27] Fejos M, Molnar K, Karger-Kocsis J. Epoxy/polycaprolactone systems with triple-shape memory effect: electrospun nanoweb with and without graphene versus co-continuous morphology. Materials 2013;6(10):4489–504.

PAPER III

NANOFIBRE BRIDGING AS A TOUGHENING MECHANISM IN CARBON/EPOXY COMPOSITE LAMINATES INTERLEAVED WITH ELECTROSPUN POLYAMIDE NANOFIBROUS VEILS

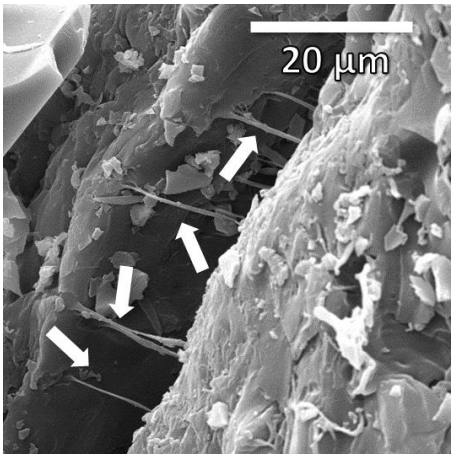

Lode Daelemans, Sam van der Heijden, Ives De Baere, Hubert Rahier, Wim Van Paepegem and Karen De Clerck

(2015) *COMPOSITES SCIENCE AND TECHNOLOGY*. 117. p.244-256

Composites Science and Technology 117 (2015) 244–256

Contents lists available at ScienceDirect

Composites Science and Technology

journal homepage: http://www.elsevier.com/locate/compscitech

Nanofibre bridging as a toughening mechanism in carbon/epoxy composite laminates interleaved with electrospun polyamide nanofibrous veils

Lode Daelemans [a], Sam van der Heijden [a], Ives De Baere [b], Hubert Rahier [c], Wim Van Paepegem [b, **], Karen De Clerck [a, *]

[a] Department of Textiles, Ghent University, Technologiepark-Zwijnaarde 907, B-9052 Zwijnaarde, Belgium
[b] Department of Materials Science and Engineering, Ghent University, Technologiepark-Zwijnaarde 903, B-9052 Zwijnaarde, Belgium
[c] Department Materials and Chemistry, Vrije Universiteit Brussel, Pleinlaan 2, B-1050 Brussels, Belgium

ARTICLE INFO

Article history:
Received 23 February 2015
Received in revised form
26 June 2015
Accepted 28 June 2015
Available online 3 July 2015

Keywords:
Nano particles
Delamination
Fibre bridging
Damage tolerance
Electro-spinning

ABSTRACT

Electrospun thermoplastic nanofibres have a large potential for the interlaminar toughening of composite laminates. They can easily be placed in resin rich interlayers between reinforcing plies prior to laminate production and require no dispersion into the matrix resin. Although there are many expected benefits, the research on composite laminates enhanced with electrospun thermoplastic nanofibres is still very limited and a thorough understanding of the toughening mechanism is still missing. This article provides thorough insights into the micromechanisms that lead to the interlaminar toughening of carbon/epoxy composite laminates interleaved with electrospun polyamide nanofibrous veils. The main mechanism leading to a higher interlaminar fracture toughness, both under Mode I and Mode II loading conditions, was the bridging of (micro)cracks by PA nanofibres. The effectiveness of the nanofibre bridging toughening mechanism is dependent on a good load transfer to the nanofibres. Crack propagation under Mode II loading conditions resulted in much higher improvements than under Mode I loading due to an optimal loading of the nanofibres along their fibre direction in the plane of the nanofibrous veil. In Mode I crack propagation, however, the loading of the nanofibres is less optimal and was shown to be dependent on both the primary reinforcement fabric architecture, as well as on the presence of a carbon fibre bridging zone.

1. Introduction

Recently, the use of electrospun thermoplastic nanofibres has been proposed for the interlaminar toughening of composites [1,2]. Nanofibrous veils produced by electrospinning can be easily placed in the resin rich interlayer between two reinforcing plies prior to composite production. Their nanoscale diameter offers the possibility of very thin interlayers, while their macroscopic length poses no health hazards. The large surface area to volume ratio and superior mechanical performance compared to the bulk polymer only adds to the advantages of using electrospun thermoplastic nanofibres [3,4]. Furthermore, since there is no need to disperse them into the resin, there are no disadvantages such as an increased viscosity or inhomogeneous dispersion which makes them suited for most laminate production routes [2].

Although there are many obvious benefits, the research on composites enhanced with (electrospun) thermoplastic nanofibres is still very limited. Several researchers focused on using electrospun nanofibres which dissolve in the matrix resin such as PCL, PEK-C, PSF or phenoxy-based nanofibres [5–10]. They reported improvements in interlaminar toughness due to a phase separation of the dissolved nanofibres which resulted in tough particulate phases. Another approach to produce enhanced composite laminates is to use thermoplastic nanofibres which keep their nanofibrous structure in the final laminate. The advantages of keeping the nanofibrous structure are that the nanofibres' physical and mechanical properties can be retained and that there is no increase in viscosity of the matrix resin due to dissolution of the nanofibres.

* Corresponding author.
** Corresponding author.
E-mail addresses: Wim.VanPaepegem@UGent.be (W. Van Paepegem), Karen.DeClerck@UGent.be (K. De Clerck).

http://dx.doi.org/10.1016/j.compscitech.2015.06.021
0266-3538/

Furthermore, retaining the nanofibrous structure can enable other toughening mechanisms to take place such as nanofibre bridging at the crack tip.

Several polymer types which retain their nanofibrous structure in the final laminate have already been investigated, e.g. PAN [8], PCL [2], P(St-coGMA) [11,12], PI [13], PA 6 [14–16] and PA 6.6 [17–22]. Regular fibrous veils, with a larger diameter of the fibres compared to nanofibrous veils, have also been investigated to study the interlaminar toughening effect [23–26]. The Mode I and Mode II interlaminar fracture toughness, G_{Ic} and G_{IIc} respectively, are most often studied since they can be used to assess the damage resistance of composite laminates [23,24,27]. Indeed, one of the most encountered forms of damage in composite applications is the propagation of cracks through the interlaminar region between reinforcing plies or other dissimilar interfaces where a resin rich layer is present, resulting in delaminations. These delaminations are mainly due to Mode I and Mode II loading conditions of cracks in frequently encountered loadings such as impact and fatigue [23,28–30].

A variety of effects on the G_{Ic} and G_{IIc} are reported in literature when laminates are interleaved with electrospun nanofibrous veils. Zhang et al. [8] reported no improvements in G_{Ic} upon interleaving of PAN nanofibres as compared to using dissolvable PCL or PEK-C nanofibres. Van der Heijden et al. [2] showed that the nanofibrous structure of PCL can be retained when typical infusion epoxy resins which cure at room temperature are used. The G_{Ic} of an already tough composite increased from 640 J/m^2 to 1240 J/m^2 upon interleaving the laminates with PCL nanofibrous veils. However, the low melting temperature of PCL at around 60 °C limits its use for prepreg based laminates which typically cure at temperatures above 60 °C, resulting in a loss of the PCL nanofibrous structure. In order to allow a wide range of curing temperatures, polymers with higher melting temperatures should be used in order to retain the nanofibrous structure.

Polyamide nanofibres have great potential as they have typical melting temperatures above 200 °C and their electrospinning process is widely studied [31–34]. Hence, there is a relatively large amount of research dedicated to the effect of polyamides, and PA 6.6 in particular, on the interlaminar fracture toughness of composite laminates [14–23]. Saghafi et al. [17] and Beckermann et al. [19] reported an increase in G_{Ic} and G_{IIc} of UD laminates interleaved with PA 6.6 nanofibres. However, these improvements in G_{Ic} only occur during precracking or crack initiation, while G_{Ic} was not affected or even decreased at further crack growth. The effect of PA 6.6 nanofibres on woven laminates has been studied by Hamer et al. [18] and Palazzetti et al. [20,21]. Although Hamer et al. report an increase in G_{Ic}, only minor improvements and even decreases on both G_{Ic} and G_{IIc} are reported by Palazetti et al. [18,20,21]. De Schoenmaker et al. [14] state that G_{Ic} increases slightly upon addition of PA 6 nanofibres in UD laminates. Furthermore, tensile tests on crossply laminates showed that the presence of PA 6 nanofibrous interlayers decreased or even stopped the formation of delaminations between reinforcing plies. Although these results illustrate the potential of interleaving laminates with PA nanofibrous veils, some of the findings seem to contradict each other or improvements only occur during crack initiation. This leads the authors to believe that some fundamental aspects of PA nanofibre toughening have not been analysed in these previous works. A thorough understanding of the fracture and toughening mechanism is clearly needed in order to link the presence of nanofibres to the observed increase or decrease in interlaminar fracture toughness.

In this article, the authors hope to provide thorough insights into the micromechanisms that are present and lead to interlaminar toughening in laminates interleaved with electrospun thermoplastic nanofibres. Electrospun nanofibrous veils of PA 6.6 are used since this is the most studied nanofibre interleaving system. This system will be compared with PA 6.9 nanofibrous veils since Beckermann et al. [19] suggest that polymers with a higher elongation at break can result in higher improvements of G_{Ic}. It is generally accepted that polyamides with longer hydrocarbon chains between the amide groups, e.g. PA 6.9, PA 11 or PA 12, have a higher elongation at break compared to PA 6 or PA 6.6 [35]. Furthermore, PA 6.9 has less moisture take-up compared to PA 6.6 which can have a positive effect on the quality of the resulting laminate [15,23]. The interlaminar fracture toughness in Mode I and Mode II of nanofibre interleaved composite laminates is determined by Double Cantilever Beam (DCB) and End Notched Flexure (ENF) experiments. Resistance curves (R-curves) and Scanning Electron Microscopy (SEM) of the fracture surface are used to analyse and determine the micromechanisms and fracture behaviour of virgin and nanofibre interleaved composite laminates. Following parameters which can affect the toughening behaviour of the nanofibres are taken into account:

- Polymer type: PA 6.6 and PA 6.9
- Nanofibre areal weight: 3 g/m^2 and 18 g/m^2
- Primary reinforcement architecture: unidirectional and twill weave carbon prepregs
- Relative position of the nanofibrous veil and the initiation film in the DCB and ENF specimen design

2. Material and methods

2.1. Materials

PA 6.6 pellets were obtained from Sigma–Aldrich, while PA 6.9 pellets were purchased from Scientific Polymer Products. The PA pellets were dissolved for electrospinning in a mixture of 98–100% formic acid (FA) and 98% acetic acid (AA), both from Sigma–Aldrich. Both solvents are used as received. Unidirectional (M10R/38%/UDT300 – 300 g/m^2) and 2×2 twill weave (MTM49-3/T800 – 200 g/m^2) carbon fibre/epoxy prepregs were purchased from Gazechim Composites and Saroléa respectively.

2.2. Methods

Mechanical experiments were performed on an electromechanical Instron 5800R machine equipped with a load cell of 500 N; load and displacement were recorded. A Jeol Quanta 200F Field Emission Gun and a Phenom ProX scanning electron microscope (SEM) were used to determine the diameter of the electrospun nanofibres and to examine the fracture surface of specimens.

2.3. Electrospinning of polyamide nanofibrous veils

Uniform PA nanofibrous veils were produced by electrospinning on an in-house multinozzle system [14]. A linear lateral motion of the electrospinning nozzles perpendicular to the production direction guarantees the uniformity of the nanofibrous veils. A FA/AA mixture was used to dissolve the PA pellets for electrospinning solutions according to previous studies [15,34]. A 14 wt% 70:30 FA:AA solution was used to electrospin PA 6.6 nanofibres, and a 16 wt% 50:50 FA:AA solution was used for PA 6.9 nanofibres. The applied voltage was set at approximately 35 kV, the feed rate was 1 ml/h per nozzle and the distance between the collector and the needle tip was set at 9 cm and 6 cm for PA 6.6 and PA 6.9 respectively. The internal diameter of the nozzles was 0.84 mm. Special care was taken to ensure stable electrospinning conditions and

uniform deposition of the nanofibres. The nanofibrous veils were produced in 3.0 ± 0.5 g/m^2 and 18 ± 1 g/m^2 and were collected on thick aluminium foil. The average diameter of the PA 6.6 and PA 6.9 nanofibres were 158 ± 19 nm and 245 ± 28 nm, respectively.

2.4. Composite laminate production

Virgin and nanofibre interleaved composite laminates were produced by stacking several layers of prepreg material. The plies were cut to 160 × 160 mm before stacking. Unidirectional $[0^\circ]_{10}$ laminates were produced with M10R/T300 UD prepregs, while woven $[(0/90)^\circ]_{20}$ laminates were produced with MTM49-3/T800 2×2 twill weave prepregs. A release foil was placed in the mid-plane of the prepregs to serve as an initial delamination in the DCB and ENF experiments. For the nanofibre interleaved laminates, the nanofibrous veils were first placed on the prepreg surface after which the aluminium foil was carefully peeled off. Since the nanofibres do not adhere to the aluminium foil, the nanofibrous veil can be easily transferred onto the tacky prepreg surface. The advantage of this method compared to electrospinning onto the prepreg surface directly, is that there is no interaction between the electrospinning solvents and the prepreg material. The laminates were cured in an autoclave according to the resin's prescribed curing cycle. There was no measurable difference in thickness between virgin and nanofibre interleaved laminates. The impregnation of the PA nanofibres by the prepreg epoxy resin was checked with SEM and showed that the nanofibrous veils were completely infused with epoxy resin. Furthermore, transversal crosssection images also showed good quality of the impregnation, see Fig. 1. Specimens for DCB and ENF experiments were sectioned from the 160 × 160 mm composite laminates with a water-cooled diamond saw. In order to assess the deviation between plates, three virgin laminates were produced and reference samples were cut from each of these plates.

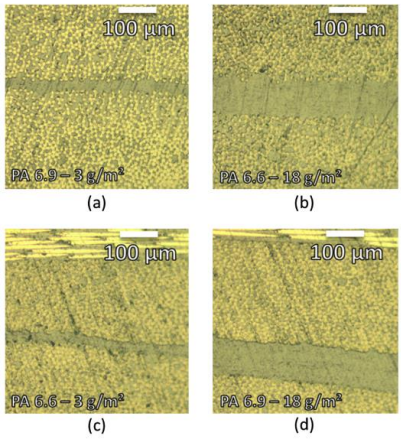

Fig. 1. Transversal cross-section images of the nanofibre interleaved unidirectional (a–b) and twill woven (c–d) composite laminates showing the impregnation of the nanofibrous interlayer.

2.5. Double cantilever beam experiments

The Mode I interlaminar fracture toughness G_{Ic} was determined according to ASTM D5528 [36] as follows:

$$G_I = \frac{3P\delta}{2b(a+|\Delta|)}F \tag{1}$$

where: $P$is the load, δ is the displacement, b is the width, a is the delamination length, $|\Delta|$ corrects for crack front rotations and F corrects for large displacement effects. The $G_{Ic,ini}$ value was determined from the 5%/max point on the load–displacement curves [36]. The $G_{Ic,prop}$ value was determined as the mean G_{Ic} value once the R-curve stabilizes after the fibre bridging zone has formed. Specimens were cut to 150 × 20 mm and had a thickness of 2.95 mm and 4.20 mm for the UD and woven laminates respectively. An initial delamination length of 50 mm was used. The load was introduced to the specimens by piano hinges and a natural Mode I precrack of 3 mm was introduced in the samples after which the sample was unloaded again and tested. The DCB-specimens were opened at 2 mm/min while the crack front propagation was followed by a travelling microscope. At least three specimens were tested for each configuration.

2.6. End notched flexure experiments

The ENF experiments consist out of three-point bending experiments on specimens with an initial delamination. The Mode II interlaminar fracture toughness (G_{IIc}) values were determined according to the Compliance Based Beam Method [37,38]:

$$G_{IIc} = \frac{9P^2a_{eq}^2}{2E_f b^2(2h)^3} \tag{2}$$

where: P is the load, a_{eq} is a corrected delamination length which accounts for subcritical crack growth, b is the width, E_f is the flexural modulus and 2 h is the thickness. This method has several advantages: (1) there is no need to visually measure the delamination length during the experiment, (2) the flexural stiffness is calculated for each specimen separately and (3) it takes subcritical crack growth into account. An R-curve is obtained by plotting Eq. (2) as a function of the equivalent crack growth. The initiation fracture toughness $G_{IIc,ini}$ is defined as the G_{IIc} value at maximum load during the experiment [39], while the propagation fracture toughness $G_{IIc,\ prop}$ is defined as the value of the plateau in the R-curve. The toughness at the onset of subcritical crack growth, i.e. microcrack formation at the crack tip before the crack propagates macroscopically, is described by $G_{IIc,NL}$ and corresponds with nonlinear behaviour before the maximum load is reached during the experiment.

Specimens were cut to 130 × 10 mm and a span length (2 L) of 110 mm was used. In order to establish stable crack growth in the specimens, the ratio of initial delamination length on the half-span length was selected to be higher than 0.7, i.e. $a_0/L > 0.7$: the initial delamination a_0 was 40 mm. The experiment was displacement controlled and the crosshead movement was set to 1 mm/min. At least three specimens were tested for each configuration.

3. Results and discussion

3.1. Mode I interlaminar fracture toughness

3.1.1. Woven laminates

Virgin and nanofibre interleaved woven composite laminates

were produced with the MTM49-3/T800 2×2 twill weave prepreg as described in Section 2.4. Although the force-displacement curve of woven laminates often shows stick-slip crack growth behaviour, the data can still be used to generate an R-curve [37,40], see Fig. 2. There is some scatter of the G_{Ic} values in the resulting R-curve associated with the local differences in toughness due to interlaminar resin pockets and the woven architecture of the carbon fibre fabric [36]. From the R-curve in Fig. 2 (b), it is clear that there is no significant amount of fibre bridging present in the woven laminates, leading to a relatively flat R-curve. For the virgin laminates without nanofibres, the difference between $G_{Ic,ini}$ and $G_{Ic,prop}$ is relatively small, especially when compared to the differences observed due to fibre bridging in unidirectional laminates as described in Section 3.1.2.

The results of the DCB experiments are given in Table 1. From these results, it is clear that both PA 6.6 and PA 6.9 nanofibrous veils of 3 g/m^2 toughen woven composite laminates considerably, leading to an increase in Mode I interlaminar fracture toughness of around 45%. For relatively thick nanofibrous veils of 18 g/m^2 a similar interlaminar toughening as with thin nanofibrous veils was found for PA 6.9 nanofibres. However, the PA 6.6 nanofibre interleaved woven laminates showed a decrease in $G_{Ic,ini}$ of almost 22%. This decrease was mainly due to two specimens which showed unstable crack growth near the initiation zone. The other specimen had similar G_{Ic} values as the virgin laminate.

The R-curve of the nanofibre interleaved woven laminates shows a rising behaviour, see Fig. 3 (a–b), resulting in a larger difference between $G_{Ic,ini}$ and $G_{Ic,prop}$. The rising R-curve behaviour was not observed for the virgin laminates and indicates the formation of a PA nanofibre bridging zone in the nanofibre interleaved specimens. The bridging nanofibres effectively bridge the crack tip and lead to a toughening of the interlaminar region. When the crack propagates further under Mode I loading conditions, the bridging nanofibres are stretched and eventually break by plastic failure. This is confirmed by SEM images of the fracture surface of the woven DCB specimens, see Fig. 3(c–d). The fracture surface showed zones where necking was visible on failed PA nanofibres, see Fig. 4. Hence, there was a good load transfer to the PA nanofibres in these zones and the nanofibres hindered the crack growth. Since plastic failure of the PA nanofibres requires energy, this resulted in higher G_{Ic} values for the nanofibre enhanced woven laminates.

3.1.2. Unidirectional laminates

Virgin and nanofibre interleaved unidirectional composite laminates were produced with the M10R/T300 UD prepreg as described in Section 2.4. In order to interpret the DCB results from the nanofibre interleaved UD composite laminates, it is necessary to understand the fracture behaviour of the virgin UD laminates. The force-displacement curve and the resulting R-curve of a virgin specimen are given in Fig. 5. Three different fracture toughness values will be used to describe the fracture behaviour of these laminates. In order to exclude any fibre bridging, $G_{Ic,0}$ is determined by the point of non-linearity during the first loading cycle where the crack growth starts from the initiation film. This ensures that there are no bridging fibres. The initiation fracture toughness $G_{Ic,ini}$ is determined by the 5%/max point in the force-displacement curve after precracking, while the propagation fracture toughness $G_{Ic,prop}$ is determined by the plateau level in the R-curve. It can be seen from Fig. 5 (b) that there is a relatively large increase in G_{Ic} with increasing crack growth which is mainly due to carbon fibres bridging the DCB specimen halves. This fibre bridging is considered to be an artefact of the DCB experiment on UD laminates [36]. Hence, the exact value of $G_{Ic,prop}$ is of lesser importance as most delaminations in realistic laminates form between plies of dissimilar orientation or between woven plies where fibre bridging is minimal or does not occur. Nevertheless, the R-curve and the related $G_{Ic,prop}$ are still discussed since they provide valuable

Table 1
Mode I interlaminar fracture toughness of virgin and nanofibre interleaved laminates.

Specimen	$G_{Ic,0}$ (J/m^2)	$G_{Ic,ini}$ (J/m^2)	$G_{Ic,prop}$ (J/m^2)
Woven laminates			
Virgin	–	*421 ± 30*	*557 ± 40*
PA 6.6–3 g/m^2	–	**588 ± 30**	**803 ± 60**
PA 6.6–18 g/m^2	–	**329 ± 60**	**523 ± 90**
PA 6.9–3 g/m^2	–	**624 ± 90**	**837 ± 140**
PA 6.9–18 g/m^2	–	**560 ± 30**	**901 ± 190**
UD Laminates			
Virgin	*397 ± 25*	*538 ± 25*	*829 ± 40*
PA 6.6–3 g/m^2	**314 ± 10**	322 ± 10	491 ± 150
PA 6.6–18 g/m^2	**564 ± 30**	557 ± 30	608 ± 40
PA 6.9–3 g/m^2	**377 ± 10**	292 ± 30	533 ± 70
PA 6.9–18 g/m^2	**508 ± 30**	530 ± 10	542 ± 30
[a]PA 6.9–3 g/m^2	398 ± 40	**542 ± 35**	759 ± 100
[a]PA 6.9–18 g/m^2	389 ± 20	**675 ± 25**	752 ± 110

Values in bold indicate which G_{Ic} value is important to compare to the virgin values.
[a] Modified geometry: 3 mm gap between initiation film and nanofibrous veil.

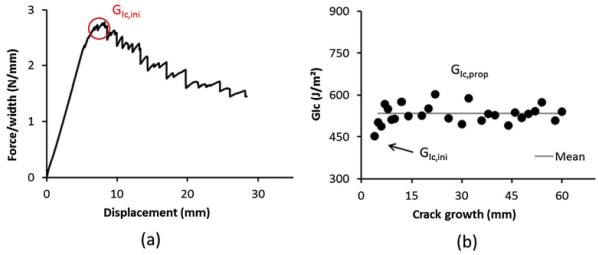

Fig. 2. Force-displacement curve for a virgin woven DCB specimen (a) and the resulting relatively flat R-curve showing no significant amount of fibre bridging (b).

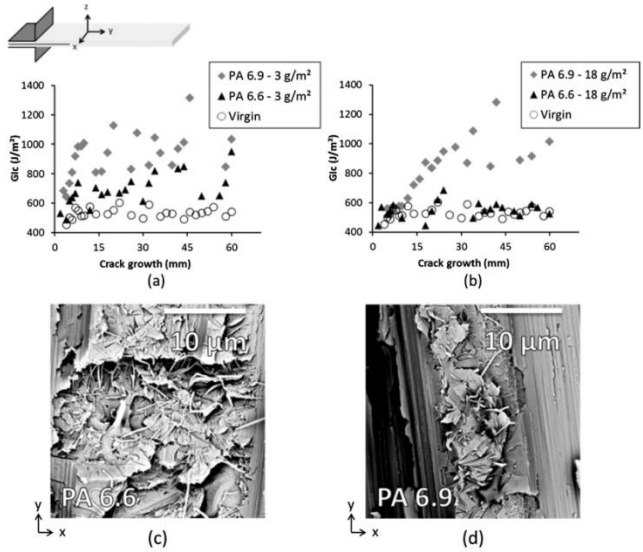

Fig. 3. R-curves for the woven laminates enhanced with PA 6.6 or PA 6.9 nanofibrous veils of 3 g/m^2 (a) and 18 g/m^2 (b) show that the laminates are considerably toughened by incorporation of the nanofibres in the interlaminar regions. SEM images of the fracture surface show zones of broken/necked PA nanofibres (c–d).

information on the fracture behaviour of UD laminates and fibre bridging in particular.

The results of the DCB experiments are given in Table 1. Apparently, the presence of the nanofibres in the interlayer region between UD plies blocked the formation of a carbon fibre bridging zone resulting in relatively flat R-curves, see Fig. 6 (a—b). Although some specimens still showed a slightly rising R-curve due to bridging carbon fibres, the extent of the fibre bridging zone was much less compared to that of the virgin laminates. Furthermore, from the appearance of the fracture surface of the tested DCB specimens and SEM images, it was clear that most of the carbon fibres were covered by a resin rich layer, see Fig. 6 (c). The nanofibres in this resin rich layer did not show much necking as opposed to the nanofibres in woven laminates visible in Fig. 3 (c—d). This suggests that most of the nanofibres seem to have been peeled off from the matrix resin without much deformation. Hence, debonding occurred mainly at the nanofibre-resin interface resulting the absence of a carbon fibre bridging zone. This explains the higher $G_{Ic,prop}$ values (and to lesser extent $G_{Ic,ini}$) of the virgin laminates since they are increased by carbon fibre bridging, while this mechanism is absent in the nanofibre interleaved laminates. Hence, $G_{Ic,0}$ values are better suited as a measure of the interlaminar toughness in order to compare virgin and nanofibre interleaved UD laminates with each other since it is not affected by fibre bridging. For UD laminates modified with nanofibrous veils of 3 g/m^2 the $G_{Ic,0}$ is not significantly affected by PA 6.9 nanofibres while a slight decrease in $G_{Ic,0}$ is observed for PA 6.6 nanofibres. However, laminates modified with a thicker nanofibrous veil of 18 g/m^2 are effectively toughened by the presence of the nanofibres. The $G_{Ic,0}$ value increases from 420 J/m^2 for the virgin laminate to 510 J/m^2 and 560 J/m^2 for the PA 6.9 and PA 6.6 modified laminates which is an increase of 28% and 42% respectively.

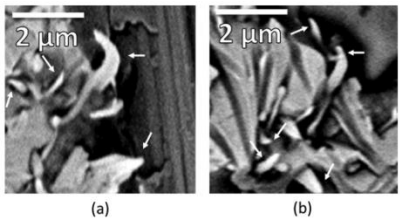

Fig. 4. Close-up of the necking phenomenon visible on failed PA nanofibres.

3.1.3. *The effect of nanofibrous veil position in UD laminates*

The previous sections illustrated the difficulty of interpreting the DCB results of UD laminates due to the absence of carbon fibre bridging in nanofibre interleaved laminates as opposed to virgin laminates. It is necessary to compare the $G_{Ic,0}$ values in order to see

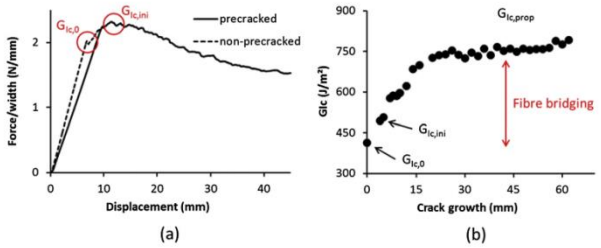

Fig. 5. Force-displacement curve for a virgin UD DCB specimen with and withouth a precrack showing the characteristic points used to determine $G_{Ic,0}$ and $G_{Ic,ini}$ (a) and the resulting R-curve with an increase in G_{Ic} with crack growth due to fibre bridging (b).

the effect that the nanofibres have on the fracture toughness in the absence of fibre bridging. However, the $G_{Ic,ini}$ value which is obtained from a (3 mm) Mode I natural precrack, is better suited and also recommended by the ASTM standard [36]. Therefore, the specimen geometry was modified in such a way that there was a gap of 3 mm between the initiation film and the nanofibrous veil. Hence, a sharp natural precrack can be formed in the virgin matrix material up to the point where it reaches the nanofibrous veil after

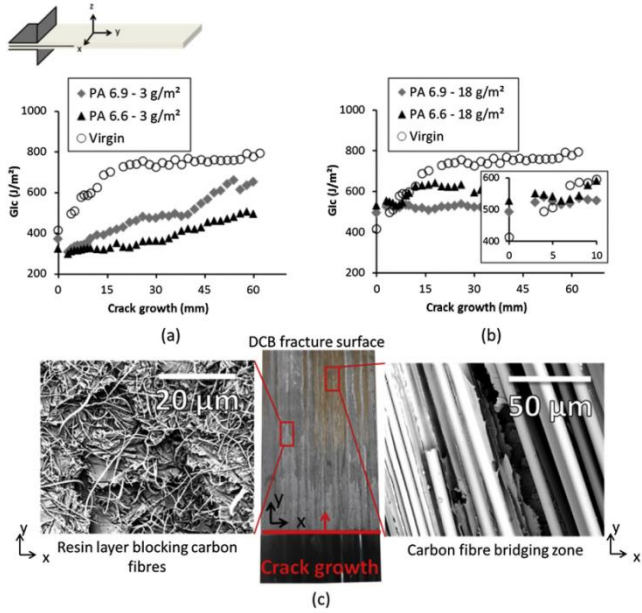

Fig. 6. R-curves for the UD laminates enhanced with a PA nanofibrous veils of 3 g/m^2 (a) and 18 g/m^2 (b) show that the nanofibres (partially) block the formation of a carbon fibre bridging zone, leading to relatively flat R-curves and lower Glc, prop values compared to virgin laminates. This was also visible on the DCB fracture surface which shows small zones of carbon fibre bridging, however, most of the specimen half is covered in a resin rich layer embedded with nanofibres (c).

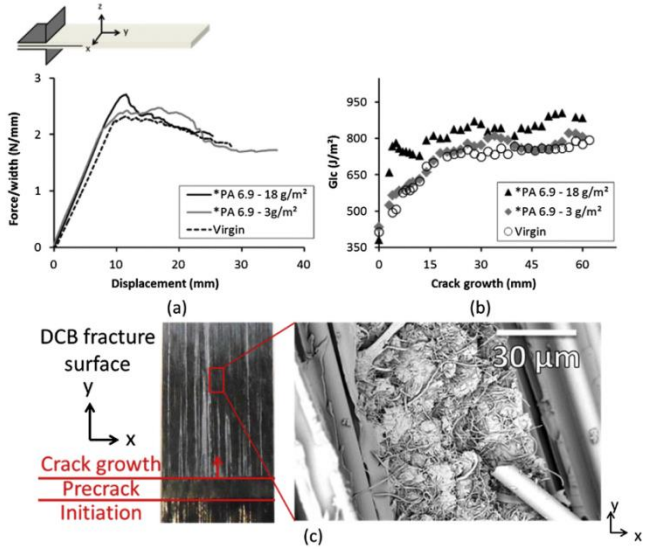

Fig. 7. Force-displacement curve (a) and resulting R-curve (b) show a significant increase in $G_{Ic,ini}$ for the 18 g/m² PA 6.9 nanofibre interleaved laminates with a modified geometry (3 mm gap). The DCB fracture surface shows large amounts of carbon fibre bridging and zones of torn nanofibres in between the carbon fibres (c).

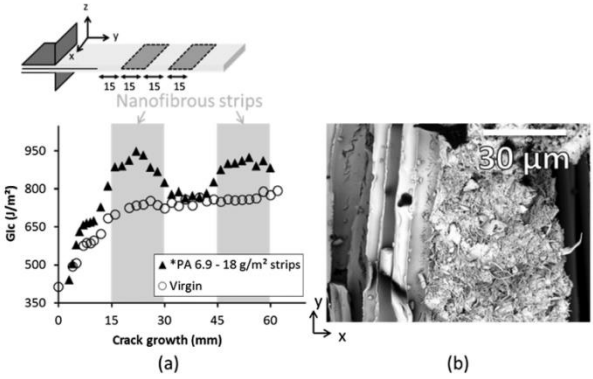

Fig. 8. The Mode I interlaminar toughness increases significantly when the delamination encounters a region of nanofibre enhanced matrix material as can be seen on the R-curve (a). Zones of failed PA nanofibres were visible in between carbon fibres on SEM images of the fracture surface from DCB specimens (b).

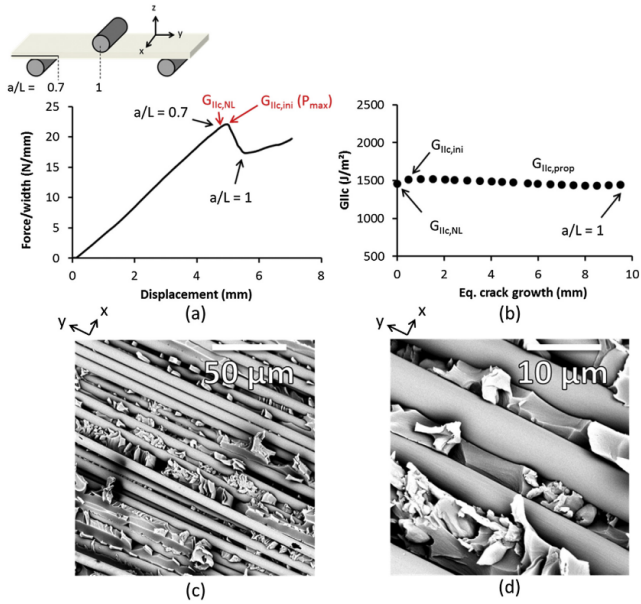

Fig. 9. Force-displacement curve of a virgin UD ENF specimen (a) and the resulting R-curve (b) showing the characteristic points used to describe the Mode II interlaminar fracture toughness. The fracture surface of the ENF specimens shows typical hackle markings (c–d).

which the specimen is closed again. Upon reopening the specimen, the delamination will initiate from a natural crack and grow further into the nanofibre modified interlayer. The results of these experiments are also given in Table 1. As expected, there is no difference between the $G_{Ic,0}$ values of the virgin and nanofibre interleaved laminates as the precrack is formed in the virgin material for all specimens. However, a significant increase in $G_{Ic,ini}$ is obtained when the laminate is enhanced with a PA 6.9 nanofibrous veil of 18 g/m^2, see Fig. 7 (a–b). Furthermore, the $G_{Ic,prop}$ values are also higher than those of nanofibre interleaved laminates in Section 3.1.2. These results indicate that the fracture behaviour changes considerably when the delamination initiates from a natural crack in the virgin material. It was clear that there was a relatively large quantity of carbon fibre bridging present during the experiment which is also visible on the fracture surface of the DCB specimen halves. Furthermore, SEM images showed zones of failed PA 6.9 nanofibres in between the carbon fibres, see Fig. 7 (c), which were not observed on the fracture surface of the UD laminates in Section 3.1.2.

It is clear that a small difference in crack initiation geometry has a big influence on the resulting G_{Ic} values. A second modified geometry was also used to study this effect. Nanofibrous strips with a length of 15 mm were placed at 15 mm and at 45 mm ahead of the initiation film. Hence, a relatively large zone of carbon fibre bridging is allowed to develop before the delamination encounters the nanofibres. This resulted in a significant increase in G_{Ic} in the zones where nanofibres were present, see Fig. 8.

Both nanofibre enhanced laminates with a modified initiation geometry showed large increases in G_{Ic} values compared to the nanofibre enhanced specimens where the initiation film touched the nanofibrous veils. This mechanism can be of use to toughen laminates where the delamination will start from a known region, e.g. around (drilled) holes, free edges or inserts. If the nanofibrous veils are placed several millimetres away from these regions in order for a fibre bridge zone to develop, they can act as "delamination-stoppers". Furthermore, in order to interpret the DCB data of nanofibrous interleaved composites it is very important that the interleaving of the nanofibres is done carefully and reported in detail since a small gap between initiation film and nanofibres has a large effect on the fracture behaviour.

3.1.4. Discussion

The previous sections have shown that the observed toughening effect of polyamide nanofibre interleaved laminates depends on the fabric architecture as well as the nanofibrous veil position. During the electrospinning process, nanofibres are deposited in the plane of the nanofibrous veil. Hence, the nanofibres are parallel with the delamination plane of the DCB specimen. As the crack is initiated in

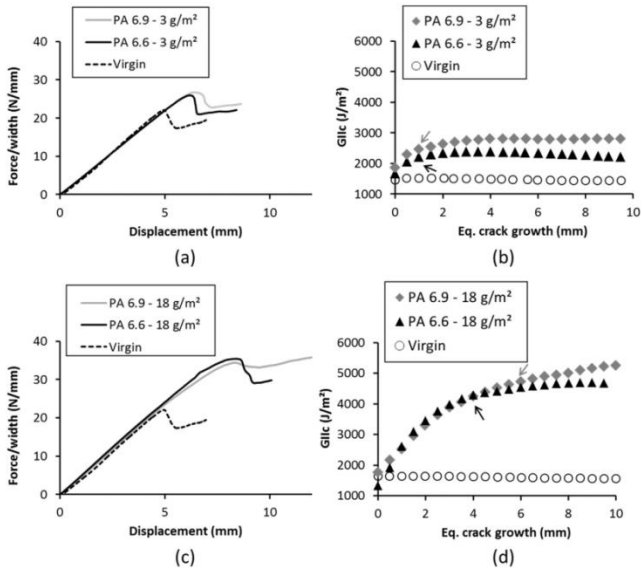

Fig. 10. Force-displacement curves and resulting R-curves for laminates interleaved with 3 g/m² (a–b) and 18 g/m² (c–d) of PA nanofibres show significant increases in G_{IIc}. The interlaminar toughness $G_{IIc,ini}$ (indicated by arrows) is even doubled and almost tripled for 18 g/m² of PA 6.6 and PA 6.9 nanofibrous webs respectively. Furthermore, the subcritical crack growth region increases with increasing nanofibre content.

Table 2
Mode II interlaminar fracture toughness of virgin and nanofibre interleaved composite laminates.

Specimen	$G_{IIc,NL}$ (J/m²)	$G_{IIc,ini}$ (J/m²)	$G_{IIc,prop}$ (J/m²)
UD laminates			
Virgin	*1403 ± 170*	*1578 ± 50*	*1611 ± 60*
PA 6.6–3 g/m²	1622 ± 350	2302 ± 130	2290 ± 110
PA 6.6–18 g/m²	1299 ± 530	4459 ± 220	4645 ± 140
PA 6.9–3 g/m²	1414 ± 248	2585 ± 114	2684 ± 83
PA 6.9–18 g/m²	1683 ± 134	4439 ± 318	5010 ± 362
Woven laminates			
Virgin	*668 ± 20*	*930 ± 40*	–
PA 6.6–3 g/m²	708 ± 10	1085 ± 70	–
PA 6.6–18 g/m²	656 ± 90	1860 ± 100	–
PA 6.9–3 g/m²	697 ± 10	1260 ± 40	–
PA 6.9–18 g/m²	898 ± 170	2666 ± 340	–

Note: compared to Mode I G_{Ic}-values, all G_{IIc}-values (NL, initiation and propagation) can be used to describe the toughening behaviour of nanofibre interleaved laminates.

the nanofibre modified interlayer and grows by Mode I crack growth, the nanofibres are loaded transversally and subjected to peeling forces [19]. This results in the absence of carbon fibre bridging in these laminates. Furthermore, most of the nanofibres that were visible on the fracture surface did not show much plastic deformation resulting in no or minor improvements of G_{Ic}. In the nanofibre interleaved woven laminates, zones of PA nanofibres with plastic failure (necking) were visible. This indicates that the load transfer to the nanofibres was more efficient in woven laminates. The woven architecture probably resulted in small zones where the local crack growth was not purely Mode I or where the crack growth direction was not parallel with the plane of the interlayer resulting in a better load transfer to the nanofibres. The same mechanism probably resulted in the relatively high improvements in G_{Ic} for the nanofibre interleaved UD laminates in which there was a gap between the initiation film and the nanofibrous veil. When a zone of bridging carbon fibres develops, these carbon fibres need to tear through the nanofibre enhanced interlaminar region. Consequently, zones of plastically deformed PA nanofibres are visible on the fracture surface and this tearing of the nanofibres takes up energy leading to a higher interlaminar fracture toughness.

The difference between PA 6.6 and PA 6.9 is most expressed in the results of the woven laminates where the toughening effect of PA 6.9 was much higher than that of PA 6.6. In general, the results

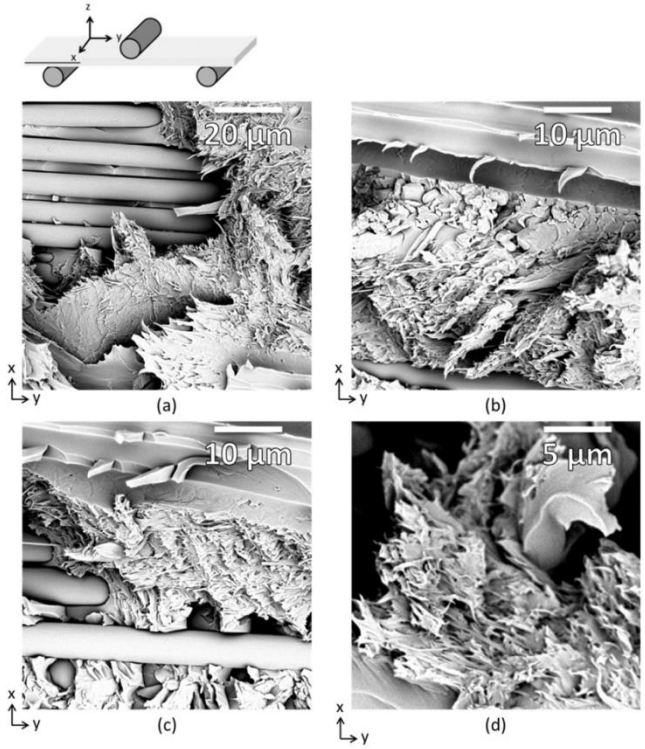

Fig. 11. SEM images taken from the fracture surface of a PA 6.9–3 g/m^2 specimen showing zones of embedded PA nanofibres (a)–(d). Necking can be observed on the broken nanofibres which indicates plastic failure of bridging nanofibres.

indicate that the toughening behaviour of PA 6.9 is more consistent and often leads to a larger observed toughening effect. Possible reasons for this observation might be the smaller moisture take-up of PA 6.9 or the difference in mechanical properties between both polymers. Furthermore, the G_{Ic} increased when the amount of PA 6.9 nanofibres increased.

3.2. Mode II interlaminar fracture toughness

3.2.1. Unidirectional laminates

End notch flexure specimens were sectioned from the same plates as the DCB specimens. The force-displacement curve of a virgin specimen and its resulting R-curve are given in Fig. 9 (a–b). All UD specimens showed stable crack propagation. For the UD laminates the $G_{IIc,NL}$, $G_{IIc,ini}$ and $G_{IIc,\ prop}$ values were very similar around 1600 J/m^2. As opposed to the Mode I R-curves obtained from the DCB results in Section 3.1.2, the virgin UD laminates show no rising R-curve behaviour in Mode II crack propagation. This indicates that carbon fibre bridging zones do not develop and that the effects due to fabric architecture and nanofibrous veil position will probably be of lesser importance for the Mode II interlaminar fracture toughness. The fracture surface of the virgin ENF specimens showed deformed matrix material and hackle markings typical for Mode II crack growth, see Fig. 9 (c–d).

The results of the ENF experiments on virgin and nanofibre interleaved UD laminates are shown in Fig. 10 and Table 2. Both PA 6.6 and PA 6.9 show a very large increase in G_{IIc} in initiation as well as in propagation. Similar to the results in Mode I, PA 6.9 nanofibres show the best improvement and increase the $G_{IIc,ini}$ and $G_{IIc,\ prop}$ about 165% and 190% respectively. From the force-displacement curves given in Fig. 10 (a) and (c), it can be seen that the maximum force during the experiment increases for nanofibre

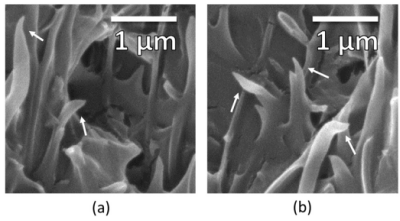

Fig. 12. Close-up of the necking of the PA nanofibres.

interleaved laminates. Furthermore, the propagation of the crack is slowed down as is apparent by the change in slope of the curve after the maximum load has been reached (crack propagation region). As compared to the virgin laminates, the difference between $G_{IIc,NL}$ and $G_{IIc,ini}$ is relatively large. At the point of non-linearity in the force-displacement during the experiment, sub-critical crack growth will occur before the force reaches its maximum value and macroscopic crack growth is observed. For the virgin specimens, this subcritical crack growth is almost neglible. However, the nanofibre interleaved specimens showed a relatively large zone of sub-critical crack growth before macroscopic crack growth is observed. At the point of non-linearity, microcracks are initiated in the matrix material which explains why $G_{IIc,NL}$ is similar for virgin and nanofibre interleaved specimens. The microcracks are subsequently bridged by PA nanofibres in the nanofibre interleaved specimens. This results in the formation of a nanofibre bridging zone. The bridging of the nanofibres absorbs large amounts of energy, leading to a highly increased $G_{IIc,ini}$ and $G_{IIc,\ prop}$. This effect is clearly visible on the R-curves of nanofibre interleaved specimens which show a rising behaviour and from SEM images taken from the fracture surface, see Fig. 11 and Fig. 12.

3.2.2. The effect of nanofibrous veil position in UD laminates

In order to exclude any influence from the UD fibre architecture and carbon fibre bridging, the same modified ENF specimens as in Section 3.1.3 with a gap of 3 mm between the initiation film and nanofibrous veil were tested. As compared to the results obtained in Mode I crack growth, no difference in delamination behaviour was observed in Mode II crack growth. Initially, the G_{IIc} values are similar to those of the virgin laminate material since the crack is initiated in the virgin material. They increase with further crack growth into the nanofibre modified interlayer region to values similar to those of the nanofibre interleaved laminates in the previous section. Hence, as expected, the carbon fibre bridging and nanofibrous veil position is of lesser importance to study the effect of nanofibres by ENF experiments.

3.2.3. Woven laminates

End notch flexure specimens were sectioned from the same woven laminates as the DCB specimens, both for 3 g/m^2 and 18 g/m^2 of PA 6.6 and PA 6.9. The crack growth was stable but exhibited stick-slip behaviour due to the woven architecture. This is visible on the force-displacement curves in Fig. 13. The stick-slip crack growth behaviour made it difficult to construct an R-curve with the used data reduction scheme. Hence, only $G_{IIc,NL}$ and $G_{IIc,ini}$ values defined at the point where the first maximum of the force occurred, are reported in Table 2. From the force-displacement curves it is clear that the nanofibre interleaved specimens showed crack growth at higher loads and that the crack growth is slowed down due to the presence of the nanofibres similar to the results of the UD laminates. The toughening behaviour is also similar to that of the UD laminates: $G_{IIc,NL}$ values of nanofibre interleaved and virgin laminates are comparable indicating the onset of crack growth is similar in both laminates, while a large increase in $G_{IIc,ini}$ is obtained for nanofibre interleaved laminates due to the development of a nanofibre bridging zone. The Mode II interlaminar fracture toughness $G_{IIc,ini}$ increased from 930 ± 40 J/m^2 up to 2666 ± 340 J/m^2 upon addition of 18 g/m^2 of PA 6.9 nanofibrous veils.

3.2.4. Discussion

The high increase in Mode II interlaminar fracture toughness of the nanofibre interleaved composite laminates can be explained by the ideal loading case for the nanofibres. Under Mode II crack growth, the shear stresses result in an in-plane loading of the nanofibrous veil in the interlayer. Hence, the load transfer to the nanofibres is much better as compared to Mode I crack growth resulting in the large increase in G_{IIc} values. This was also apparent from SEM images taken from the fracture surface of the ENF specimens. Zones of plastic deformation are clearly visible and relatively large in size. These zones showed plastically failed and necked PA nanofibres which bridged (micro)cracks in the specimen. The failure of the bridging PA nanofibres absorbs large amounts of energy, thus leading to a highly increased Mode II interlaminar fracture toughness. The toughening effect of the PA 6.9

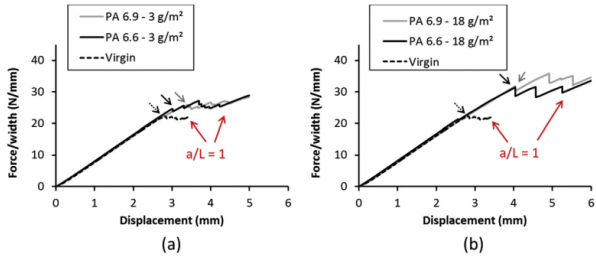

Fig. 13. Force-displacement curves for laminates enhanced with 3 g/m^2 (a) and 18 g/m^2 (b) of PA nanofibres show an increase in load before crack growth, indicating an increase in $G_{IIc,ini}$ (indicated by arrows). Furthermore, the crack propagation is slower for the nanofibre enhanced specimens as indicated by the larger crack growth displacement interval.

interleaved specimens was higher compared to PA 6.6 interleaved specimens which was also the case in the DCB experiments. Furthermore, the $G_{IIc,ini}$ and $G_{IIc,\ prop}$ increased if the weight of the nanofibrous veils increased.

4. Conclusion

Electrospun polyamide nanofibres have a large potential for the interlaminar toughening of prepreg based composite laminates. They are easily integrated in the final laminate and have no significant effect on the production process of the laminates. The main mechanism leading to a higher interlaminar fracture toughness, both in Mode I and Mode II, was observed to be the bridging of cracks by PA nanofibres.

The effectiveness of the nanofibre bridging toughening mechanism depends on a proper load transfer to the nanofibres. Crack propagation under Mode II loading conditions resulted in much higher improvements than under Mode I loading due to an optimal loading of the nanofibres along their fibre direction in the plane of the nanofibrous veil. The nanofibre interleaved specimens showed large improvements of G_{IIc} both for UD and woven laminates. In Mode I crack propagation, however, the loading of the nanofibres is less optimal and was shown to be dependent on both the primary reinforcement fabric architecture, as well as on the presence of a carbon fibre bridging zone.

Woven laminates showed good improvements in G_{Ic} due to the woven fabric architecture which resulted in zones of plastically failed PA nanofibres indicating that there was a good load transfer to the nanofibres in these zones. Furthermore, the rising R-curve behaviour of the nanofibre interleaved woven laminates indicated the formation of a PA nanofibre bridging zone.

In unidirectional laminates, the nanofibres blocked the formation of a carbon fibre bridging zone and the delamination propagated in between the nanofibres resulting in relatively low improvements of the G_{Ic} values. However, if a zone of carbon fibre bridging was able to develop before the delamination encountered the nanofibre modified region, the G_{Ic} increased significantly in this nanofibre modified region. Analysis of the fracture surface showed that the bridging carbon fibres were torn through the nanofibre modified interlayer resulting in a good load transfer to the nanofibres and thus in high G_{Ic} values. Furthermore, this mechanism is of general importance in order to interpret DCB data of nanofibrous interleaved composites since small gaps between initiation film and nanofibrous veil can have a large effect on the observed fracture behaviour.

Acknowledgements

Financial support from the Agency for Innovation by Science and Technology of Flanders (IWT) is gratefully acknowledged. Results in this paper were obtained within the framework of the IWT Strategic Basic Research Grant 141344.

References

[1] J. Kim, D.H. Reneker, Mechanical properties of composites using ultrafine electrospun fibers, Polym. Compos 20 (1999) 124–131, http://dx.doi.org/10.1002/pc.10340.

[2] S. Van der Heijden, L. Daelemans, B. De Schoenmaker, I. De Baere, H. Rahier, W. Van Paepegem, et al., Interlaminar toughening of resin transfer moulded glass fibre epoxy laminates by polycaprolactone electrospun nanofibres, Compos Sci. Technol. 104 (2014) 66–73, http://dx.doi.org/10.1016/j.compscitech.2014.09.005.

[3] Z.-M. Huang, Y.-Z. Zhang, M. Kotaki, S. Ramakrishna, A review on polymer nanofibers by electrospinning and their applications in nanocomposites, Compos Sci. Technol. 63 (2003) 2223–2253, http://dx.doi.org/10.1016/S0266-3538(03)00178-7.

[4] A. Baji, Y.-W. Mai, S.-C. Wong, M. Abtahi, P. Chen, Electrospinning of polymer nanofibers: effects on oriented morphology, structures and tensile properties, Compos Sci. Technol. 70 (2010) 703–718, http://dx.doi.org/10.1016/j.compscitech.2010.01.010.

[5] S. Lin, Q. Cai, J. Ji, G. Sui, Y. Yu, X. Yang, et al., Electrospun nanofiber reinforced and toughened composites through in situ nano-interface formation, Compos Sci. Technol. 68 (2008) 3322–3329, http://dx.doi.org/10.1016/j.compscitech.2008.08.033.

[6] J. Zhang, T. Lin, X. Wang, Electrospun nanofibre toughened carbon/epoxy composites: effects of polyetherketone cardo (PEK-C) nanofibre diameter and interlayer thickness, Compos Sci. Technol. 70 (2010) 1660–1666, http://dx.doi.org/10.1016/j.compscitech.2010.06.019.

[7] G. Li, P. Li, C. Zhang, Y. Yu, H. Liu, S. Zhang, et al., Inhomogeneous toughening of carbon fiber/epoxy composite using electrospun polysulfone nanofibrous membranes by in situ phase separation, Compos Sci. Technol. 68 (2008) 987–994, http://dx.doi.org/10.1016/j.compscitech.2007.07.010.

[8] J. Zhang, T. Yang, T. Lin, C.H. Wang, Phase morphology of nanofibre interlayers: critical factor for toughening carbon/epoxy composites, Compos Sci. Technol. 72 (2012) 256–262, http://dx.doi.org/10.1016/j.compscitech.2011.11.010.

[9] J. Zhang, H. Niu, J. Zhou, X. Wang, T. Lin, Synergistic effects of PEK-C/VGCNF composite nanofibres on a trifunctional epoxy resin, Compos Sci. Technol. 71 (2011) 1060–1067, http://dx.doi.org/10.1016/j.compscitech.2011.03.008.

[10] K. Magniez, T. Chaffraix, B. Fox, Toughening of a carbon-fibre composite using electrospun poly(hydroxyether of bisphenol A) nanofibrous membranes through inverse phase separation and inter-domain etherification, Mater. (Basel) 4 (2011) 1967–1984, http://dx.doi.org/10.3390/ma4111967.

[11] K. Bilge, E. Ozden-Yenigun, E. Simsek, Y.Z. Menceloglu, M. Papila, Structural composites hybridized with epoxy compatible polymer/MWCNT nanofibrous interlayers, Compos Sci. Technol. 72 (2012) 1639–1645, http://dx.doi.org/10.1016/j.compscitech.2012.07.005.

[12] K. Bilge, S. Venkataraman, Y.Z. Menceloglu, M. Papila, Global and local nanofibrous interlayer toughened composites for higher in-plane strength, Compos Part A Appl. Sci. Manuf. 58 (2014) 73–76, http://dx.doi.org/10.1016/j.compositesa.2013.12.001.

[13] S. Jiang, G. Duan, J. Schöbel, S. Agarwal, A. Greiner, Short electrospun polymeric nanofibers reinforced polyimide nanocomposites, Compos Sci. Technol. 88 (2013) 57–61, http://dx.doi.org/10.1016/j.compscitech.2013.08.031.

[14] B. De Schoenmaker, S. Van der Heijden, I. De Baere, W. Van Paepegem, K. De Clerck, Effect of electrospun polyamide 6 nanofibres on the mechanical properties of a glass fibre/epoxy composite, Polym. Test. 32 (2013) 1495–1501, http://dx.doi.org/10.1016/j.polymertesting.2013.09.015.

[15] B. De Schoenmaker, S. van der Heijden, S. Moorkens, H. Rahier, G. van Assche, K. De Clerck, Effect of nanofibres on the curing characteristics of an epoxy matrix, Compos Sci. Technol. 79 (2013) 35–41, http://dx.doi.org/10.1016/j.compscitech.2013.02.009.

[16] S. Van der Heijden, B. De Schoenmaker, H. Rahier, G. Van Assche, K. De Clerck, The effect of the moisture content on the curing characteristics of an epoxy matrix in the presence of nanofibrous structures, Polym. Test. 40 (2014) 265–272, http://dx.doi.org/10.1016/j.polymertesting.2014.08.019.

[17] H. Saghafi, A. Zucchelli, R. Palazzetti, G. Minak, The effect of interleaved composite nanofibrous mats on delamination behavior of polymeric composite materials, Compos Struct. 109 (2014) 41–47, http://dx.doi.org/10.1016/j.compstruct.2013.10.039.

[18] S. Hamer, H. Leibovich, A. Green, R. Intrater, R. Avrahami, E. Zussman, et al., Mode I interlaminar fracture toughness of Nylon 66 nanofibrilmat interleaved carbon/epoxy laminates, Polym. Compos 32 (2011) 1781–1789, http://dx.doi.org/10.1002/pc.21210.

[19] G.W. Beckermann, K.L. Pickering, Mode I and Mode II interlaminar fracture toughness of composite laminates interleaved with electrospun nanofibre veils, Compos Part A Appl. Sci. Manuf. 72 (2015) 11–21, http://dx.doi.org/10.1016/j.compositesa.2015.01.028.

[20] R. Palazzetti, A. Zucchelli, C. Gualandi, M.L. Focarete, L. Donati, G. Minak, et al., Influence of electrospun Nylon 6,6 nanofibrous mats on the interlaminar properties of Gr–epoxy composite laminates, Compos Struct. 94 (2012) 571–579, http://dx.doi.org/10.1016/j.compstruct.2011.08.019.

[21] R. Palazzetti, X. Yan, A. Zucchelli, Influence of geometrical features of electrospun nylon 6,6 interleave on the CFRP laminates mechanical properties, Polym. Compos 35 (2014) 137–150, http://dx.doi.org/10.1002/pc.22643.

[22] P. Akangah, S. Lingaiah, K. Shivakumar, Effect of Nylon-66 nano-fiber interleaving on impact damage resistance of epoxy/carbon fiber composite laminates, Compos Struct. 92 (2010) 1432–1439, http://dx.doi.org/10.1016/j.compstruct.2009.11.009.

[23] T.K. Tsotsis, Interlayer toughening of composite materials, Polym. Compos 30 (2009) 70–86, http://dx.doi.org/10.1002/pc.20535.

[24] V.A. Ramirez, P.J. Hogg, W.W. Sampson, The influence of the nonwoven veil architectures on interlaminar fracture toughness of interleaved composites, Compos Sci. Technol. 110 (2015) 103–110, http://dx.doi.org/10.1016/j.compscitech.2015.01.016.

[25] M. Guo, X. Yi, G. Liu, L. Liu, Simultaneously increasing the electrical conductivity and fracture toughness of carbon–fiber composites by using silver nanowires-loaded interleaves, Compos Sci. Technol. 97 (2014) 27–33, http://dx.doi.org/10.1016/j.compscitech.2014.03.020.

[26] S.-H. Lee, J.-H. Lee, S.-K. Cheong, H. Noguchi, A toughening and strengthening technique of hybrid composites with non-woven tissue, J. Mater. Process

Technol. 207 (2008) 21–29, http://dx.doi.org/10.1016/j.jmatprotec.2007.12.047.
[27] I. Chou, T. Inutake, K. Namba, Correlation of damage resistance under low velocity impact and Mode II delamination resistance in CFRP laminates, Adv. Compos Mater. 8 (1999) 167–176, http://dx.doi.org/10.1163/156855199X00173.
[28] A.C. Garg, Delamination—a damage mode in composite structures, Eng. Fract. Mech. 29 (1988) 557–584, http://dx.doi.org/10.1016/0013-7944(88)90181-6.
[29] N. Sela, O. Ishai, Interlaminar fracture toughness and toughening of laminated composite materials: a review, Composites 20 (1989) 423–435, http://dx.doi.org/10.1016/0010-4361(89)90211-5.
[30] M. Hojo, T. Ando, M. Tanaka, T. Adachi, S. Ochiai, Y. Endo, Modes I and II interlaminar fracture toughness and fatigue delamination of CF/epoxy laminates with self-same epoxy interleaf, Int. J. Fatigue 28 (2006) 1154–1165, http://dx.doi.org/10.1016/j.ijfatigue.2006.02.004.
[31] S. De Vrieze, B. De Schoenmaker, Depuydt J. Ceylan Ö, L. Van Landuyt, H. Rahier, et al., Morphologic study of steady state electrospun polyamide 6 nanofibres, J. Appl. Polym. Sci. 119 (2011) 2984–2990, http://dx.doi.org/10.1002/app.33036.
[32] P. Heikkilä, A. Harlin, Parameter study of electrospinning of polyamide-6, Eur. Polym. J. 44 (2008) 3067–3079, http://dx.doi.org/10.1016/j.eurpolymj.2008.06.032.
[33] C. Mit-uppatham, M. Nithitanakul, P. Supaphol, Ultrafine electrospun polyamide-6 fibers: effect of solution conditions on morphology and average fiber diameter, Macromol. Chem. Phys. 205 (2004) 2327–2338, http://dx.doi.org/10.1002/macp.200400225.
[34] B. De Schoenmaker, A. Goethals, L. Van der Schueren, H. Rahier, K. De Clerck, Polyamide 6.9 nanofibres electrospun under steady state conditions from a solvent/non-solvent solution, J. Mater. Sci. 47 (2012) 4118–4126, http://dx.doi.org/10.1007/s10853-012-6266-9.
[35] T.D. Fornes, D.R. Paul, Structure and properties of nanocomposites Based on Nylon-11 and -12 compared with those based on Nylon-6, Macromolecules 37 (2004) 7698–7709, http://dx.doi.org/10.1021/ma048757o.
[36] ASTM Standard D5528-13, Standard Test Method for Mode I Interlaminar Fracture Toughness of Unidirectional Fiber Reinforced Polymer Matrix Composites, ASTM Int, 2013, http://dx.doi.org/10.1520/D5528.
[37] I. De Baere, S. Jacques, W. Van Paepegem, J. Degrieck, Study of the Mode I and Mode II interlaminar behaviour of a carbon fabric reinforced thermoplastic, Polym. Test. 31 (2012) 322–332, http://dx.doi.org/10.1016/j.polymertesting.2011.12.009.
[38] A. Arrese, N. Carbajal, G. Vargas, F. Mujika, A new method for determining mode II R-curve by the end-notched flexure test, Eng. Fract. Mech. 77 (2010) 51–70, http://dx.doi.org/10.1016/j.engfracmech.2009.09.008.
[39] ASTM Standard D7905-14, Standard Test Method for Determination of the Mode II Interlaminar Fracture Toughness of Unidirectional Fiber-Reinforced Polymer Matrix Composites, ASTM Int, 2014, http://dx.doi.org/10.1520/D7905_D7905M-14.
[40] A.F. Gill, P. Robinson, S. Pinho, Effect of variation in fibre volume fraction on modes I and II delamination behaviour of 5HS woven composites manufactured by RTM, Compos Sci. Technol. 69 (2009) 2368–2375, http://dx.doi.org/10.1016/j.compscitech.2009.02.008.

PAPER IV

USING ALIGNED NANOFIBRES FOR IDENTIFYING THE TOUGHENING MICROMECHANISMS IN NANOFIBRE INTERLEAVED LAMINATES

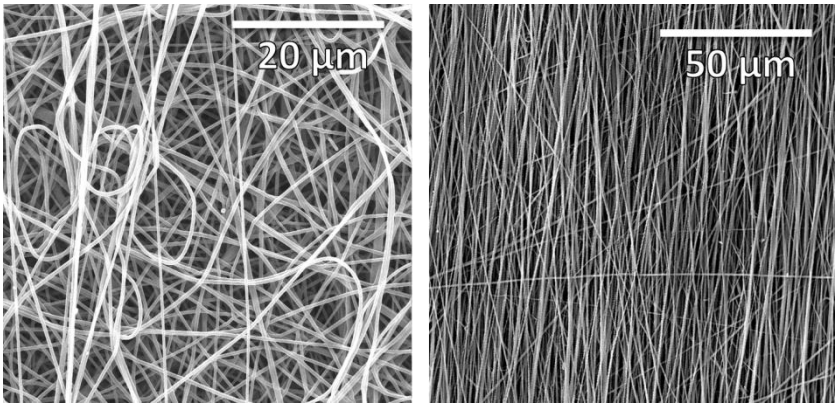

Lode Daelemans, Sam van der Heijden, Ives De Baere, Hubert Rahier, Wim Van Paepegem and Karen De Clerck

(2016) *COMPOSITES SCIENCE AND TECHNOLOGY*. 124. p.17-26

Composites Science and Technology 124 (2016) 17–26

Contents lists available at ScienceDirect

Composites Science and Technology

journal homepage: http://www.elsevier.com/locate/compscitech

Using aligned nanofibres for identifying the toughening micromechanisms in nanofibre interleaved laminates

Lode Daelemans [a], Sam van der Heijden [a], Ives De Baere [b], Hubert Rahier [c], Wim Van Paepegem [b, **], Karen De Clerck [a, *]

[a] Department of Textiles, Ghent University, Technologiepark-Zwijnaarde 907, B-9052 Zwijnaarde, Belgium
[b] Department of Materials Science and Engineering, Ghent University, Technologiepark-Zwijnaarde 903, B-9052 Zwijnaarde, Belgium
[c] Department Materials and Chemistry, Vrije Universiteit Brussel, Pleinlaan 2, B-1050 Brussels, Belgium

ARTICLE INFO

Article history:
Received 12 October 2015
Received in revised form
17 November 2015
Accepted 19 November 2015
Available online 2 December 2015

Keywords:
Nano particles
Delamination
Fibre bridging
Damage tolerance
Electro-spinning

ABSTRACT

The susceptibility to delamination is one of the main concerns in many advanced laminated composite applications. Laminates interleaved with electrospun nanofibrous veils provide a potential solution in order to increase the material's resistance to interlaminar fracture. Previous studies have shown that nanofibres are able to bridge microcracks in the laminates resulting in an increased interlaminar fracture toughness (IFT). However, the exact micromechanisms resulting in these nanofibre bridging zones are still unclear. In this article, aligned nanofibrous structures are used to identify and study the different micromechanisms which take place during Mode II crack propagation. Three nanofibrous veil morphologies with a distinct orientation of the nanofibres are used: (1) a random deposition of nanofibres, (2) nanofibres oriented parallel to the crack growth direction, and (3) nanofibres oriented perpendicular to the crack growth direction. A thorough analysis of the fracture surface of tested specimens and crack path behaviour is performed in order to determine the micromechanisms associated with the development of nanofibre bridging zones. A strong effect of the nanofibre orientation distribution on the Mode II IFT and the underlying toughening mechanisms was observed: different micromechanisms were observed depending on the nanofibre orientation.

1. Introduction

Delaminations between reinforcing plies remain one of the most important types of damage encountered in composite laminates during service. Hence, the susceptibility to delamination of composite laminates is a critical design factor in many applications [1–3]. It is often expressed in terms of interlaminar fracture toughness (IFT) and a lot of research is dedicated to developing methods that increase the IFT of composite laminates.

A recently proposed method of increasing the IFT is the interleaving of laminates with electrospun nanofibrous veils [4–21]. The nanoscale diameter of electrospun nanofibres offers the possibility of obtaining very thin veils with a very high surface area to volume ratio and superior mechanical performance compared to the bulk polymer. Although the use of electrospun nanofibrous veils offers many benefits compared to traditional toughening methods, the research on composites enhanced with electrospun thermoplastic nanofibrous veils is still limited. Several studies indicate that electrospun polyamide nanofibrous veils have a lot of potential to be used as an interlaminar toughener [4–6,9,14,17,19]. In a previous article by the authors [4], the development of nanofibre bridging zones was suggested to be the main mechanism resulting in an increased toughness of PA nanofibre interleaved laminates. However, a detailed analysis of the fracture process and the nanofibre bridging development in nanofibre interleaved laminates has yet to be performed. Hence, it is necessary to investigate the fracture behaviour of the nanofibre interleaved composites in detail in order to determine the critical factors for toughening.

In this article, the authors aim to provide thorough insight into the micromechanisms that govern the interlaminar fracture of nanofibre interleaved composite laminates. The focus will be on Mode II IFT as delamination growth during service often occurs under Mode II dominated loadings. Mode II IFT can also be related

* Corresponding author.
** Corresponding author.
E-mail addresses: Karen.DeClerck@UGent.be (K. De Clerck), Wim.VanPaepegem@UGent.be (W. Van Paepegem).

http://dx.doi.org/10.1016/j.compscitech.2015.11.021
0266-3538/

to the damage resistance of the material when laminates are subjected to, for example, impact [1,22]. Furthermore, Mode II IFT experiments are less prone to artefacts related to the specimen design as compared to Mode I IFT experiments [4], and thus, provide for a more robust analysis of the micromechanisms.

It will be shown that there are two distinct mechanisms which can result in nanofibre bridging zones and which are dependent on the nanofibre orientation distribution. Three nanofibrous veil morphologies will be used in order to study the effect of nanofibre orientation distribution on the IFT: (1) random deposition of nanofibres, (2) nanofibres oriented parallel to the crack growth direction, and (3) nanofibres oriented transversely to the crack growth direction.

In the first section of this article, the nanofibre orientation influence on the Mode II IFT is discussed. The Mode II IFT is determined by End Notched Flexure (ENF) experiments on unidirectional carbon/epoxy composite laminates. Analysis of the R-curves provides information about the development of nanofibre bridging zones which result in an increased Mode II IFT. In the second section, a detailed fractographic analysis of the tested specimens is used in order to complement the results of the ENF experiments. The micromechanisms resulting in toughening were observed by combining SEM images of the fracture surface and optical microscopy on polished cross-sections of tested specimens. Finally, the effect of precracking on the observed IFT, i.e. crack initiation starting from an initiation film or from a natural formed crack, is discussed.

2. Materials and methods

2.1. Materials

PA 6.9 pellets were purchased from Scientific Polymer Products. The pellets were dissolved for electrospinning in a mixture of 98–100% formic acid (FA) and 98% acetic acid (AA), both purchased from Sigma–Aldrich. Both solvents are used as received. Composite laminates are produced with unidirectional (M10R/38%/UD T300 – 300 g/m^2) carbon fibre/epoxy prepregs purchased from Gazechim Composites.

2.2. Methods

2.2.1. Electrospinning of nanofibrous veils

Uniform PA 6.9 nanofibrous veils were produced with an in-house developed electrospinning system with a rotating drum collector. By using a rotating drum collector in the electrospinning process, it is possible to obtain aligned nanofibres [23–25]. The drum has a diameter of 100 mm and a length of 400 mm, allowing the production of relatively large aligned nanofibrous veils. The rotational speed can be set between 0 rpm and 4000 rpm in order to produce randomly oriented or aligned nanofibrous veils. The electrospinning nozzles move at a constant velocity parallel to the drum's axis in order to produce uniform nanofibrous veils with constant areal density. A FA/AA mixture was used as an electrospinning solvent for the PA 6.9 pellets according to previous studies [26]. The electrospinning mixture consisted of a 20 wt% PA 6.9 1:1 FA/AA solution. The solution was pumped through a hollow needle with an inner diameter of 1.024 mm at a flow rate of 1.5 ml/h. The tip-to-collector distance was set at 6 cm and the applied voltage was chosen between 20 and 25 kV until a stable Taylor cone was obtained. Special care was taken to ensure stable electrospinning conditions and uniform deposition of the nanofibres onto the collector. The nanofibrous veils had an areal weight of 11 $\pm$ 0.5 g/m^2 and were collected directly on the rotating drum collector.

In order to produce aligned nanofibrous veils, the rotational speed of the drum collector was set to its maximum value of 4000 rpm, resulting in a tangential speed at the collector's surface of approximately 41 m/s. Nanofibrous veils with randomly oriented nanofibres were obtained by using a very low rotational speed of 150 rpm, see Fig. 1a. The high rotational velocity of the rotating drum collector induces a preferred orientation in the nanofibrous veil resulting in aligned nanofibres, see Fig. 1b. The average diameter of the randomly oriented and aligned nanofibres were 457 $\pm$ 53 nm and 464 $\pm$ 110 nm respectively.

2.2.2. Composite laminate production

Virgin and nanofibre interleaved composite laminates were produced by stacking 12 layers of unidirectional prepreg plies in a $[0^\circ]_{12}$ layup. The plies were cut to 200 $\times$ 200 mm before stacking. An ETFE-based release film was placed in the midplane of the stacking to serve as an initial delamination in the ENF experiments. For the nanofibre interleaved laminates, one nanofibrous veil was placed in the midplane adjacent to the initiation film. The laminates were cured in an autoclave according to the manufacturer's prescribed curing cycle: 2 h at 120 °C at a pressure of 5 bar while a vacuum of 0.9 bar was applied to the vacuum bag. Four different laminates were produced: (i) a virgin laminate without nanofibres which serves as a baseline (VIRGIN), (ii) an interleaved laminate with the nanofibres oriented parallel to the carbon fibres (PAR), (iii) an interleaved laminate with the nanofibres oriented transversely to the carbon fibres (TRANS), and (iv) an interleaved laminate with a random deposition of the nanofibres (RNDM). There was no difference in thickness between the virgin and nanofibre interleaved laminates: all laminates had a thickness of approximately 3.7 mm.

2.2.3. Mode II interlaminar fracture toughness

The ENF experiment consists of a UD specimen with an initial delamination, loaded in three-point bending. Upon loading, the delamination/crack grows in the 0°-direction, parallel to the carbon fibres. The specimen geometry was chosen in order to comply with the recent ASTM D7905-14 standard for determining the Mode II IFT of UD composites by ENF experiments [27]. Specimens were sectioned from the laminates with a water-cooled diamond saw and cut to 160 $\times$ 20 mm. An initial delamination length of 30 mm and a span length of 100 mm were used in accordance with ASTM D7905-14. The support and loading roller radii were 2.2 mm. A sharp natural Mode II precrack was produced by loading a non-precracked specimen to crack initiation after which the sample was unloaded again. The precrack length was determined according to the procedure outlined in the ASTM D7905-14 standard by using a compliance calibration method. The precracked specimens were then used in order to determine the precracked Mode II IFT according to the Compliance Based Beam Method [4,28,29]:

$$G_{IIc} = \frac{9P^2 a_{eq}^2}{2E_f b^2 (2h)^3} \quad (1)$$

where: P is the load, a_{eq} is the delamination length which accounts for subcritical crack growth and is determined from the actual compliance of the specimen, E_f is the flexural modulus which is measured for each specimen separately, b is the width and $2h$ is the thickness. This method has several advantages over the data reduction method proposed in ASTM D7905-14: (1) there is no need to visually measure the delamination length during the experiment in order to construct an R-curve, (2) it does not require a compliance calibration for each specimen, and (3) it takes subcritical crack growth into account.

Two Mode II IFT values will be used throughout the article, G_{IIc}(initiation) and G_{IIc}(non-linear). The initiation fracture toughness

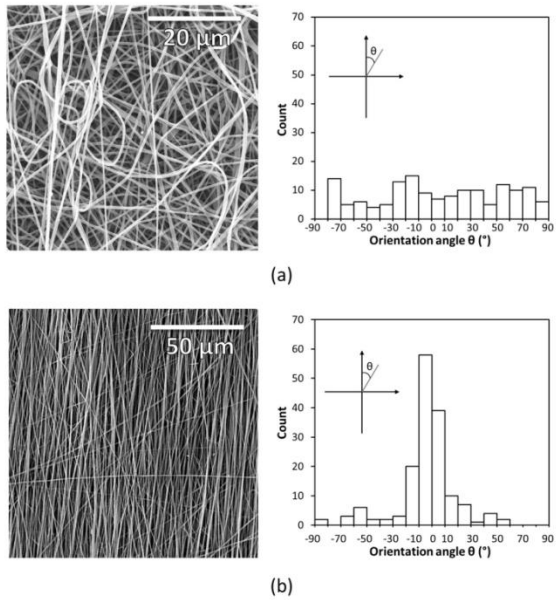

Fig. 1. SEM image of the nanofibrous veils produced on a rotating drum collector at 150 rpm (a) and at 4000 rpm (b) and their resulting orientation distributions. Good alignment of the PA 6.9 nanofibres is obtained at 4000 rpm.

$G_{IIc,ini}$ is defined as the G_{IIc} value at maximum load during the experiment ($P = P_{max}$) in accordance with ASTM D7905-14. This is the most commonly used Mode II IFT parameter as it is related to the point at which macroscopic crack growth will occur. The toughness at the onset of subcritical crack growth, i.e. microcrack formation at the crack tip before the crack propagates macroscopically (fracture processing zone), is described by $G_{IIc,NL}$ and corresponds with non-linear load behaviour before the maximum load is reached. Furthermore, an R-curve is obtained by plotting Eq. (1) as a function of the equivalent crack growth Δa_{eq}. The value of $G_{IIc,NL}$ is obtained from the R-curve as the toughness before any crack growth occurs ($\Delta a_{eq} = 0$). This is illustrated in Fig. 2 for a typical ENF experiment.

The ENF experiments were displacement-controlled with a crosshead movement of 0.5 mm/min (loading and unloading) on an electromechanical Instron 3369 machine equipped with a load cell of 2 kN; load and displacement were recorded during loading and unloading of the specimens. All experiments were performed at 20 ± 2 °C and 65 ± 4% RH. Three specimens were tested for each configuration. A Jeol Quanta 200F Field Emission Gun SEM, a Phenom ProX SEM and an Olympus BX51 optical microscope with an Olympus UC30 camera were used to examine the fracture surface of the specimens.

3. Results and discussion

3.1. Mode II IFT of laminates interleaved with nanofibrous veils

Representative load–displacement curves and the resulting Mode II IFT $G_{IIc,ini}$ values of each configuration (VIRGIN, PAR, TRANS and RNDM) are given in Fig. 3. The introduction of PA 6.9 nanofibrous veils in the interlaminar region results in a higher maximum load before fracture and thus in a higher $G_{IIc,ini}$. Furthermore, there is a clear effect of nanofibrous veil orientation on the $G_{IIc,ini}$. The Mode II IFT increased by approximately 50% for specimens in which the nanofibres were parallel to the crack growth direction, by 75% for nanofibres oriented transversely to the crack growth direction and even by 100% when a random deposition of nanofibres was used.

Since there is a difference in observed $G_{IIc,ini}$ between PAR and TRANS interleaved specimens, indicating that both orientations induce a different toughening of the interleaved laminate, it can be expected that, in extremum, a RNDM interleaved laminate may combine both effects of PAR and TRANS interleaved laminates. Indeed, the random oriented nanofibrous veil is composed of both nanofibres more or less parallel and more or less transversely oriented to the delamination growth direction. Hence, the toughening effect of both parallel and transversely oriented nanofibres can be

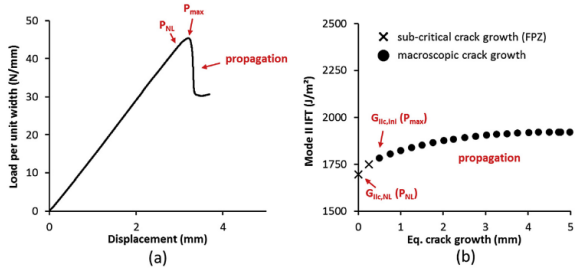

Fig. 2. Typical load–displacement curve (a) and resulting R-curve (b) from the ENF experiment with an indication of the different points at which $G_{IIc,NL}$ and $G_{IIc,ini}$ are defined. Subcritical crack growth in the fracture processing zone (FPZ) is taken into account as an equivalent crack growth.

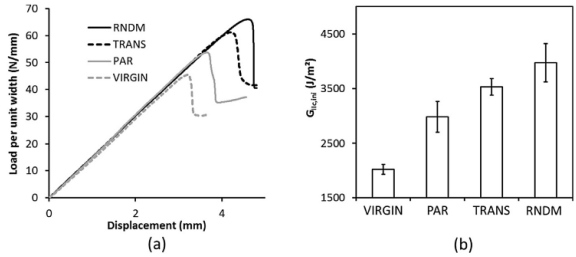

Fig. 3. Representative load–displacement curves (a) and resulting $G_{IIc,ini}$ values (b) for the four different configurations. All nanofibre interleaved laminates show an increase in maximum load before fracture and in $G_{IIc,ini}$ compared to the virgin laminate. A random deposition of nanofibres results in the largest increase.

associated to the RNDM interleaved laminates. This might explain why the RNDM specimens have the highest observed $G_{IIc,ini}$.

The toughened response of nanofibre interleaved laminates can be associated with the development of nanofibre bridging zones [4]. The increase in toughness during subcritical crack growth, i.e. $\Delta G_{IIc} = G_{IIc,ini} - G_{IIc,NL}$, is a measure for the effectiveness, or "size", of the nanofibre bridging zone. A larger ΔG_{IIc} indicates a more effective nanofibre bridging zone which takes up more energy. However, it should be noted that ΔG_{IIc} is not purely a measure of nanofibre bridging, but is associated to the complex crack growth mechanism under Mode II loading, see also Sections 2.2.3 and 3.2.2. Hence, ΔG_{IIc} can be non-zero for virgin laminates. However, the development of nanofibre bridging zones in interleaved laminates results in an increase in ΔG_{IIc} compared to the virgin material due to nanofibres which will bridge the microcracks and result in a higher toughness.

The R-curves in Fig. 4a show that $G_{IIc,NL}$ remains similar for all nanofibre interleaved configurations, while $G_{IIc,ini}$ is dependent on the nanofibre orientation. Hence, there is a significant effect of nanofibre orientation on the nanofibre bridging zone's effectiveness, see Fig. 4b. The effectiveness of the toughening mechanism characteristic to PAR interleaved specimens is less effective compared to the toughening mechanism in TRANS interleaved specimens. The RNDM interleaved laminates show the largest ΔG_{IIc} values, indicating that the nanofibre bridging zone in this configuration is the most effective – or the "largest" – compared to PAR and TRANS configurations. Furthermore, the interleaved laminates have a higher $G_{IIc,NL}$ value than that of the virgin laminate. In order to explain these mechanisms, a fractographic analysis of the specimens is performed in the following section.

3.2. Fractographic analysis

3.2.1. Crack path behaviour

A typical cross-sectional image of the virgin ENF specimens after loading is shown in Fig. 5a. There is no distinguishable interlaminar region present in the virgin laminate between the reinforcing plies due to the use of unidirectional prepregs. The crack will grow into the laminate under Mode II loading conditions and is mainly located at the carbon fibre/matrix interface in the intralaminar region. The failure mechanism is a combination of interfacial failure at the fibre/matrix interface and hackle formation in the matrix resin due to shear stresses. It is designated as Type A failure and it is typical for Mode II crack growth.

The introduction of a nanofibrous veil in the midplane of the laminates resulted in the formation of an interlaminar region with a thickness of 40–50 μm. Cross-sectional images of nanofibre interleaved ENF specimens show that the crack is deflected away from the toughened interlayer into the intralaminar region and only crosses the interlaminar region at certain locations designated as Type B failure, see Fig. 5b. This results in a very distinct fracture

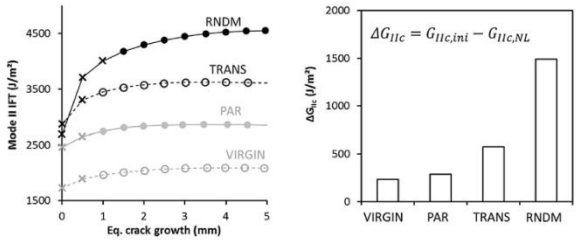

Fig. 4. Representative R-curves for each configuration (a) show the effect of nanofibre orientation on the fracture behaviour. While $G_{IIc,NL}$ remains similar for all the interleaved configurations, $G_{IIc,ini}$ increases substantially for the RNDM interleaved laminates (b). This indicates that the nanofibre bridging zone developed in RNDM interleaved laminates is more effective than those in PAR and TRANS interleaved laminates.

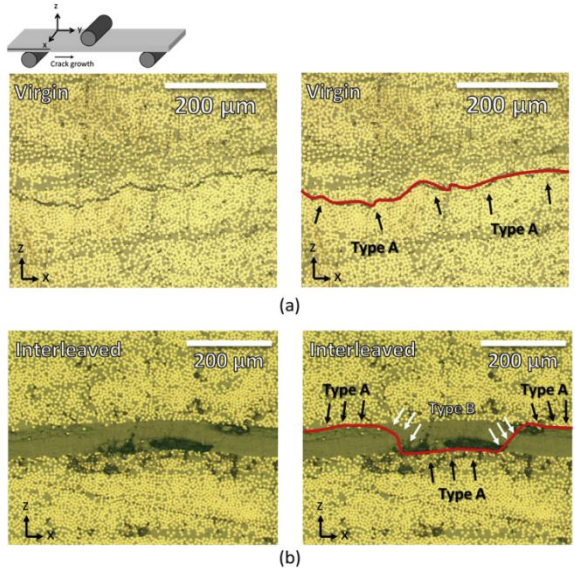

Fig. 5. Cross-sectional images of virgin laminates (a) show that the crack path is located at the carbon fibre/matrix resin interface in the intralaminar region (Type A). Nanofibre interleaved laminates (b) show a similar crack path, however, the crack path crosses the interlaminar region at certain locations (Type B). The crack path behaviour was similar for all nanofibre interleaved configurations (Left image: unmodified; right image: crack path visualised).

surface topology which consists of intralaminar failure similar to the virgin laminates (Type A), and, interlaminar failure at points where the crack passes from one side of the interlayer to the other (Type B), see Fig. 6. Furthermore, it can be seen that the interlaminar failure mainly propagates parallel to the crack growth direction resulting in a "banded" structure on the fracture surface.

3.2.2. Fracture surface analysis

3.2.2.1. Virgin laminates (without nanofibres). The fracture surface of a virgin ENF specimen after loading is shown in Fig. 7. During

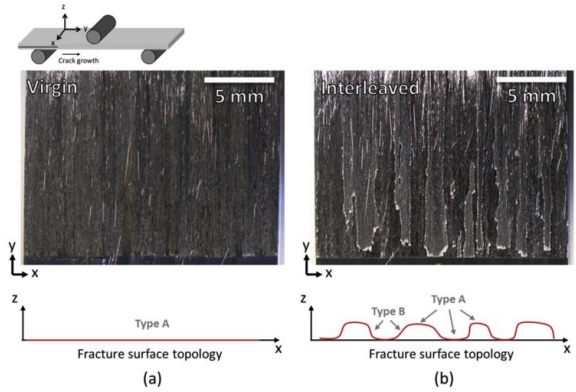

Fig. 6. The fracture surface of a virgin (a) and a nanofibre interleaved (b) show the distinct fracture surface topology due to regular interlaminar crossings of the crack path (Type B failure) in nanofibre interleaved laminates. The fracture surface topology is similar for all nanofibre interleaved configurations.

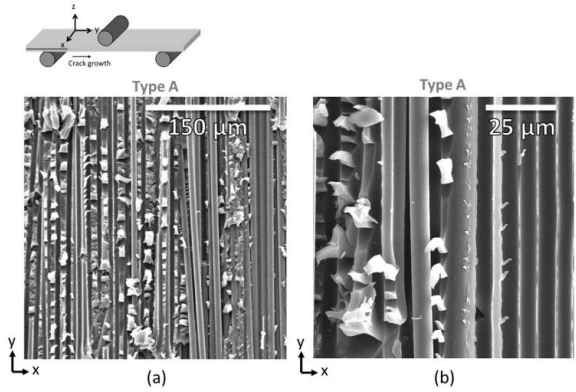

Fig. 7. SEM images of the fracture surface of virgin ENF specimens show that the Type A failure mechanism is a combination of hackle formation and interfacial failure.

Mode II loading, the material in front of the crack tip experiences shear stresses, which results in the formation of tensile microcracks in the matrix resin ahead of the crack tip at 45° relative to the macroscopic crack growth direction [2,30]. These microcracks will coalesce to form a macroscopic continuous crack, while subsequent shear failure of the ligaments results in the formation of hackles [31–33]. This mechanism of hackle formation is typical for Mode II crack growth in Type A failure regions and can clearly be seen on SEM images of the fracture surfaces.

As described in Section 3.2.1, the crack path behaviour of interleaved laminates differs from that of virgin laminates by regular interlaminar crossings in Type B failure regions. Although hackle formation can still occur in Type A failure regions similar to hackle formation in virgin laminates, the failure plane of Type B failure zones is inclined to the macroscopic delamination plane which might give rise to different micromechanisms of failure in these zones.

3.2.2.2. Nanofibres oriented parallel to the crack propagation (PAR). The fracture surface of a PAR interleaved specimen is shown in

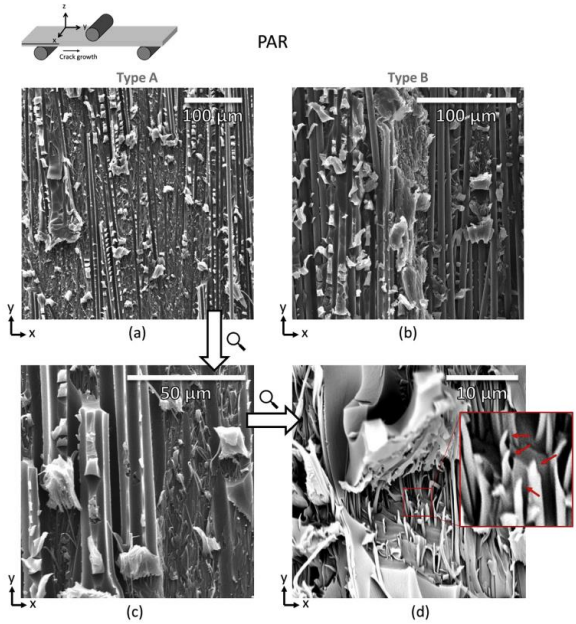

Fig. 8. SEM images of the fracture surface showing an overview of the Type A (a) and Type B (b) failure regions in a PAR interleaved specimen. Close-up images of the Type A regions show nanofibre bridging zones developed during hackle formation (c–d). The insert shows the plastically deformed and necked PA 6.9 nanofibres protruding from the epoxy matrix.

Fig. 8. An overview of the Type A and Type B failure regions are given in Fig. 8a and Fig. 8b respectively. Although nanofibres were present in both failure regions, severe nanofibre bridging and deformed nanofibres were mainly visible in the Type A failure regions, see Fig. 8c and Fig. 8d. The nanofibres bridge (micro)cracks in the specimen and eventually fail by plastic deformation (necking). Since the nanofibres are oriented parallel to the Type B failure plane (yz-plane), the crack can advance parallel to the nanofibres in Type B regions without having to go through the nanofibres themselves. Hence, only a very limited amount of nanofibre bridging was observed in these regions.

In Type A failure regions, nanofibre bridging can develop during hackle formation since hackles are initiated by small tensile cracks in the interlaminar matrix resin at 45° relative to the macroscopic delamination plane. These microcracks go through the nanofibres and cause severe nanofibre bridging, see Fig. 8d. Nevertheless, it only results in the bridging of nanofibres which are near the surface of the nanofibrous veil, and, the total amount of bridging nanofibres is relatively low. Since the amount of bridging nanofibres is relatively low in both Type A as well as Type B failure regions, the induced toughening effect will also be relatively low. This is in agreement with the Mode II IFT results in Section 3.1.

3.2.2.3. Nanofibres oriented transversely to the crack propagation (TRANS). The fracture surface of a TRANS interleaved specimen is shown in Fig. 9. As opposed to PAR interleaved laminates, plastically deformed nanofibres are mainly located at the interlaminar crossings in the Type B failure regions, see Fig. 9c and Fig. 9d, while almost no bridging nanofibres are observed at the Type A failure regions. Since the nanofibres are oriented perpendicular to the crack growth direction, hackle formation can occur in Type A regions without causing nanofibre bridging as the crack can advance parallel with the nanofibres. Similarly, severe nanofibre bridging occurs at the interlaminar crossings in Type B regions as the crack has to go through the nanofibres.

The interlaminar crossings have very distinct features with a preferred orientation of the interlaminar fracture surface at 45° relative to the crack growth direction in the xy-plane. Fig. 9c and Fig. 9d show a detailed image of the interlaminar fracture surface in the Type B failure regions. The extent of necking on the nanofibres is less visible than in PAR interleaved specimens as the nanofibres are not protruding as much from the fracture surface. Furthermore, the protruding ends are somewhat bent and parallel to the fracture surface indicating that both sides of the fracture surface have sheared past each other. Since the nanofibres are transversely

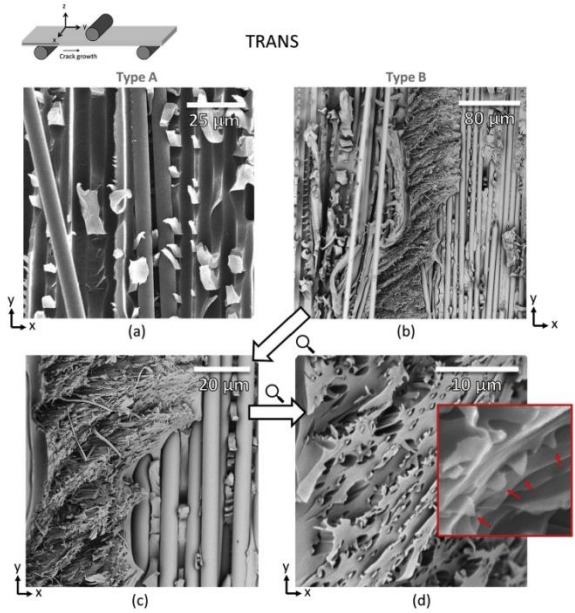

Fig. 9. SEM images of the fracture surface showing Type A failure (a) and Type B failure (b) in a TRANS interleaved specimen. Nanofibre bridging is mainly observed in Type B failure regions. Close-up images of the interlaminar crossings show the characteristic orientation of the interlaminar crossings at 45° relative to the crack propagation direction in the xy-plane (c–d). The insert shows necked PA 6.9 nanofibres protruding from the fracture surface in a Type B failure region.

oriented to the crack growth direction, each interlaminar crossing results in the failure of almost all the nanofibres which are present in the modified interlayer. Hence, the effectiveness of these nanofibre bridging zones is relatively high compared to PAR interleaved laminates resulting in the higher observed Mode II IFT in Section 3.1.

It is interesting to note that the fracture behaviour of TRANS interleaved laminates is opposite to that of PAR interleaved laminates – nanofibre bridging zones develop mainly in the Type B failure regions for TRANS interleaved laminates and not in the Type A failure regions as opposed to PAR interleaved laminates where they develop mainly in the Type A failure regions and not at the interlaminar crossings in Type B regions – only due to the difference in orientation between the fracture surface in Type A and Type B regions.

3.2.2.4. Nanofibres oriented randomly (RNDM). The fracture surface of a RNDM interleaved laminate is shown in Fig. 10. It can be seen that both nanofibre bridging zones characteristic to PAR and TRANS interleaved laminates are present: nanofibre bridging zones develop during hackle formation in Type A failure regions and at the interlaminar crossings in Type B failure regions. This indicates that each failure mode requires a certain orientation distribution of the nanofibres. Nanofibre bridging zones develop during hackle formation when the nanofibres are oriented more or less parallel to the crack growth direction. Similarly, they develop at interlaminar crossings when the nanofibres are oriented more or less perpendicular to the crack growth direction. Hence, a random distribution of nanofibres results in the initiation of both toughening mechanisms.

Since both nanofibre bridging zones develop independently of each other in different failure regions, their effect in a RNDM interleaved laminate can be seen as a superposition of both mechanisms, each resulting in an increased IFT. The amount of energy related to each mechanism can be obtained from the results of the ENF experiments in Section 3.1. The PAR and TRANS interleaved specimens resulted in an increase in $G_{IIc,ini}$ of approximately 1000 J/m^2 and 1500 J/m^2 respectively, compared to the virgin laminates. Hence, for RNDM interleaved laminates where both mechanisms of nanofibre bridging are present, the increase in $G_{IIc,ini}$ can be approximated as the sum of 1000 J/m^2 and 1500 J/m^2. However, this is an overestimation due to the random orientation distribution of the nanofibres: only a certain fraction of nanofibres will develop nanofibre bridging zones as their effectiveness is dependent on their orientation. This is in agreement with the results obtained in Section 3.1: RNDM interleaved laminates showed

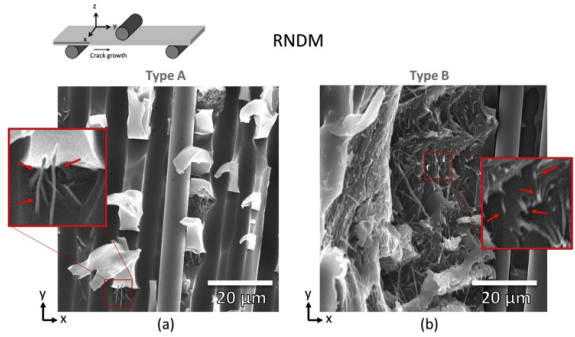

Fig. 10. The fracture surface of specimens interleaved with a random deposition of nanofibres shows both failure modes characteristic to parallel (a) and transversely (b) oriented nanofibres. Nanofibre bridging and necked nanofibres can be observed at hackles and at interlaminar crossings.

the highest increase in Mode II IFT resulting in an increase in $G_{IIc,ini}$ compared to the virgin laminates of approximately 2000 J/m^2.

3.3. Non-precracked VS precracked ENF specimens

As stated in Section 2.1.3, a natural Mode II precrack was produced in the specimens prior to testing by loading a non-precracked (NPC) specimen to crack initiation. The load–displacement data during precracking is used to determine the non-precracked Mode II IFT. Afterwards, the exact length of the precrack was determined by a compliance calibration procedure and the specimen was loaded again, resulting in a precracked (PC) Mode II IFT value. In general, the non-precracked Mode II IFT is slightly higher due to initiation film effects [27]. However, a relatively large difference between NPC- and PC-values was obtained for the PAR interleaved laminates, see Fig. 11. In interleaved specimens, the Type B failure regions initiate a small distance away from the initiation film, see Fig. 6b. Hence, these interlaminar crossings still need to be initiated in non-precracked specimens, but not in precracked specimens. Furthermore, the Type B failure regions seem to initiate parallel to the crack front (x-direction) after which they propagate parallel to the crack growth direction (y-direction). Since the nanofibres in PAR interleaved specimens are parallel to the crack growth direction, the initiation of the interlaminar crossings is perpendicular to the nanofibre direction which leads to a relatively large amount of bridging nanofibres. Hence, this results in non-precracked Mode II IFT values that are significantly higher than those for precracked specimens.

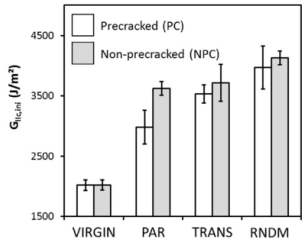

Fig. 11. Precracking ENF specimens results in a significant difference between $G_{IIc,ini}$(NPC) and $G_{IIc,ini}$(PC) for PAR interleaved laminates since interlaminar crossings still need to be initiated in non-precracked specimens and are initiated perpendicular to the nanofibre direction.

4. Conclusions

PA 6.9 nanofibrous veils with different morphologies were successfully interleaved in UD carbon/epoxy laminates and resulted in an increase of the Mode II IFT. A strong effect of nanofibrous veil morphology on the toughening mechanisms was observed. Two distinct failure regions were observed in interleaved laminates: intralaminar failure (Type A) and interlaminar crossings (Type B).

The main toughening mechanism in laminates interleaved with aligned nanofibres oriented parallel to the crack growth direction is the development of nanofibre bridging zones during hackle formation in Type A failure regions. On the other hand, laminates interleaved with aligned nanofibres oriented transversely to the crack growth direction show that nanofibre bridging zones developed mainly at the interlaminar crossings in Type B failure regions. Furthermore, the toughening effectiveness of the transversely oriented nanofibres is higher, since a larger amount of nanofibres are able to bridge cracks. Laminates interleaved with a random deposition of nanofibres resulted in the largest increase in Mode II IFT. Due to their random orientation, both mechanisms of nanofibre bridging were present on the fracture surface of these specimens in Type A as well as in Type B failure regions. The Mode II initiation IFT increased from 2000 J/m^2 for the virgin laminates up to 4000 J/m^2 for a random deposition of PA 6.9 nanofibres. The effectiveness of random deposition is advantageous for applications since it is usually unknown prior to failure in which direction delaminations will grow. Furthermore, randomly oriented nanofibres are automatically produced in the electrospinning process and do not require a dedicated collector as compared to aligned nanofibres.

Acknowledgements

Financial support from the Agency for Innovation by Science and Technology, Flanders is gratefully acknowledged. Results in this paper were obtained within the framework of the IWT Strategic Basic Research Grant 141344.

References

[1] T.K. Tsotsis, Interlayer toughening of composite materials, Polym. Compos. 30 (2009) 70–86, http://dx.doi.org/10.1002/pc.20535.
[2] M. Hojo, T. Ando, M. Tanaka, T. Adachi, S. Ochiai, Y. Endo, Modes I and II interlaminar fracture toughness and fatigue delamination of CF/epoxy laminates with self-same epoxy interleaf, Int. J. Fatigue 28 (2006) 1154–1165, http://dx.doi.org/10.1016/j.ijfatigue.2006.02.004.
[3] N. Sela, O. Ishai, Interlaminar fracture toughness and toughening of laminated composite materials: a review, Composites 20 (1989) 423–435, http://dx.doi.org/10.1016/0010-4361(89)90211-5.
[4] L. Daelemans, S. van der Heijden, I. De Baere, H. Rahier, W. Van Paepegem, K. De Clerck, Nanofibre bridging as a toughening mechanism in carbon/epoxy composite laminates interleaved with electrospun polyamide nanofibrous veils, Compos. Sci. Technol. 117 (2015) 244–256, http://dx.doi.org/10.1016/j.compscitech.2015.06.021.
[5] P. Akangah, S. Lingaiah, K. Shivakumar, Effect of Nylon-66 nano-fiber interleaving on impact damage resistance of epoxy/carbon fiber composite laminates, Compos. Struct. 92 (2010) 1432–1439, http://dx.doi.org/10.1016/j.compstruct.2009.11.009.
[6] G.W. Beckermann, K.L. Pickering, Mode I Mode II interlaminar fracture toughness of composite laminates interleaved with electrospun nanofibre veils, Compos. Part A Appl. Sci. Manuf. 72 (2015) 11–21, http://dx.doi.org/10.1016/j.compositesa.2015.01.028.
[7] K. Bilge, E. Ozden-Yenigun, E. Simsek, Y.Z. Menceloglu, M. Papila, Structural composites hybridized with epoxy compatible polymer/MWCNT nanofibrous interlayers, Compos. Sci. Technol. 72 (2012) 1639–1645, http://dx.doi.org/10.1016/j.compscitech.2012.07.005.
[8] Q. Chen, L. Zhang, Y. Zhao, X.-F. Wu, H. Fong, Hybrid multi-scale composites developed from glass microfiber fabrics and nano-epoxy resins containing electrospun glass nanofibers, Compos. Part B Eng. 43 (2012) 309–316, http://dx.doi.org/10.1016/j.compositesb.2011.08.044.
[9] S. Hamer, H. Leibovich, A. Green, R. Intrater, R. Avrahami, E. Zussman, et al., Mode I interlaminar fracture toughness of Nylon 66 nanofibrilmat interleaved carbon/epoxy laminates, Polym. Compos. 32 (2011) 1781–1789, http://dx.doi.org/10.1002/pc.21210.
[10] J. Kim, D.H. Reneker, Mechanical properties of composites using ultrafine electrospun fibers, Polym. Compos. 20 (1999) 124–131, http://dx.doi.org/10.1002/pc.10340.
[11] G. Li, P. Li, C. Zhang, Y. Yu, H. Liu, S. Zhang, et al., Inhomogeneous toughening of carbon fiber/epoxy composite using electrospun polysulfone nanofibrous membranes by in situ phase separation, Compos. Sci. Technol. 68 (2008) 987–994, http://dx.doi.org/10.1016/j.compscitech.2007.07.010.
[12] S. Lin, Q. Cai, J. Ji, G. Sui, Y. Yu, X. Yang, et al., Electrospun nanofiber reinforced and toughened composites through in situ nano-interface formation, Compos. Sci. Technol. 68 (2008) 3322–3329, http://dx.doi.org/10.1016/j.compscitech.2008.08.033.
[13] K. Magniez, T. Chaffraix, B. Fox, Toughening of a carbon-fibre composite using electrospun poly(hydroxyether of bisphenol A) nanofibrous membranes through inverse phase separation and inter-domain etherification, Materials 4 (2011) 1967–1984, http://dx.doi.org/10.3390/ma4111967.
[14] H. Saghafi, A. Zucchelli, R. Palazzetti, G. Minak, The effect of interleaved composite nanofibrous mats on delamination behavior of polymeric composite materials, Compos. Struct. 109 (2014) 41–47, http://dx.doi.org/10.1016/j.compstruct.2013.10.039.
[15] S. van der Heijden, L. Daelemans, B. De Schoenmaker, I. De Baere, H. Rahier, W. Van Paepegem, et al., Interlaminar toughening of resin transfer moulded glass fibre epoxy laminates by polycaprolactone electrospun nanofibres, Compos. Sci. Technol. 104 (2014) 66–73, http://dx.doi.org/10.1016/j.compscitech.2014.09.005.
[16] J. Zhang, T. Lin, X. Wang, Electrospun nanofibre toughened carbon/epoxy composites: effects of polyetherketone cardo (PEK-C) nanofibre diameter and interlayer thickness, Compos. Sci. Technol. 70 (2010) 1660–1666, http://dx.doi.org/10.1016/j.compscitech.2010.06.019.
[17] S. Hamer, H. Leibovich, A. Green, R. Avrahami, E. Zussman, A. Siegmann, et al., Mode I and Mode II fracture energy of MWCNT reinforced nanofibrilmats interleaved carbon/epoxy laminates, Compos. Sci. Technol. 90 (2014) 48–56, http://dx.doi.org/10.1016/j.compscitech.2013.10.013.
[18] K. Magniez, C. De Lavigne, B.L. Fox, The effects of molecular weight and polymorphism on the fracture and thermo-mechanical properties of a carbon-fibre composite modified by electrospun poly (vinylidene fluoride) membranes, Polymer 51 (2010) 2585–2596, http://dx.doi.org/10.1016/j.polymer.2010.04.021.
[19] R. Palazzetti, A. Zucchelli, C. Gualandi, M.L. Focarete, L. Donati, G. Minak, et al., Influence of electrospun Nylon 6,6 nanofibrous mats on the interlaminar properties of Gr–epoxy composite laminates, Compos. Struct. 94 (2012) 571–579, http://dx.doi.org/10.1016/j.compstruct.2011.08.019.
[20] J. Zhang, T. Yang, T. Lin, C.H. Wang, Phase morphology of nanofibre interlayers: critical factor for toughening carbon/epoxy composites, Compos. Sci. Technol. 72 (2012) 256–262, http://dx.doi.org/10.1016/j.compscitech.2011.11.010.
[21] K. Bilge, S. Venkataraman, Y.Z. Menceloglu, M. Papila, Global and local nanofibrous interlayer toughened composites for higher in-plane strength, Compos. Part A Appl. Sci. Manuf. 58 (2014) 73–76, http://dx.doi.org/10.1016/j.compositesa.2013.12.001.
[22] I. Chou, T. Inutake, K. Namba, Correlation of damage resistance under low velocity impact and Mode II delamination resistance in CFRP laminates, Adv. Compos. Mater. 8 (1999) 167–176, http://dx.doi.org/10.1163/156855199X00173.
[23] D. Li, Y. Xia, Electrospinning of nanofibers: reinventing the wheel? Adv. Mater. 16 (2004) 1151–1170, http://dx.doi.org/10.1002/adma.200400719.
[24] Z. Sun, J.M. Deitzel, J. Knopf, X. Chen, J.W. Gillespie, The effect of solvent dielectric properties on the collection of oriented electrospun fibers, J. Appl. Polym. Sci. 125 (2012) 2585–2594, http://dx.doi.org/10.1002/app.35454.
[25] W.E. Teo, S. Ramakrishna, A review on electrospinning design and nanofibre assemblies, Nanotechnology 17 (2006) R89–R106, http://dx.doi.org/10.1088/0957-4484/17/14/R01.
[26] B. De Schoenmaker, A. Goethals, L. Van der Schueren, H. Rahier, K. De Clerck, Polyamide 6.9 nanofibres electrospun under steady state conditions from a solvent/non-solvent solution, J. Mater. Sci. 47 (2012) 4118–4126, http://dx.doi.org/10.1007/s10853-012-6266-9.
[27] ASTM Standard D7905-14, Standard Test Method for Determination of the Mode II Interlaminar Fracture Toughness of Unidirectional Fiber-Reinforced Polymer Matrix Composites, ASTM International, 2014, http://dx.doi.org/10.1520/D7905_D7905M-14.
[28] I. De Baere, S. Jacques, W. Van Paepegem, J. Degrieck, Study of the Mode I and Mode II interlaminar behaviour of a carbon fabric reinforced thermoplastic, Polym. Test. 31 (2012) 322–332, http://dx.doi.org/10.1016/j.polymertesting.2011.12.009.
[29] A. Arrese, N. Carbajal, G. Vargas, F. Mujika, A new method for determining mode II R-curve by the End-Notched Flexure test, Eng. Fract. Mech. 77 (2010) 51–70, http://dx.doi.org/10.1016/j.engfracmech.2009.09.008.
[30] S. Matsuda, M. Hojo, S. Ochiai, Mesoscopic fracture mechanism of mode ii delamination fatigue crack propagation in interlayer-toughened CFRP, JSME Int. J. Ser. A 40 (1997) 423–429, http://dx.doi.org/10.1299/jsmea.40.423.
[31] B.R.K. Blackman, A.J. Kinloch, M. Paraschi, The determination of the mode II adhesive fracture resistance, GIIC, of structural adhesive joints: an effective crack length approach, Eng. Fract. Mech. 72 (2005) 877–897, http://dx.doi.org/10.1016/j.engfracmech.2004.08.007.
[32] S. Sridharan, Delamination Behaviour of Composites, first ed., Woodhead Publishing, 2008.
[33] Z.C. Xia, J.W. Hutchinson, Mode II fracture toughness of a brittle adhesive layer, Int. J. Solids Struct. 31 (1994) 1133–1148, http://dx.doi.org/10.1016/0020-7683(94)90168-6.

PAPER V

IMPROVED FATIGUE DELAMINATION BEHAVIOUR OF COMPOSITE LAMINATES WITH ELECTROSPUN THERMOPLASTIC NANOFIBROUS INTERLEAVES USING THE CENTRAL CUT-PLY METHOD

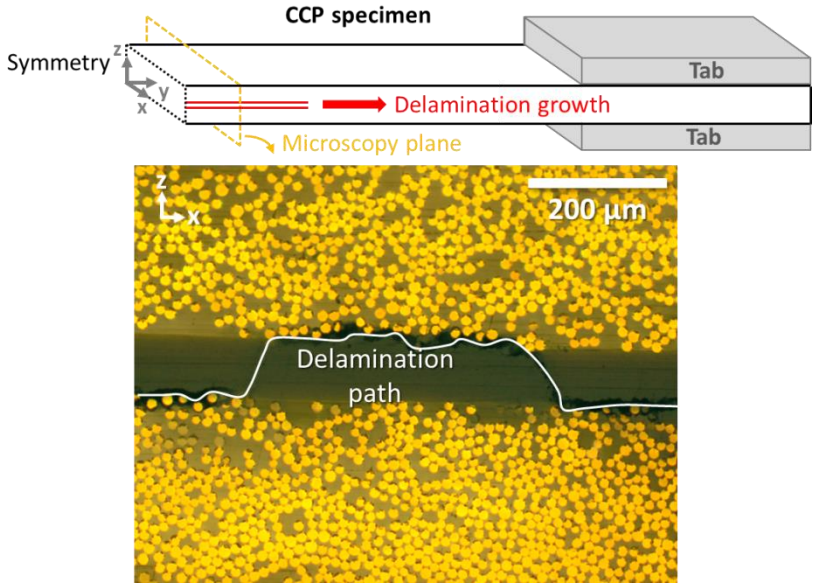

Lode Daelemans, Sam van der Heijden, Ives De Baere, Hubert Rahier, Wim Van Paepegem and Karen De Clerck

(2016) *COMPOSITES : PART A : APPLIED SCIENCE AND MANUFACTURING*. 94. p.1-31

Composites: Part A 94 (2017) 10–20

Contents lists available at ScienceDirect

Composites: Part A

journal homepage: www.elsevier.com/locate/compositesa

Improved fatigue delamination behaviour of composite laminates with electrospun thermoplastic nanofibrous interleaves using the Central Cut-Ply method

Lode Daelemans [a], Sam van der Heijden [a], Ives De Baere [b], Hubert Rahier [c], Wim Van Paepegem [b], Karen De Clerck [a,*]

[a] Department of Textiles, Ghent University, Technologiepark-Zwijnaarde 907, B-9052 Zwijnaarde, Belgium
[b] Department of Materials Science and Engineering, Ghent University, Technologiepark-Zwijnaarde 903, B-9052 Zwijnaarde, Belgium
[c] Department Materials and Chemistry, Vrije Universiteit Brussel, Pleinlaan 2, B-1050 Brussels, Belgium

ARTICLE INFO

Article history:
Received 20 May 2016
Received in revised form 29 November 2016
Accepted 2 December 2016
Available online 5 December 2016

Keywords:
A. Nanocomposites
B. Damage tolerance
B. Fatigue
E. Electrospinning

ABSTRACT

Adding toughening particles to composite laminates is a common approach to increase their delamination resistance. More recently, interleaving the laminated structures with electrospun (thermoplastic) nanofibrous veils is shown to be a viable toughening method. Where toughening composite laminates with nanofibrous interleaves becomes more and more evident under static conditions, the effectiveness under fatigue loadings has yet to be proven. This article provides insight in the nanofibre toughening mechanisms acting under fatigue conditions. Several nanofibre types with a high potential for toughening are considered. A substantial decrease of the delamination propagation rate up to one order of magnitude was obtained for all tested nanofibre types. Furthermore, two distinct zones of delamination behaviour are observed in nanofibre interleaved laminates on exposure to cyclic loading. These insights reveal the crucial design parameters which allow for the production of nanofibre toughened composites with an improved fatigue life.

1. Introduction

The relatively low delamination resistance of most composite laminates remains one of the limiting factors during their in-service life. Increasing the delamination resistance of these materials results in higher damage resistance and improved performance and lifetime. Hence, many methods of interlaminar toughening have been proposed and researched over the past decades [1–12]. The more recent principle of interleaving composite laminates with electrospun nanofibrous veils has shown to be a viable interlaminar toughening method [13–20]. There are several advantages associated to these veils which adds to their commercial applicability. During electrospinning, nanofibrous veils are formed as a self-supporting non-woven membrane which can be handled in a similar way as regular fabrics. They can also be deposited directly on fabrics by guiding dry fabric through an electrospinning set-up [20]. Hence, the veils can easily be placed in between the primary reinforcing plies either as standalone membranes or as nanofibre deposited fabrics prior to composite production and there is no change in the composite manufacturing process required. The nanoscale diameter of the nanofibres offers relatively thin interlayers, while their macroscopic length (continuous fibres) poses no health hazards in comparison with other nanomaterials. The electrospinning process itself is relatively simple in design and proven to be upscalable [22,23] making it a cost-effective nanofibre production method. Furthermore, the electrospinning process used to obtain nanofibrous veils is applicable to many polymer types adding to its versatility [21].

Notwithstanding the numerous expected benefits, the research into composite laminates toughened by electrospun nanofibrous interleaves is still limited. It consists mainly of Mode I and Mode II interlaminar fracture tests performed on interleaved laminates under static conditions [14,20,24–30]. Although these experiments provide useful information about critical parameters, toughening (micro)mechanisms and general concerns of the delamination behaviour in nanofibre interleaved laminates under static conditions, an analysis of the effect of nanofibrous interleaves under fatigue loadings has not been reported in literature to date. Nevertheless, a thorough understanding of the fatigue delamina-

* Corresponding author.
E-mail address: Karen.DeClerck@UGent.be (K. De Clerck).

http://dx.doi.org/10.1016/j.compositesa.2016.12.004
1359-835X/

tion behaviour of interleaved laminates is of major concern since almost all composite laminate structures experience fatigue loading during their in-service life. Furthermore, it is known that the delamination behaviour in (toughened) composite laminates can differ substantially between static and fatigue loading [31–33].

This article gives thorough insight into the fatigue delamination behaviour of electrospun nanofibre interleaved composite laminates. Nanofibrous veils are electrospun from polycaprolactone (PCL), polyamide 6 (PA 6) and polyamide 6.9 (PA 6.9) since these systems have proven their effectiveness under static loading conditions [14,20,27]. The focus is on Mode II delamination behaviour as delamination growth during service often occurs under Mode II dominated loadings. The Central Cut-Ply (CCP) method [34] is used to determine the crack propagation rate under cyclic loading as this method is representative for delamination initiation encountered in structural applications, where, for example, delaminations initiate from terminated plies, near free edges or in tapered sections. The observed toughening micromechanisms are linked to the results obtained from static experiments, thus providing the necessary insights in order to design novel fatigue resistant structures.

2. Materials and methods

2.1. Materials

PCL (M_N 80 000) and PA 6 (M_W 51,000 g/mol) pellets were purchased from Sigma-Aldrich; PA 6.9 pellets (M_W 58,000 g/mol) were obtained from Scientific Polymer Products. The polymers are dissolved for electrospinning in a mixture of 98–100% purity formic acid (FA) and 98% purity acetic acid (AA), both purchased from Sigma-Aldrich and used as received. Uniform electrospun nanofibrous veils are produced on an in-house developed multinozzle electrospinning machine; more details can be found in Ref. [27]. Standalone nanofibrous veils are produced with an areal density in the range of 14 ± 0.5 g/m^2. The PCL, PA 6 and PA 6.9 nanofibres had diameters of 650 ± 150 nm, 195 ± 35 nm and 250 ± 30 nm respectively as measured from SEM images (Fig. 1a–c).

2.2. Methods

The Central Cut-Ply (CCP) method is used to determine the crack propagation rate under cyclic loading [34]. This method has several advantages compared to the traditional End Notched Flexure (ENF) specimen design such as the use of a simple grip fixture and easy in-situ crack growth monitoring using a clip-on extensometer. Delamination growth in the CCP specimen design initiates from (artificially) interrupted plies instead of an initiation film. Hence, it is much more representative for the type of delamination initiation encountered in structural applications where delaminations initiate for example from terminated plies, near free edges or in tapered sections. The CCP specimen consists of a unidirectional laminated specimen in which a certain number of plies is artificially interrupted symmetrically with respect to the laminate midplane, see Fig. 2. When subjected to a far field axial tensile load, four delaminations will grow under Mode II conditions as interlaminar compression prevents Mode I opening of the delaminations [34].

The Mode II energy release rate (ERR) G_{II} associated with a single delamination can be determined using beam theory as [34]

$$G_{II} = \frac{P^2}{4EB^2t}\left(\frac{\chi}{1-\chi}\right) \tag{1}$$

with load P, Young's modulus of the unidirectional material without cut plies E, specimen width B, specimen thickness t and the ratio of cut plies to the total number of plies in the specimen χ [34]. Eq. (1) shows that the Mode II ERR is independent of delamination length and thus remains constant during fatigue tests at constant maximum load. The delamination growth during the fatigue tests is monitored using a clip-on extensometer which is placed in the middle of the specimen. Furthermore, a video camera is used to monitor the delamination length visually and validate the extensometer measurements. Let ε^* be the strain corresponding to the peak load P^* in each loading cycle during the fatigue tests, the delamination length of a single delamination can then be expressed as [34]

$$a = \frac{1-\chi}{\chi} L\left(\frac{EBt}{P^*}\varepsilon^* - 1\right) \tag{2}$$

Differentiation of Eq. (2) results in an expression for the delamination propagation rate which is determined by the slope of the extensometer peak strain measurements during the fatigue tests [34]

$$\frac{da}{dN} = \frac{1-\chi}{\chi} L\left(\frac{E}{P^*}\right)\frac{d\varepsilon^*}{dN} \tag{3}$$

A more detailed derivation and validation of these equations for the CCP method can be found in Ref. [34].

Composite laminates are produced by vacuum assisted resin transfer moulding (VARTM) with unidirectional E-glass plies with an areal density of 500 g/m^2 (UDO ES500 manufactured by SGL group) and a high toughness epoxy/amine thermoset resin system (EPIKOTE MGS RIMR135 and EPIKURE MGS RIMH137 supplied by Momentive) typically used for wind turbine blades. More details on the used VARTM process can be found in Ref. [35]. A total amount of 8 plies is used with the two middle plies cut prior to stacking. Special care was taken to produce a straight cut along the whole ply in order to have a sharply defined cut region in the final laminate. The standalone nanofibrous veils, which have the same size as a reinforcing ply (300 × 300 mm^2), are interleaved in the two interlaminar regions where delamination growth will occur (Fig. 1d). The manufacturer's recommended curing cycle is used to cure the laminates (24 h at room temperature followed by a post-cure for 15 h at 80 °C). The nominal thickness of the final laminates is 3 mm. The glass fibre volume fraction (52 vol%) did not change when nanofibrous veils were interleaved as a two-piece mould with a fixed thickness was used to produce the laminates. Furthermore, the nanofibres had no measurable influence on the infusion process and the final quality of the laminates. The infusion resin could easily impregnate the nanofibrous veils in the interlayers. Visual inspection and microscopic images of the interlayers showed no dry spots in the final laminates (transparent epoxy resin) indicating that the porosity did not increase.

Six different laminated plates were produced: two non-interleaved (virgin), two PA 6.9 interleaved, one PA 6 interleaved and one PCL interleaved laminated plate. To validate the CCP results, the same nanofibrous veils were also used to produce composite laminated plates with an initiation film and nanofibrous veil in the midplane for ENF experiments. The CCP and ENF specimens were cut from the respective laminates with a water-cooled diamond cutting machine to nominal dimensions of 140 × 15 mm^2 and 140 × 20 mm^2 respectively. The edges of the specimens were polished in order to remove any edge defects introduced by the cutting machine.

The CCP specimens were tested on an Instron 8801 servo-hydraulic machine equipped with an Instron Dynacell load cell of 100 kN both under static and fatigue loading conditions. Hydraulic wedge grips were used to fix the specimens and the alignment was assured using an Instron alignment kit. An Instron clip-on dynamic extensometer with 25 mm gauge length was used to monitor delamination growth during fatigue tests and mounted centrally

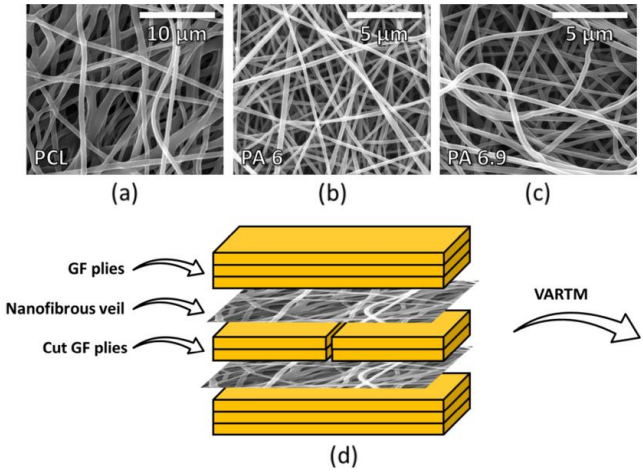

Fig. 1. SEM images of electrospun PCL (a), PA 6 (b) and PA 6.9 (c) nanofibres. The nanofibrous veils are subsequently interleaved at the delamination interfaces near the Cut-Ply region (d). (For interpretation of the references to colour in this figure legend, the reader is referred to the web version of this article.)

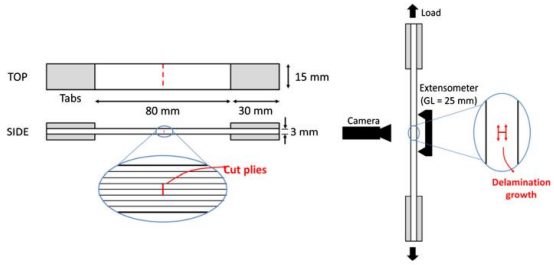

Fig. 2. Central Cut-Ply specimen design. Four delaminations emanate under Mode II loading conditions from the interrupted plies due to far field axial tensile loading. The delamination growth is monitored in-situ by an extensometer and a videocamera. (For interpretation of the references to colour in this figure legend, the reader is referred to the web version of this article.)

on the specimen. Tension-tension fatigue loading was applied at a stress ratio R of 0.1 and test frequency of 5 Hz (load-controlled). Depending on the desired load level, the maximum fatigue stress was adjusted between 260 MPa and 620 MPa. Self-heating of the specimens was monitored using a FLIR T420 infrared camera and was found to be acceptable (maximum heating up to 30 °C at the highest load levels). The equations given in Section 2 were used to analyse the data from the experiments. A Young's modulus of 42 GPa was used in Eqs. (1)–(3) as measured on unidirectional samples without cut plies. Quasi-static delamination tests were also performed using the same set-up with a displacement-controlled movement of the grips of 2 mm/min. The first significant drop in load represents the point of major delamination and its value is used to determine the static Mode II interlaminar fracture toughness $G_{IIc,CCP}$ obtained by the CCP method.

The ENF specimens were statically tested on an Instron 3369 electromechanical machine using a load cell of 2 kN. The Beam Theory including Bending Rotations (BTBR) described in Ref. [36] was used to determine $G_{IIc,ENF}$. This method is similar to the Compliance Based Beam Method (CBBM) used in previous work [14,27], but corrects for large displacements. The loading roller was displaced at a speed of 1 mm/min. The span length was 100 mm and the ratio of initial delamination length to half-span length was 0.7 in order to have stable delamination growth.

3. Results and discussion

3.1. Applicability and validation of the CCP method

3.1.1. Applicability to nanofibre interleaved composite laminates

Static CCP tests were performed in order to check if the increase in G_{IIc} for nanofibre interleaved laminates is not dependent on the testing method and is comparable to the results obtained in the more commonly used ENF method, i.e. $G_{IIc,CCP}$ should be similar to $G_{IIc,ENF}$. Cui et al. [37] showed that through the thickness normal compressive stress is present at the crack tips in CCP specimens. Such compressive stresses are known to increase the measured Mode II interlaminar fracture toughness [38–40]. In order to account for this effect, Cui et al. [37] proposed following correction for a glass fibre/epoxy CCP specimen with a ratio of 2/8 cut plies:

$$G'_{IIc,CCP} = \frac{G_{IIc,CCP}}{1 + 0.008 \times 37.72 \times 10^{-3}\sigma_c} \quad (4)$$

in which σ_c is the experimentally determined nominal failure stress of the CCP specimen. For the CCP specimens reported in this work, correcting for the interlaminar compressive stress yielded values about 20% lower than directly computed from Eq. (1). The results show good agreement between the G_{IIc} values obtained in both tests as shown in Fig. 3. The most notable difference between $G_{IIc,CCP}$ and $G_{IIc,ENF}$ is noted for the virgin laminates with a difference of approximately 15%. This is in agreement with the difference between both methods reported by other researchers and is probably related to the simple beam theory used to derive Eq. (1) [34]. Furthermore, the load-displacement curves of CCP specimens show a more pronounced stick-slip crack growth (sudden drops in load upon crack extension) compared to the stable crack growth obtained in the ENF tests. This indicates some stress build-up at the crack tip in CCP specimens, which might be due to local through thickness compressive stresses causing a local enhancement in G_{IIc}, resulting in an overestimation of G_{IIc}.

Although the Mode II interlaminar fracture toughness of the virgin laminates is already relatively high, the nanofibrous interleaves result in a significant improvement up to a toughness of approximately 3000 J/m² which is in the range of thermoplastic composites [41]. Previous research by the authors has shown that this increase is due to the development of so-called nanofibre bridging zones which occur when the delamination path crosses the toughened interlaminar region [27]. Microscopic images of tested CCP specimens show the same delamination crack path behaviour as observed in ENF specimens: regular crossings of the interlaminar region in which nanofibre bridging zones can develop (Fig. 4).

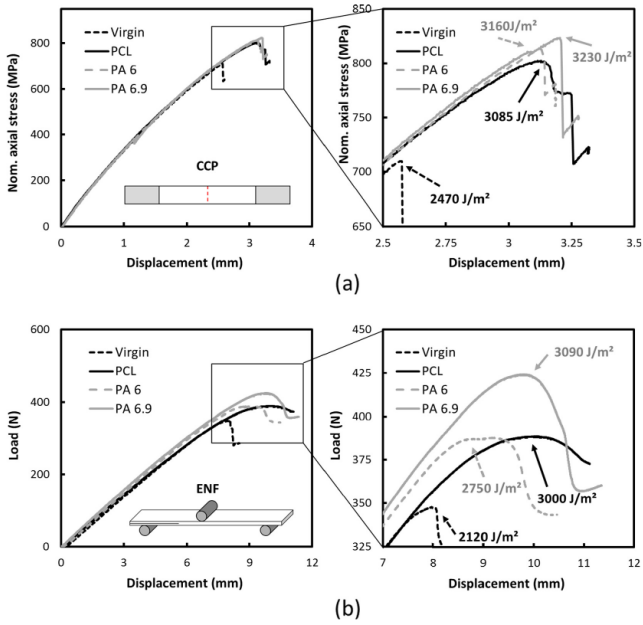

Fig. 3. Nominal axial stress versus displacement curves for representative CCP specimens show that G_{IIc} increases upon interleaving the laminates with nanofibrous veils (a). Similar results are obtained using the standard ENF method (b) which indicates that the applicability of the CCP method to determine the G_{IIc} of nanofibre interleaved laminates is good. (For interpretation of the references to colour in this figure legend, the reader is referred to the web version of this article.)

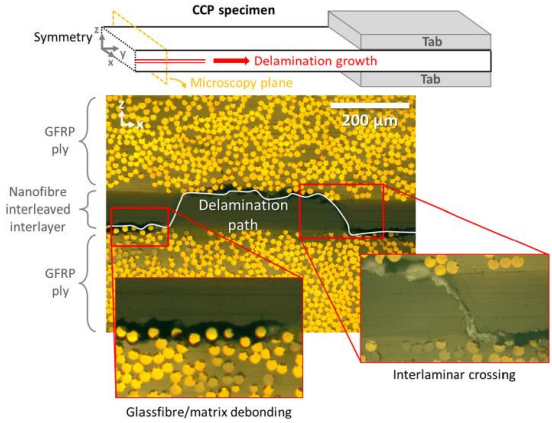

Fig. 4. The delamination path in an interleaved CCP specimen shows interlaminar crossings through the nanofibre modified interlayer. Nanofibre bridging zones mainly develop in these crossings resulting in an improved toughness. (For interpretation of the references to colour in this figure legend, the reader is referred to the web version of this article.)

These crossings are important as they are suggested to be the main cause of an increased interlaminar fracture toughness [42]. In the region between the crossings, delamination progresses at the reinforcing fibre/matrix interface (Fig. 4), similar to non-interleaved (untoughened) laminates, and as such is less affected by the electrospun nanofibres. Hence, the same nanofibre bridging toughening mechanism occurs both in CCP and ENF specimens. Furthermore, delamination initiation in a CCP specimen is more "natural" as it does not require an initiation film, and is thus more closely related to the type of initiation that can be expected in composite applications. This is advantageous for testing nanofibre interleaved laminates since we have previously shown that the relative position of the initiation film and the nanofibrous veil can artificially affect the observed interlaminar fracture toughness resulting in IFT values that may not well represent the actual material [27].

3.1.2. Validation of delamination growth measured by extensometer

As shown above, the CCP method is well suited to determine the Mode II interlaminar fracture toughness of nanofibre interleaved laminates. Furthermore, the CCP method allows for an accurate monitoring of the delamination growth during fatigue testing, as needed to determine the fatigue delamination behaviour, from relatively simple extensometer measurements through Eq. (3). Fig. 5 shows the delamination length – as calculated by Eq. (2) from the strain measurements – as a function of the amount of loading cycles for virgin (non-interleaved) laminates at a high and a low value of load severity $G_{IImax}/G_{IIc,virgin}$. The delaminations grow linearly with the amount of loading cycles and the slope of this curve is equal to the delamination growth rate da/dN as defined by Eq. (3). A linear delamination growth behaviour is observed for all virgin specimens, independent of the applied load severity. In addition, a visual observation of the delamination front also enables the calculation of the delamination growth rate by measuring the delamination length after a certain amount of loading cycles. Fig. 6a reveals that the delamination growth rate determined by Eq. (3) agrees well with the growth rate determined from visual observation. Hence, the CCP method provides the means to accurately determine the delamination length in-situ based on relatively simple strain measurements. This is advantageous as the Mode II delamination front is usually difficult to determine visually from the edges of a specimen when the laminates are not translucent [43]. The delamination growth rate of the virgin laminates decreases proportionally to the load ratio and the datapoints fit well to the semi-empirical model proposed by Allegri et al.

$$\frac{da}{dN} = C\left(\frac{G_{IImax}}{G_{IIc,virgin}}\right)^{\frac{b}{1-R^2}} \tag{5}$$

where C and b are empirically derived constants [34], see Fig. 6b. The datapoints in Fig. 6b were fitted to Eq. (5) using a least squares regression algorithm. The model gives a linear dependency between da/dN and $G_{IImax}/G_{IIc,virgin}$ on a double logarithmic scale. Table 1 represents the fitting coefficients and a quantitative measure for the fitting accuracy of Eq. (5) using the coefficient of determination (CoD). The semi-empirical model describes the behaviour of the virgin laminates well with a CoD of 96.4%.

3.2. Analysis of the fatigue behaviour of nanofibre interleaved composites

3.2.1. Delamination growth behaviour

The delamination growth behaviour during the fatigue testing of nanofibre interleaved specimens is found to be different from that of the virgin specimens. A distinct transition in delamination propagation rate was often observed after a few millimetres of delamination growth in the CCP specimens. Initially, the delamination grows relatively slowly for several millimetres at a constant rate after which the delamination growth rate increases to values similar to those of the virgin specimens. This is schematically represented in Fig. 7. Microscopic images of the cross-section of failed

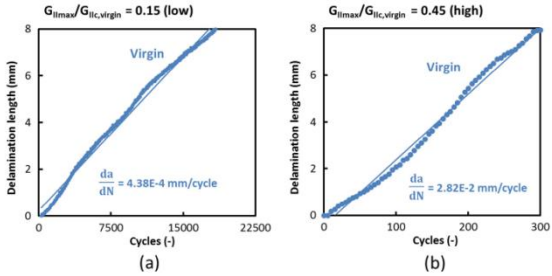

Fig. 5. Delamination length in function of the amount of loading cycles at low (a) and high (b) load severity. The delamination grows linearly with the amount of loading cycles and the slope corresponds to the delamination growth rate. (For interpretation of the references to colour in this figure legend, the reader is referred to the web version of this article.)

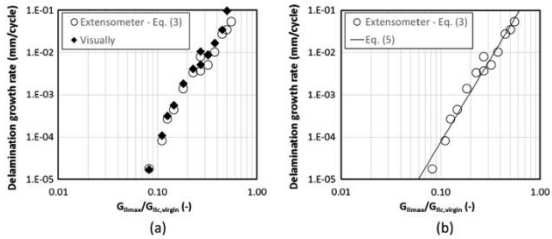

Fig. 6. Delamination growth rate *da*/*dN* in function of the applied load for virgin (non-interleaved) specimens (each point represents an individual specimen). Good agreement is observed between *da*/*dN* determined by strain measurements according to Eq. (3) and *da*/*dN* determined by visual observation of the delamination front (a). The virgin material's fatigue behaviour is well approximated by the semi-empirical model of Eq. (5) (b).

Table 1
Fitting parameters *C* and *b* for Eq. (5) and the resulting fitting accuracy determined by the coefficient of determination (CoD).

Specimen series	C (mm/cycle)	b (–)	CoD (%)
Virgin (non-interleaved)	0.65	3.18	96.9
PA 6.9 interleaved	0.08	2.95	94.1
PA 6 interleaved	0.10	2.68	94.3
PCL interleaved	0.10	3.28	90.3

CCP specimens taken near the initiation region showed the same delamination behaviour as observed in the static experiments, i.e. regular crossings of the nanofibre toughened interlaminar region (Fig. 4). At several millimetres away from the initiation region, some specimens showed almost complete glass fibre/epoxy debonding with none or very few interlaminar crossings. Hence, at these points, the delamination growth rate starts to approach that of the virgin non-interleaved specimens as the amount of interlaminar crossings is minimal. Observation of the fracture surface indicates that the distance between two neighbouring interlaminar crossings can become smaller with increasing delamination growth. Eventually, both crossings combine at a certain point of delamination growth after which the delamination grows by glass fibre/epoxy debonding without crossing the interlayer (Fig. 8). This mechanism of interlaminar crossing suppression causes the distinct delamination behaviour observed in nanofibre interleaved specimens.

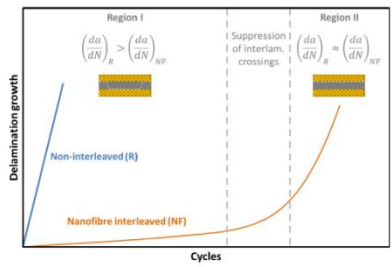

Fig. 7. The delamination growth of nanofibre interleaved CCP specimens exhibits three regions during fatigue testing: (i) relatively constant delamination growth rate smaller than that of the non-interleaved material (Region I), (ii) rapidly increasing delamination growth rate due to suppression of interlaminar crossings (transition zone), and (iii) delamination growth rate similar to that of the non-interleaved material (Region II). (For interpretation of the references to colour in this figure legend, the reader is referred to the web version of this article.)

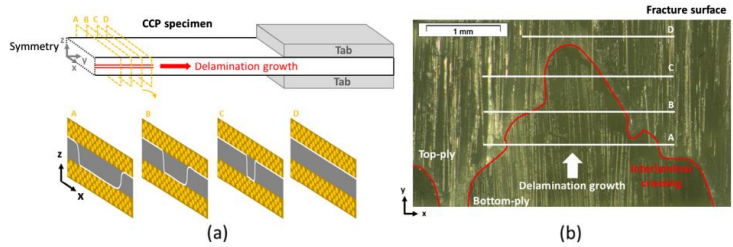

Fig. 8. Interlaminar crossings get suppressed, resulting in complete interfacial debonding without interlaminar crossings after a certain distance of delamination growth. Schematic representation of cross-section views (a). Fracture surface of a failed CCP specimen with two interlaminar crossings that disappear after 2–3 mm of delamination growth (b). (For interpretation of the references to colour in this figure legend, the reader is referred to the web version of this article.)

The transition from a delamination path with interlaminar crossings (Region I delamination growth) to one without (Region II delamination growth) is not instantaneous, but spans a certain amount of cycles and a certain amount of delamination growth. This transition zone is associated with the disappearance of individual interlaminar crossings. Observation of the fracture surface showed that these crossings do not disappear at the same time (same point of delamination growth). In addition, the transition zone is further broadened as this effect is present at each of the four delamination interfaces.

3.2.2. Effect of load severity on delamination growth behaviour

The transition from Region I to Region II delamination growth in nanofibre interleaved specimens seems to be predominantly present at low load levels, while a constant delamination growth rate is more often observed at high load levels (Fig. 9). Inspection of the fracture surface of failed specimens showed that the suppression mechanism is still present at high load levels, but takes place after a longer length of delamination. As such, the transition from Region I to Region II delamination growth was not always visible on the delamination growth data as it happened at delamination lengths higher than the maximum measurable delamination length (using an extensometer of 25 mm travel).

Particularly at the lower load levels, the driving force for the suppression of interlaminar crossings seems to be high, which results in complete glass fibre/epoxy interfacial failure without crossings after several millimetres. As the amount of delamination growth per cycle decreases substantially at lower load severities, the delamination has more time (i.e. more cycles) to realign itself in a more energetic favourable position outside of the toughened interlayer (i.e. at the glass fibre/epoxy interface) after only a few millimetres. Furthermore, the plasticity of the epoxy matrix increases at lower strain rates [44] which adds to the driving force for the suppression of interlaminar crossings at low load severities as the increased plasticity also causes an increased matrix toughness.

The interlaminar crossing suppression was also observed on the fracture surfaces of CCP and ENF specimens tested under static conditions, but there it took several centimetres before all the interlaminar crossings have disappeared. Hence, the mechanism of interlaminar crossing suppression seems to always be present in nanofibre interleaved specimens, but the length at which all the crossings have disappeared depends on the type of loading (high load severity, low load severity, static). Furthermore, it also depends on the type of nanofibre system (Fig. 9). In general, for the same kind of loading, PCL nanofibres result in a longer Region I delamination growth compared to PA 6.9 and PA 6 nanofibres.

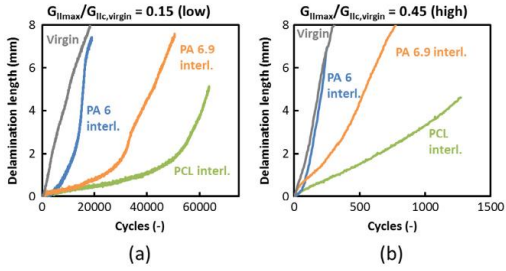

Fig. 9. At low load levels, nanofibre interleaved specimens show a substantial reduction in delamination growth rate compared to the virgin specimens during Region I delamination growth (a). At higher load levels, a constant delamination growth rate is more often observed throughout the test (b). (For interpretation of the references to colour in this figure legend, the reader is referred to the web version of this article.)

3.2.3. Improved fatigue delamination resistance

The delamination growth rate as a function of the load severity for the nanofibre interleaved laminates is given in Fig. 10. The plotted delamination growth rates were calculated from strain measurements in Region I. All nanofibre interleaved specimens showed an overall decrease in da/dN as compared to the virgin (non-interleaved) specimens, indicating an improved delamination resistance under fatigue loading. Improvements in delamination growth rate up to 15 times compared to the virgin material were obtained for individual specimens. It is worth noting that the PCL nanofibre interleaved specimens performed best over the range of load severities tested. Furthermore, the delamination behaviour of the nanofibre interleaved laminates is well described by the semi-empirical model of Eq. (5) with CoD values between 90 and 95% (Table 1). As described in Section 3.1.1, the improved delamination resistance can be associated with the formation of nanofibre bridging zones in interlaminar crossings. Analysis of the fracture surface of tested CCP specimens showed that these nanofibre bridging zones also form under fatigue loading conditions, see Fig. 11. They mainly develop at interlaminar crossings where the delamination causes a relatively large zone of interlaminar failure, but also occur at other interlaminar (micro)cracks, for example during hackle formation (tensile microcracking at 45° relative to the delamination plane).

A more detailed SEM analysis of the nanofibre bridging zones in interlaminar crossings is represented in Fig. 12. The electrospun nanofibres protrude from the epoxy resin and show a high degree of plastic deformation (Fig. 12a and c). Their morphology is typical for static tensile failure of (thermoplastic) fibres with a clearly defined necked region resulting in a tip-like fibre end. A similar nanofibre morphology is observed on statically tested CCP specimens. Crazing is observed at the interface between PCL nanofibres and epoxy indicative of a good adhesion between both polymers (Fig. 12b) as reported earlier [42]. In the case of polyamide nanofibres, the interface is mainly governed by relatively weak Van der Waals forces or hydrogen bonds resulting in a relatively weak PA-epoxy interface [45]. Indeed, the PA nanofibres occasionally debond from the epoxy resin without much deformation, resulting in smooth nanofibre imprints in the epoxy (Fig. 12d). This peeling mechanism most likely results in a lower energy uptake than if the nanofibres would plastically deform. Hence, the difference in interface quality between PCL-epoxy and PA-epoxy can explain why PCL nanofibres outperform the PA nanofibres in the fatigue tests.

4. Conclusion

This article describes the Mode II delamination behaviour of composite laminates toughened with electrospun nanofibrous

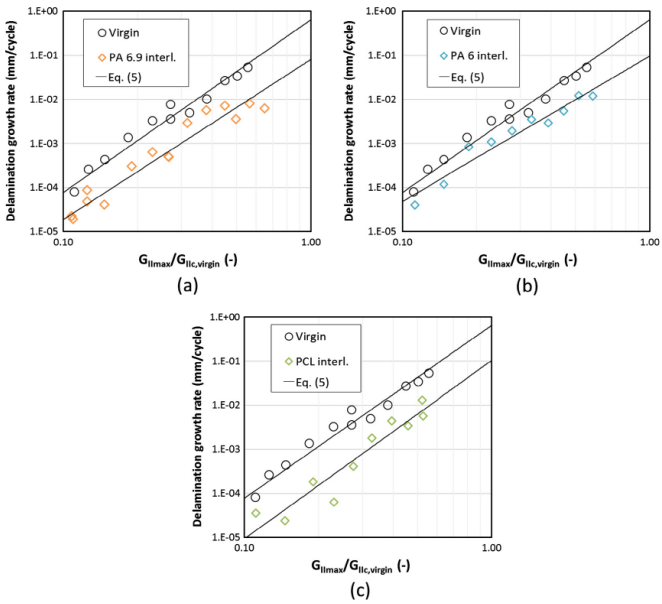

Fig. 10. The delamination growth rate decreases for laminates interleaved with PA 6.9 (a), PA 6 (b) and PCL (c) nanofibrous veils (each point represents an individual specimen). Overall improvements up to one order of magnitude are obtained for the nanofibre interleaved laminates. The PCL interleaved specimens show the best improvements over the whole load severity range considered (c). (For interpretation of the references to colour in this figure legend, the reader is referred to the web version of this article.)

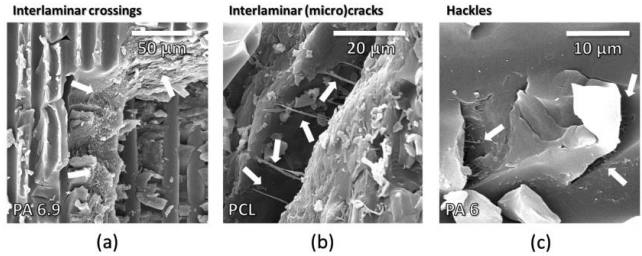

Fig. 11. Bridging nanofibres are observed on the fracture surface of tested CCP specimens at interlaminar crossings (a), in interlaminar microcracks (b), and at the base of hackles (c).

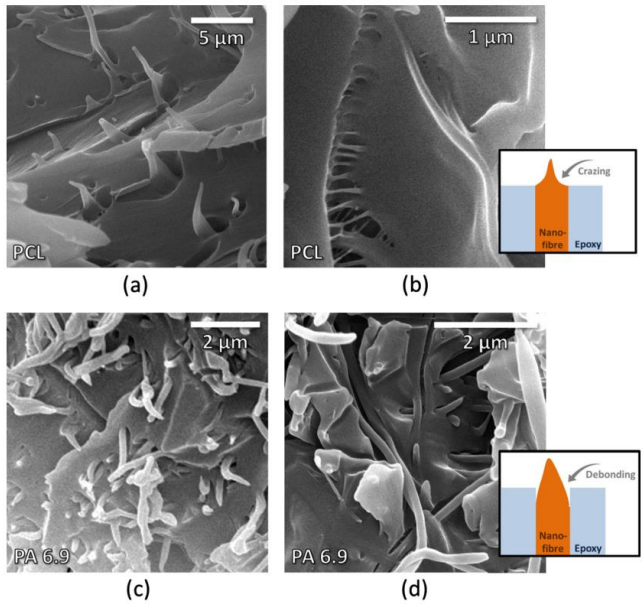

Fig. 12. Detailed SEM images of bridging nanofibres observed on interlaminar crossings: protruding PCL nanofibres (a), crazing observed at the PCL-epoxy interface (b), protruding PA 6.9 nanofibres (c), and imprints left by debonded PA 6.9 nanofibres (d). (For interpretation of the references to colour in this figure legend, the reader is referred to the web version of this article.)

interleaves under fatigue loading. The Central Cut-Ply method is used as it allows for a natural crack initiation into the nanofibre toughened interlayers similar to the initiation mechanism expected during service. The CCP method is found to give similar results for the Mode II interlaminar fracture toughness as the more commonly used ENF method. The CCP method however allows for an accurate monitoring of the delamination growth during fatigue testing from relatively simple extensometer measurements. This was validated by comparing the delamination growth rate obtained by strain measurements with the actual delamination

growth rate obtained from visual observation of the delamination front.

Static experiments showed that the increase in interlaminar fracture toughness is associated with the development of nanofibre bridging zones at interlaminar crossings. Under fatigue loading, the same mechanism of nanofibre bridging at interlaminar crossings is observed. This results in a substantial decrease in delamination growth rate up to one order of magnitude, and thus, an improved delamination behaviour under fatigue conditions of nanofibre interleaved composite laminates. A distinct fatigue delamination behaviour is observed for nanofibre interleaved laminates: depending on the applied load severity, there is a tendency for suppression of interlaminar crossings after a certain amount of delamination growth. The delamination growth of nanofibre interleaved specimens thus exhibits three regions during fatigue testing. Initially (Region I), the delamination propagation rate remains relatively constant and is smaller than the rate of the non-interleaved material. As more and more interlaminar crossings disappear, the delamination growth rapidly increases and the delamination growth rate of the nanofibre interleaved specimens approaches the rate of the non-interleaved material when no interlaminar crossings remain (Region II). Both regions are separated by a transition zone in which the interlaminar crossings combine and disappear. Especially at low load severities, the driving force for this suppression mechanism is found to be high.

All three nanofibre types tested, i.e. PA 6, PA 6.9 and PCL, result in improved fatigue delamination resistance, and the PCL interleaved laminates have the best performance over the range of load severities tested. Analysis of the fracture surfaces with SEM shows bridging nanofibres protruding from the epoxy matrix. Upon crack extension, these nanofibres will strain, yield and fail resulting in a significant amount of absorbed energy. Despite the fact that the CCP specimens are subjected to fatigue loading, the protruding nanofibres failure mode is similar to that found for (quasi-)static tensile failure of polymer fibres with a necked region resulting in a tip-like fibre end after failure.

The results obtained in this work indicate that nanofibrous veils are suitable as an interlaminar toughener under both static and fatigue (Mode II) loading conditions as they improve the delamination resistance considerably. Furthermore, the veils are easily integrated in composite laminates without any changes to the composite production process or the quality of the final laminates. As such, they are a viable interlaminar toughening material for high-end and demanding composite applications.

Acknowledgements

Financial support from the Agency for Innovation by Science and Technology of Flanders (IWT) and the Special Research Fund (BOF) Ghent University is gratefully acknowledged. Results in this paper were obtained within the framework of the IWT Strategic Basic Research Grant 141344 and the BOF 13/24J/020 project.

References

[1] Quaresimin M, Schulte K, Zappalorto M, Chandrasekaran S. Toughening mechanisms in polymer nanocomposites: from experiments to modelling. Compos Sci Technol 2015;123:187–204. doi: http://dx.doi.org/10.1016/j.compscitech.2015.11.027.

[2] Manjunatha CM, Taylor AC, Kinloch AJ, Sprenger S. The tensile fatigue behaviour of a silica nanoparticle-modified glass fibre reinforced epoxy composite. Compos Sci Technol 2010;70:193–9. doi: http://dx.doi.org/10.1016/j.compscitech.2009.10.012.

[3] Khan SU, Iqbal K, Munir A, Kim J-K. Quasi-static and impact fracture behaviors of CFRPs with nanoclay-filled epoxy matrix. Compos Part A Appl Sci Manuf 2011;42:253–64. doi: http://dx.doi.org/10.1016/j.compositesa.2010.11.011.

[4] Wong DWY, Lin L, McGrail PT, Peijs T, Hogg PJ. Improved fracture toughness of carbon fibre/epoxy composite laminates using dissolvable thermoplastic fibres. Compos Part A Appl Sci Manuf 2010;41:759–67. doi: http://dx.doi.org/10.1016/j.compositesa.2010.02.008.

[5] Sohn M-S, Hu X-Z. Mode II delamination toughness of carbon-fibre/epoxy composites with chopped Kevlar fibre reinforcement. Compos Sci Technol 1994;52:439–48. doi: http://dx.doi.org/10.1016/0266-3538(94)90179-1.

[6] Kuwata M, Hogg PJ. Interlaminar toughness of interleaved CFRP using non-woven veils: Part 2. Mode-II testing. Compos Part A Appl Sci Manuf 2011;42:1560–70. doi: http://dx.doi.org/10.1016/j.compositesa.2011.07.017.

[7] Hogg PJ. Toughening of thermosetting composites with thermoplastic fibres. Mater Sci Eng A 2005;412:97–103. doi: http://dx.doi.org/10.1016/j.msea.2005.08.028.

[8] Ramirez VA, Hogg PJ, Sampson WW. The influence of the nonwoven veil architectures on interlaminar fracture toughness of interleaved composites. Compos Sci Technol 2015;110:103–10. doi: http://dx.doi.org/10.1016/j.compscitech.2015.01.016.

[9] Yasaee M, Bond IP, Trask RS, Greenhalgh ES. Damage control using discrete thermoplastic film inserts. Compos Part A Appl Sci Manuf 2012;43:978–89. doi: http://dx.doi.org/10.1016/j.compositesa.2012.01.011.

[10] Tsotsis TK. Interlayer toughening of composite materials. Polym Compos 2009;30:70–86. doi: http://dx.doi.org/10.1002/pc.20535.

[11] Yokozeki T, Iwahori Y, Ishibashi M, Yanagisawa T, Imai K, Arai M, et al. Fracture toughness improvement of CFRP laminates by dispersion of cup-stacked carbon nanotubes. Compos Sci Technol 2009;69:2268–73. doi: http://dx.doi.org/10.1016/j.compscitech.2008.12.017.

[12] Sato N, Hojo M, Nishikawa M. Intralaminar fatigue crack growth properties of conventional and interlayer toughened CFRP laminate under mode I loading. Compos Part A Appl Sci Manuf 2015;68:202–11. doi: http://dx.doi.org/10.1016/j.compositesa.2014.09.031.

[13] Dzenis Y. Structural nanocomposites. Science 2008;319:419–20. doi: http://dx.doi.org/10.1126/science.1151143 (80-).

[14] Daelemans L, van der Heijden S, De Baere I, Rahier H, Van Paepegem W, De Clerck K. Using aligned nanofibres for identifying the toughening micromechanisms in nanofibre interleaved laminates. Compos Sci Technol 2015;124:17–26. doi: http://dx.doi.org/10.1016/j.compscitech.2015.11.021.

[15] Zhang H, Bharti A, Li Z, Du S, Bilotti E, Peijs T. Localized toughening of carbon/epoxy laminates using dissolvable thermoplastic interleaves and electrospun fibres. Compos Part A Appl Sci Manuf 2015;79:116–26. doi: http://dx.doi.org/10.1016/j.compositesa.2015.09.024.

[16] Bilge K, Ozden-Yenigun E, Simsek E, Menceloglu YZ, Papila M. Structural composites hybridized with epoxy compatible polymer/MWCNT nanofibrous interlayers. Compos Sci Technol 2012;72:1639–45. doi: http://dx.doi.org/10.1016/j.compscitech.2012.07.005.

[17] Wu X-F, Rahman A, Zhou Z, Pelot DD, Sinha-Ray S, Chen B, et al. Electrospinning core-shell nanofibers for interfacial toughening and self-healing of carbon-fiber/epoxy composites. J Appl Polym Sci 2013;129:1383–93. doi: http://dx.doi.org/10.1002/app.38838.

[18] Huang Z-M, Zhang Y-Z, Kotaki M, Ramakrishna S. A review on polymer nanofibers by electrospinning and their applications in nanocomposites. Compos Sci Technol 2003;63:2223–53. doi: http://dx.doi.org/10.1016/S0266-3538(03)00178-7.

[19] Kim J, Reneker DH. Mechanical properties of composites using ultrafine electrospun fibers. Polym Compos 1999;20:124–31. doi: http://dx.doi.org/10.1002/pc.10340.

[20] van der Heijden S, Daelemans L, De Schoenmaker B, De Baere I, Rahier H, Van Paepegem W, et al. Interlaminar toughening of resin transfer moulded glass fibre epoxy laminates by polycaprolactone electrospun nanofibres. Compos Sci Technol 2014;104:66–73. doi: http://dx.doi.org/10.1016/j.compscitech.2014.09.005.

[21] Greiner A, Wendorff JH. Electrospinning: a fascinating method for the preparation of ultrathin fibers. Angew Chem Int Ed Engl 2007;46:5670–703. doi: http://dx.doi.org/10.1002/anie.200604646.

[22] Persano L, Camposeo A, Tekmen C, Pisignano D. Industrial upscaling of electrospinning and applications of polymer nanofibers: a review. Macromol Mater Eng 2013;298:504–20. doi: http://dx.doi.org/10.1002/mame.201200290.

[23] Agarwal S, Burgard M, Greiner A, Wendorff J. Electrospinning: A Practical Guide to Nanofibers 2016.

[24] Hamer S, Leibovich H, Green A, Avrahami R, Zussman E, Siegmann A, et al. Mode I and Mode II fracture energy of MWCNT reinforced nanofibrilmats interleaved carbon/epoxy laminates. Compos Sci Technol 2014;90:48–56. doi: http://dx.doi.org/10.1016/j.compscitech.2013.10.013.

[25] Beckermann GW, Pickering KL. Mode I and Mode II interlaminar fracture toughness of composite laminates interleaved with electrospun nanofibre veils. Compos Part A Appl Sci Manuf 2015;72:11–21. doi: http://dx.doi.org/10.1016/j.compositesa.2015.01.028.

[26] Nash NH, Ray D, Young TM, Stanley WF. The influence of hydrothermal conditioning on the Mode-I, thermal and flexural properties of carbon/benzoxazine composites with a thermoplastic toughening interlayer. Compos Part A Appl Sci Manuf 2015;76:135–44. doi: http://dx.doi.org/10.1016/j.compositesa.2015.04.023.

[27] Daelemans L, van der Heijden S, De Baere I, Rahier H, Van Paepegem W, De Clerck K. Nanofibre bridging as a toughening mechanism in carbon/epoxy composite laminates interleaved with electrospun polyamide nanofibrous veils. Compos Sci Technol 2015;117:244–56. doi: http://dx.doi.org/10.1016/j.compscitech.2015.06.021.

[28] Zhang J, Lin T, Wang X. Electrospun nanofibre toughened carbon/epoxy composites: effects of polyetherketone cardo (PEK-C) nanofibre diameter and interlayer thickness. Compos Sci Technol 2010;70:1660–6. doi: http://dx.doi.org/10.1016/j.compscitech.2010.06.019.

[29] Li G, Li P, Zhang C, Yu Y, Liu H, Zhang S, et al. Inhomogeneous toughening of carbon fiber/epoxy composite using electrospun polysulfone nanofibrous membranes by in situ phase separation. Compos Sci Technol 2008;68:987–94. doi: http://dx.doi.org/10.1016/j.compscitech.2007.07.010.

[30] Magniez K, Chaffraix T, Fox B. Toughening of a carbon-fibre composite using electrospun poly(hydroxyether of bisphenol A) nanofibrous membranes through inverse phase separation and inter-domain etherification. Materials (Basel) 2011;4:1967–84. doi: http://dx.doi.org/10.3390/ma4111967.

[31] Hojo M, Ando T, Tanaka M, Adachi T, Ochiai S, Endo Y. Modes I and II interlaminar fracture toughness and fatigue delamination of CF/epoxy laminates with self-same epoxy interleaf. Int J Fatigue 2006;28:1154–65. doi: http://dx.doi.org/10.1016/j.ijfatigue.2006.02.004.

[32] Hojo M, Matsuda S, Tanaka M, Ochiai S, Murakami A. Mode I delamination fatigue properties of interlayer-toughened CF/epoxy laminates. Compos Sci Technol 2006;66:665–75. doi: http://dx.doi.org/10.1016/j.compscitech.2005.07.038.

[33] Knoll JB, Riecken BT, Kosmann N, Chandrasekaran S, Schulte K, Fiedler B. The effect of carbon nanoparticles on the fatigue performance of carbon fibre reinforced epoxy. Compos Part A Appl Sci Manuf 2014;67:233–40. doi: http://dx.doi.org/10.1016/j.compositesa.2014.08.022.

[34] Allegri G, Jones MI, Wisnom MR, Hallett SR. A new semi-empirical model for stress ratio effect on mode II fatigue delamination growth. Compos Part A Appl Sci Manuf 2011;42:733–40. doi: http://dx.doi.org/10.1016/j.compositesa.2011.02.013.

[35] Daelemans L, van der Heijden S, De Baere I, Muhammad I, Van Paepegem W, Rahier H, et al. Bisphenol A based polyester binder as an effective interlaminar toughener. Compos Part B Eng 2015;80:145–53. doi: http://dx.doi.org/10.1016/j.compositesb.2015.05.044.

[36] Arrese A, Carbajal N, Vargas G, Mujika F. A new method for determining mode II R-curve by the end-notched flexure test. Eng Fract Mech 2010;77:51–70. doi: http://dx.doi.org/10.1016/j.engfracmech.2009.09.008.

[37] Cui W, Wisnom MR, Jones M. An experimental and analytical study of delamination of unidirectional specimens with cut central plies. J Reinf Plast Compos 1994;13:722–39. doi: http://dx.doi.org/10.1177/073168449401300804.

[38] Bing Q, Sun CT. Effect of compressive transverse normal stress on mode II fracture toughness in polymeric composites. Int J Fract 2007;145:89–97. doi: http://dx.doi.org/10.1007/s10704-007-9103-4.

[39] Johnson W, Masters J, Cui W, Wisnom M, Jones M. Effect of through thickness tensile and compressive stresses on delamination propagation fracture energy. J Compos Technol Res 1994;16:329. doi: http://dx.doi.org/10.1520/CTR10593J.

[40] Li X, Hallett SR, Wisnom MR. Predicting the effect of through-thickness compressive stress on delamination using interface elements. Compos Part A Appl Sci Manuf 2008;39:218–30. doi: http://dx.doi.org/10.1016/j.compositesa.2007.11.005.

[41] De Baere I, Jacques S, Van Paepegem W, Degrieck J. Study of the Mode I and Mode II interlaminar behaviour of a carbon fabric reinforced thermoplastic. Polym Test 2012;31:322–32. doi: http://dx.doi.org/10.1016/j.polymertesting.2011.12.009.

[42] Daelemans L, van der Heijden S, De Baere I, Rahier H, Van Paepegem W, De Clerck K. Damage resistant composites using electrospun nanofibers: a multiscale analysis of the toughening mechanisms. ACS Appl Mater Interfaces 2016. doi: http://dx.doi.org/10.1021/acsami.6b02247.

[43] Blackman BRK, Kinloch AJ, Paraschi M. The determination of the mode II adhesive fracture resistance, GIIC, of structural adhesive joints: an effective crack length approach. Eng Fract Mech 2005;72:877–97. doi: http://dx.doi.org/10.1016/j.engfracmech.2004.08.007.

[44] Allaer K, De Baere I, Van Paepegem W, Degrieck J. Direct fracture toughness determination of a ductile epoxy polymer from digital image correlation measurements on a single edge notched bending sample. Polym Test 2015;42:199–207. doi: http://dx.doi.org/10.1016/j.polymertesting.2015.01.014.

[45] De Schoenmaker B, van der Heijden S, Moorkens S, Rahier H, van Assche G, De Clerck K. Effect of nanofibres on the curing characteristics of an epoxy matrix. Compos Sci Technol 2013;79:35–41. doi: http://dx.doi.org/10.1016/j.compscitech.2013.02.009.

PAPER VI

REGULAR AND CORE-SHELL ELECTROSPUN NANOFIBRES CAPABLE OF SELF-FUSING FOR NANOCOMPOSITES WITH INCREASED DAMAGE RESISTANCE

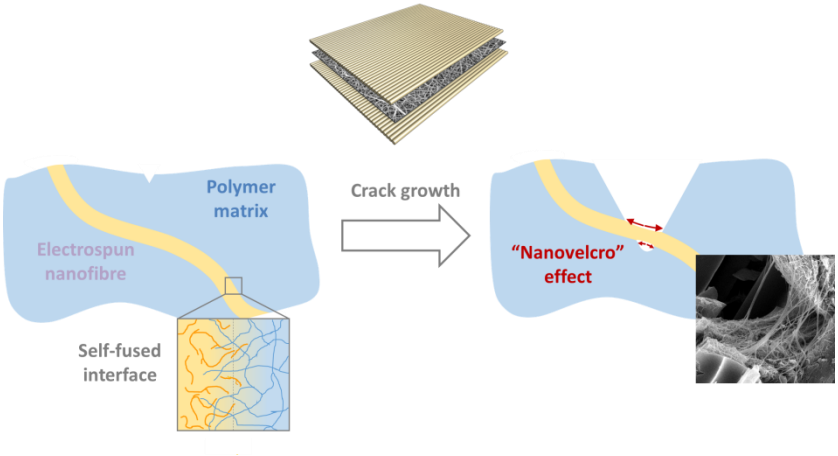

Lode Daelemans, Sam van der Heijden, Ives De Baere, Hubert Rahier, Wim Van Paepegem and Karen De Clerck

Currently in submission with *Composites Science and Technology*.

Regular and core-shell electrospun nanofibres capable of self-fusing for nanocomposites with increased damage resistance

Lode Daelemans[1], Timo Meireman[1], Nuray Kizildag[1,2], Ives De Baere[1], Hubert Rahier[3], Wim Van Paepegem[1] and Karen De Clerck[1]*

[1] Department of Materials, Textiles and Chemical Engineering (MATCH), Ghent University, Technologiepark-Zwijnaarde 907, B-9052 Zwijnaarde, Belgium

[2] Department of Textile Engineering, Istanbul Technical University, Inonu Cad. 65, 34437 Gumussuyu Istanbul, Turkey

[3] Department of Materials and Chemistry, Vrije Universiteit Brussel, Pleinlaan 2, B-1050 Brussels, Belgium

Keywords: nanocomposites, electrospinning, fracture toughness, delamination, adhesion

Abstract

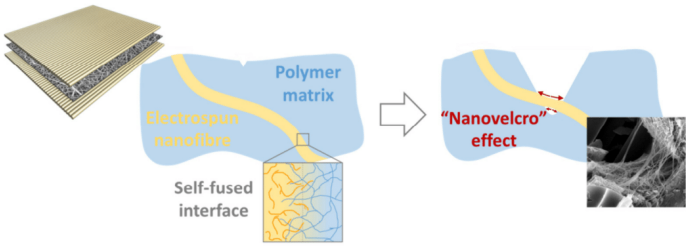

Good adhesion between the constituents in polymer based nanocomposites is often very important to have load transfer between the constituents and achieve a material with better (mechanical) properties. Therefore, a new methodology is presented to create enhanced bonding between electrospun nanofibres and a thermosetting polymer matrix in a nanocomposite material based on the interdiffusion of both polymers at their interface during the curing of the thermosetting component. This cure-induced self-fusing mechanism enables the bond strength to be tuned from weak to strong depending on the curing temperature and time. As such, novel nanocomposites or nano-engineered laminates can be obtained in which there is a tuneable bond strength. This article shows the potential of nano-engineering fibre reinforced composites for better delamination resistance using electrospun poly(ε-caprolacton) (PCL) nanofibres and a thermosetting epoxy. These hybrid laminates, consisting of electrospun PCL nanofibrous veils interleaved between glass fibre plies, are produced with varying PCL/epoxy bond strength. Two concepts are introduced to optimize the delamination resistance using either multiple curing cycles or core/shell structured nanofibres. These concepts proved to be able to retain the nanofibrous morphology while

providing a strong bond with the matrix material and as such resulted in significant improvements of the delamination resistance.

1. Introduction

Polymer composites are a class of materials consisting of multiple constituents that have a synergistic effect on the macroscopic properties of the material which would not be achievable by either component alone. Most often, a reinforcing filler is dispersed within a polymer matrix material resulting in better mechanical properties. Today, high modulus/high strength fibre reinforced polymer (FRP) composites are one of the main polymer composites used in engineering applications and can be found in applications ranging from space- and aircraft, wind turbine blades, cars, bridge decks to bicycles, fishing rods and canoes. Their high mechanical properties at low weight makes them especially advantageous compared with other engineering materials when light and strong components are required. These FRP composites are usually made with glass, carbon or aramid fibres with diameters of 5 – 30 µm which are dispersed under the form of a textile structure (woven fabric, non-woven mat, unidirectional tapes, …) into an epoxy polymer matrix. However, as applications demand more and more of the material, research into improving these materials has surged over the past decades. Due to their laminated structure, the weak point of traditional composite laminates is the interlayer between reinforcing fibre plies causing typical delamination failure. At the same time, the development and production of nanomaterials such as carbon nanotubes (CNTs), clay particles and electrospun nanofibrous veils has seen an increase. Nano-engineering the polymer composites to improve their mechanical performance – such as delamination and damage resistance – has thus been one of the main aims of today's research in this field.[1–6]

Electrospinning is a versatile and relatively straight-forward technique to produce fibrous nanomaterials at a scale necessary for composite applications.[7–9] During (solvent) electrospinning, a polymer solution is pumped through a nozzle connected to a high voltage source. The electric field between the nozzle and the (grounded or opposite potential) collector, results in the expulsion of a polymer solution jet from the nozzle tip. During the deposition, the solvent will evaporate while the jet will experience whipping forces which elongate the jet several orders of magnitude resulting in the formation of continuous fibres with a typical diameter of 50 – 500 nm. The nanofibrous veils formed in this process are typically self-supporting non-woven membranes which gives them a similar ease of handling as regular textiles. Furthermore, a large variety of polymers can be used to electrospin nanofibres and the health risks of the nanofibrous veils are typically non-existent compared with other nanomaterials due to the fact that they consist of long continuous nanofibres with diameters between 50 – 500 nm which limits their mobility to diffuse through the body/skin.

These advantages have resulted in a lot of interest of the community over the past years into electrospun veils for nano-engineered polymer composites.[10–15] One of the main topics within this research is to incorporate electrospun nanofibrous veils within traditional laminated glass fibre or carbon fibre composites to obtain hybrid composites with both nano- and microscale fibres.[16–21] Incorporating electrospun nanofibres within the damage prone interlayers results in a nano-engineered interlayer with for example improved fracture toughness.[4] As such, the nano-engineered hybrid laminates have much better failure properties with increased delamination resistance while the main properties of the composite – such as high strength and stiffness at low weight – are retained. Especially when the nanofibres have a mechanical purpose, e.g. toughening, strengthening, …, there must be an adequate adhesion with the matrix material to have good load transfer and thus good mechanical performance similar to traditional fibre reinforced composites. Little research has been dedicated to determine the adhesion properties between an electrospun nanofibre and matrix material and no direct test methods exist until today.

However, several researchers have indicated the importance of good adhesion for properties such as damage resistance or mechanical performance.[4,14,22,23]

This article proposes a new method to tune the adhesion between an electrospun nanofibre and an epoxy matrix. Poly(ε-caprolacton) (PCL) is used as a model material as its combination with epoxy resins under the form of polymer blends is already well studied.[24–28] However, the principle is general and can be broadened to other polymer types as well. It is based on the intermolecular mixing of PCL and epoxy molecules during curing of the epoxy resin and requires no special processing steps compared to other adhesion improving methods such as plasma-treatment, chemical surface modification, etc. To underpin the self-fusing mechanism, an analysis on macroscopic PCL/epoxy interfaces is provided. These results are further used to design nano-engineered hybrid fibre reinforced composite laminates with a variation in the nanofibre PCL/epoxy interfacial strength to study the effect on the delamination resistance under both Mode I and Mode II loading conditions.

2. Results and discussion

2.1. Mechanism of cure-induced self-fusion

The mechanism of cure-induced self-fusion is a physical way to create bonding between two types of polymer during the curing of one of them. In the case of a PCL/epoxy system, PCL is often dissolved into the epoxy monomer before any curing agent is added to have full dissolution of PCL into the epoxy resin. Depending on the curing conditions (time, temperature, concentration) different microstructures can be obtained ranging from a single homogeneous phase to a (inverse) phase separated material.[27,29] The PCL/epoxy blend can thus result in a single homogeneous amorphous phase with a glass transition temperature which is intermediate between those of both single components, i.e. $T_{g,PCL} < T_{g,blend} < T_{g,epoxy}$. Hence, the PCL and epoxy are miscible at the molecular level and form a single phase in which there is no macroscopic distinction between both components. This mechanism can be exploited to create a strong interfacial bond between an epoxy resin and a solid PCL polymer. Indeed, as a solid PCL phase is brought into contact with the uncured liquid epoxy resin, the PCL/epoxy miscibility can result in the formation of a blended structure at the interface. This creates molecular diffusion/mixing between the PCL and epoxy which, upon curing, can result in better interfacial strength between both polymers due to molecular interlocking. The formation of this blend interface will of course depend on the mobility of both PCL and epoxy molecules, the contact time, temperature and affinity between both polymers. During curing of the epoxy resin – which is often an auto-catalytic reaction performed at temperatures well above $T_{g,PCL}$ (-60 °C) – the mobility of the epoxy resin will quickly decline after gelation or vitrification. Hence, the contact time in which PCL and epoxy can blend, is limited by the curing reaction itself. The temperature at which the curing occurs thus has a direct effect on the available contact time for blending. The temperature also influences the mobility of the PCL polymer, especially when the temperature reaches the melting onset. As such, the curing cycle that is used will evoke a cure-induced self-fusion or not. This mechanism is illustrated in **Figure 1**.

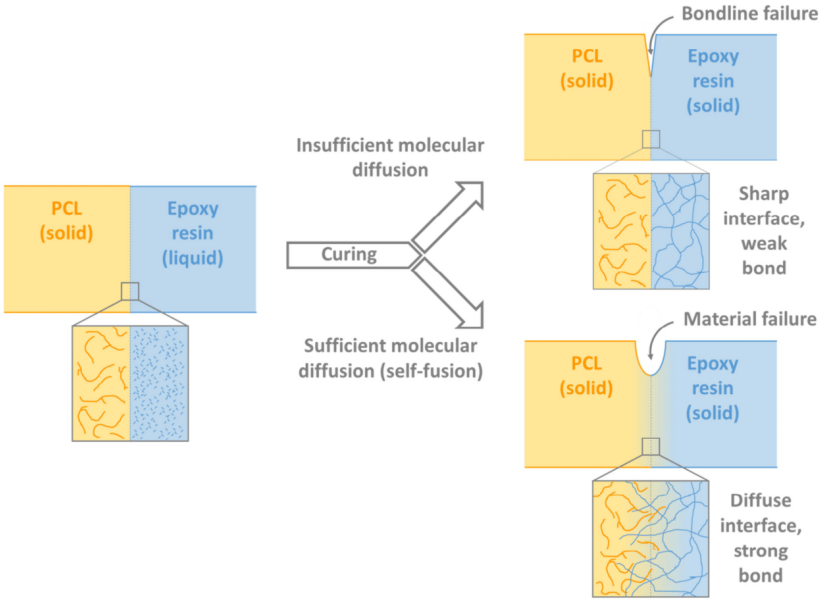

Figure 1: Mechanism of cure-induced self-fusion resulting in a strong bond between PCL and epoxy.

2.2. Evaluation of self-fusion in a PCL/epoxy system

Double butt-jointed dogbone tensile specimens were developed which allowed for the mechanical testing of a controlled PCL/epoxy interface, see **Figure 2**. First, PCL polymer was moulded as a short beam with flat sides in a silicon dogbone mould with silicon dummy spacers inserted at both ends. After solidification of the PCL polymer, the silicon spacers were removed which results in a PCL block with two exposed flat sides. The sides were cleaned with aceton to remove possible silicone residue. The silicon mould is then filled at each side with liquid epoxy resin to the same level as the height of the PCL beam. At this point, the self-fusion of the PCL/epoxy can occur at both interfaces. After curing of the epoxy resin, the specimens are taken out of the mould and tested for their tensile strength. The curing time for each temperature is determined by isothermal DSC experiments on the epoxy resin. When a specimen breaks at the bond line, the maximum stress gives an indication of the bond strength. If the specimen fails by bulk failure however, the bond strength is sufficient enough and no longer the weakest point in the specimen. Note that the tensile strength of bulk PCL (14 ± 1 MPa) is much lower than that of the epoxy resin (65 MPa[30]) and bulk failure will thus occur in the PCL section.

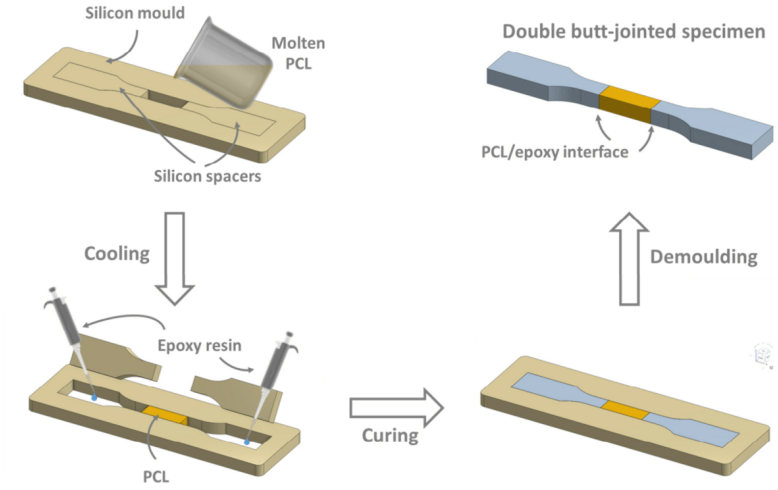

Figure 2: Production of double butt-jointed tensile specimens with a controlled PCL/epoxy interface to determine the self-fusion efficiency.

The results of the tensile tests are illustrated in **Figure 3** and show a clear trend in increasing strength with increasing cure temperature. For cure temperatures between 25 °C and 35 °C, the failure of the tensile specimens was within one of the PCL/epoxy interfaces due to limited bond strength between PCL and epoxy. Nevertheless, the bond strength increases from 2 MPa at a cure temperature of 25 °C to 6 MPa at a cure temperature of 35 °C which is three times higher. Note that a bond strength of essentially zero was obtained for specimens in which no self-fusion was allowed to occur (epoxy is first fully cured before it is brought into contact with PCL). At cure temperatures equal to or above 40 °C, the bond strength becomes higher than the bulk PCL yield strength. The tensile specimens showed yielding of the PCL near one of the interfaces at a stress equal to the bulk PCL yield stress and failed by extensive elongation of the bulk PCL phase instead of the clear interfacial fracture in the specimens cured below 40 °C. The results show that cure cycles above 40 °C resulted in enough molecular mixing between PCL and epoxy near the interface, resulting in a diffuse boundary which increased the bond strength above the bulk PCL strength. When $\sigma_{bond} > \sigma_{PCL}$, failure will occur in the PCL polymer phase and the PCL/epoxy interface is no longer a limiting parameter for load transfer to occur.

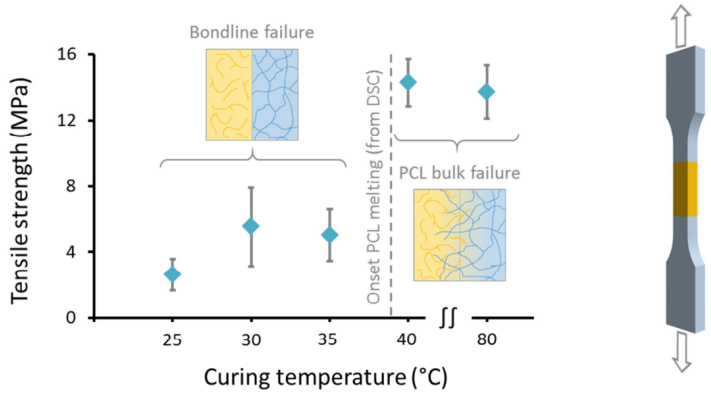

Figure 3: Tensile strength of the double butt-jointed specimens at different isothermal cure temperatures show an increased bond strength at higher curing temperatures (specimens in which no self-fusing occurred had a bond strength of essentially zero).

SEM images of the fracture surfaces of the butt-jointed tensile specimens for different cure temperatures are shown in **Figure 4**. These reveal that the fracture surface of the specimens transitioned from smooth (at low interface strength) to rough (at high interface strength). Due to an increased interfacial bond strength by the cure induced fusion, the failure changed from adhesive to cohesive at cure temperatures of 40 °C or higher. A DSC scan of the bulk PCL confirms that high bond strengths are achieved when the cure temperature of the resin reaches the melting point of PCL. This indicates the main limitation for the molecular mixing is the mobility of the PCL polymer.

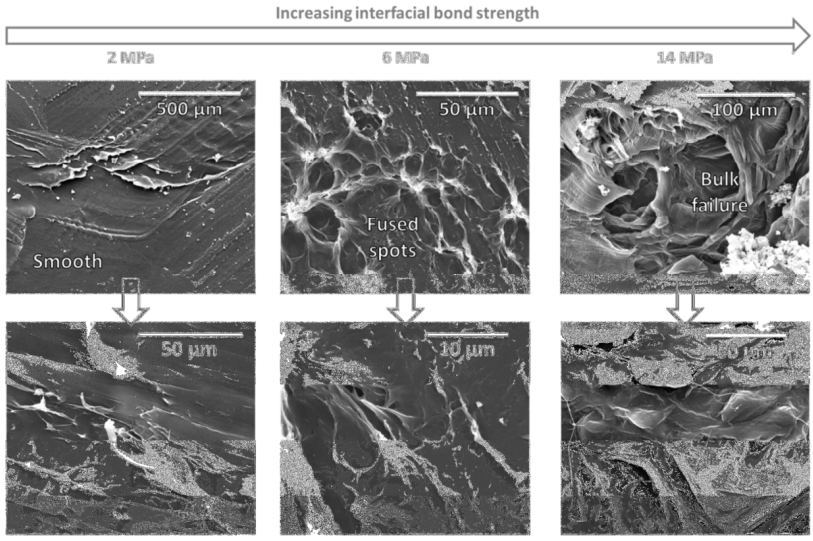

Figure 4: SEM images taken on the fracture surface of the tensile specimens showing increased plasticity indicating better adhesion with increasing curing temperature.

2.3. Self-fusion in nano-engineered hybrid composite laminates

The principle of the cure-induced fusing mechanism is exploited to produce nano-engineered composite laminates with different degrees of nanofibre/matrix bond strength by interleaving electrospun PCL nanofibrous veils in between the reinforcing glass fibre plies (**Figure 5**). The stacking of dry glass fibre plies and nanofibrous veils is infused with unreacted epoxy resin and isothermally cured at a fixed temperature of 30 °C, 40 °C, 50 °C or 80 °C. Unmodified reference composite laminates are produced to compare with the nano-engineered ones.

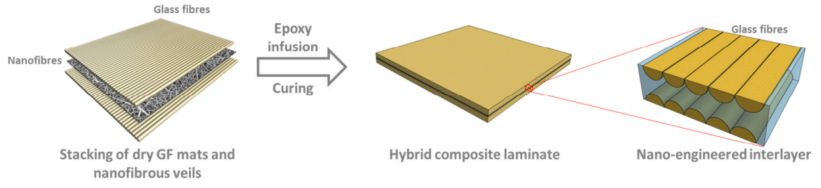

Figure 5: Production of hybrid composite laminates by interleaving nanofibrous veils.

Composite laminates typically fail by delamination of the reinforcing plies due to a lack of out-of-plane reinforcement. By introducing nanofibres in between the reinforcing plies, the delamination resistance can be largely improved.[4] Upon (micro)crack formation in the composite, the nanofibres will bridge the cracks and absorb energy by yielding. This relieves the stress at the crack tip and more energy will be required to propagate the crack further into the material.[4,18] The two major delamination modes are studied in accordance to traditional fracture mechanics: Mode I delamination (opening mode) and Mode II delamination (shearing mode). The results are shown in **Figure 6**. Note that for the unmodified virgin specimens both the Mode I as well as Mode II interlaminar fracture toughness were independent of the cure cycle as its delamination resistance is mostly determined by glass fibre/matrix debonding.[4]

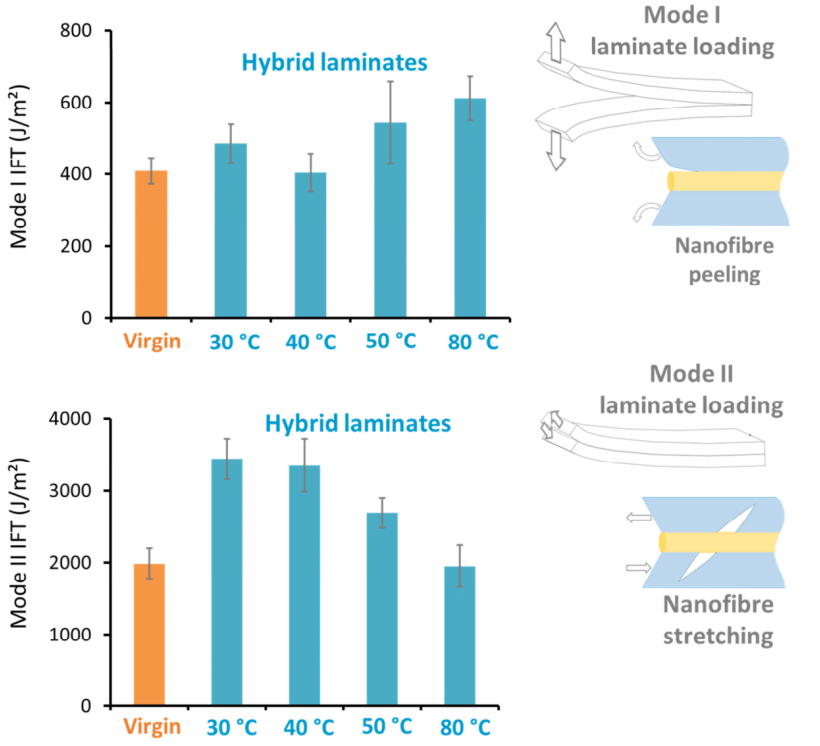

Figure 6: Mode I and Mode II interlaminar fracture toughness for reference (virgin) and hybrid laminates cured at different temperatures. Increasing the curing temperature results in a better Mode I delamination resistance, but a lower Mode II delamination resistance.

Under Mode I loading of the specimens, the nanofibres are subjected to peeling forces which can cause relatively easy debonding of the nanofibres without much energy uptake. The delamination will propagate by interfacial debonding of the nanofibres instead of stretching the nanofibres and as such, the delamination resistance is hardly improved.[4] However, when the bonding between the nanofibres and the epoxy is improved by the self-fusion mechanism, the energy uptake of the nanofibres increases as they will yield before debonding which absorbs energy, resulting in an improvement of the Mode I interlaminar fracture toughness. This mechanism is illustrated by the experimental results. The Mode I interlaminar fracture toughness increases with increasing cure temperature similar to the tensile specimens of Section 2.2. Note that the morphology of the nanofibres was lost when the composite was cured at 80 °C as this temperature is above the melting point of PCL resulting in a blended zone larger than the nanofibres themselves. The highest improvements are found for cure cycles of 50 °C and above.

Analysis of the delaminated fracture surfaces with SEM confirms that the adhesion between the nanofibres and epoxy improves with increasing cure temperature while their nanofibrous morphology disappears, see **Figure 7**. At low curing temperatures (30 °C and 40 °C), clearly outlined nanofibres are visible on the fracture surface. Furthermore, the nanofibres of the Mode I subjected specimens show a high degree of debonding which is visible on the SEM images as imprints left by peeled nanofibres. The specimens cured at 50 °C show better bonding, but the morphology of the nanofibres becomes less clear. For the specimens cured at 80 °C, no clear nanofibres are observed anymore and the interlayer is comprised of a single homogeneous phase. As 80 °C is above the melting range of PCL, this cure cycle allowed full dissolution of the nanofibres into the epoxy resin resulting in a total loss of the nanofibrous morphology.

Under Mode II loading conditions, the interlayer will be subjected to shearing forces. This results in the formation of tensile microcracks at 45° relative to the loading direction. This not only subjects the nanofibres to shearing forces, but also results in stretching of the nanofibres which bridge cracks. Since there are no significant peeling forces acting on the nanofibres in this case, it is expected that the adhesion between the nanofibres and the epoxy becomes less important. Indeed, peeling forces create a very local debonding while shearing forces are spread over a larger area. Typically, the bond strength under shearing forces is about an order of magnitude higher than under peeling forces due to the high amount of surface area of nanofibres[31]. As such, one would expect a relatively stable Mode II interlaminar fracture toughness independent of the isothermal curing temperature. However, there is a clear decreasing trend with increasing cure temperature visible which is opposite to the trend observed under Mode I loading. This trend cannot be associated with a difference in interfacial strength, but instead, reveals that the Mode II toughness improvement is dependent on the nanofibrous morphology itself. Indeed, with increasing cure temperature, a more diffuse interface is created and the morphology of the nanofibres starts to differ from their initial morphology. At 80 °C, the nanofibrous morphology is completely lost resulting in a decrease of the Mode II fracture toughness compared to the reference specimens.

These results indicate the importance and duality of both adhesion and morphology aspects to optimize the nano-engineered composites. From a practical aspect, the nano-engineered composites would perform best if a significant increase in both Mode I and Mode II delamination resistance can be obtained at the same time as real-life structures often experience a combination of both modes (mixed mode).

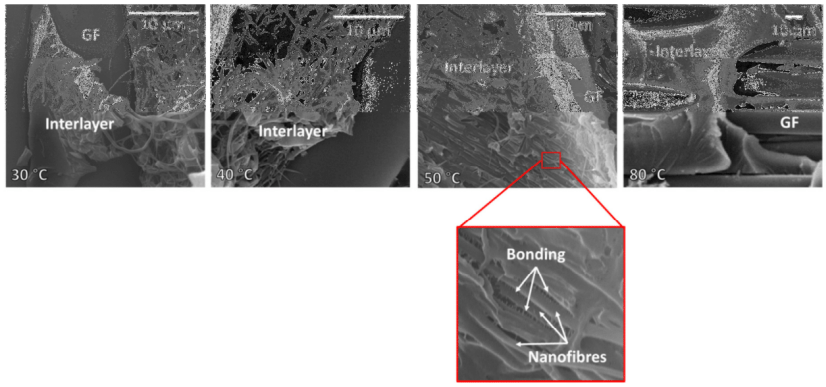

Figure 7: SEM images of the fracture surface of hybrid laminates tested under Mode I loading conditions with the nano-engineered interlayers visualised. For cure cycles of 30 °C to 50 °C, increased bonding is observed between the nanofibres and the epoxy matrix, while their morphology becomes less clear. At 80 °C, the interlayer is a homogeneous phase indicating that the nanofibres completely dissolved into the epoxy resin.

2.4. Optimizing interfacial bond strength while maintaining the nanofibrous morphology

Two different methodologies are investigated which can be used to produce nano-engineered hybrid composites with an optimized interfacial bond strength and maintaining the morphology of the nanofibres.

2.4.1. Multi-step curing cycle

The first methodology is based on multiple curing steps at different temperatures. The previous results have shown that with increasing (isothermal) curing temperature, the fusing mechanism is more pronounced, but at the same time the nanofibre morphology starts to disappear. This limits the optimizing procedure as both effects are fixed for a certain curing temperature. However, by introducing multiple curing steps at different temperatures, both effects can be more or less separated from each other. More specifically, a low temperature ($T < T_{m,PCL}$) curing step will fix the nanofibre morphology as the diffusion of PCL will be limited while the epoxy resin reacts. A second curing step at elevated temperature ($T > T_{m,PCL}$) can then be used to allow enough diffusion of the PCL into the partially reacted epoxy to have substantial self-fusing. Of course, this implies that diffusion of the PCL in the epoxy can still happen. Therefore, it is important that the time and temperature of the first curing step is chosen such that the epoxy is viscous/solid enough to maintain the nanofibre morphology (as a sort of self-formed mould), while still be "open" enough to allow sufficient mixing between PCL and epoxy molecules. The added advantage of this method is that the epoxy resin can be fully cured during the second step at higher temperature. This will increase its glass transition temperature and is often desirable for better mechanical properties at elevated temperatures in applications.

A two-step curing procedure was used with a curing step at 25 °C for 24 hours followed by a curing step at 80 °C for 15 hours. A DSC analysis of the curing reaction of the epoxy resin was performed to determine the conversion-time relationship for the epoxy resin at 25 °C. This showed that the conversion after 24 hours at 25 °C was approximately 63% (the maximum conversion reached at 25 °C is 81%). The 24h-period of the first curing step was selected because the Mode I and Mode II delamination resistance of specimens that were allowed to reach their maximum conversion at 25 °C was not affected by subjecting them to a second cure step at 80 °C. This indicates that the conversion was already too high in those specimens limiting the interdiffusion of PCL and epoxy during the high temperature step. Reference and PCL nanofibre interleaved composite plates were produced using the two-step curing process and subsequently tested to determine the Mode I and Mode II interlaminar fracture toughness. The results show that both Mode I and Mode II interlaminar fracture toughness are significantly increased at the same time, which was not possible using a single curing step (**Figure 8**). The Mode I interlaminar fracture toughness is even higher than all the ones obtained for single step curing. The Mode II interlaminar fracture toughness was similar to those of the laminates isothermally cured at 30 °C and 40 °C and significantly higher than obtained with a single curing step at 50 °C or 80 °C.

Analysis of the fracture surface with SEM showed the duality between the bond strength and morphology of the nanofibres. The specimens showed no real signs of bad bonding such as imprints or peeled nanofibres, but rather showed a lot of deformation due to a good load transfer at the epoxy/PCL interface. It can also be seen that the morphology of the nanofibres is in between a complete dissolution (as observed during a single curing step at 80 °C) and the non-dissolved morphology (as observed during a single curing step at low temperature). A nanofibrous morphology is obtained with a diffuse PCL-epoxy blend interface.

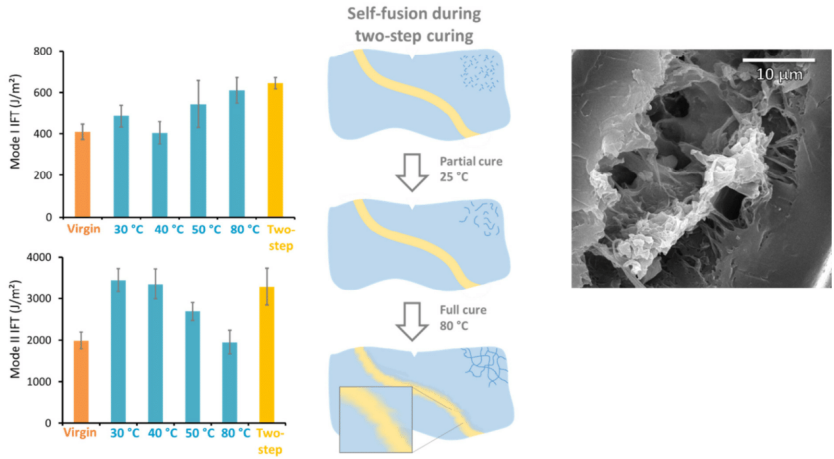

Figure 8: Using a two-step curing cycle results in good improvements of both Mode I and Mode II interlaminar fracture toughness.

2.4.2. *Core-shell structured nanofibres*

Another interesting approach to obtain good bonding and maintain the nanofibre morphology is the use of electrospun core-shell nanofibres. The technique of coaxial electrospinning allows the production of core-shell structured nanofibres for which there is a wide variety in core and shell polymer possible. Apart from the requirement of a coaxial needle, this technique does not differ that much from regular electrospinning and is thus also capable of producing nanofibrous veils for nano-engineered composites. By selecting a polymer that is not (or very little) affected by the self-fusion mechanism and a polymer capable of self-fusing with the epoxy resin, the morphology and bond strength can be tuned at the same time. Hence, the core and shell of the nanofibres can consist of different polymers, or even the same polymer type but with different molecular weights which have different dissolution rates.

The coaxial electrospinning technique is used to produce 70/30 m% PA 6/PCL core-shell nanofibres. Previous research has indicated that PA 6 nanofibres maintain their morphology at common curing temperatures ($T_{m,PA6}$ = 220 °C) and are a good choice to nano-engineer composite laminates for increased toughness and maintain their morphology for common curing temperatures.[18,32] However, the adhesion of PA 6 nanofibres with the epoxy matrix can be a limiting factor resulting in only low improvements under Mode I delamination loading.[4,18] The PCL shell which surrounds the PA 6 nanofibres will bond with the epoxy matrix due to the self-fusion mechanism. It is expected that there will also be some interdiffusion, and thus adhesion, between the PA 6 core and PCL shell as both solutions are spun from the same solvent and come into contact in the coaxial needle. The specimens were made similar to the single component nanofibre interleaved composites with a single curing step at 80 °C to have a high conversion of the epoxy resin and limiting the curing time.

The Mode I and Mode II interlaminar fracture toughness values of reference laminates and hybrid laminates containing PCL nanofibres, PA 6 nanofibres or PA 6/PCL core-shell nanofibres are shown in **Figure 9**. All specimens underwent the same curing conditions and had the same amount of nanofibres inside. Compared to the single component nanofibre systems, the core-shell structured nanofibres result in toughness improvements under both Mode I and Mode II loading conditions. This indicates that the bonding is improved due to the PCL shell, while the nanofibre morphology remains due to the PA 6 core which is hardly affected by the temperature or the epoxy resin. Analysis of the fracture surface with SEM indeed shows clearly distinguishable nanofibres which bridge cracks without much debonding/peeling of the nanofibres.

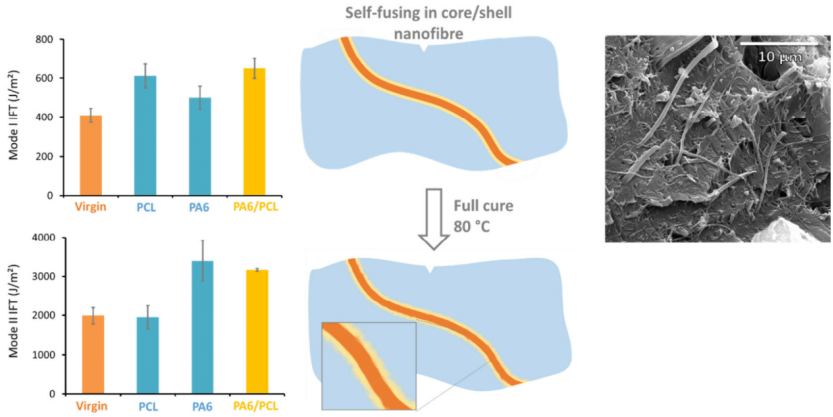

Figure 9: Self-fusion with PA6/PCL core/shell nanofibres results in a synergetic effect between bond strength and nanofibre morphology. The core/shell nanofibre based hybrid laminates have a better delamination resistance under both loading conditions than by using single component nanofibres.

3. Conclusions

This article describes a method to obtain good interfacial bonding between two polymers which is based on molecular interdiffusion during curing of one of both polymers. More specifically, a PCL/epoxy system was analysed. The mechanism is first illustrated using simple tensile specimens with a controlled interface. It was found that increasing the cure temperature caused an increased interfacial bond strength. At temperatures equal to or above the melting point of PCL, the bond strength exceeded the bulk PCL strength and specimens failed by bulk PCL failure. These tests proved that the cure-induced self-fusion mechanism can result in sufficient molecular mixing near the polymers' interface which increases the interfacial bond strength substantially.

The self-fusion is applied to nano-engineered fibre reinforced polymer composites to increase their delamination resistance. The nanofibres are interleaved within the glass fibre plies to produce hybrid composite laminates. Previous work has shown that the nanofibres will bridge microcracks and subsequently stretch and fail which absorbs energy which increases the delamination resistance of the composites. However, under Mode I loading, the nanofibers are subjected to peeling forces and the interfacial bond strength becomes a limiting factor for improving the delamination resistance. The results described in this article show that good bonding between the nanofibres and the resin is indeed essential to improve the Mode I delamination resistance significantly. In line with the tensile specimens, increasing the curing temperature of the hybrid laminates increased their Mode I interlaminar fracture toughness. Analysis of the fracture surfaces with SEM indicated a better bonding at higher temperatures, but at the same time, the nanofibre morphology disappeared due to complete dissolution into the epoxy. Under Mode II loading, the nanofibres do not experience peeling forces, but rather shearing and stretching forces. As such, the bond strength becomes less important compared to Mode I loading. However, the results showed a trend for the Mode II interlaminar fracture toughness which was opposite to the one found under Mode I loading. It indicated a strong

dependence of the Mode II interlaminar fracture toughness on the nanofibrous morphology: a decrease in delamination resistance with increasing curing temperature due to dissolution of the nanofibres at elevated temperature.

Next, two concepts were introduced which allowed to tune the bond strength and nanofibre morphology to obtain hybrid laminates with both improved Mode I and Mode II delamination resistance. One concept is based on the use of multiple curing steps. The first curing step is performed at relatively low temperature until the resin is partially cured to fix the nanofibre morphology. A second curing step at higher temperature is then performed in order to have sufficient molecular diffusion at the PCL/epoxy interface which increases the bond strength. The other concept is based on the use of coaxially electrospun core/shell structured nanofibres. A PA6 core – which is not affected by the epoxy resin or high curing temperatures – was selected and spun with PCL as shell material. Both concepts resulted in strong improvement of both the Mode I and Mode II interlaminar fracture toughness of the hybrid laminates at the same time.

The results presented in this article show the importance of the bonding between nanofibres and a polymer matrix to have better load transfer to the nanofibres. This is important when one wants to produce novel nanocomposites in which the nanofibres have a mechanical purpose such as damage resistance. Furthermore, they showed the importance of both interfacial bond strength and nanofibrous morphology on the delamination resistance of nano-engineered hybrid composite laminates.

4. Materials and methods

Double butt-jointed tension test. The double butt-jointed tensile specimens were produced as illustrated in Figure 2 and consisted of a short PCL beam bonded at both sides with epoxy. The narrow section of the dogbone had dimensions of 50 x 10 mm². PCL (Sigma-Aldrich, M_N 80 000) is allowed to melt at 90 °C and casted as a short beam (nominal length 20 mm, nominal thickness 7 mm) into a silicone dogbone mould. The mould is then air-cooled by placing it in an acclimatized environment of 23 °C and 50% RH. When the PCL is solidified, the silicone spacers are removed and epoxy resin is casted at both ends of the mould. The epoxy resin (EPIKOTE MGS RIMR135) and hardener (EPIKURE MGS RIMH137) were first mixed in a 100:30 mass ratio as recommended by the manufacturer using a mechanical stirrer and then placed under vacuum for 15 minutes in order to remove any trapped air introduced during mixing. The mould is then cured at a fixed temperature in an oven. Dummy specimens were used in order to monitor the temperature inside the epoxy resin with a thermocouple. After curing, the specimens are carefully demoulded and tested for their tensile strength. An Instron 3369 tensile machine was used with wedge grips and a load cell of 2 kN. The tensile test was displacement controlled at a ratio of 1 mm/min. The maximum stress was calculated by dividing the maximum force by the surface area of the failed interface in the case of bond failure, or by the cross-section of the PCL block in the case of bulk failure.

Nanofiber veil preparation. PCL (Sigma-Aldrich, M_N 80 000) and PA6 nanofibres (Sigma-Aldrich, M_W 51 000 g/mol) were electrospun from a formic acid (FA, Sigma-Aldrich, 98%) / acetic acid (AA, Sigma-Aldrich, 98%) solution according to previously reported procedures[33,34]. The electrospinning was performed on an in-house developed multinozzle electrospinning machine[35]. The PCL and PA6 nanofibers had average diameters of 345 ± 150 nm and 195 ± 35 nm respectively. Using a coaxial electrospinning nozzle (Raméhart Custom Needle, 100-10-COAXIAL-2016, outer needle: 1.7 mm OD, inner needle: 0.9 mm OD), core-shell nanofibres were produced with a PA6 core and PCL shell. Two pumps (KD Scientific Pump Series 100) were used to feed the core (18 wt% PA6 in 50/50 FA/AA) and shell (8 wt% PCL in 50/50 FA/AA) solutions, respectively. A high voltage power supply (Glassman High Voltage Series) was used to apply high voltage to the outer needle. The tip to collector distance (TCD), the flow rates (FR) of the solutions and the voltage were

adjusted to obtain stable electrospinning and uniform coaxial nanofibers (TCD = 80 mm, V = 30 kV). The nanofibres had a diameter of 235 ± 30 nm. The core/shell morphology was validated by dissolving the PCL shell with anisole after which the nanofibres were again analysed with SEM. All nanofibrous veils were directly electrospun onto the glass fibre mats with an areal density between 5 – 6 g/m². Representative SEM images of the nanofibres can be found in **Figure 10**.

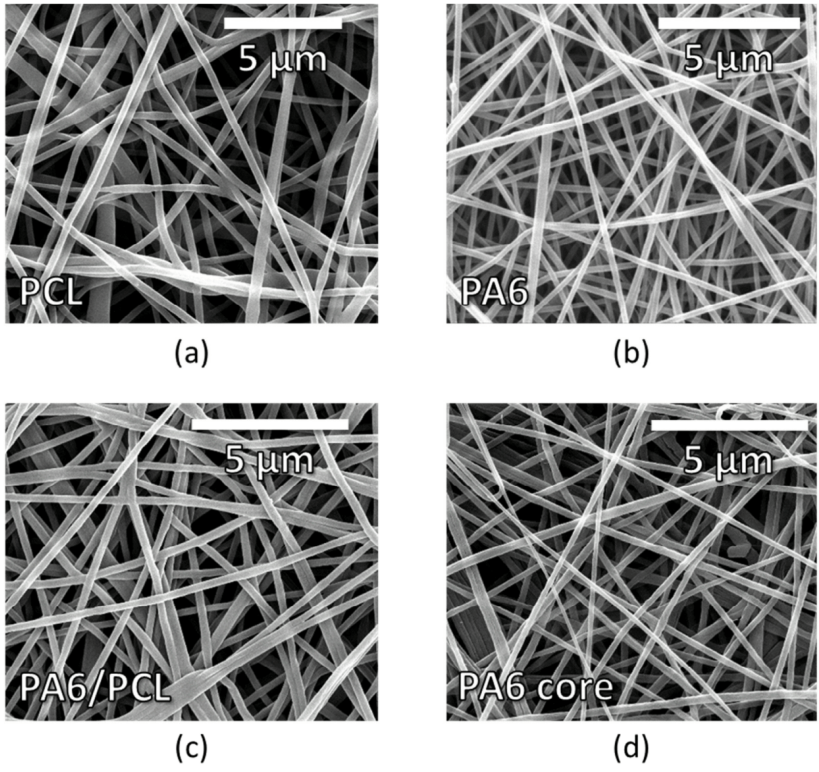

Figure 10: Representative SEM images of PCL (a), PA6 (b) and core/shell structured PA6/PCL nanofibres (c). The core structure is visualized in (d) after dissolving the PCL shell with anisole.

(Hybrid) composite laminate production. Unidirectional $[0°]_8$ glass fibre reinforced (UDO ES500) composite laminates were produced by Vacuum Assisted Resin Transfer Moulding according to a previously reported procedure.[36] For the hybrid laminates, the two middle plies consisted of a glass fibre ply with nanofibres spun on them (either PCL, PA6 or PA6/PCL) facing the midplane. The laminates had a nominal thickness of 3 mm. The Mode I and Mode II interlaminar fracture toughness were determined by Double Cantilever Beam[37] and End Notched Flexure[38,39] tests accordingly.

Fracture surface analysis. A Jeol Quanta 200F Field Emission Gun SEM, a Phenom ProX SEM and an Olympus BX51 optical microscope were used to examine the fracture surface of the tested specimens.

5. Acknowledgements

Financial support from the Agency for Innovation by Science and Technology of Flanders (IWT) and the Special Research Fund (BOF) Ghent University is gratefully acknowledged. Results in this paper were obtained within the framework of the IWT Strategic Basic Research Grant 141344 and the BOF 13/24J/020 project. Nuray Kizildag would like to thank The Scientific and Technological Research Council of Turkey (TUBITAK) for the scholarship (2214-A/1059B141500560) for her research study at Ghent University.

6. Bibliography

[1] U. Khan, P. May, A. O'Neill, A. P. Bell, E. Boussac, A. Martin, J. Semple, J. N. Coleman, Y. K. Gun'ko, W. J. Blau, J. Chen, J. Z. Wang, A. I. Minett, V. Nicolosi, J. N. Coleman, G. T. Kim, G. S. Duesberg, T. Hallam, J. J. Boland, J. J. Wang, J. F. Donegan, J. C. Grunlan, G. Moriarty, A. Shmeliov, R. J. Nicholls, J. M. Perkins, E. M. Grieveson, K. Theuwissen, D. W. McComb, P. D. Nellist, V. Nicolosi, *Nanoscale* **2013**, *5*, 581.

[2] H. Yang, L. Ye, J. Gong, M. Li, Z. Jiang, X. Wen, H. Chen, N. Tian, T. Tang, W. J. Blau, R. Harris, J. Douglas, *Mater. Chem. Front.* **2017**, *54*, 3524.

[3] F. Yavari, M. A. Rafiee, J. Rafiee, Z.-Z. Yu, N. Koratkar, *ACS applied materials & interfaces* **2010**, *2*, 2738.

[4] L. Daelemans, S. van der Heijden, I. De Baere, H. Rahier, W. Van Paepegem, K. De Clerck, *ACS applied materials & interfaces* **2016**, DOI 10.1021/acsami.6b02247.

[5] Q. Cheng, B. Wang, C. Zhang, Z. Liang, *Small* **2010**, *6*, 763.

[6] Q. Zhang, J.-Q. Huang, W.-Z. Qian, Y.-Y. Zhang, F. Wei, *Small* **2013**, *9*, 1237.

[7] L. Persano, A. Camposeo, C. Tekmen, D. Pisignano, *Macromolecular Materials and Engineering* **2013**, *298*, 504.

[8] A. Greiner, J. H. Wendorff, *Angewandte Chemie International Edition* **2007**, *46*, 5670.

[9] B. Lu, Y. Wang, Y. Liu, H. Duan, J. Zhou, Z. Zhang, Y. Wang, X. Li, W. Wang, W. Lan, E. Xie, *Small* **2010**, *6*, 1612.

[10] K. Bilge, E. Ozden-Yenigun, E. Simsek, Y. Z. Menceloglu, M. Papila, *Composites Science and Technology* **2012**, *72*, 1639.

[11] H. Yano, J. Sugiyama, A. N. Nakagaito, M. Nogi, T. Matsuura, M. Hikita, K. Handa, *Advanced Materials* **2005**, *17*, 153.

[12] R. Neppalli, C. Marega, A. Marigo, M. P. Bajgai, H. Y. Kim, V. Causin, *Polymer* **2011**, *52*, 4054.

[13] Z.-M. Huang, Y.-Z. Zhang, M. Kotaki, S. Ramakrishna, *Composites Science and Technology* **2003**, *63*, 2223.

[14] A. Romo-Uribe, L. Arizmendi, M. E. Romero-Guzmán, S. Sepúlveda-Guzmán, R. Cruz-Silva, *ACS Applied Materials & Interfaces* **2009**, *1*, 2502.

[15] L. Daelemans, S. van der Heijden, I. De Baere, H. Rahier, W. Van Paepegem, K. De Clerck, *Composites Part A: Applied Science and Manufacturing* **2017**, *94*, 10.

[16] Y. Dzenis, *Science* **2008**, *319*, 419.

[17] K. Bilge, S. Venkataraman, Y. Z. Menceloglu, M. Papila, *Composites Part A: Applied Science and Manufacturing* **2014**, *58*, 73.

[18] L. Daelemans, S. van der Heijden, I. De Baere, H. Rahier, W. Van Paepegem, K. De Clerck, *Composites Science and Technology* **2015**, *117*, 244.

[19] G. W. Beckermann, K. L. Pickering, *Composites Part A: Applied Science and Manufacturing* **2015**, *72*, 11.

[20] S. Hamer, H. Leibovich, A. Green, R. Avrahami, E. Zussman, A. Siegmann, D. Sherman, *Composites Science and Technology* **2014**, *90*, 48.

[21] H. Saghafi, A. Zucchelli, R. Palazzetti, G. Minak, *Composite Structures* **2014**, *109*, 41.

[22] E. Özden, Y. Z. Menceloğlu, M. Papila, *ACS Applied Materials & Interfaces* **2010**, *2*, 1788.

[23] E. Özden-Yenigün, Y. Z. Menceloğlu, M. Papila, *ACS Applied Materials & Interfaces* **2012**, *4*, 777.

[24] J. Zhang, T. Yang, T. Lin, C. H. Wang, *Composites Science and Technology* **2012**, *72*, 256.

[25] A. Cohades, E. Manfredi, C. J. G. Plummer, V. Michaud, *European Polymer Journal* **2016**, *81*, 114.

[26] X. Luo, R. Ou, D. E. Eberly, A. Singhal, W. Viratyaporn, P. T. Mather, *ACS Applied Materials & Interfaces* **2009**, *1*, 612.

[27] P. M. Remiro, M. M. Cortazar, M. E. Calahorra, M. M. Calafel, *Macromolecular Chemistry and Physics* **2001**, *202*, 1077.

[28] J. Rotrekl, L. Matějka, L. Kaprálková, A. Zhigunov, J. Hromádková, I. Kelnar, *Express Polymer Letters* **2012**, DOI 10.3144/expresspolymlett.2012.103.

[29] J.-L. Chen, F.-C. Chang, *Macromolecules* **1999**, *32*, 5348.

[30] K. Allaer, I. De Baere, W. Van Paepegem, J. Degrieck, *Polymer Testing* **2015**, *42*, 199.

[31] J. F. Najem, S.-C. Wong, G. Ji, *Langmuir : the ACS journal of surfaces and colloids* **2014**, *30*, 10410.

[32] L. Daelemans, S. van der Heijden, I. De Baere, H. Rahier, W. Van Paepegem, K. De Clerck, *Composites Science and Technology* **2015**, *124*, 17.

[33] L. Van der Schueren, B. De Schoenmaker, Ö. I. Kalaoglu, K. De Clerck, *European Polymer Journal* **2011**, *47*, 1256.

[34] B. De Schoenmaker, S. Van der Heijden, I. De Baere, W. Van Paepegem, K. De Clerck, *Polymer Testing* **2013**, *32*, 1495.

[35] P. Westbroek, T. Van Camp, S. De Vrieze, K. De Clerck, **2008**.

[36] S. van der Heijden, L. Daelemans, B. De Schoenmaker, I. De Baere, H. Rahier, W. Van Paepegem, K. De Clerck, *Composites Science and Technology* **2014**, *104*, 66.

[37] "ASTM Standard D5528, Standard Test Method for Mode I Interlaminar Fracture Toughness of Unidirectional Fiber Reinforced Polymer Matrix Composites," DOI 10.1520/D5528can be found under www.astm.org, **2013**.

[38] "ASTM Standard D7905-14, Standard Test Method for Determination of the Mode II Interlaminar Fracture Toughness of Unidirectional Fiber-Reinforced Polymer Matrix Composites," DOI 10.1520/D7905_D7905M-14, **2014**.

[39] A. Arrese, N. Carbajal, G. Vargas, F. Mujika, *Engineering Fracture Mechanics* **2010**, *77*, 51.

PAPER VII

NOVEL COMPOSITE MATERIALS WITH TUNABLE DELAMINATION RESISTANCE USING FUNCTIONALIZABLE ELECTROSPUN SBS FIBERS

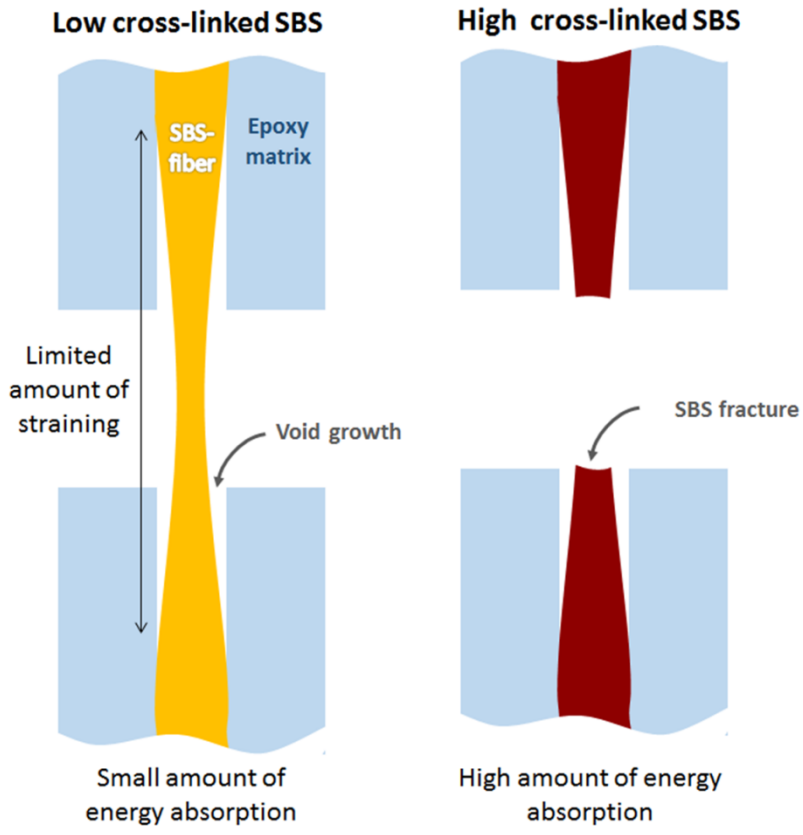

Sam van der Heijden, Lode Daelemans, Kevin De Bruycker, Robin Simal, Ives De Baere, Wim Van Paepegem, Hubert Rahier and Karen De Clerck

(2017) *COMPOSITE STRUCTURES*. 159. p.12-20

Composite Structures 159 (2017) 12–20

Contents lists available at ScienceDirect

Composite Structures

journal homepage: www.elsevier.com/locate/compstruct

Novel composite materials with tunable delamination resistance using functionalizable electrospun SBS fibers

Sam van der Heijden [a], Lode Daelemans [a], Kevin De Bruycker [d], Robin Simal [a], Ives De Baere [b], Wim Van Paepegem [b], Hubert Rahier [c], Karen De Clerck [a,*]

[a] Department of Textiles, Ghent University, Technologiepark-Zwijnaarde 907, B-9052 Zwijnaarde, Belgium
[b] Department of Materials Science and Engineering, Ghent University, Technologiepark-Zwijnaarde 903, B-9052 Zwijnaarde, Belgium
[c] Department of Materials and Chemistry, Vrije Universiteit Brussel, Pleinlaan 2, B-1050 Brussels, Belgium
[d] Department of Organic and Macromolecular Chemistry, Polymer Chemistry Research Group, Ghent University, Krijgslaan 281 S4-bis, B-9000 Ghent, Belgium

ARTICLE INFO

Article history:
Received 24 May 2016
Revised 9 August 2016
Accepted 19 September 2016
Available online 20 September 2016

Keywords:
Nano composites
Resin transfer molding (RTM)
Delamination
SBS
Electrospinning

ABSTRACT

Electrospun fibers have shown great potential for the interlaminar toughening. In this work, electrospun SBS fibers were incorporated into glass epoxy laminates. The mechanical properties of these SBS fibers are tuned using a triazolinedione cross-linker, where a higher amount of cross-linking gives rise to a lower elongation at break and a higher stiffness of the SBS fibers. Consequently, insights are provided into the relation between mechanical properties of electrospun fibers and enhancements in both Mode I and Mode II interlaminar fracture toughness. The SBS fiber's mechanical properties affect the crack path in composites. Non and low cross-linked SBS fibers which have a very low stiffness promote crack growth with SBS fiber bridging under both Mode I and Mode II loading conditions. However, these SBS fibers need to elongate substantially in order to take up a significant amount energy (>300%). As this only occurs under Mode I loading conditions, the Mode I interlaminar fracture toughness can be improved. Nevertheless, the Mode II IFT is negatively affected. Higher cross-linked SBS fibers on the other hand, do take up more energy at much lower levels of elongation. As such, they can improve the Mode II interlaminar fracture toughness substantially.

1. Introduction

Today, fiber reinforced polymer composites are a standard material in applications where a high stiffness and strength are required at minimal weight, such as aerospace structures, ultra-light vehicles, or even flywheels for highly efficient power storage systems. Although fiber reinforced polymer composites show many advantages compared to other materials, delamination between reinforcing plies remains a major problem limiting further breakthrough. These delaminations are usually due to Mode I and Mode II loading conditions of cracks which are frequently encountered during realistic loading conditions such as impact or fatigue. Recently, the use of electrospun nanofibers has been proposed to toughen composites and prevent such delaminations [1–4]. Such nanofibrous nonwovens can easily be placed between two reinforcing plies prior to composite production, furthermore, the high porosity of the nanofibrous nonwovens allows for easy impregnations with epoxy or even thermoplastic matrix materials [5]. This will automatically result in a homogenous distribution of thermoplastic phases (nanofibers) surrounded by epoxy, unlike most traditional toughening systems which rely on a complex reaction-induced phase separation process in order to obtain such a homogenous distribution of microscopic rubber/thermoplastic phases [6,7].

As such there is also no need to disperse the nanofibers into the matrix resin as opposed to (functionalized) nanoparticles [8–12] or epoxies modified with reactive rubbers/thermoplastic materials.

This is a major advantage for infusion applications, since mixing in any particle or thermoplastic material generally causes a large increase in viscosity, thus limiting the quality of the produced composite parts.

In our previous work we have shown that for a nanotoughened epoxy resin, yielding of nanofibers in the fracture processing zone as well as nanofiber bridging increase the fracture toughness substantially. On a laminate level (glass epoxy laminates with nanofibers in the interlaminar regions), the fracture toughness of nanofiber toughened laminates is influenced by the crack path of the interlaminar cracks. More specifically, it was shown that crossings of the interlaminar region are the main contributors to the

* Corresponding author.
E-mail address: Karen.DeClerck@ugent.be (K. De Clerck).

http://dx.doi.org/10.1016/j.compstruct.2016.09.057
0263-8223/

increase in interlaminar fracture toughness as nanofiber bridging zones develop in them. The amount of these interlaminar crossings can depend on numerous parameters such as the delamination mode and the nanofibrous veil areal density [13]

In this paper we study the effect of the mechanical properties of the electrospun fibers on the resulting interlaminar fracture toughness of composites containing electrospun fibrous veils. By a change in the fibers' mechanical properties, the energy absorption during crack bridging and the crack path behavior (occurrence of interlaminar crossings) can be affected. It should be pointed out that a relatively diverse set of polymer nanofibers has already been studied in literature for the interlaminar toughening of composites. Examples include polysulfones (PSU), PEK-C, poly(ε-caprolactone) (PCL), polyamides (PA), poly(vinylidene fluoride) (PVDF), polyacrylonitrile (PAN), polyamide-imide (PAI), poly(styrene-*co*-glycidyl methacrylate), and polyvinyl butyral (PVB), Poly(vinyl alcohol) (PVA) [14–18,3,19–27]. Although all these polymers have different mechanical properties, ranging from rubbery materials such as PVB to more stiff materials such as PA and PAN, they are also very different from a chemical point of view. Hence, this difference in chemical structure will also affect other properties such as the fiber-matrix adhesion. As a such it is hard to relate the interlaminar fracture toughness of the laminates toughened using various types of electrospun nanofibers directly to the mechanical properties of the specific nanofibers. Nevertheless, this link between the electrospun fiber properties and the resulting interlaminar fracture toughness of a composite containing these electrospun fibers is crucial for designing optimal damage resistant materials.

Recently, we have shown that styrene-butadienestyrene (SBS) triblock copolymers are excellent candidates to produce tunable electrospun fibers [28]. The mechanical properties of these SBS fibers can be tuned using a post-cross-linking reaction. This cross-linking is obtained by reacting the unsaturated bonds in the butadiene segments of SBS with a bifunctional triazolinedione (TAD), i.e. 4,4′-(4,4″-diphenylmethylene)-bis-(1,2,4-triazoline-3,5-dione) (MDI-TAD), in an Alder-ene reaction (Fig. 1)[29–35].

Using the TAD-based modification, chemical cross-links are introduced into the SBS fibers, thereby allowing the mechanical properties of the SBS to be modified from an extremely ductile rubbery material, to a glassy and stiffer material. Thus allowing to report on the relation between the tunable mechanical properties of the electrospun SBS fibers and their ability to improve the interlaminar toughness of glass fiber reinforced epoxy laminates. The SBS fiber properties will be linked to the behavior of the laminates under both Mode II and Mode I loading conditions, contributing to an in-depth understanding of the mechanisms involved in toughening of epoxy based composite laminates and as such allows for designing novel, damage resistant, nanofiber toughened materials.

2. Materials and methods

2.1. Materials

The styrene butadiene styrene (SBS) copolymer Kraton D1101 was kindly supplied by Kraton Polymers LLC. Butyl acetate (99.5%) and LiBr (99%) were obtained from Sigma-Aldrich. The MDI-TAD cross-linker is prepared in three steps according to a previously reported procedure [30].

All composite laminates were reinforced with unidirectional E-glass fabric with an areal density of 500 g/m^2, UDO ES500 manufactured by SGL Group. The epoxy resin was composed of EPIKOTE resin MGS RIMR 135 with EPIKURE curing agent MGS RIMH 137 (Momentive).

2.2. Electrospinning

In our previous work, the electrospinning process of SBS from a butyl acetate solution was optimized using a design of experiments. Butyl acetate was selected as an alternative solvent as the use of carcinogenic and reprotoxic solvents such as DMF is under debate [36]. MDI-TAD and LiBr were added to an SBS solution in butyl acetate in order to increase the amount of polymer entanglements and the conductivity of the electrospinning solution respectively. The optimal electrospinning solution, giving rise to SBS fibers with a diameter of 2 μm and no beads, contained 13 wt% of SBS, 0.45 wt% MDI-TAD (relative to SBS weight) and 0.013 g/ml LiBr [28]. These parameters were also used for the production of the SBS membranes in this paper. All fibers were electrospun using an in-house developed electrospinning machine with a rotating drum collector. In this electrospinning set-up, the electrospinning needle moves at a constant speed of 0.15 m/s parallel to the drum with a tip-to-collector distance of 20 cm, while the flow rate was set at 1.25 ml/h. The voltage was set between 15 and 25 kV until a stable Taylor cone was attained. The drum has a diameter of 100 mm, a total width of 40 cm and can rotate at speeds going from 0 rpm up to 4000 rpm to allow for the production of both random (150 rpm) and aligned (4000 rpm) fibers. For the toughening of glass epoxy composites, randomly deposited fibers with a diameter of 2 ± 0.5 μm were used as presented in Fig. 2.

2.3. Mechanical characterization of electrospun SBS fibers

All fiber tensile properties were measured on aligned electrospun SBS fibers. These tensile tests were carried out on a Statimat tensile testing machine in accordance to ASTM D 882, an image of this test setup can be found in the Supplementary information. All samples were conditioned and tested at 20 ± 2 °C and 65 ± 4% relative humidity. The samples had a width of 5 mm, while the gauge

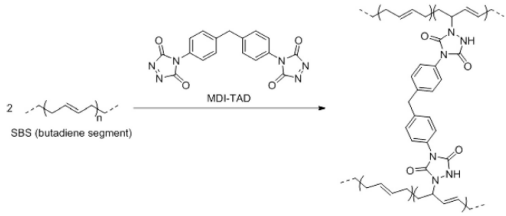

Fig. 1. Cross-linking of butadiene segments in SBS via Alder-ene reactions with MDI-TAD.

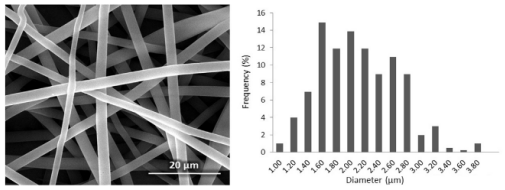

Fig. 2. Representative SEM image and diameter distribution of electrospun SBS fibers.

length was fixed on 50 mm. The cross-sectional area of the samples was estimated by measuring the mass of the rectangular samples over a length of 200 mm and dividing it by the sample length and the density of the SBS, hereby assuming a constant SBS density of 0.94 g/cm^3. The cross-head speed was adjusted to 1250 or 50 mm/min, depending on the elongation at break in a pre-test. At least 5 samples were tested for each sample type.

2.4. TAD post-cross-linking

Post-cross-linking of the SBS fibers was carried out by submerging an electrospun membrane into a solution of MDI-TAD in acetone (0.018 mol/L). The electrospun nonwovens were immersed into the reactive solution for prolonged times, ranging from 10 to 180 min, in order to create nonwovens with an increasing extent of cross-linking. Next, the nonwovens were rinsed with acetone to remove any unreacted compounds after which they were dried at ambient conditions for at least 24 h.

2.5. Laminate production

The composite laminates were manufactured by vacuum assisted resin transfer molding (VARTM). The glass fiber mats were stacked in a $[0^\circ]_8$ configuration into a steel mold. All laminates had a total thickness of 3 ± 0.1 mm. Electrospun SBS nonwovens as well as a crack initiation film were placed in the middle interlaminar region between the two middle reinforcing glass fiber plies. After infusion, the laminates were cured at room temperature for 24 h, followed by a post-cure at 80 °C for 15 h according to the manufacturer's recommended cure cycle.

2.6. End notched flexure experiments

The Mode II interlaminar fracture toughness (G_{IIc}) of the laminates was determined by End Notched Flexure experiments. The ENF experiments consist out of three-point bending experiments on specimens (140 × 20 mm) with an initial delamination a_0 of 40 mm (produced by the initiation film) and a span length of 100 mm. The experiment was displacement controlled and the crosshead movement was set to 1 mm/min. The G_{IIc} values were determined according to the Compliance-Based Beam Method [37–39]:

$$G_{IIc} = \frac{9Pmax^2 a_{eq}^2}{16b^2 E_f h^3} \quad (1)$$

where: *Pmax* is the maximum load, a_{eq} is a corrected delamination length, b is the width, E_f is the flexural modulus and h is the thickness. At least three specimens were tested for each configuration.

2.7. Double cantilever beam experiments

The Mode I interlaminar fracture toughness (G_{Ic}) of the laminates was determined using the Double Cantilever Beam (DCB) method according to ASTM D5528. An Instron 5800R machine equipped with a load cell of 500 N was used. G_{Ic} was determined as follows:

$$G_I = \frac{3P\delta}{2b(a + |\Delta|)} F \quad (2)$$

where: P is the load, δ is the displacement, b is the width, a is the delamination length, $|\Delta|$ corrects for crack front rotations and F corrects for large displacement effects. The DCB-specimens were opened at 3 mm/min and the crack front propagation was followed by a travelling microscope. The load was introduced to the specimens by piano hinges. A natural Mode I precrack of 3 mm was introduced in the samples after which the sample was unloaded and tested again. The $G_{Ic,ini}$ value was determined from the 5%/max point on the load–displacement curves [40]. The specimens were cut 150 mm by 20 mm and had a thickness of 3 mm. An initial delamination of 50 mm was used. At least three specimens were tested for each configuration.

3. Results and discussion

3.1. Effect of MDI-TAD cross-linker on tensile properties of SBS fibers

Fig. 3 illustrates the tunability of the mechanical properties of the SBS fibers as reported in our previous work [28]. These values were obtained from tensile experiments on unidirectional bundles of electrospun SBS fibers. The unmodified and low cross-linked SBS fibers have a low E-modulus and high elongation at break, around 10–30 MPa and 400–600% respectively. The highly cross-linked samples, on the other hand, have a higher E-modulus but lower elongations at break up to 140 MPa and 100% respectively. In addition, careful SEM analysis reported in our previous work showed that the fiber diameter after cross-linking was 2.1 ± 0.5 µm. As such, the post cross-linking procedure has no significant effect on the SBS fiber diameter or morphology [28].

Fig. 4 shows the work needed to introduce a certain percentage of elongation into these fibers, derived from the area underneath their stress–strain curves. The energy uptake of unmodified and low cross-linked SBS fibers only becomes significant when the SBS fibers are elongated up to high strains (>300%), whereas in the low strain region (<100%) their energy uptake is very limited. For the SBS fibers with relatively high amounts of cross-linking, the total work of rupture (10–15 MPa) is lower, but these fibers do absorb significantly more energy in the low strain region.

By incorporating SBS fibrous veils with different amounts of cross-linking in composites, the mechanical properties of these

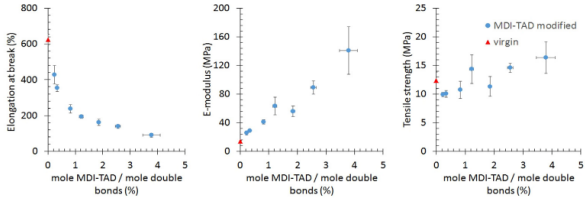

Fig. 3. Tensile properties of (aligned) SBS fibers as a function of the molar ratio of MDI-TAD cross-linker to the total SBS double bonds (i.e. a measure for the amount of cross-links) showing a reduction in elongation at break and an increase in E-modulus with an increasing extent of cross-linking, while the tensile strength remains relatively independent on the degree of cross-linking [28].

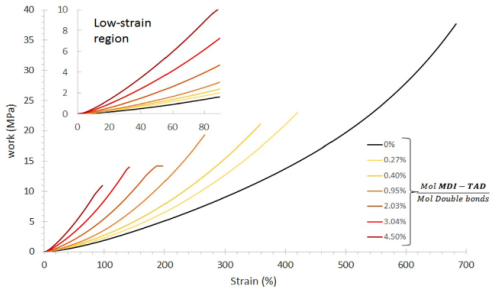

Fig. 4. The work needed to introduce a certain percentage of elongation for different amounts of cross-links (as expressed by molar ratio of MDI-TAD cross-linker to the total SBS double bonds).

cross-linked SBS fibers can now be linked to their effect on the interlaminar fracture toughness.

3.2. Effect of the mechanical properties of the SBS fibers on the interlaminar fracture toughness and the mechanism of electrospun fiber bridging

As mentioned in our previous work, the toughening mechanism of electrospun fibers consists out of fibers which bridge crack halves in the damaged epoxy resin in the interlaminar region. There are two main mechanism acting in these fibers, straining of the fibers and deboning of the fiber epoxy interface, both of which can occur simultaneously.

As mentioned in Section 3.1, the strain till break as well as the energy absorption for a particular amount of straining of the SBS fibers depends heavily on the degree of cross-linking. If only a limited amount of straining occurs, the low-cross-linked fibers will not break and will only absorb a small amount of energy. The high cross-linked SBS fibers on the other hand will be able to absorb more energy, in this low strain region. This is schematically illustrated in Fig. 5 where the SBS fiber bridging effect is shown during (tensile) matrix failure. Although this representation is rather simple as it assumes that the matrix cracks propagate perpendicular to the electrospun fibers, previous research has shown that it is still suitable to explain the observations made on tested DCB and ENF nanofiber interleaved specimens [13]. As the failure strain of the epoxy is much lower than that of the SBS fibers, the epoxy is likely to crack first, subsequently resulting in a separation of the crack surfaces which in turn causes the SBS fibers to elongate.

SBS fiber matrix debonding can limit the overall strain in the SBS fibers, since the length of the non-bonded SBS fiber segments becomes higher. Thus, in order to reach a certain elongation, this requires much larger displacements than would be the case if no debonding occurred. Post mortem SEM images of interlaminar cracks (Fig. 6), show a relatively high amount of such SBS fiber matrix debonding and little or no fiber fracture of non-cross-linked SBS fibers (Fig. 6A). Hence, it is reasonable to assume that the overall straining of the SBS fibers was limited, especially in case of Mode II delaminations where the shear forces only result in a limited displacement of crack halves in a specimen.

3.2.1. Mode II interlaminar fracture toughness

Fig. 7 shows the Mode II interlaminar facture toughness of composites containing electrospun SBS fibrous veils with different amounts of cross-linking. The results indicate an increasing trend with increasing amount of cross-linking. The non-cross-linked and low cross-linked SBS fibers even decrease the interlaminar fracture toughness, implying that even less energy is required if such SBS fibers are present than if only epoxy resin was present in the interlaminar region. Since it is very likely that the SBS fibers do not strain significantly during the Mode II delamination, their low energy absorption at small elongations explains this phenomenon. In contrast, the highly cross-linked SBS fibers do absorb a lot of energy in this low-elongation regime, resulting in the

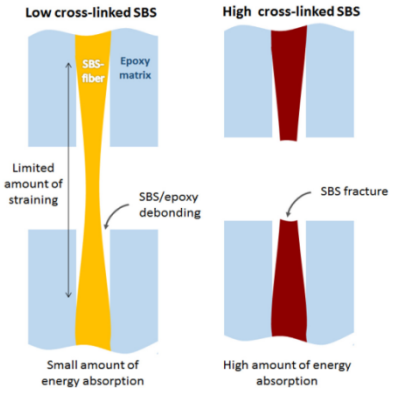

Fig. 5. Simplified representation of the fracture behavior of the SBS-fiber epoxy composite under tensile loading. The low failure strain of the epoxy compared to the SBS fibers, results in epoxy fracture and a separation of the crack surfaces which in turn causes the SBS fibers to elongate. High cross-linked SBS fibers can absorb more energy compared to low cross-linked SBS fibers when a limited amount of straining occurs in the fibers.

observed increase in fracture toughness up to 3950 ± 400 J/m^2 for the 5.45% cross-linked SBS, which is over 100% improvement as compared to the reference laminates (1900 ± 250 J/m^2).

The explanation above does not take into account a possible effect of the SBS fiber properties on the crack path in the interlaminar region. Nevertheless, it is important to also take this crack path into account since the SBS fibers can only bridge interlaminar cracks if these cracks occur in the interlaminar region. To analyze the position of the Mode II crack with respect to the SBS toughened interlayer, microscopic cross-sectional images of the tested Mode II specimens (perpendicular to the crack front) are shown in Fig. 8 (original images can be found in the Supporting information). The low cross-linked SBS fibers provide little to no resistance to the Mode II crack due to their low stiffness, causing the crack to propagate directly through the SBS/epoxy interlayer, i.e. the weakest point in the composite (Fig. 8 A and B, see Fig. 7 for coordinate system). Although this creates vast amounts of SBS fiber bridging, the SBS fibers themselves are most likely not strained to failure due to their high elongation at break, see Section 3.2.2

On the other hand, for composites containing SBS fibers with high amounts of cross-linking, propagating through the SBS modified interlayer requires a lot of energy as the SBS fibers are much stiffer, and as such, the interlayer is no longer the weakest zone in the laminate. This deflects the delamination crack towards the reinforcing plies out of the SBS toughened interlayer. Nevertheless, the shear loading stimulates the formation of interlaminar crossings (Fig. 8C and D, see Fig. 7 for coordinate system) in which SBS fiber bridging does occur. This particular fracture behavior is in line with similar to the behavior previously observed for composites containing PCL and PA nanofibers as both polymers have mechanical properties in the same order of magnitude as the high-cross-linked SBS [13].

3.2.2. Mode I interlaminar fracture toughness

Fig. 9 shows the Mode I interlaminar fracture toughness during crack initiation as a function of the amount of cross-linking of the SBS fibers Load-displacement curves as well as the interlaminar fracture toughness during propagation are included as Supplementary information. Two SBS fibrous veils with different areal densities were tested, i.e. 12 ± 1 g/m^2 as well as 22.0 ± 1.5 g/m^2. Fig. 9 shows that the laminates containing 22.0 ± 1.5 g/m^2 SBS membranes have a slightly higher $G_{Ic,ini}$. Nevertheless, the overall trend indicates that $G_{Ic,ini}$ is relatively independent on the weight of the SBS membrane for the range of areal densities tested. In contrast to the results for Mode II loading (vide supra), the virgin and low cross-linked SBS fibers do increase the Mode I interlaminar fracture toughness. This observation can be explained by the higher displacement of the two sample halves during the DCB experiments as compared to the ENF experiments which, results in a higher elongation of the electrospun SBS fibers., Hence, the Mode I opening mode increases the importance of the SBS fiber behavior at higher strain levels. Although this explains why an improvement in Mode I interlaminar fracture toughness is obtained at low amounts of cross-linking, one would not expect the improvement in Mode I interlaminar fracture toughness to be similar with that of the energy required to elongate an SBS fiber till break (Fig. 3).

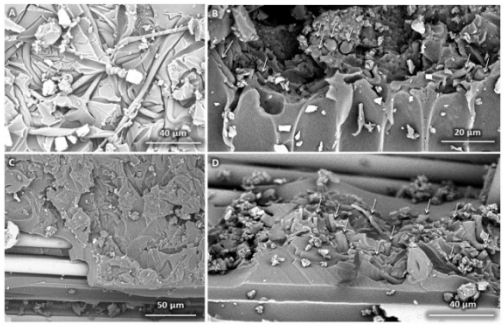

Fig. 6. Post mortem SEM images of interlaminar cracks due to Mode I loading, containing SBS fibers with different amounts of cross-linking, virgin A, 0.6% B, 0.83% C, 4.2% D.

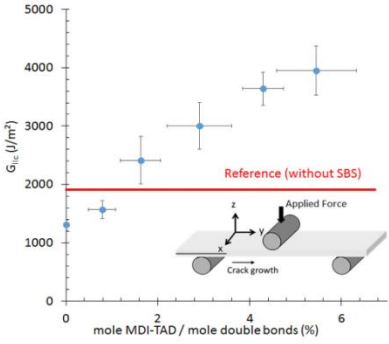

Fig. 7. The Mode II interlaminar fracture toughness for laminates interleaved with 20 g/m² of SBS fibers increases with increasing extent of cross-linking of SBS fibers (as expressed by molar ratio of MDI-TAD cross-linker to the total SBS double bonds).

However, Fig. 9 clearly reveals an optimal zone of cross-linking in which the resulting interlaminar fracture toughness is the highest.

In order to explain this phenomenon, the relationship between the mechanical properties of the SBS fiber and the crack path has to be analyzed. Previous work has already shown that the Mode I crack path is much more sensitive to changes in the electrospun fibrous veil than the Mode II delamination crack path [13]. More specifically, under Mode I loading conditions, there is a high tendency for the delamination crack to be deflected out of the toughened interlayer towards the glass fiber/epoxy interface.

Analysis of the cross section of tested Mode I specimens (Fig. 10, original images can be found in the Supporting information) reveals that the Mode I cracks again propagate directly through the SBS membrane at a low cross-linking density similar to the behavior observed under Mode II loading conditions. However, for the highly cross-linked SBS interlayers, the Mode I crack is deflected away from the toughened interlayer towards the glass fiber/epoxy interface without regular occurrences of interlaminar crossings. Consequently, almost no SBS fiber bridging can occur and $G_{Ric,ini}$ decreases to the reference level.

An intermediate amount of crosslinking, between 0.65% and 1.5%, allows for an improvement of >80% up to almost 90% in Mode I interlaminar fracture toughness. These intermediate amounts of

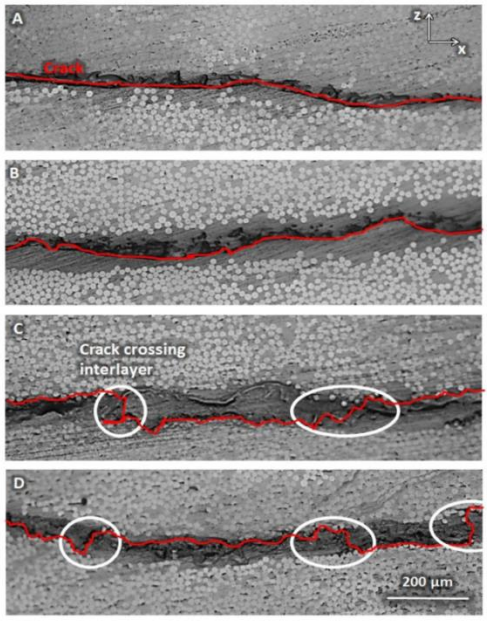

Fig. 8. Microscopic image illustrating the mode II crack (red line) propagation. For low amounts of cross-linking (virgin A, 1.25% B) the crack propagated directly through the SBS toughened interlayer. At high amounts of cross-linking (2.31% C, 3.34% D) the crack rather crosses the interlayer (white circles), see Fig. 7 for coordinate system. (For interpretation of the references to colour in this figure legend, the reader is referred to the web version of this article.)

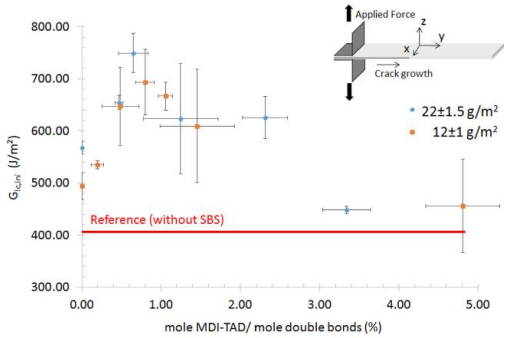

Fig. 9. Mode I fracture toughness as a function of the extent of cross-linking (as expressed by molar ratio of MDI-TAD cross-linker to the total SBS double bonds) for both laminates containing 12 g/m^2 of SBS and 22 g/m^2 of SBS in the interlayer.

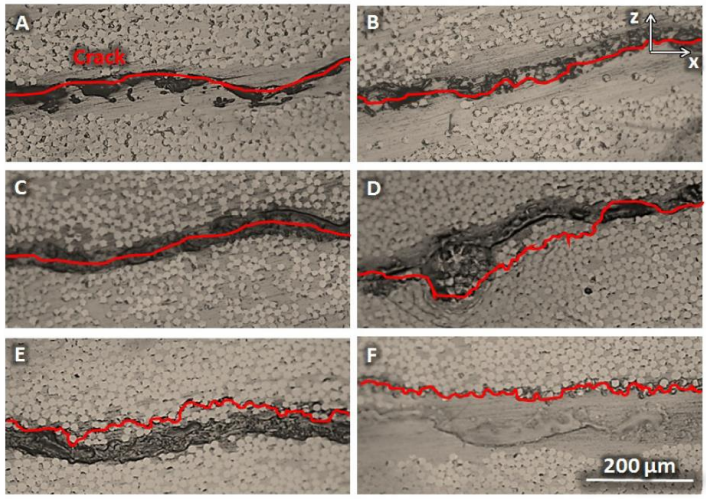

Fig. 10. Microscopic images of cross sections showing Mode I crack propagating through the SBS toughened interlayer at low amounts (A = virgin, B = 0.47%, C = 0.65%) and avoiding the interlayer for high amounts of cross-linking (D = 1.25%, E = 2.3%, F = 3.3%) see Fig. 9 for coordinate system.

cross-linking are low enough to allow the Mode I crack to propagate directly through the SBS toughed interlayer (Fig. 10 C) or at least allow for the occurrence of regular interlaminar crossings (Fig. 10 D), while it is still high enough for the SBS fibers to absorb significant amounts of energy at relatively low elongations.

4. Conclusion

In this paper, cross-linked SBS fibers were successfully embedded into resin transfer molded glass epoxy laminates in order to improve their interlaminar toughness. A homogeneous distribu-

tion of SBS phases in the epoxy interlayer was obtained, resulting in very high interlaminar fracture toughness values. A novel TAD-click chemistry allowed to modify the mechanical properties of the SBS fibers. The variation in these fiber mechanical properties, had a significant effect on both Mode II and Mode I interlaminar toughness of the glass epoxy laminates, and allowed to gain some fundamental insights into the toughening mechanisms using electrospun fibers.

SBS fibers with a low cross-linking density, characterized by high elongations at break (>300%) and low E-moduli, were demonstrated to be unsuitable for interlaminar toughening. Although these fibers have a high work of rupture, the energy absorbed when strained up to small elongations (<100%) is nearly zero. With an increasing amount of crosslinking, SBS fibers with lower elongation at break and a higher E-modulus were obtained, resulting in an increased amount of absorbed energy in the low strain region. This significantly affects the toughness of the interlayer as well as the interlaminar crack path, both in Mode II and Mode I.

For the lower cross-linking densities, the delamination crack propagates through the interlayer. The limited crack opening involved with Mode II loadings results in only low strains in the SBS fibers and thus a low energy absorption. As the amount of cross-linking is increased to intermediate amounts, the energy absorbed in the low strain region is increased. This already leads to an improvement in Mode I fracture toughness up to almost 90% (750 ± 38 J/m^2) when an intermediate amount (0.65%) of cross-linking is used. With a further increase in the extent of cross-linking the delamination crack starts to be deflected by the toughened interlayer. In Mode I this results in a decrease of the $G_{Ic,ini}$ values down to the reference level as the crack is propagating mainly in the virgin resin above the SBS rich layer. However, in Mode II, the shear forces will now promote the formation of interlaminar crossings. This results in improvements in Mode II fracture toughness of over 100%, up to a value of 3950 ± 400 J/m^2 when highly cross-linked SBS (5.45%) was used.

Acknowledgements

Financial support from The Agency for Innovation by Science and Technology of Flanders (IWT) is gratefully acknowledged. Results in this paper were obtained within the framework of the IWT Strategic Basic Research Grant 121156. Kevin De Bruycker thanks the Research Foundation-Flanders (FWO) for the funding of his fellowship.

Appendix A. Supplementary data

Supplementary data associated with this article can be found, in the online version, at http://dx.doi.org/10.1016/j.compstruct.2016.09.057.

References

[1] Papkov D, Zou Y, Andalib MN, Goponenko A, Cheng SZD, Dzenis YA. Simultaneously strong and tough ultrafine continuous nanofibers. ACS Nano 2013;7:3324–31.
[2] Kim JS, Reneker DH. Mechanical properties of composites using ultrafine electrospun fibers. Polym Compos 1999;20:124–31.
[3] van der Heijden S, Daelemans L, De Schoenmaker B, De Baere I, Rahier H, Van Paepegem W, et al. Interlaminar toughening of resin transfer moulded glass fibre epoxy laminates by polycaprolactone electrospun nanofibres. Compos Sci Technol 2014;104:66–73.
[4] Bergshoef MM, Vancso GJ. Transparent nanocomposites with ultrathin, electrospun nylon-4,6 fiber reinforcement. Adv Mater 1999;11:1362–5.
[5] Neppalli R, Marega C, Marigo A, Bajgai MP, Kim HY, Causin V. Poly(ε-caprolactone) filled with electrospun nylon fibres: a model for a facile composite fabrication. Eur Polym J 2010;46:968–76.
[6] Bascom WD, Hunston DL. Rubber-Toughened Plastics, vol. 222. Washington, DC: American Chemical Society; 1989.
[7] Bucknall C, Partridge I. Phase separation in epoxy resins containing polyethersulphone. Polymer (Guildf) 1983;24:639–44.
[8] González-Domínguez JM, Ansón-Casaos A, Díez-Pascual AM, Ashrafi B, Naffakh M, Backman D, et al. Solvent-free preparation of high-toughness epoxy-SWNT composite materials. ACS Appl Mater Interfaces 2011;3:1441–50.
[9] Yu W, Fu J, Dong X, Chen L, Jia H, Shi L. Highly populated and nearly monodispersed nanosilica particles in an organic medium and their epoxy nanocomposites. ACS Appl Mater Interfaces 2013;5:8897–906.
[10] Martinez-Rubi Y, Ashrafi B, Guan J, Kingston C, Johnston A, Simard B, et al. Toughening of epoxy matrices with reduced single-walled carbon nanotubes. ACS Appl Mater Interfaces 2011;3:2309–17.
[11] Chen L, Chai S, Liu K, Ning N, Gao J, Liu Q, et al. Enhanced epoxy/silica composites mechanical properties by introducing graphene oxide to the interface. ACS Appl Mater Interfaces 2012;4:4398–404.
[12] Kim BC, Park SW, Lee DG. Fracture toughness of the nano-particle reinforced epoxy composite. Compos Struct 2008;86:69–77.
[13] Daelemans L, van der Heijden S, De Baere I, Rahier H, Van Paepegem W, De Clerck K. Damage resistant composites using electrospun nanofibers: a multiscale analysis of the toughening mechanisms. ACS Appl Mater Interfaces 2016;8:11806–18.
[14] Daelemans L, van der Heijden S, De Baere I, Rahier H, Van Paepegem W, De Clerck K. Using aligned nanofibres for identifying the toughening micromechanisms in nanofibre interleaved laminates. Compos Sci Technol 2015.
[15] Özden-Yenigün E, Menceloğlu YZ, Papila M. MWCNTs/P(St-co-GMA) composite nanofibers of engineered interface chemistry for epoxy matrix nanocomposites. ACS Appl Mater Interfaces 2012;4:777–84.
[16] Bovicelli F, Saghafi H, Brugo TM, Belcari J, Zucchelli A, Minak G. On consideration the mode I fracture response of CFRP composite interleaved by composite nanofibers. Proc Mater Sci 2014;3:1316–21.
[17] Zhang J, Lin T, Wang X. Electrospun nanofibre toughened carbon/epoxy composites: Effects of polyetherketone cardo (PEK-C) nanofibre diameter and interlayer thickness. Compos Sci Technol 2010;70:1660–6.
[18] Zhang J, Niu H, Zhou J, Wang X, Lin T. Synergistic effects of PEK-C/VGCNF composite nanofibres on a trifunctional epoxy resin. Compos Sci Technol 2011;71:1060–7.
[19] Hamer S, Leibovich H, Green A, Intrater R, Avrahami R, Zussman E, et al. Mode I interlaminar fracture toughness of Nylon 66 nanofibrilmat interleaved carbon/epoxy laminates. Polym Compos 2011;32:1781–9.
[20] Beckermann GW, Pickering KL. Mode I and Mode II interlaminar fracture toughness of composite laminates interleaved with electrospun nanofibre veils. Compos Part A Appl Sci Manuf 2015;72:11–21.
[21] De Schoenmaker B, Van der Heijden S, De Baere I, Van Paepegem W, De Clerck K. Effect of electrospun polyamide 6 nanofibres on the mechanical properties of a glass fibre/epoxy composite. Polym Test 2013;32:1495–501.
[22] Palazzetti R, Zucchelli A, Gualandi C, Focarete ML, Donati L, Minak G, et al. Influence of electrospun Nylon 6,6 nanofibrous mats on the interlaminar properties of Gr–epoxy composite laminates. Compos Struct 2012;94:571–9.
[23] Bilge K, Venkataraman S, Menceloglu YZ, Papila M. Global and local nanofibrous interlayer toughened composites for higher in-plane strength. Compos Part A Appl Sci Manuf 2014;58:73–6.
[24] Li G, Li P, Zhang C, Yu Y, Liu H, Zhang S, et al. Inhomogeneous toughening of carbon fiber/epoxy composite using electrospun polysulfone nanofibrous membranes by in situ phase separation. Compos Sci Technol 2008;68:987–94.
[25] Palazzetti R, Zucchelli A, Trendafilova I. The self-reinforcing effect of Nylon 6,6 nano-fibres on CFRP laminates subjected to low velocity impact. Compos Struct 2013;106:661–71.
[26] Saghafi H, Zucchelli A, Palazzetti R, Minak G. The effect of interleaved composite nanofibrous mats on delamination behavior of polymeric composite materials. Compos Struct 2014;109:41–7.
[27] Phong NT, Gabr MH, Okubo K, Chuong B, Fujii T. Improvement in the mechanical performances of carbon fiber/epoxy composite with addition of nano-(Polyvinyl alcohol) fibers. Compos Struct 2013;99:380–7.
[28] Van Der Heijden S, De Bruycker K, Simal R, Du Prez F, De Clerck K. Use of triazolinedione click chemistry for tuning the mechanical properties of electrospun SBS-fibers. Macromolecules 2015;48:6474–81.
[29] Vonhören B, Roling O, De Bruycker K, Calvo R, Du Prez FE, Ravoo BJ. Ultrafast layer-by-layer assembly of thin organic films based on triazolinedione click chemistry. ACS Macro Lett 2015;4:331–4.
[30] Billiet S, De Bruycker K, Driessen F, Goossens H, Van Speybroeck V, Winne JM, et al. Triazolinediones enable ultrafast and reversible click chemistry for the design of dynamic polymer systems. Nat Chem 2014;6:815–21.
[31] Türünç O, Billiet S, De Bruycker K, Ouardad S, Winne J, Du Prez FE. From plant oils to plant foils: Straightforward functionalization and crosslinking of natural plant oils with triazolinediones. Eur Polym J 2014;65:286–97.
[32] Butler GB. Triazolinedione modified polydienes. Ind Eng Chem Prod Res Dev 1980;19:512–28.
[33] Chen TCS, Butler GB. Chemical reactions on polymers. 111. modification of diene polymers via the ene reaction with 4-substituted-1,2,4-triazoline-3,5-diones. J Macromol Sci Part A – Chem 2006;16:757–68.
[34] Leong K-W, Butler GB. Chemical Reactions on Polymers. II. Modification of Diene Polymers with Triazolinediones via the Ene Reaction. J Macromol Sci Part A - Chem 2006;14:287–319.

[35] Roling O, De-Bruycker K, Vonhören B, Stricker L, Körsgen M, Arlinghaus HF, et al. Rewritable polymer brush micropatterns grafted by triazolinedione click chemistry. Angew Chem Int Ed 2015. n/a.
[36] Agarwal S, Greiner A. On the way to clean and safe electrospinning-green electrospinning: emulsion and suspension electrospinning. Polym Adv Technol 2011;22:372–8.
[37] Daelemans L, van der Heijden S, De Baere I, Rahier H, Van Paepegem W, De Clerck K. Nanofibre bridging as a toughening mechanism in carbon/epoxy composite laminates interleaved with electrospun polyamide nanofibrous veils. Compos Sci Technol 2015;117:244–56.
[38] De Baere I, Jacques S, Van Paepegem W, Degrieck J. Study of the mode i and mode II interlaminar behaviour of a carbon fabric reinforced thermoplastic. Polym Test 2012;31:322–32.
[39] Arrese A, Carbajal N, Vargas G, Mujika F. A new method for determining mode II R-curve by the End-Notched Flexure test. Eng Fract Mech 2010;77:51–70.
[40] ASTM International. ASTM D5528–13, standard test method for mode I interlaminar fracture toughness of unidirectional fiber-reinforced polymer matrix composites. Am Soc Test Mater 2013:1–13.

PAPER VIII

ELECTROSPUN NANOFIBROUS INTERLEAVES FOR IMPROVED LOW VELOCITY IMPACT RESISTANCE OF GLASS FIBRE REINFORCED COMPOSITE LAMINATES

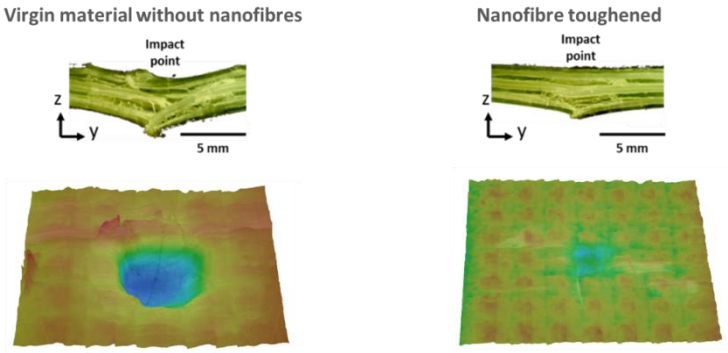

Lode Daelemans, Amaël Cohades, Timo Meireman, Jasper Beckx, Siebe Spronk, Mathias Kersemans, Ives De Baere, Hubert Rahier, Véronique Michaud, Wim Van Paepegem and Karen De Clerck

Currently in submission with *Materials & Design*.

Electrospun nanofibrous interleaves for improved low velocity impact resistance of glass fibre reinforced composite laminates

Lode Daelemans[*1], Amaël Cohades[2], Timo Meireman[1], Jasper Beckx[1], Siebe Spronk[1], Mathias Kersemans[1], Ives De Baere[1], Hubert Rahier[3], Véronique Michaud[2], Wim Van Paepegem[1], Karen De Clerck[1]*

[1] *Department of Materials, Textiles and Chemical Engineering (MATCH), Ghent University, Technologiepark 907, B-9052 Zwijnaarde, Belgium*

[2] *Laboratory for Processing of Advanced Composites (LPAC), Institut Des Matériaux, Ecole Polytechnique Fédérale de Lausanne, Station 12, CH-1015 Lausanne, Switzerland*

[3] *Department Materials and Chemistry, Vrije Universiteit Brussel, Pleinlaan 2, B-1050 Brussels, Belgium*

** Lode.Daelemans@UGent.be Tel.: +32 9 264 57 40 Fax.: +32 9 264 58 46*

Abstract

This study analyses the damage tolerance of nanofibre interleaved composites when subjected to low velocity impact. Drop-weight impact and residual compressive strength measurements are performed according to the ASTM D7136 and ASTM D7137 standards for a range of impact energies around the Barely Visible Impact Damage energy limit. PA6, PA6.9 and PCL nanofibrous veils with two different veil densities are selected to assess their effect on the damage tolerance. The low velocity impact resistance of nanofibre interleaved laminates increases considerably compared to the virgin material. The (projected) damage area decreases up to 50 – 60%, especially at higher impact energies where the virgin material shows widespread delamination. As more energy is absorbed in the interleaved laminates by the nanofibres, less damage to reinforcing fibres and matrix resin is produced. Analysis of fracture surfaces shows that the development of nanofibre bridging zones is the main reason for the improved impact damage tolerance.

***Keywords*:** Nano particles, Damage tolerance, Electrospinning, Toughening, Compression After Impact, CAI

1. Introduction

The poor impact tolerance of laminated fibre reinforced polymer composites is often stated to be one of the main drawbacks of these materials [1]. Their laminated nature results in a low interlaminar fracture toughness, which can cause delamination between the reinforcing plies. This delamination is a critical and major failure event during impact loading. The reduced load bearing capability of impacted composites is of major concern as even relatively small impact events such as tool drops or runway debris can already cause an important degradation of the mechanical properties of the composite structure without causing visible damage [2]. Improving the impact resistance of composite laminates would thus result in a better damage tolerance, performance and lifetime. Hence, many methods have been proposed to toughen the materials over the past decades [3], e.g. rubber/thermoplastic toughening [4,5], addition of rigid nanoparticles [6–8], interlayering toughening particles [9], or using through-thickness reinforcements [10,11]. Yet, these methods often result in a decrease of the in-plane properties, a higher cost or an increase in weight.

A novel and promising toughening method is the interleaving of electrospun nanofibrous veils [12,13]. These veils can be easily integrated into laminated composites as self-supporting veils or by using reinforcing plies on which electrospun nanofibres have been directly

deposited [14]. The small diameter of the nanofibres offers relatively thin interlayers, and since they are continuous, their macroscopic length poses no health hazards in comparison to other nanomaterials. Reneker, Kim and Dzenis [15–17] produced the pioneering work of interlaminar toughened composites using electrospun fibres in 1999. Since then, work from our own group as well as other research groups has confirmed the toughening potential of electrospun nanofibres for composite laminates [18–29]. This research, however, is mainly carried out by delamination experiments such as the double cantilever beam or end notch flexure method. Although important, the results cannot be easily translated to an improved impact damage tolerance.

The research into nanofibre interleaved composite laminates subjected to out-of-plane impact is still very limited. To the authors' best knowledge, there are currently only a handful of published articles regarding this topic. Akangah et al. [30] studied the effect of polyamide 6.6 (PA6.6) nanofibres on the impact resistance of carbon fibre reinforced polymer (CFRP) composite laminates. Due to limited material, they used smaller specimens than those recommended by the ASTM D7136 standard and no repetitions were performed. Furthermore, the areal density of the PA6.6 nanofibrous veils was only 1.7 g/m², which is quite low to have a substantial increase in the interlaminar fracture toughness [13]. Nevertheless, the results indicated an improved impact tolerance of the nanofibre interleaved laminates with less internal damage and smaller damage areas. Akangah and Shivakumar [31] later analysed the impact response of PA6.6 interleaved CFRP laminates according to the ASTM D7136 standard. The nanofibrous veils in this study were even thinner and had an areal density of about 0.7 g/m². In contrast to their earlier work, the nanofibrous veils did not result in a decrease in damage area, which was attributed to the low areal density of the used veils. A small increase in impact damage threshold was however observed. Palazzetti et al. [32] also investigated the impact properties of CFRP laminates interleaved with PA6.6 nanofibrous veils. The laminates were not fully interleaved as the veils were only placed at specific interlayers. Analysis of the force data during the impact event showed no differences between the reference and the nanofibre modified material. The damage area of the impacted specimens was not determined. Saghafi et al. [33] investigated the effect of polyvinylidene fluoride nanofibres, but found no improvement in impact resistance. Beylergil et al. [34] and Neisiany et al. [35] reported improvements in the in-plane impact absorption energy using Charpy and Izod experiments, indicating the potential of using nanofibrous veils. However, these impact experiments are inherently different from typical drop-weight out-of-plane impact and it is currently not clear if the same toughening mechanisms will act for both types of impact loading.

From these studies, it is not clear if interleaving nanofibrous veils is an effective method to improve the impact tolerance of composite laminates. Furthermore, one of the main limitations in these studies is the relatively low amount of specimens and low areal density of the nanofibrous veils. Based on our own research where interleaving certain nanofibrous veils increased the delamination resistance considerably, we would also expect them to positively affect the impact tolerance. It is clear that further analysis of the impact response of nanofibre interleaved composite laminates is required.

This study addresses the toughening effect of interleaved composites when subjected to low velocity impact. A much broader experimental campaign is performed than what has been reported in literature up till now. The drop-weight impact and residual compressive strength measurements have been performed following the well-recognized ASTM D7136 and ASTM D7137 standards. A wide range of impact energies was analysed around the Barely Visible Impact Damage (BVID) energy limit [36]. Based on our own previous findings, polycaprolactone (PCL) as well as polyamide 6 (PA6) and polyamide 6.9 (PA6.9) were

selected since these systems have already proven to be able to considerably increase the delamination resistance under static loading [12–14,37,38] and showed some potential in preliminary impact experiments [13]. Likewise, the nanofibrous veils under consideration were produced with two different selected areal weights (6 g/m² and 12 g/m²) in order to assess their effect on impact tolerance. The veils were interleaved in glass fibre reinforced polymer (GFRP) laminates at each interlayer between plies of dissimilar orientation.

2. Materials and methods

2.1. Electrospinning of nanofibrous veils

PA6 (M_W 51 000 g/mol) pellets were purchased from Sigma Aldrich; PA6.9 (M_W 58 000 g/mol) and PCL (M_W 100 000 g/mol) pellets were purchased from Scientific Polymer Products. The pellets were dissolved for electrospinning in a mixture of formic acid (98%-100%) and acetic acid (98%) both purchased from Sigma Aldrich and used as received. Table 1 gives an overview of the parameters used for electrospinning. These were based on previous studies [39–41]. A representative SEM image for each system is given in Figure 1. All stated nanofibre diameters were measured on dry specimens (before any resin infusion) as the average of at least 50 fibres.

Table 1 – Overview of the electrospinning systems.

System		Electrospinning parameters			Electrospun veil properties	
		Flow rate per nozzle (ml/h)	Nozzle-to-collector distance (cm)	Voltage (kV)	Areal density (g/m²)	Nanofibre diameter (nm)
#1	PA6.9	1.5	6	35	6	200 ± 25
	16 wt%, 1:1 FA/AA				12	
#2	PA6	1.5	8	35	6	150 ± 20
	16 wt%, 1:1 FA/AA				12	
#3	PCL	2	23	25 – 30	6	370 ± 200
	23 wt%, 3:7 FA/AA				12	

Self-supporting nanofibrous veils were produced on an in-house developed multinozzle electrospinning system (Figure 1d). An array of 2 – 8 nozzles is used to allow a larger throughput of nanofibres as necessary for the relatively large amount of nanofibres required for impact testing. The collector is a moving conveyor belt out of aluminium foil (grounded) to continuously produce sheets of fixed thickness and size. The array of needles travels back and forth in a linear motion, while the collector moves perpendicular to the needle movement at constant speed. The speed of the collector determines the amount of nanofibres deposited per square meter.

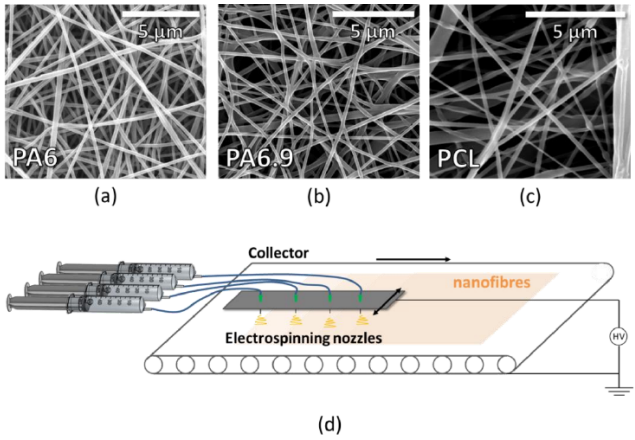

Figure 1 – Representative SEM image of PA6 (a), PA6.9 (b) and PCL (c) electrospun nanofibres. A schematic view of the multinozzle system used to produce the nanofibrous veils (d).

2.2. Composite production

Glass fibre composite laminates are produced by vacuum assisted resin transfer moulding (VARTM) with unidirectional E-glass plies with an areal density of 500 g/m² and a width of 300 mm (UDO ES500 manufactured by SGL group) and a high toughness epoxy/amine thermoset resin system typically used for wind turbine blades (EPIKOTE MGS RIMR135 and EPIKURE MGS RIMH137 supplied by Momentive). An in-house developed VARTM setup is used, consisting of a two-piece flat mould with internal dimensions of 3 x 350 x 350 mm³. The stacking sequence was $[0°/90°]_{2S}$. For the nanofibre interleaved plates, a (self-supporting) nanofibrous veil was inserted at each interface between 0°- and 90°-oriented plies. The manufacturer's recommended curing cycle is used to cure the laminates: curing for 24 hours at 23°C (room temperature) followed by a post-cure at 80°C for 15 hours. The overall glass fibre volume fraction (52 vol%) did not change when nanofibrous veils were interleaved since the mould had a fixed thickness of 3 mm. For each configuration, i.e. virgin (reference material without nanofibrous interlayers), PA6 6 g/m², PA6 12 g/m², PA6.9 6 g/m², PA6.9 12 g/m², PCL 6 g/m² and PCL 12 g/m², at least two plates were produced. From each plate, six specimens where cut for impact testing. A veil density of 6 g/m² resulted in an interlayer thickness of 32 ± 5 µm and a veil density of 12 g/m² resulted in an interlayer thickness of 61 ± 20 µm. Note that although the post-cure happens at a temperature above the melting point of PCL, the nanofibrous morphology is retained in the composite due to the curing step at room temperature [12,13].

2.3. Low velocity impact experiments

Low velocity impact tests were conducted according to the procedures described in ASTM D7136. The specimens were cut from the laminates at a nominal size of 98 x 148 mm^2 with a water-cooled diamond cutter (blade thickness 2 mm). This is slightly smaller (2 mm in each direction) than recommended by the standard, but allowed us to section six instead of four specimens per plate. Initial trials on reference specimens showed no influence of the reduced size. Although the ASTM D7136 standard recommends thicker specimens, the choice for

plates of 3 mm thickness was made to be consistent with our previous work. The test was executed on an in-house developed impact test machine. It consists of a drop tower with an impactor (8.17 kg) with a hemispherical nose (diameter of 16 mm). It is guided through two smooth guide columns and impact occurs on the centre of the specimen. The specimen is firmly fastened by four clamps at its corners. The test machine is equipped with a Gen. 5I oscilloscope to record acceleration, load and displacement data of the impactor [42]. Two Photron SA4 high-speed cameras were used to observe the upper and lower face of the specimens during impact. A third Photron APX-RS high-speed camera was used to measure displacement, velocity and acceleration of the impactor by the use of a specific line pattern on the impactor. The three cameras were synchronized by triggering them at the moment a force of 200 N was detected by the oscilloscope. Images were recorded at 10 000 – 15 000 fps. The initial height of the impactor could be varied in order to obtain various impact energies. Six different heights were set: 20, 40, 60, 80, 100 and 120 cm. They correspond to impact energies of 14, 28, 41, 54, 67, 79 J respectively (taking into account frictional losses due to the sliding mechanism of the impactor). An anti-rebound device was used to avoid a second strike. For each type of composite and for each impact energy, the drop weight impact test was repeated at least three times on different specimens. Note that not all impact energies were always applied to each configuration depending on the amount of produced specimens.

2.4. Post inspection of specimens

The maximum depth of the permanent indentation of the impacted specimens was measured with a micrometre using a fine tip. The indentation profile was also investigated with a Keyence VHX-2000 digital microscope for one specimen of each configuration at each impact energy. The surface profile of the indent and outdent was obtained by 3D stitching of several microscopic images using a dynamic focus depth.

The damage area after impact was measured optically as the specimens were translucent. To validate the optical measurements, water-coupled ultrasonic C-scans in transmission were performed on a specimen of each configuration at each impact energy. The obtained C-scans in transmission provided an integrated view of damage through the depth of the specimens. A short ultrasonic pulse with a central frequency f_c = 5 MHz was used (H5K transducer with diameter 13 mm, General Electric). The pulser/receiver apparatus operates at a sampling frequency of 400 MHz (USIP40, General Electric), and the maximum transmission pulse amplitude is evaluated in the selected time gate. The distance between the transducers was approximately 130 mm, with the sample positioned in between. The resolution of the scan grid was set 1 mm and 0.1 mm for the index axis and the scan axis respectively, with an actual scanning speed of 50 mm/s.

Another specimen was sacrificed for microscopic analysis of the cross-section using optical (Olympus BX51) and scanning electron microscopy (Jeol Quanta 200F Field Emission GUN).

2.5. Residual compressive strength

The impacted specimens were tested for their residual compressive strength, i.e. the compression after impact (CAI) strength, according to ASTM D7137 using a 600 kN Schenk universal testing machine. An anti-buckling device was used to prevent buckling of the specimens during compression. Specimens with an invalid failure mode (edge failure) were discarded.

3. Results and discussion

3.1. Impact event data

3.1.1. Contact load

An example of the dynamic load exerted by the specimen on the impactor during a typical impact test with damage is shown in Figure 2. The curve was characterised by four temporal regions, which relate to the mechanical response of the composite specimen. Time t_1 and t_5 correspond to the beginning, respectively the end of an impact event, i.e. the impactor contacts and rebounds from the specimen. Region $t_1 - t_2$ represents elastic bending of the specimen. At this point, no measurable stiffness degradation of the specimen is visible on the load-time curve, although initiation of sub-critical matrix cracks and delaminations could already happen [43]. Region $t_2 - t_3$ was characterised by a small load drop at t_2 and a change in slope of the load-time curve, indicating a first degradation of the stiffness of the specimen due to more pronounced matrix cracking and delamination onset [44]. At t_3, the velocity of the impactor was zero and its kinetic energy has been transferred completely to the specimen. Region $t_3 - t_4$ showed a sharp drop in load due to major damage propagation in the specimen which caused a sudden loss of the stiffness in the contact region. The final stage, $t_4 - t_5$, corresponds to the residual stiffness of the specimen causing the impactor to be rebounded from the specimen.

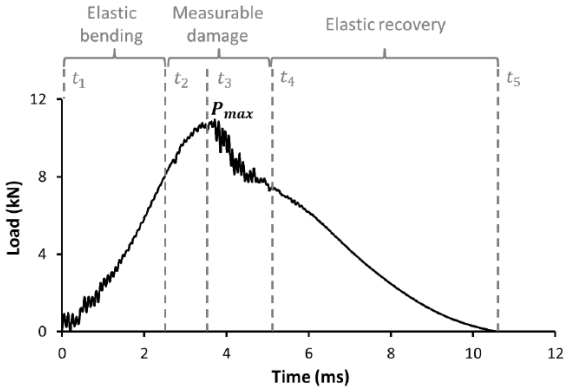

Figure 2 – Load versus time recorded during an impact event shows four regions: elastic bending ($t_1 - t_2$), (minor) damage initiation ($t_2 - t_3$), major damage ($t_3 - t_4$) and elastic recovery ($t_4 - t_5$).

Figure 3 shows the impact event as recorded by high-speed cameras at different times. Small damage already occurred in the $t_1 - t_2$ region, but was localised underneath the impact point. The damage zone then extended considerably in the $t_2 - t_4$ region as the delaminations propagated in the specimen. Depending on the impact energy, occurrence of cracks and splits were also visible on the bottom and top surfaces in this region. After t_4, the specimen bended back to its unloaded state and a second impact of the impactor was prevented by the anti-rebound mechanism (not illustrated).

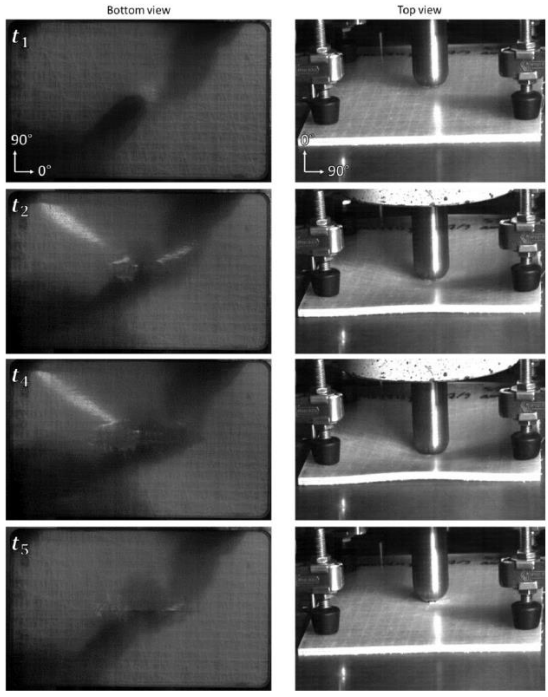

Figure 3 – Images obtained from high-speed camera during an impact event (67 J) giving a bottom and top view of the specimen at times t_1, t_2, t_4 and t_5.

The load-time curves obtained from experiments show the development of damage in the specimens with increasing impact energy (Figure 4). The results show that the $t_1 - t_3$ region did not differ much between the virgin and nanofibre interleaved laminates, indicating that the addition of the nanofibrous interleaves did not affect the elastic behaviour of the material. At low impact energies (< 41 J), the curves show a smooth Gaussian-like response for all configurations, corresponding to a minor amount of damage in the specimens. At higher energies, more damage occurred, resulting in the sharp drop in contact load between $t_3 - t_4$. For the virgin specimens, this happened at impact energies of 54 J. At these energies, a relatively large delaminated surface was visible on the high-speed camera images. For the nanofibre interleaved specimens – which have an improved interlaminar fracture toughness [13] – the occurrence of the steep drop in contact load is shifted to 67 J for both PA6 and PA6.9 interleaved laminates and even up to 79 J for PCL interleaved laminates.

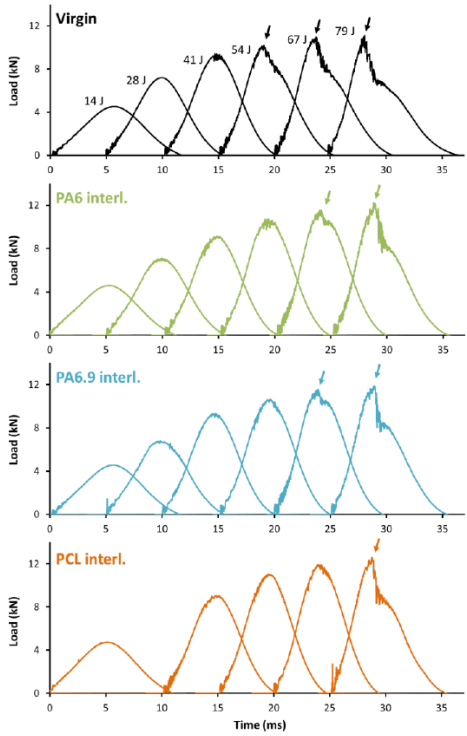

Figure 4 – Load-time curves at increasing impact energies show the damage progression during impact. A steep drop in load represents damage processes that cause a sudden loss of stiffness of the material (indicated by arrows). Nanofibrous interleaves improve the damage resistance as the loss in stiffness occurred at higher impact energies. (curves are taken from different tests and plotted with a 5 ms offset for clarity)

The maximum load P_{max} increased with increasing impact energy (Figure 5). A higher P_{max} was recorded for the nanofibre interleaved laminates compared to the virgin material at impact energies in the 54 J – 79 J range. There was no clear difference between laminates interleaved with 6 g/m² or 12 g/m² indicating that increasing the veil density to 12 g/m² had no measurable effect. The higher P_{max} of the nanofibre interleaved laminates means that they can withstand a higher load before sub-critical cracks reached the limit where major damage and a sudden loss of stiffness occurred. This is very similar to the improvements in Mode II delamination resistance that we reported earlier [37,38], where the energy during sub-critical crack growth increased due to nanofibre bridging. Indeed, when cracks or delaminations occur in the toughened interlayer(s) during impact, nanofibres will bridge the newly formed fracture surfaces and take up energy by straining.

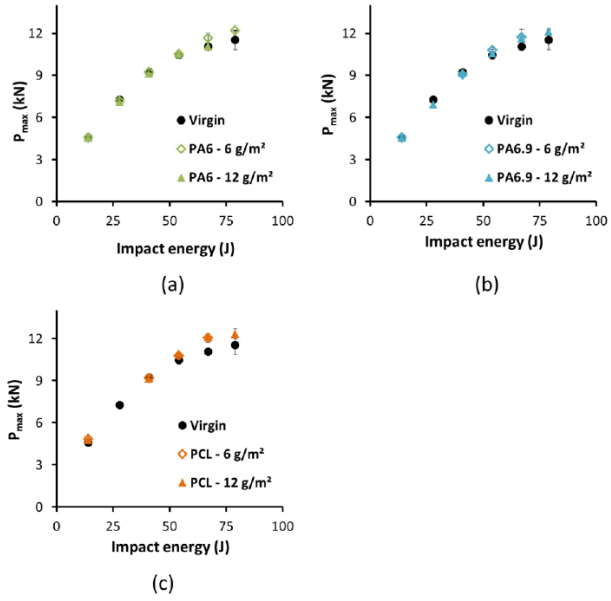

Figure 5 – P_{max} versus impact energy for PA6 (a), PA6.9 (b) and PCL (c) interleaved specimens. P_{max} increases with increasing impact energy and is slightly higher for nanofibre interleaved specimens at impact energies of 67 J and higher.

3.1.2. Contact duration

Figure 6 shows the contact duration versus impact energy for the impact experiments. Longer contact durations were typically observed in virgin composites. This implies that more damage propagation occurred in the virgin specimens as compared to the nanofibre toughened specimens [1]. The largest differences in contact duration were again recorded for impact energies of 67 J and higher. The evolution of the contact duration in function of the impact energy has a particular shape. First, a decrease in contact duration was observed with increasing impact energy, followed by an increase in contact duration. When the impact energy increases, its velocity increases, resulting in shorter contact durations. However, more damage will also be created which eventually results in longer contact duration. This latter point was clearly shifted to higher impact energies for the nanofibre interleaved laminates in accordance with the results of Section 3.1.1.

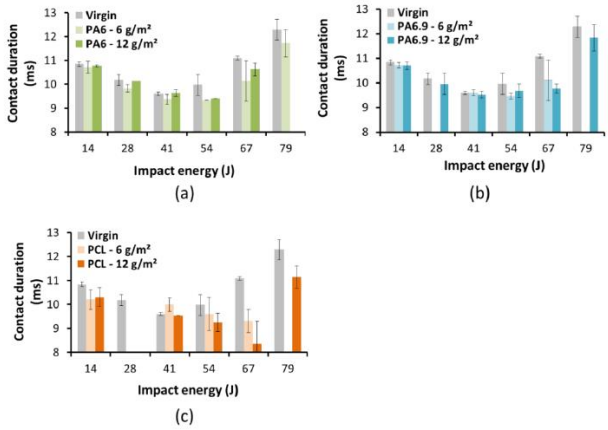

Figure 6 – Contact time versus impact energy for PA6 (a), PA6.9 (b) and PCL (c) interleaved composite laminates.

3.2. Damage analysis

3.2.1. Projected damage area

The (projected) damage area after impact was determined by measuring the delaminated area on impacted specimens. As the specimens were translucent, the damage area was determined visually. A series of C-scans on impacted specimens showed that the agreement between the damage areas measured by both methods was very good (Figure 7). The shape of the damage area was rhombus-like for all tested impact energies. It showed a larger damage growth in the 0°-direction compared to the 90°-direction, most likely caused by the rectangular shaped specimen fixture recommended by the ASTM standard and the cross-ply layup. Hence, the reduction in damage area is mainly attributed due to a reduction in damage length (0°-direction) and not in damage width (90°-direction).

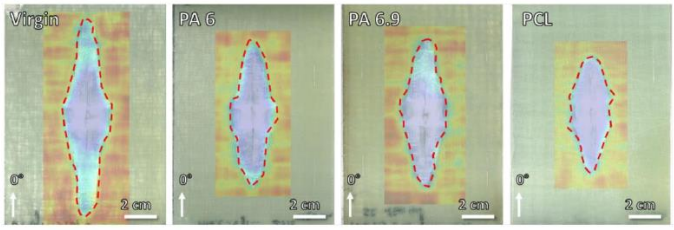

Figure 7 – The optical measured damage area (dashed line) corresponded well with the overlaid C-scan (blue area) results (impact energy of 79 J). Nanofibre interleaved specimens showed a smaller damage area, mainly due to a reduction in damage length. PCL nanofibres resulted in the best improvements.

The (projected) damage area in function of the impact energy is given in Figure 8. The curves show a bilinear behaviour, likely caused by a difference in failure mechanisms present at low and high impact energies. The toughening effect of the nanofibres was relatively small at low

impact energies, especially for PA6 and PA6.9 interleaved specimens, but increased significantly at impact energies higher than 41 J. There was no clear difference between nanofibrous veils of 6 g/m² or 12 g/m². Overall, specimens interleaved with PCL nanofibres showed the highest reductions in damage area, which indicates the best improvement in impact damage resistance for the range of impact energies tested. The damage area reduced up to 60% for PCL nanofibre interleaved specimens.

3.2.2. Indentation depth

The sharp drop in load recorded on the load-time curves in Figure 4 corresponds to a sudden loss of stiffness of the material in the contact region. Such degradation of the material also results in large indentations due to ply failure underneath the impactor. The depth of the indentation after impact is illustrated in Figure 9. The change from relatively minor to major damage occurrence is clearly visible by a sudden increase of the indentation depth at higher impact energies. At impact energies above 50 J, severe ply splitting and almost full penetration of the impactor in the virgin specimens occurred, resulting in very large indents on the top surface and outdents on the bottom surface of the specimens (Figure 10). This behaviour also resulted in higher standard deviations on the average dent depth. Since the damage formation in the nanofibre interleaved specimens was less severe, higher impact energies were required to obtain the same indentation as the virgin material. Contrary to the damage area however, the difference between PCL and PA6.9 nanofibres is relatively small. Again, no clear difference in dent formation was obtained for both veil densities. The PA6 interleaved specimens show a similar trend, although it is less clear due to the high standard variation obtained for the PA6 – 6 g/m² specimens subjected to an impact energy of 67 J.

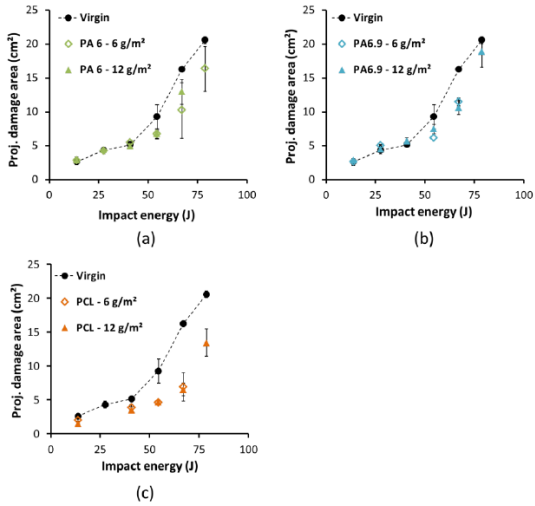

Figure 8 – Projected damage area versus impact energy for PA6 (a), PA6.9 (b) and PCL (c) interleaved composite laminates. The damage area decreases compared to the virgin material, especially at impact energies higher than 41 J. PCL nanofibre interleaved specimens showed the best improvements.

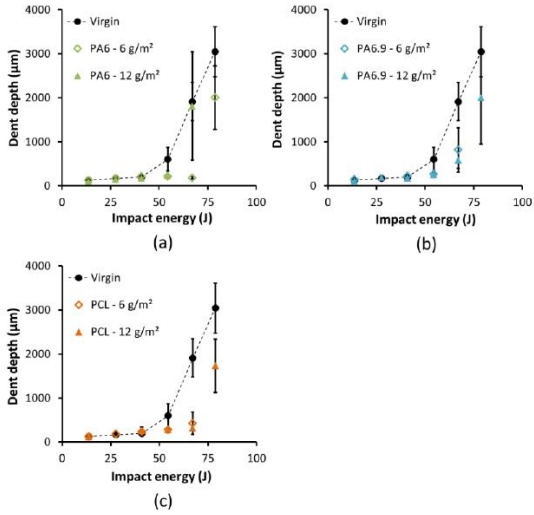

Figure 9 – Dent depth versus impact energy for PA6 (a), PA6.9 (b) and PCL (c) interleaved composite laminates. Macroscopic dent formation occurs at energies higher than 50 J. The nanofibre interleaved specimens showed much smaller dents due to better damage resistance. The veil density had no effect for both nanofibre types.

The Barely Visible Impact Damage (BVID) range is limited by the energy level at which a permanent indentation smaller than 300 µm is formed (by definition) [36]. The results indicate that the upper limit of the BVID range is improved when nanofibres are interleaved. This limit was 41 J for the virgin specimens, around 54 J for the PA6 and PA6.9 interleaved specimens and around 67 J for the PCL interleaved specimens, which represents improvements of 30% and 65% respectively.

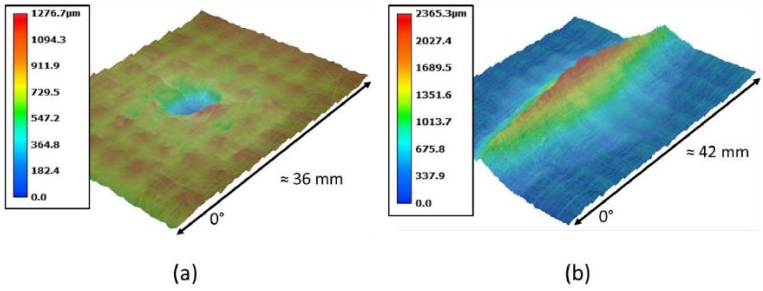

Figure 10 – 3D reconstruction of the indent (a) and outdent (b) geometry which are characteristic for impact energies above the Barely Visible Impact Damage limit on impacted specimens (reconstruction was done on a Keyence microscope by automatic z-stitching). While the indent is hemispherical similar to the impactor, the outdent is rhombus shaped and often showed ply splitting of the bottom layer (0° orientation).

3.2.3. Microscopic analysis

A microscopic investigation of the damage mechanisms was performed by analysing cross-sectional images taken at the impact point along the transversal direction, i.e. along the 90° direction (Figure 11). As expected, the damage region increased as the impact energy increased. At 14 J, few intralaminar cracks and delaminations were present, resembling the typical pine tree pattern. Intralaminar tensile cracks were seen in the lowest reinforcing ply due to the bending of the specimens during impact (external light sources were used to produce a high contrast between the cracks/delaminations and the 0°-oriented plies). At an intermediate impact energy of 41 J, more intralaminar cracks were observed and the delaminations were longer. The lower plies also started to show signs of glass fibre failure. At this point, the indentation was still limited and thus the material beneath the impact point was still able to take up the load induced by the impact event. At higher energies of 67 J however, the specimens were severely damaged. Many cracks and delaminations were observed at further distances away from the impact point. Pulled-out glass fibres were also visible. In the virgin specimens, the material beneath the impact point showed failure throughout the thickness of the specimen explaining the sharp drop in contact load. On the contrary, the nanofibre toughened specimens showed less cracks. Furthermore, the structural integrity of the material underneath the impact point was maintained much better in the interleaved laminates.

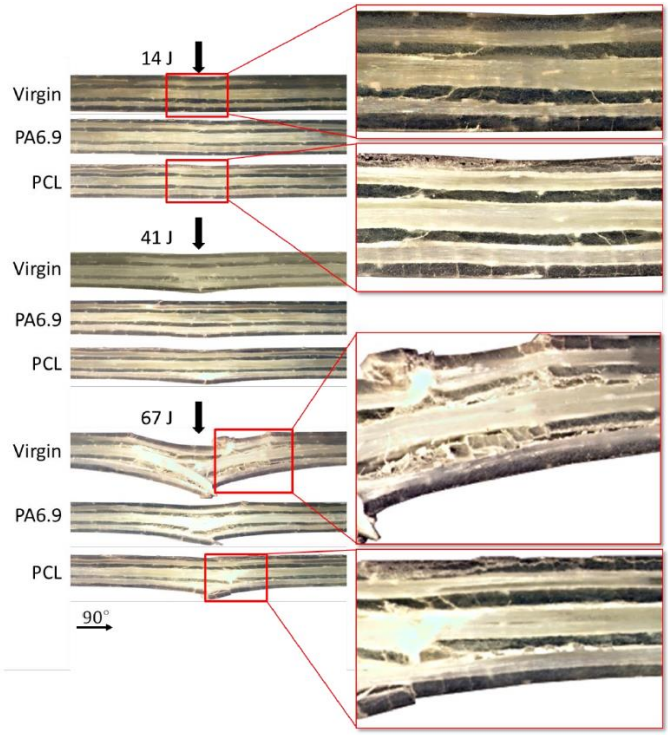

Figure 11 – Cross-section view of impacted specimens. The amount of interlaminar cracks and delaminations was found to be lower in the nanofibre interleaved laminates. At impact energies of 67 J, severe dent formation is visible for the virgin specimens due to complete ply failure underneath the impact, while much less damage and smaller dents are observed for the nanofibre interleaved specimens. PA6 interleaved laminates are not shown as they were similar to PA6.9 interleaved laminates.

Previous work has shown that nanofibres can improve the delamination resistance by interacting with the crack path and bridging newly created crack surfaces [13]. They then take-up load by stretching and deforming, resulting in more energy required for propagating the delamination. Typically, the delamination propagates at the reinforcing ply interface by (reinforcing) fibre/matrix debonding and only interacts with the toughened interlayer at points where it crosses the interlayer. Under Mode I loading, the adhesion between the nanofibres and the matrix resin is very important to effectively increase the delamination resistance. Indeed, previous delamination experiments showed poor performance of polyamide nanofibres due to low adhesion with the matrix compared to PCL nanofibres under Mode I delamination growth [13,38]. Under Mode II loadings, this adhesion effect is of lesser importance and both polyamide and PCL nanofibres resulted in similar improvements in delamination resistance.

For the impacted specimens, the majority of the delaminations were found at the reinforcing ply interface with regular crossings of the delamination path through the toughened

interlayers (Figure 12a), similar to the findings in delamination experiments. However, interlaminar cracks through the nanotoughened interlayers were also observed in regions without clear delamination failure (Figure 12b-c). Hence, nanofibre bridging zones can develop in both regions due to the interaction between the crack path and the toughened interlayer.

SEM analysis of the fracture surface confirmed the existence of nanofibre bridging zones (Figure 13). PA6, PA6.9 as well as PCL nanofibres showed signs of plastic deformation indicating energy take-up. However, a certain fraction of PA6 and PA6.9 nanofibres was also peeled off from the matrix resin. Previous research showed that this peeling effect is due to Mode I delamination and typically will not result in toughness improvement [13,38]. The fracture surface thus showed signs of both Mode I (peeling) and Mode II conditions (hackle formation, Figure 12d). Such Mixed Mode behaviour is to be expected for relatively thin composite laminates as failure of the bottom plies allows an opening mode deformation between the delaminated plies. Indeed, the delaminations in Figure 11 were "open" indicating at least partial Mode I conditions. PCL interleaved laminates showed better impact resistance, most likely due to an increased delamination resistance under both Mode I and Mode II loading. The results show that the toughening mechanisms under impact loading are very similar to those previously reported in delamination studies.

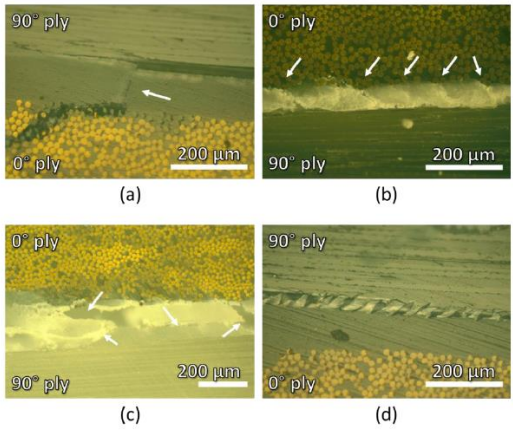

Figure 12 – Interlaminar crossing of the nanotoughened interlayer by a delamination which jumps from the 0°-interface to the 90°-interface (a). Interlaminar cracks formed between plies with different orientation due to shear stresses (b,c). Hackle formation caused by shear loading (Mode II) near a 90° ply interface (d). The arrows indicate cracks through the nanotoughened interlayer.

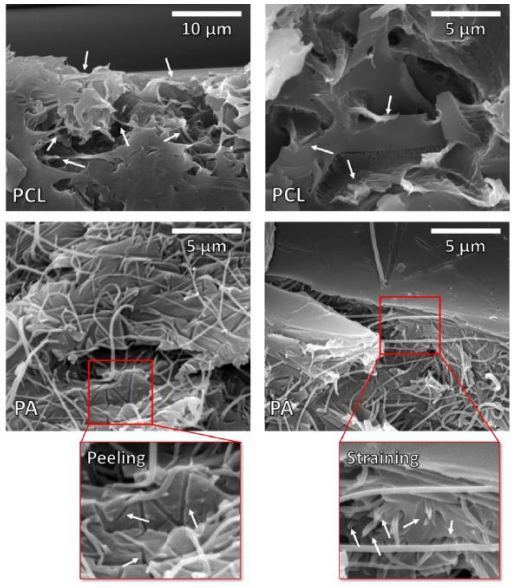

Figure 13 – SEM analysis of the fracture surface showed nanofibre bridging zones. The PCL nanofibres were severely deformed without signs of a weak interface thus indicating good load transfer and energy take-up by the nanofibres. The PA6.9 and PA6 nanofibres also showed plastic deformation (straining), but many peeled off nanofibres were also visible due to the low interfacial strength. The arrows indicate nanofibres that deformed during nanofibre bridging.

3.2.1. Penetration threshold

The nanofibre interleaved specimens had a slightly higher P_{max}, a smaller projected damage area and a lower dent depth than the virgin material, especially at higher impact energies. The reason for this behaviour is attributed to more pronounced delamination and interlaminar crack occurrence failure at higher energies. With increasing impact energy, the value of P_{max} started to level off to a constant value which corresponds to the penetration threshold of the material [45]. At this value, the laminate will not be able to withstand the impact event and the impactor will fully penetrate through the specimens. The increase in P_{max} thus indicated a higher penetration threshold for nanofibre interleaved laminates due to better damage resistance.

3.3. Residual compressive strength

The results of the CAI experiments are given in Figure 14. The specimens are compressed in their longitudinal direction according to the ASTM standard (Figure 14d). The individual measurements are plotted for the nanofibre interleaved laminates as it was not always possible to obtain multiple valid measurements. As the specimens were relatively thin, they tended to fail in an invalid manner in which the failure was initiated near the edges of the fixture and not at the impact zone. For the same reason, no valid measurements were obtained at the for the virgin material at 0 J (compression strength) and 14 J.

On average, the nanotoughened interlayers did not improve the CAI strength although the damage area was considerably smaller. However, the damage area was mainly reduced in length and not in width for the interleaved specimens. This means that the effective cross-section that experiences the compressive load is more or less similar for virgin and nanofibre interleaved specimens. The stiffness in the compression direction will thus hardly be affected by the difference in damage length. Furthermore, the impact energies considered were relatively high. As such, the material under the impact point degraded to that extent that it likely acted as a local failure initiation point before the delaminated sub-laminates could buckle out. Indeed, glass fibre failure already occurred at impact energies of 40 J. Therefore, it is unlikely that at energies higher than 40 J, the failure event is governed by delamination between the sub-laminates, and thus, the toughened interlayers will not affect the CAI strength.

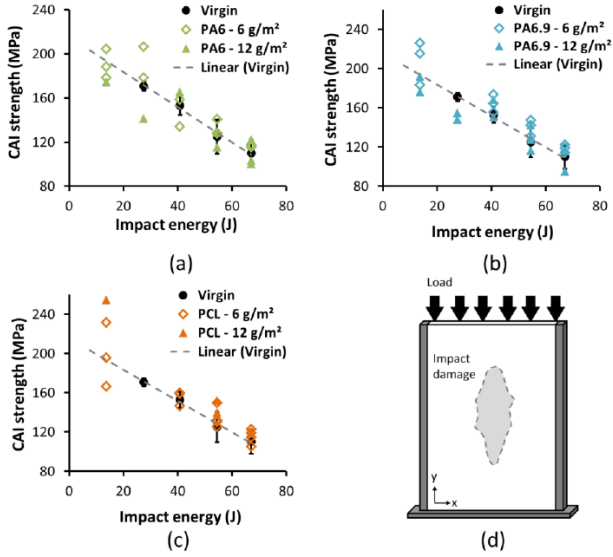

Figure 14 – CAI strength for PA6.9 (a), PCL (b) and PA6 (c) interleaved composite laminates. Individual measurements are plotted for the nanofibre interleaved specimens, while the average and standard deviation is plotted for the virgin material (including a linear fit). The CAI strength decreases with increasing impact energy. On average, the nanofibres do not differ significantly from the virgin material. Illustration of the experimental setup for CAI testing (d).

Only considering the datapoints within the BVID region of the material, the average CAI strength of the nanofibre interleaved specimens was still comparable to that of the virgin material. Yet several specimens showed a CAI strength that could be considered to be relatively high based on the trend visible in Figure 14, especially at the lowest impact energy of 14 J. This is in accordance with the work of Akangah and Shivakumar [31], who similarly only recorded improvements in CAI strength at the lowest impact energies.

For example, two of the four specimens interleaved with PCL nanofibres and subjected to an impact of 14 J had a very high CAI strength. At this energy level, damage was still limited to relatively small matrix cracks and delaminations. For the three specimens interleaved with

6 g/m² PCL nanofibres, the bottom surfaces before and after CAI testing are shown in Figure 15. The lowest CAI strength was recorded for specimen #1 and it also showed the largest delaminated area after CAI testing. Furthermore, the highest CAI strength was recorded for specimen #3, which was the specimen with the smallest delamination area after CAI testing. As the initial damage size of the three specimens was similar, and assuming that the compression failure is governed by delamination of the sub-laminates, these results indicate a difference in interlaminar fracture toughness between the three specimens. A possible explanation for this behaviour is that the onset of delamination induced by sub-laminate buckling in specimen #3 had more interlaminar crossings where nanofibre bridging occurred and thus a higher interlaminar fracture toughness [13]. Hence, it could take up more load before the delamination reached a critical size and abrupt compressive failure occurred.

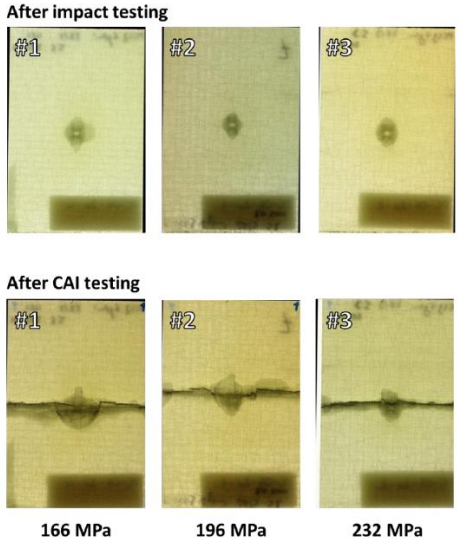

Figure 15 – Images of the specimens interleaved with 6 g/m² of PCL nanofibres subjected to an impact energy of 14 J before and after CAI testing. When a lower CAI strength was recorded, a larger delaminated area can be seen on the failed specimens.

4. Conclusion

Electrospun nanofibrous veils (PA6, PA6.9 and PCL) were interleaved in GFRP cross-ply composite laminates to determine their effect on the low velocity impact properties of the material. The results show that interleaving nanofibrous veils is an effective method to improve the damage tolerance during low velocity impact. The presence of the nanofibre toughened interlayers resulted in a reduction in projected damage area, an increase in maximum load, shorter contact times, an increase in the BVID upper energy limit, less internal damage and a higher penetration threshold.

The toughening mechanisms that were observed are in line with those observed in static delamination experiments. Nanofibre bridging zones developed throughout the specimen

when (micro)cracks and delaminations occurred in the toughened interlayers. In these zones, the nanofibres will bridge the crack surfaces and take up energy by straining, yielding and breaking. This was confirmed by SEM analysis on the (internal) fracture surface of impacted specimens.

There was not much difference in impact properties between laminates interleaved with veils of 6 g/m² or 12 g/m². This is a positive result as lower veil densities are economically more interesting.

Overall, PCL nanofibres resulted in much better improvements compared to PA6 or PA6.9 nanofibres. Interleaving the composite laminates with PCL nanofibres decreased the projected damage area about 50%, resulted in a higher penetration threshold and even increased the BVID range by 63% compared to the virgin material. Both PA6 and PA6.9 nanofibres were less effective for improving the impact damage tolerance. This was due to the low adhesion between polyamide nanofibres and the epoxy matrix causing debonding of the nanofibres. On the contrary, PCL nanofibres do have a good adhesion with the epoxy matrix resulting in much better load transfer to the nanofibres.

No clear improvements in CAI strength were recorded. This was most likely due to the rhombus shaped damage area and the relatively high impact energies that were used. Future studies should consider lower impact energies and/or thicker (quasi-isotropic) laminates to analyse the potential of nanofibrous interleaves for improving the CAI strength as this will result in a more delamination dominant failure mode and less buckling of the specimens during testing (to prevent invalid measurements).

5. Acknowledgments

Financial support from the Agency for Innovation by Science and Technology of Flanders (IWT) and the Special Research Fund (BOF) Ghent University is gratefully acknowledged. Results in this paper were obtained within the framework of the IWT Strategic Basic Research Grant 141344, the BOF 13/24J/020 project and the BOF.PDO.2015.0028.01 project.

6. Bibliography

[1] M.O.W. Richardson, M.J. Wisheart, Review of low-velocity impact properties of composite materials, Composites Part A: Applied Science and Manufacturing. 27 (1996) 1123–1131. doi:10.1016/1359-835X(96)00074-7.

[2] J.C. Prichard, P.J. Hogg, The role of impact damage in post-impact compression testing, Composites. 21 (1990) 503–511. doi:10.1016/0010-4361(90)90423-T.

[3] N.H. Nash, T.M. Young, P.T. McGrail, W.F. Stanley, Inclusion of a thermoplastic phase to improve impact and post-impact performances of carbon fibre reinforced thermosetting composites — A review, Materials & Design. 85 (2015) 582–597. doi:10.1016/j.matdes.2015.07.001.

[4] A. Bahrami, F. Cordenier, P. Van Velthem, W. Ballout, T. Pardoen, B. Nysten, C. Bailly, Synergistic local toughening of high performance epoxy-matrix composites using blended block copolymer-thermoplastic thin films, Composites Part A: Applied Science and Manufacturing. 91 (2016) 398–405. doi:10.1016/j.compositesa.2016.08.038.

[5] F. Xu, X.S. Du, H.Y. Liu, W.G. Guo, Y.W. Mai, Temperature effect on nano-rubber toughening in epoxy and epoxy/carbon fiber laminated composites, Composites Part B: Engineering. 95 (2016) 423–432. doi:10.1016/j.compositesb.2016.04.019.

[6] C. Kostagiannakopoulou, T.H. Loutas, G. Sotiriadis, A. Markou, V. Kostopoulos, On

the interlaminar fracture toughness of carbon fiber composites enhanced with graphene nano-species, Composites Science and Technology. 118 (2015) 217–225. doi:10.1016/j.compscitech.2015.08.017.

[7] S. Chandrasekaran, N. Sato, F. Tölle, R. Mülhaupt, B. Fiedler, K. Schulte, Fracture toughness and failure mechanism of graphene based epoxy composites, Composites Science and Technology. 97 (2014) 90–99. doi:10.1016/j.compscitech.2014.03.014.

[8] I. Taraghi, A. Fereidoon, F. Taheri-Behrooz, Low-velocity impact response of woven Kevlar/epoxy laminated composites reinforced with multi-walled carbon nanotubes at ambient and low temperatures, Materials & Design. 53 (2014) 152–158. doi:10.1016/j.matdes.2013.06.051.

[9] M. Ho, K. Lau, Design of an impact resistant glass fibre/epoxy composites using short silk fibres, Materials & Design. 35 (2012) 664–669. doi:10.1016/j.matdes.2011.10.003.

[10] F. Pegorin, K. Pingkarawat, A.P. Mouritz, Comparative study of the mode I and mode II delamination fatigue properties of z-pinned aircraft composites, Materials and Design. 65 (2015) 139–146. doi:10.1016/j.matdes.2014.08.072.

[11] K.T. Tan, N. Watanabe, Y. Iwahori, X-ray radiography and micro-computed tomography examination of damage characteristics in stitched composites subjected to impact loading, Composites Part B: Engineering. 42 (2011) 874–884. doi:10.1016/j.compositesb.2011.01.011.

[12] S. van der Heijden, L. Daelemans, T. Meireman, I. De Baere, H. Rahier, W. Van Paepegem, K. De Clerck, Interlaminar toughening of resin transfer molded laminates by electrospun polycaprolactone structures: Effect of the interleave morphology, Composites Science and Technology. 136 (2016) 10–17. doi:10.1016/j.compscitech.2016.09.024.

[13] L. Daelemans, S. van der Heijden, I. De Baere, H. Rahier, W. Van Paepegem, K. De Clerck, Damage resistant composites using electrospun nanofibers: a multiscale analysis of the toughening mechanisms., ACS Applied Materials & Interfaces. (2016). doi:10.1021/acsami.6b02247.

[14] S. van der Heijden, L. Daelemans, B. De Schoenmaker, I. De Baere, H. Rahier, W. Van Paepegem, K. De Clerck, Interlaminar toughening of resin transfer moulded glass fibre epoxy laminates by polycaprolactone electrospun nanofibres, Composites Science and Technology. 104 (2014) 66–73. doi:10.1016/j.compscitech.2014.09.005.

[15] Y.A. Dzenis, D.H. Reneker, Delamination resistant composites prepared by small diameter fiber reinforcement at ply interfaces, United States Patent 6265333:, 2001. http://www.mendeley.com/research/united-states-patent-6265333-delamination-resistant-composites-prepared-small-diameter-fiber-reinfor/.

[16] J. Kim, D.H. Reneker, Mechanical properties of composites using ultrafine electrospun fibers, Polymer Composites. 20 (1999) 124–131. doi:10.1002/pc.10340.

[17] Y.A. Dzenis, D.H. Reneker, Delamination resistant composites prepared by small fiber reinforcement at ply interfaces, 1999. https://encrypted.google.com/patents/WO1999062705A1?cl=und.

[18] N. Zheng, Y. Huang, H.Y. Liu, J. Gao, Y.W. Mai, Improvement of interlaminar fracture toughness in carbon fiber/epoxy composites with carbon nanotubes/polysulfone interleaves, Composites Science and Technology. 140 (2017) 8–15. doi:10.1016/j.compscitech.2016.12.017.

[19] G.W. Beckermann, Nanofiber interleaving veils for improving the performance of composite laminates, Reinforced Plastics. (2017). doi:10.1016/j.repl.2017.03.006.

[20] T. Brugo, R. Palazzetti, The effect of thickness of Nylon 6,6 nanofibrous mat on Modes I–II fracture mechanics of UD and woven composite laminates, Composite Structures. 154 (2016) 172–178. doi:10.1016/j.compstruct.2016.07.034.

[21] L. Daelemans, S. van der Heijden, I. De Baere, H. Rahier, W. Van Paepegem, K. De Clerck, Improved fatigue delamination behaviour of composite laminates with electrospun thermoplastic nanofibrous interleaves using the Central Cut-Ply method, Composites Part A: Applied Science and Manufacturing. 94 (2017) 10–20. doi:10.1016/j.compositesa.2016.12.004.

[22] S. van der Heijden, L. Daelemans, K. De Bruycker, R. Simal, I. De Baere, W. Van Paepegem, H. Rahier, K. De Clerck, Novel composite materials with tunable delamination resistance using functionalizable electrospun SBS fibers, Composite Structures. 159 (2017) 12–20. doi:10.1016/j.compstruct.2016.09.057.

[23] H. Zhang, A. Bharti, Z. Li, S. Du, E. Bilotti, T. Peijs, Localized toughening of carbon/epoxy laminates using dissolvable thermoplastic interleaves and electrospun fibres, Composites Part A: Applied Science and Manufacturing. 79 (2015) 116–126. doi:10.1016/j.compositesa.2015.09.024.

[24] G.W. Beckermann, K.L. Pickering, Mode I and Mode II interlaminar fracture toughness of composite laminates interleaved with electrospun nanofibre veils, Composites Part A: Applied Science and Manufacturing. 72 (2015) 11–21. doi:10.1016/j.compositesa.2015.01.028.

[25] N.H. Nash, D. Ray, T.M. Young, W.F. Stanley, The influence of hydrothermal conditioning on the Mode-I, thermal and flexural properties of Carbon/Benzoxazine composites with a thermoplastic toughening interlayer, Composites Part A: Applied Science and Manufacturing. 76 (2015) 135–144. doi:10.1016/j.compositesa.2015.04.023.

[26] S. Hamer, H. Leibovich, A. Green, R. Avrahami, E. Zussman, A. Siegmann, D. Sherman, Mode I and Mode II fracture energy of MWCNT reinforced nanofibrilmats interleaved carbon/epoxy laminates, Composites Science and Technology. 90 (2014) 48–56. doi:10.1016/j.compscitech.2013.10.013.

[27] G. Li, P. Li, C. Zhang, Y. Yu, H. Liu, S. Zhang, X. Jia, X. Yang, Z. Xue, S. Ryu, Inhomogeneous toughening of carbon fiber/epoxy composite using electrospun polysulfone nanofibrous membranes by in situ phase separation, Composites Science and Technology. 68 (2008) 987–994. doi:10.1016/j.compscitech.2007.07.010.

[28] J. Zhang, T. Lin, X. Wang, Electrospun nanofibre toughened carbon/epoxy composites: Effects of polyetherketone cardo (PEK-C) nanofibre diameter and interlayer thickness, Composites Science and Technology. 70 (2010) 1660–1666. doi:10.1016/j.compscitech.2010.06.019.

[29] K. Magniez, T. Chaffraix, B. Fox, Toughening of a Carbon-Fibre Composite Using Electrospun Poly(Hydroxyether of Bisphenol A) Nanofibrous Membranes Through Inverse Phase Separation and Inter-Domain Etherification, Materials. 4 (2011) 1967–1984. doi:10.3390/ma4111967.

[30] P. Akangah, S. Lingaiah, K. Shivakumar, Effect of Nylon-66 nano-fiber interleaving on impact damage resistance of epoxy/carbon fiber composite laminates, Composite

Structures. 92 (2010) 1432–1439. doi:10.1016/j.compstruct.2009.11.009.

[31] P. Akangah, K. Shivakumar, Assessment of Impact Damage Resistance and Tolerance of Polymer Nanofiber Interleaved Composite Laminates, Journal of Chemical Science and Technology. (n.d.). http://www.academicpub.org/jcst/paperInfo.aspx?PaperID=12067 (accessed September 5, 2014).

[32] R. Palazzetti, A. Zucchelli, I. Trendafilova, The self-reinforcing effect of Nylon 6,6 nano-fibres on CFRP laminates subjected to low velocity impact, Composite Structures. 106 (2013) 661–671. doi:10.1016/j.compstruct.2013.07.021.

[33] H. Saghafi, R. Palazzetti, A. Zucchelli, G. Minak, Impact response of glass/epoxy laminate interleaved with nanofibrous mats, Engineering Solid Mechanics. 1 (2013) 85–90. http://growingscience.com/beta/esm/1141-impact-response-of-glass-epoxy-laminate-interleaved-with-nanofibrous-mats.html (accessed September 5, 2014).

[34] B. Beylergil, M. Tano?lu, E. Akta?, Enhancement of interlaminar fracture toughness of carbon fiber-epoxy composites using polyamide-6,6 electrospun nanofibers, Journal of Applied Polymer Science. (2017) 45244. doi:10.1002/app.45244.

[35] R.E. Neisiany, S.N. Khorasani, M. Naeimirad, J.K.Y. Lee, S. Ramakrishna, Improving Mechanical Properties of Carbon/Epoxy Composite by Incorporating Functionalized Electrospun Polyacrylonitrile Nanofibers, Macromolecular Materials and Engineering. 302 (2017) 1600551. doi:10.1002/mame.201600551.

[36] M. de Freitas, L. Reis, Failure mechanisms on composite specimens subjected to compression after impact, Composite Structures. 42 (1998) 365–373. doi:10.1016/S0263-8223(98)00081-6.

[37] L. Daelemans, S. van der Heijden, I. De Baere, H. Rahier, W. Van Paepegem, K. De Clerck, Using aligned nanofibres for identifying the toughening micromechanisms in nanofibre interleaved laminates, Composites Science and Technology. 124 (2016) 17–26. doi:10.1016/j.compscitech.2015.11.021.

[38] L. Daelemans, S. van der Heijden, I. De Baere, H. Rahier, W. Van Paepegem, K. De Clerck, Nanofibre bridging as a toughening mechanism in carbon/epoxy composite laminates interleaved with electrospun polyamide nanofibrous veils, Composites Science and Technology. 117 (2015) 244–256. doi:10.1016/j.compscitech.2015.06.021.

[39] B. De Schoenmaker, A. Goethals, L. Van der Schueren, H. Rahier, K. De Clerck, Polyamide 6.9 nanofibres electrospun under steady state conditions from a solvent/non-solvent solution, Journal of Materials Science. 47 (2012) 4118–4126. doi:10.1007/s10853-012-6266-9.

[40] L. Van der Schueren, B. De Schoenmaker, Ö.I. Kalaoglu, K. De Clerck, An alternative solvent system for the steady state electrospinning of polycaprolactone, European Polymer Journal. 47 (2011) 1256–1263. doi:10.1016/j.eurpolymj.2011.02.025.

[41] S. De Vrieze, B. De Schoenmaker, Ö. Ceylan, J. Depuydt, L. Van Landuyt, H. Rahier, G. Van Assche, K. De Clerck, Morphologic study of steady state electrospun polyamide 6 nanofibres, Journal of Applied Polymer Science. 119 (2011) 2984–2990. doi:10.1002/app.33036.

[42] S. Van Dam, J. Pelfrene, S. De Pauw, W. Van Paepegem, Experimental study on the dynamic behaviour of glass fitted with safety window film with a small-scale drop weight set-up, International Journal of Impact Engineering. 73 (2014) 101–111.

doi:10.1016/j.ijimpeng.2014.06.002.

[43] ASTM International, ASTM D7136 / D7136M - 15 Standard Test Method for Measuring the Damage Resistance of a Fiber-Reinforced Polymer Matrix Composite to a Drop-Weight Impact Event, (n.d.). https://www.astm.org/Standards/D7136.htm.

[44] S. Denneulin, P. Viot, F. Leonardi, J.-L. Lataillade, The influence of acrylate triblock copolymer embedded in matrix on composite structures' responses to low-velocity impacts, Composite Structures. 94 (2012) 1471–1481. doi:10.1016/j.compstruct.2011.11.021.

[45] P. Wang, X. Zhang, G. Lim, H. Neo, A.A. Malcolm, Y. Xiang, G. Lu, J. Yang, Improvement of impact-resistant property of glass fiber-reinforced composites by carbon nanotube-modified epoxy and pre-stretched fiber fabrics, Journal of Materials Science. 50 (2015) 5978–5992. doi:10.1007/s10853-015-9145-3.